THESE DE DOCTORAT

Synthesis of novel phosphinate flame retardants for poly butylene(terephthalate) (PBT) and polyamide 6 (PA6)

Présentée et soutenue publiquement à
L'UNIVERSITE DE LILLE 1 – SCIENCES ET TECHNOLOGIES

Pour obtenir le grade de
Docteur
Spécialité : Molécules et Matière condensée

Par

Renaud DUPRETZ

Ingénieur diplômé de l'Ecole Nationale Supérieure de Chimie de Lille
Titulaire du Master Ingénierie des Systèmes Polymères de l'Université Lille 1

Thèse dirigée par
Prof. Serge BOURBIGOT et Prof. Sophie DUQUESNE

Soutenue le 27 Octobre 2015 devant la Commission d'Examen composée de :

Prof. Gaëlle FONTAINE, Université Lille 1	Président du Jury
Prof. Annie-Claude GAUMONT, Université de Caen	Rapporteur
Prof. Manfred DÖRING, Fraunhofer LBF	Rapporteur
Prof. Serge BOURBIGOT, Université Lille 1	Directeur de thèse
Prof. Sophie DUQUESNE, Université Lille 1	Co-directeur de thèse
Dr. Sebastian WAGNER, BASF SE	Examinateur
Dr. Michel KELLER, BASF SE	Examinateur

"Qui souffle sur le feu a des étincelles dans les yeux."

Proverbe Allemand

"Hilf mir,
Das Feuer liebt mich."

Rammstein – Hilf Mir

Acknowledgements

The work presented in this manuscript was carried out in the UMET laboratory (CNRS UMR 8207), led by Prof. Alexandre Legris, and more precisely within the team ISP-R2F (Reaction and Resistance to Fire) led by Prof. Serge Bourbigot. I would like to thank them for giving me the opportunity to join their labs, work on this project and achieve this PhD in excellent job conditions.

I would obviously like to thank my supervisors, Prof. Sophie Duquesne and Prof. Serge Bourbigot for their expertise and advice in this project. I really enjoyed working and sharing social moments with them at work or during meetings.

I would like to thank all the BASF team, without which the project would not have existed. I thank Martin Klatt, Alexander Koenig, Sebastian Wagner and Roland Kramer, for their welcoming attitude during the many meetings in Ludwigshafen. Thanks for the trust they have placed in me to lead this research.

I would like to acknowledge any technique expert who helped me during the time I spent in the lab. First, the NMR team, Bertrand Revel for his patient formation and his trust in my ability to use their equipment, and Bertrand Doumert for the time he spent in designing experiments with me. Thanks as well to Severine Bellayer for her patient and tricky work in microscopy techniques. Finally, I would like to thank Pierre Bachelet for his technical support in our lab.

I would like to acknowledge Prof. Annie-Claude Gaumont and prof. Manfred Döring who accepted to take on their time and to bring their expertise as examiners to assess this manuscript. I would also like to thank Prof. Gaëlle Fontaine for agreeing to chair the jury of this PhD, and also for helping me throughout the past four years in the ENSCL.

I thank all members of the R2F team for all the moments we shared in easy-going atmosphere, thanks for their contagious good mood in the hardest moments of these three years. First thanks to those who left before me but brought me a real pleasure to work in the beginning of this PhD: Jérémie, who left me a powerful scientific legacy as basis for my work and shared with me nice moments in our music band; special thanks to Gwenaëlle for our endless conversations and nice tea-times, thanks to Marion, Marianne (thanks for having me discover *Delain*), Nicolas R. (my dear homonymous), Andrea *alias* Francis, Antoine, Bastien, Franck, Maryska, Carmen and Mathieu. Thanks to all the lab's permanent members: Fabienne, Mathilde, Michel, Maude, Charaffedine, Catherine, and particular thanks to Brigitte, who really acted as a mother for all of PhD students in the lab. Thanks to my two internship students, Hajar and Emil (Diablo-fan-little-brother). Thanks to Agnès, Anil, Trang, Nittaya, Caroline, Hirak, Laurie, Pauline, Audrey, Sarah, Martin, and also Benjamin, Bertrand and Nicolas for the gaming-evenings we shared.

Last but not least I would like to thank my friends, Seb, Greg and Yann, Alex and Laure, Romain and Adrien, and most of all my fiancée, Gaëlle, and our families, for their invaluable daily support in the best and worst moments.

TABLE OF CONTENTS

List of abbreviations

2-POO: 2-phenyl-1,2-oxaphospholan-5-one 2-oxide

3-HPP: 3-hydroxyphenyl(phosphonyl) propanoïc acid

ACN: Acetonitrile

AlPi: Aluminum diethylphosphinate

ATH: Aluminum trihydrate

BA-3-HPP: Benzyl amide of 3-hydroxyphenyl(phosphonyl) propanoïc acid

BAS: Aluminum salt of BA-3-HPP

CP: Cross Polarization

CSA: Chemical shift anisotropy

DCP: Double Cross Polarization

D-HMQC: Dipolar heteronuclear multiple quantum correlation

DMF: DImethylformamide

DMSO: Dimethylsulfoxide

DOPO: Dyhydro-oxa-phosphaphenathrene-oxide

DPP: Dichlorophenylphosphine

DSC: Differential scanning calorimetry

dTG: Derivative of the thermogravimetric curve

E&E or **EEE:** Electrical and electronic equipment

EDA-3-HPP: ethylene diamide of 3-hydroxyphenyl(phosphonyl) propanoïc acid

EDAS: Aluminum salt of EDA-3-HPP

EGA/MS: Evolved gas analysis through mass spectrometry

EPMA: Electron probe micro analysis

FR: Flame retardant

FTIR: Fourier transform infra-red

GF: Glass fibers

GSMP: Guanidine sulfamate /melamine polyphosphate 1:1 mixture

GWFI: Glow wire flaming index

GWIT: Glow wire ignition temperature

HCN: Hydrogen cyanide

HP: Hot press

IM: Injection molding

LOI: Limiting oxygen index

MAS: Magic angle spinning

MCA: Melamine cyanurate

MDH: Magnesium dyhydrate

MLC: Mass loss cone calorimeter

MPP: Melamine polyphosphate

MPY: Melamine pyrophosphate

NMR: Nuclear magnetic resonance

OxP: Oxaphospholane

PA-3-HPP: Phenyl amide of 3-hydroxyphenyl(phosphonyl) propanoïc acid

PA6: Polyamide 6

PA6.6: Polyamide 6.6

PA6GF: Glass fiber reinforced Polyamide 6

PAS: Aluminum salt of PA-3-HPP

PBT: Poly(butylene terephthalate)

PBTGF: Glass fiber reinforced PBT

PBTGF-PAS: PBTGF loaded with 20 wt% PAS

PBT-PAS: PBT loaded with 20 wt% PAS

PC: Polycarbonate

PCFC: Pyrolysis combustion flow calorimeter

PET: Poly(ethylene terephthalate)

pHRR: peak of heat released rate

PPD-3-HPP: para-phenylene diamide of 3-hydroxyphenyl(phosphonyl) propanoïc acid

PPDS: Aluminum salt of PPD-3-HPP

PPZ-3-HPP: piperazine diamide of 3-hydroxyphenyl(phosphonyl) propanoïc acid

PPZS: Aluminum salt of PPZ-3-HPP

py-GC/MS: Pyrolysis-gas chromatography-mass spectrometry

SEM: Scanning electron microscopy

TGA: Thermogravimetric analysis

THF: Tetrahydrofuran

THR: Total heat release

TMS: Tetramethylsilane

_____

General Introduction

_____

Human has benefited from the use of plastics since Antiquity, when the ancient Mesoamericans first processed natural rubber into balls or figurines. However, it is most of all at the end of XIXth century that their uses developed. Synthetic plastics were then discovered and created to cover a broadest range of uses. Bakelite was the first polymer completely synthetic to be designed and used. After the First World War, improvements in chemical technology led to an explosion in new forms of plastics and mass production began around the 1940s. The production of plastics grew fast in the 1950s and never decreased since that time (Figure 1), except during the oil shocks in 1973 and 1979, and because of the crisis in 2008.
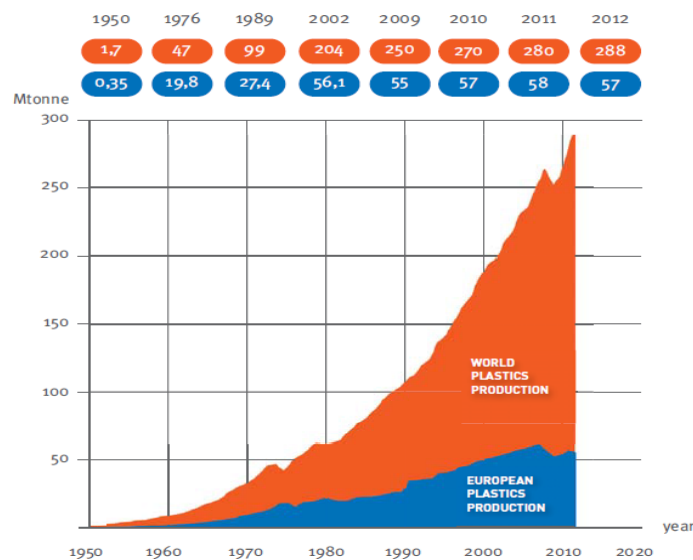
Figure 1: World plastic production 1950-2012 [1]

During those years, plastics have gradually replaced traditional materials such as wood or metal in many applications (Figure 2) since they present a great variety of properties and a processing versatility, which make them part of our everyday life.
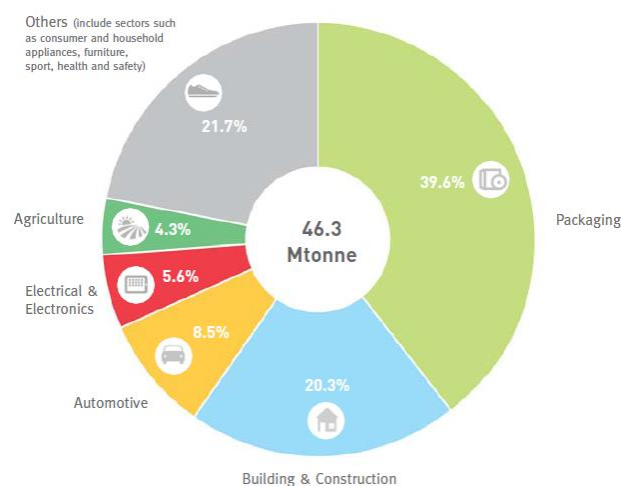
Figure 2: European plastics demand by segment in 2013 [2]

Among the various, engineering plastics are a group of plastic materials exhibiting higher properties than the "commodity" polymers (such as polystyrene, polyvinyl chloride, polypropylene and polyethylene)**[3]**. Moreover, they are much easier to process, especially when complicated shapes

are required. However, their better properties make them more expensive, so that they are produced in lower quantities and used for "low-volume" applications. The term "engineering plastics" usually refers to thermoplastic materials rather than thermosetting ones.

The global market for engineering plastics in terms of revenue was estimated to be worth $45.2 billion in 2011 and is expected to reach $76.8 billion by 2017 **[4]**. Many parts are made of engineering polymers, in particular poly(butylene terephthalate) (PBT) and polyamide 6 (PA6). These polymers are used in fields such as automotive **[5]**, electronics and electrical (E&E) **[6]**, building and construction, packaging or textile. In these fields, their exceptional properties are required: high stiffness, dimensional stability, low moisture absorption, durability (high resistance to chemical agents, light or weathering), and dielectric properties. They are the fastest growing segment of the plastics industry with an anticipated growth rate from 8 to 10%.

In spite of their properties and the variety of their uses, engineering plastics exhibit one major drawback: they are highly flammable. In case of fire, these materials will tend to release fuel and toxic smokes. Statistics in the US report that 1,240,000 fires occurred in 2013 **[7]**. This corresponds to a fire every 25 s, and more tragically also causes civilian fire deaths and casualties. In this frame, plastics represent heavy contributors to the development and propagation of a fire.

In many applications, where fire hazard cannot be neglected **[8]**, high safety levels must be met. Strict regulations or standard ensure that these materials or products meet the required level of safety (ignitability, fire behavior). For example, the Consumer Protection Act regulates requirements in the UK **[9]**; NF P.92.507 **[10]** and NF EN 13501-1 **[11]** give specifications in France; NFPA 701 **[12]** is the US industry specification; as a consequence, flame retardancy of plastics is a major security and economic issue. In that frame, it has become really necessary to develop Flame Retardants (FR) to reduce the risk inherent to the use of plastics.

FR represent a large group of chemicals consisting mainly in organic and inorganic compounds based on halogens, nitrogen, boron, phosphorus, sulfur, and metals (such as aluminum and magnesium) **[13]**. The global consumption of FR reached about 2 million tons a year in 2011. This number is particularly important in E&E field. The repartition of consumption of FR by type is reported in Figure 3.
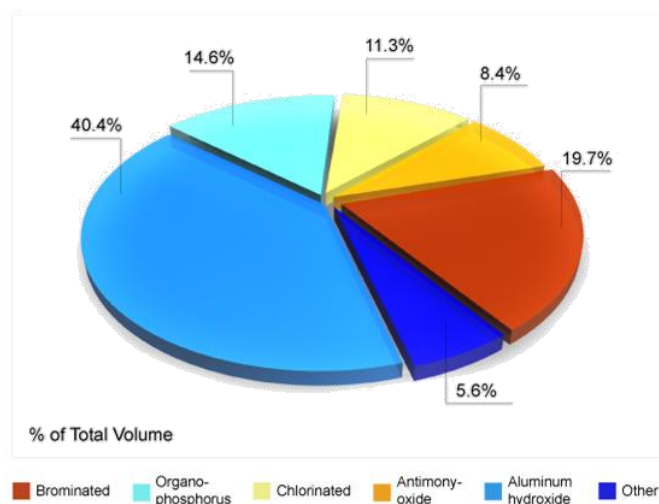
Figure 3: Global consumption of flame retardants by type (2011 data) [14]

The flame retardancy of a polymeric matrix can also be achieved in different ways [13, 15]. FR additives can be incorporated prior to, during, or more frequently, after polymerization; FR are not bonded to the polymer in that case. FR can be grafted on polymer chains [16]. A protecting substrate can be deposited on the material or grafted at the surface of the material [16]. Finally FR additives or functionalized monomers can be polymerized (or copolymerized with classical monomers), the result being an intrinsically modified polymer. In this work, the first approach was used to enhance fire properties of PBT and PA6.

Among all FR, phosphorus containing flame retardants represent a versatile class of compounds that are used either as main FRs or synergists, additive or reactive. Many commercial compounds such as aluminum phosphinates (aluminum diethylphosphinate [17-19]) are part of this category and are nowadays widely used in industrial formulations (organo-phosphorus compounds represented 14,6 % of global consumption of FR in 2011 [14]). The flame retardancy of PBT and PA6 using phosphinates was studied many times in literature.

This PhD thesis was done in collaboration with the company BASF SE (Ludwigshafen, Germany). The aim of the project was to design new phosphinate based flame retardants, thus exploring the additive route of fire retardancy. A good understanding of the modes of action and decomposition of obtained compounds was also necessary to allow developing new structures.

The first chapter of this manuscript will be dedicated to a short literature review on the flame retardancy of PBT and PA6, and their various properties and uses. A focus will be made on the literature of phosphinate salts, their use as flame retardants with or without synergist, their mode of action and decomposition. As this PhD followed the work of Dr. Jeremie Louisy [20], a special attention will be paid to the previous work achieved in our laboratory on the synthesis and uses of novel phosphinate salts.

The second chapter will present the materials, processing methods, as well as the experimental techniques used in the characterization of the products and formulations. The methods implemented to evaluate the flame retardant behavior of formulations and to perform a comprehensive study of the flame retardant mechanisms will also be presented. This chapter further outlines the experimental procedures used for the synthesis of various phosphinate salts.

In a third chapter, the synthesis and characterization of the phosphinate salts will be depicted. Novel compounds were prepared by grafting nitrogen-containing building-blocks on 2-phenyl-1,2-oxaphospholan-5-one 2-oxide (similar to those studied by Louisy [20] and to Clariant OP systems [18]). The thermal behavior of these salts will also be presented.

The fourth chapter will report the results of a screening based on the use of the synthesized additives in glass fiber-reinforced PBT (PBTGF) and PA6 (PA6GF). The objective is to find which compounds are efficient flame retardants and in which polymeric matrix. The results will then be discussed and the best formulation will be selected to take part in the methodology of comprehension of mechanisms.

The fifth chapter of this manuscript will be dedicated to the instrumentation of the UL-94 test. The UL-94 is widely used in the determination of formulations that have a potential to be commercialized. However, the answer of this test is only a "pass or fail" test. This chapter will show that the instrumentation allows obtaining novel information to understand the mode action of the flame retardants and also at which level this mode of action of a FR differs between two matrices. A

setup of the test on formulations developed in UMET laboratory in the past will first be presented. The instrumentation will then be used on the selected system in the fourth chapter and will be compared to a commercial formulation including FR additives.

Finally, the last chapter will focus on the comprehension of mechanisms introduced throughout the manuscript. Various analyses of gas and condensed phases during the degradation of additives or formulations will be presented. Gathering all the information obtained this way and in the other chapters will allow drawing a global mechanism of decomposition and determining modes of action of the selected flame retardant.

After concluding, an outlook to this study will be drawn from the different parts of the PhD that would need further investigation.

_____

Chapter I. State of the art - Fire retardancy of engineering plastics: the use of phosphinates

_____

This chapter aims at giving a review of the literature on the flame retardancy of engineering plastics, and in particular of PBT and PA6. The synthesis of these polymers, their properties and their applications will first be exposed. After giving a listing of general FR, a focus will be made on the use of phosphorus FR in such matrices and phosphinate salts will be further detailed.

I.1. POLY(BUTYLENE TEREPHTHALATE) AND POLYAMIDE 6

Poly(butylene terephthalate) (PBT) and polyamide 6 (PA6) are nowadays among the most used commercialized engineering polymers. They are sold under Ultradur® and Ultramid® trademarks by BASF for instance, but also Solvay or DuPont. They are used in a variety of applications where their inherent properties are a real benefit. In order to position this work in recent literature, this section of the chapter will be dedicated to a summary of their history, synthesis, properties and uses.

I.1.1   Polyesters – history

In the late 1920's, Carothers and his research group investigated the formation of polyesters from the reaction of aliphatic dicarboxylic acids with diols. However, the low melting points of obtained compounds made them inadequate as fiber precursors. That is why polyamides bypassed polyesters between the 1920's and the 1940's, as their properties were higher.

Polyesters really had their beginning in 1941 when Whinfield and Dickson discovered high melting point crystalline polymers by replacing aliphatic diacids with terephthalic acid. ICI, DuPont and other industrials developed these new compounds into familiar polyester fibers and films. Whinfield and Dickson realized that the polymer based on ethylene glycol (poly(ethylene terephthalate), PET) was the best suited for fibers; PBT was also discovered in the meantime. However, and many years later, a number of polyester producers became interested in PBT as its properties were close to those of nylons.

Polyesters did not only see their expansion in the domain of fibers. Many companies were simultaneously interested in adapting PET for molding applications. In 1966, the first injection molding grades of PET were introduced. However, these early materials were not very successful. It was observed that PET does not crystallize very rapidly; a crystallizable polymer in an amorphous or partially crystallized state would be useless, because of the potential crystallization and shrinkage of the part during use. Many methods were tested to obtain crystallized PET parts, and in 1978 DuPont introduced a PET injection-molding compound, under the trade name Rynite. A number of companies followed DuPont on the market. However, even if PET-based molding compounds are gaining acceptance at a substantial rate, the actual market volume is still relatively small. While studies were led on PET, Celanese (nowadays Ticona) chemists focused their attention on PBT. They released in 1970 a glass-fiber reinforced PBT designated as X-917. Eastman Kodak, GE and a dozen additional companies entered the business since that time.

I.1.2   Synthesis of PBT

Poly(butylene terephthalate) (Figure 4) is a semicrystalline thermoplastic polyester produced by the melt polycondensation of butan-1,4-diol with Pure Terephthalic Acid (PTA process **[21]**) or its DiMethyl ester (DMT process **[22]**).
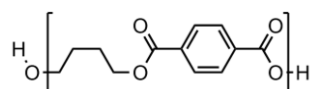
Figure 4: Structure of poly(butylene terephthalate)

Since both processes are based on an equilibrated reaction, catalysts are added to the bulk (e.g. Ti(OBu)$_4$) to reach higher conversion and speed up the reaction [23]. Tetrahydrofuran (THF, obtained by the backbiting reaction of PBT) is the main byproduct of both processes. The industrial production exhibits two general steps. First, transesterification (for DMT), or direct esterification (for PTA), lead to bis(4-hydroxybutyl) terephthalate and oligomers. Then, proper polymerization of hydroxybutyl-terminated oligomers leads to high molecular weight chains of PBT. The linear chains only contain low amounts of oligomers (around 1%)[23]. If an ultra-high molecular weight is needed, a further solid-state polycondensation stage is required. The main technologies for the manufacture of PBT were developed by Zimmer and Ems-Inventa-Fischer [23].

Both DMT and PTA routes (whatever continuous or discontinuous) constitute a basis for the current polycondensation processes; however PTA is more developed in the new facilities as it presents some advantages compared to DMT. PTA exhibits less process stages and higher polycondensation speed. It consumes fewer raw materials and does not need methanol which is carcinogenic and toxic. Finally, in PTA, THF (which is a commercially valuable product) can be easily recycled (in DMT, it forms an azeotrope with methanol).

I.1.3   Structure and properties of PBT

PBT exhibits a degree of crystallinity of 35 to 40% [24], with two possible phases, α and β, of triclinic structure as depicted in Figure 5. α phase is a relaxed crystalline state obtained while cooling PBT from the melt. It can be converted in β phase by uniaxial stretching. PBT crystallizes faster than most engineering polymers for comparable properties [25]. This makes it a polymer really suitable for injection molding. Compared to PET, the shorter cycle times lead to economical advantage.
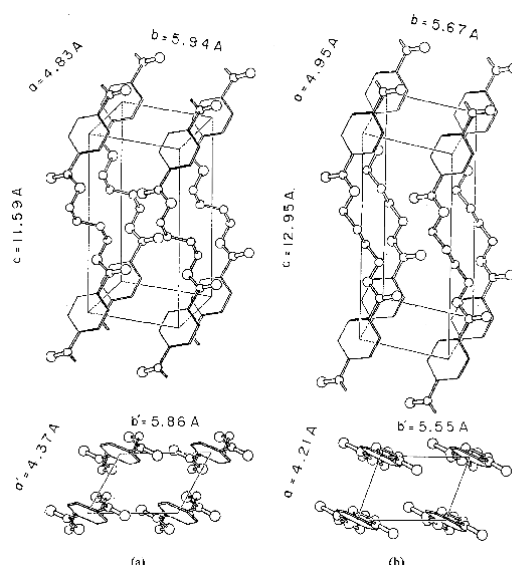
Figure 5: Crystal structure of poly(butylene terephthalate), a) α form and b) β form

PBT exhibits a glass transition temperature (Tg) between 30 and 50 °C, with a higher Tg value for a higher crystallinity [26] due to the lower mobility of the polymer chains. The melting behavior of PBT has been widely studied by DSC in the literature [27-32]. The DSC thermograms obtained by scanning the polymer from below Tg up to melting temperature often show multiple melting peaks. This illustrates the different crystal structures with proper thermal stabilities. Most researchers now attribute these multiple melting peaks to simultaneous melting, recrystallization and crystal perfection of the polymer.

PBT is generally used for its high strength, stiffness and heat deflection stability. Neat PBT shows a tensile strength of 55 MPa, a flexural modulus of 2500 MPa and a heat-deflection temperature of 170 °C at 0.46 MPa. These mechanical properties are generally modified by the addition of glass fibers (GF). Tensile strength increases up to 140 MPa, flexural modulus to 9000 MPa and heat-deflection temperature to 215 °C with 30 wt% GF **[5]**.

This polyester has also good electrical and dielectrical properties which make it a material of choice for E&E applications: outstanding creep current and arc-tracking resistance **[5, 24]**. Moreover, moisture has a low impact on its electrical properties.

The water uptake of PBT after immersion in boiling water is around 0.8%, so that it exhibits a good dimensional stability. Below 60 °C, PBT shows a good resistance to most common chemicals such as organic solvents, oils, brake fluids, aromatic products, diluted acids or bases, and water. Above 60 °C, its resistance to ketones, aromatics, acids and bases is reduced.

I.1.4   *Thermal decomposition and burning behavior of PBT*

The crystallinity of PBT induces a high thermal stability. It can be maintained close to its melting point without significant degradation **[5]**. In TGA under inert atmosphere, the thermal decomposition of PBT starts around 350 °C and occurs in one step, as the polymer decomposes completely into volatile products, following a pattern (Figure 6) that has been widely studied in pyrolysis coupled to gas chromatography/mass spectrometry **[33-35]**. Thermal scissions can occur at different points, involving either heterolytic or homolytic cleavages (according to different experimental conditions). These scissions lead to high boiling point ester fragments with vinyl, phenyl or acid end groups (E, I, K, M), terephthalic acid monoester (C) or diester (A), benzoic ester (F), terephthalic acid (D) and benzoic acid (G), and more volatile species such as THF (J), butadiene (B), benzene (L) and biphenyl (H). Vinyl end groups would illustrate heterolytic cleavages **[33]** while THF formation would be explained by homolytic cleavages (backbiting reaction) **[36]**.
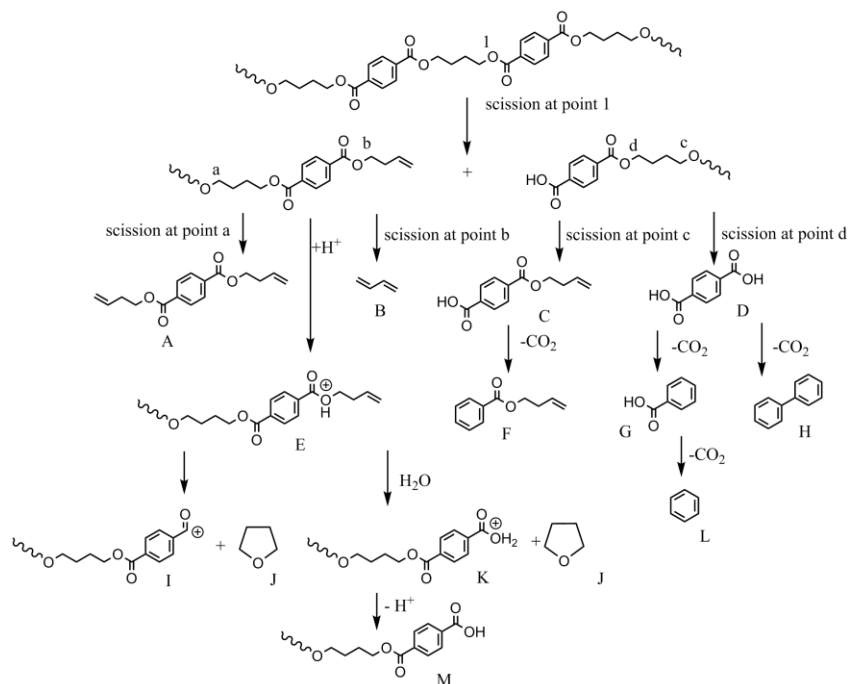
Figure 6: Degradation pattern of PBT [35]

As most engineering polymers, PBT is flammable, so that it is not classified in the UL-94 vertical test, whatever neat or reinforced with glass fibers [37, 38]. Its limiting oxygen index (LOI) is 22 vol% O_2, and decreases to 19-20 w% with GF. The measurement of the LOI values illustrates the inherent burning character of a material. A LOI of 21% or below ignite easily and burn rapidly in ambient atmosphere. Materials presenting higher LOI (above 21% but in most cases around 26-28%) can be considered as flame-retardant and generally pass ignition tests in horizontal and vertical orientations [39, 40]. Casu et al. [41] investigated the effect of glass fibers on the flammability of PBT. They came to the conclusion that because of their alignment in the polymer matrix and due to a higher heat conduction of glass compared to the polymeric material, glass fibers bring a "wick effect" leading to the increase of the flame propagation.

In cone calorimeter test, the tendency is opposite and GF help improving fire properties. The presence of GF drastically reduces the peak of heat release by forming an insulating shield at the surface of the polymer. However, the total heat release is comparable, combustion of the polymer being extended in time in the presence of GF, as depicted in Figure 7. It was then concluded that glass fibers tended to change the degradation pattern of PBT and to favor the release of more combustible volatile products.
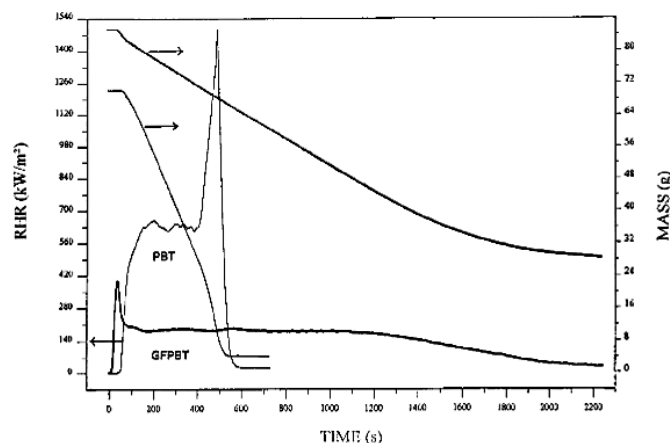
Figure 7: Cone calorimeter results on PBT and PBTGF (30 wt% GF) at 50 kW/m², rate of heat release (RHR and mass loss)

I.1.5   Additives and uses of PBT

PBT is rarely used in its pure form, but generally compounded with additives or blended with other polymers to reach a material with defined properties for given applications.

In most cases, GF are added to PBT to improve properties such as stiffness, strength, creep, and to increase its dimensional stability [42]. The amount of fibers, as well as their size or orientation [43], represent key factors that have a direct impact on mechanical properties of the composite. A sizing treatment can be applied to fibers so as to obtain more efficient transfers of mechanical stresses inside the material [44]. It should be highlighted that glass fiber reinforced PBT represents nowadays about 70 to 80% of PBT consumption [45]. Besides glass fibers, other additives or fillers are usually used. Chalk or talc can be used as fillers.

Additives mainly consist in antioxidants, UV stabilizers, flame retardants and processing agents. PBT can also be blended with other polymers to bring it new properties. PBT and polycarbonates alloys have for instance found some applications in the automotive industry [45]. About 15% of PBT is consumed in alloys, particularly with Polycarbonates (PC) or PET, although it can also be blended

with elastomers. Most PC/PBT applications are in automotive bumper systems where they are used for fascias and beams.

Globally, the main applications for PBT are in automotive uses (accounts for about 50% of total consumption including electrical/electronic uses), while nonautomotive electrical/electronic uses account for about 25%. In E&E, PBT can be used for connectors, relays, bobbins, contactors (Figure 8), capacitors, switches, plugs, lamp sockets, terminal boards, integrated circuit carriers, etc. PBT finds also its place in household appliances, like in hair dryers handles, oven doors, iron bases etc. **[5]**.

Figure 8: Flame retardant glass-fibre reinforced PBT is used in contactors for the French railways

Automotive use has risen as a result of increases in the number of safety and user comfort elements in vehicles, such as airbags, collision warning systems, or various electric motors (e.g., for seating mechanisms). In cars, PBT is used in air conditioning valves, gas cap, rear and side view mirror panels, lamp socket inserts, structural brackets, brake system and hydraulic transmission parts, together with door handles, wiper systems, cowl vents, bumpers, fender extension. Automotive applications account for the largest use in North America, Europe and Japan, while electrical/electronic applications are most significant in Other Asia.

Global consumption of PBT is greatest in Asia (50–55% of total 2008 global consumption), followed by Western Europe (21%) and the Americas (20%) (Figure 9). Growth rates are expected to remain highest in Asia, with more mature rates in North America and Western Europe, as some customer base continues to migrate toward Asia, especially China. The overall global market is expected to resume its historical growth rate of about 6% per year once the global economies recover. Growth in China is expected to average 12% per year, while in other areas of Asia, except Japan, it is expected to be about 10% per year. In Japan, average annual growth is expected to be about 2% **[45]**.

Figure 9: World repartition of PBT consumption in 2008 [45]

I.1.6   Polyamides – history

Polyamides, commonly called nylons, were the first commercial thermoplastic engineering polymers and represent a model for many engineering plastics. The first synthesis of PA6 was done in 1889 by heating aminocaproïc acid, but the real interest for polyamides grew up in the 1930s. In 1928, Carothers discovered a polymer by reacting hexamethylenediamine and adipic acid: polyamide 6.6 (PA6.6) was born. DuPont began its commercialization in 1938 as fiber, the commercial name *Nylon* appeared in 1939 on the American market. In 1941, nylon was developed as molding compound. In parallel in 1938, Schlack discovered a way to polymerize ε-caprolactam into PA6 with a small amount of water. World War II accelerated the development of polyamides since new synthetic fibers were required to replace silk in military equipment.

Nylon was a new concept in the domain of plastics for several reasons. It is semicrystalline, and undergoes a sharp transition from solid to melt and has a relatively high service temperature. The combination of toughness and rigidity performance suited for many applications. Nylons acquired the reputation of quality materials as they could perform better than metals in some cases, which gave nylons the label of "engineering plastics".

PA6 and PA6.6 are the most produced aliphatic nylons (still accounting for more than 90% of nylon use), whereas Polyamide 6.10, Polyamide 10, Polyamide 11 or Polyamide 12 for instance are specialty products for niche or small volume market. In recent years, there has been increasing interest in polyamides with higher melting points to extend the boundaries of this polymer type and to satisfy more stringent high temperature automotive and electronic applications. This has resulted in the development of Polyamide 4.6 and several semi-aromatic nylons **[46]**. Nowadays, these polymers are used in transportation, E&E, building and construction as well as packaging.

I.1.7   Synthesis of PA6

Polyamides contain a recurring amide group obtained in general by the reaction of a dicarboxylic acid and a diamine with removal of water. This is for instance the case of PA6.6. However in the case of PA6, the polymer is obtained by the ring-opening polymerization of ε-caprolactam followed by addition-condensation processes. The general structure of PA6 is reported in Figure 10.
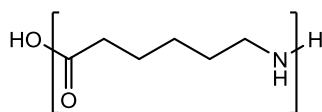
Figure 10: Structure of Polyamide 6

In the industry, PA6 is manufactured from benzene via cyclohexane. Hydrogen is passed through liquid benzene in the presence of a nickel catalyst under pressure (Figure 11-a). Cyclohexane is oxidized by passing air through the liquid under pressure in the presence of a catalyst (often a cobalt salt) to yield two products (Figure 11-b). The mixture of cyclohexanol and cyclohexanone is known as "mixed oil" or KA (ketone/alcohol). An alternative route to cyclohexanol is via the hydrogenation of phenol using a nickel catalyst at 400 K and 5 atm (Figure 11-c). A more recent route to cyclohexanol is the Asahi process from benzene via its hydrogenation to cyclohexene and subsequent hydration to alcohol. This is more energy efficient than the other processes.

To make PA6, pure cyclohexanone is required. When the mixed oil is heated under pressure with copper(II) and chromium(III) oxides, the cyclohexanol, which is a secondary alcohol, is

dehydrogenated to the corresponding ketone, cyclohexanone (Figure 11-d). Cyclohexanone is then converted into caprolactam via the oxime (produced by the reaction of the ketone with hydroxylamine - in the form of the salt, hydroxylamine hydrogen sulfate) (Figure 11-e). The isomerisation of the oxime to caprolactam by sulfuric acid is an example of the Beckmann rearrangement in which an oxime is transformed into an amide in the presence of acid. A zeolite, with acidic sites, is also being used to affect the rearrangement. The zeolite is regenerated and saves the use of sulfuric acid.
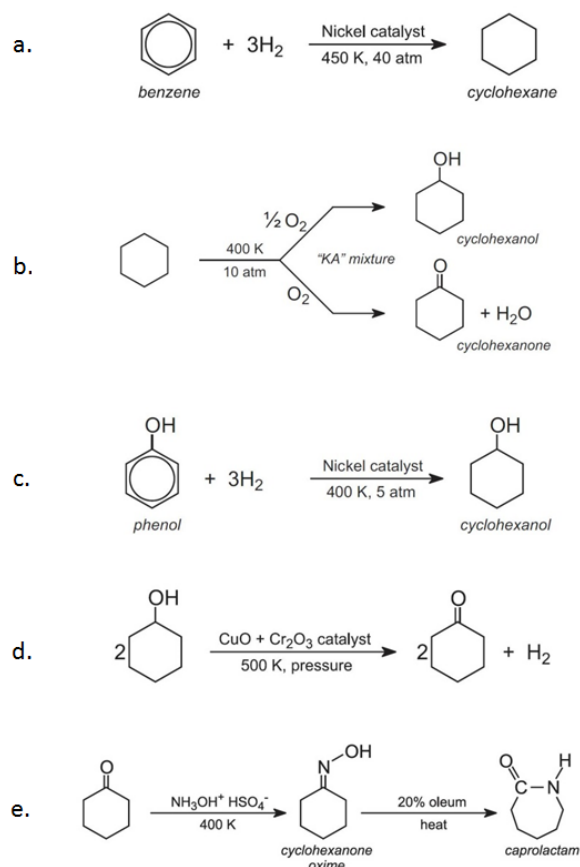
Figure 11: Schemes of the production of ε-caprolactam from benzene

After obtaining ε-caprolactam, the ring-opening polymerization of the monomer is initiated by water and the temperature range of operation is 250-260 °C. The applied pressure is up to 10 bars. The polymerization of PA6 takes place in two main steps: the ring opening of ε-caprolactam by water **[47]** and the polycondensation.

In the presence of water, the carbonyl group of caprolactam is protonated. Then a rearrangement occurs to form a carbocation, which is attacked by the hydroxyl group coming from water. The obtained unstable cyclic diol opens to form the linear ε-aminocaproïc acid as depicted in Figure 12.
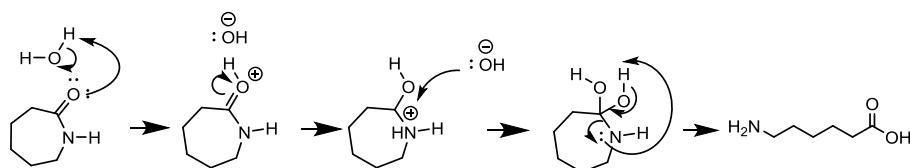
Figure 12: ε-caprolactam ring opening by water

The previously formed amino acid can react with a caprolactam molecule as illustrated in Figure 13. The carbonyl function is protonated and leads to a carbocation, which reacts with the amine function of the amino acid and gives an ammonium specie. The latter is submitted to the ring-opening rearrangement followed by an intramolecular rearrangement leading to the dimer. The dimer then acts as the linear amino acid and the ring-opening occurs multiple times to reach long chains of PA6 (Figure 13).
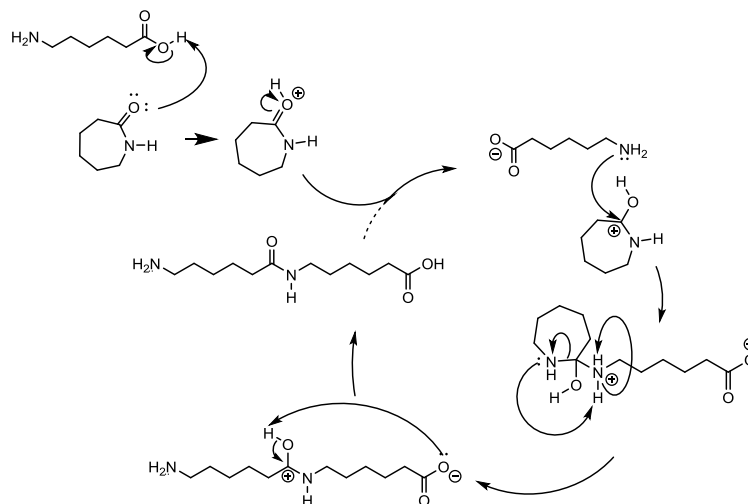
Figure 13: Ring-opening polymerization of ε-caprolactam

An anionic polymerization of PA6 is also possible, which requires lower temperatures (about 100 °C) and a strong base initiator like Na. The reaction of Na with ε-caprolactam leads to a lactam anion which attacks another caprolactam carbonyl. The anionic ring opening leads to the generation of another anion that follows the same reaction scheme and produces long chains of PA6. However the chain end is different, as depicted in Figure 14 **[48]**. Anionic polymerization and other techniques such as interfacial polymerization and solid-state polymerization also exist but they are not developed at an industrial scale **[49]**.
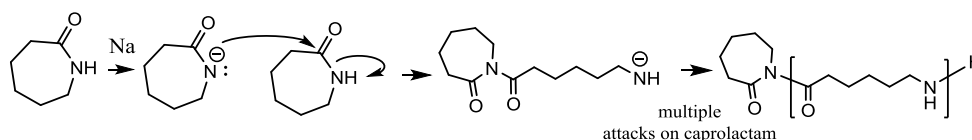
Figure 14: anionic polymerization of ε-caprolactam

I.1.8   Structure and properties of PA6

As PA6 is known to crystallize into different structures, it is said polymorphic. Many authors that studied PA6 found a plethora of crystalline, paracrystalline and mesomorphic forms with sometimes different authors using different names for a same or a very similar form. However, an overview of literature by Gianchandani et al. **[50]** suggest that PA6 exists in three general forms: amorphous, and two crystalline forms, α and γ **[51]**, as illustrated in Figure 15. A β form was also reported when PA6 crystallizes under constrain **[52]**. Due to the chemical structure of PA6 (C=O and N-H polar groups), hydrogen bonds are formed in both amorphous and crystalline phases. However polymer chains spontaneously organize to maximize these interactions to produce α and γ crystalline forms. It should be highlighted that several authors observed metastable phases under specific conditions,

which have varying degrees of disorder and defects stacking **[53]**, but α and γ remain the most encountered forms.

These two structures are very similar, however α phase if the most thermodynamically stable **[54]**, which leads to better mechanical properties. α phase is composed of molecules in an extended chain conformation, in which carbon, nitrogen and hydrogen forming the hydrogen bonds are located in the same plane. In the γ crystalline structure, the molecules form pleated sheets in which the hydrogen bonds link parallel chains. This involves higher constrains than for the α structure.

Nylon 6 (α)   Nylon 6 (γ)
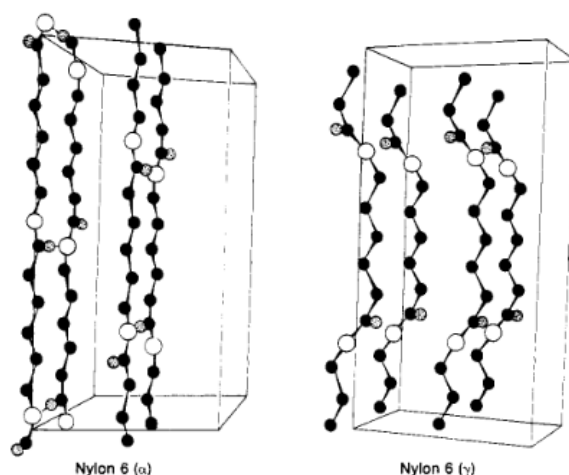
Figure 15: Schematic illustration of α and γ crystalline forms of PA6 [51]

These two structures can be distinguished through various techniques such as Fourier Transform Infra-Red spectroscopy **[55]**, differential scanning calorimetry (DSC) **[56]**, or also solid-state Nuclear magnetic Resonance (NMR) **[57]**. Vasanthan and Salem calculated an α / γ ratio thanks to the absorption band at 930 and 973 cm^{-1} in FTIR and considering a relation with the Beer-Lambert law. DSC is a useful technique in this case as the two crystalline forms melt at different temperatures. However, differences in the melting temperatures can be found depending on the PA6 molecular weight. For instance, Ho et al. found melting temperatures for γ and α forms of 226 °C and 231 °C respectively **[58]**, while Liu et al. found 214 °C and 223 °C respectively **[59]**. Finally, solid-state NMR also helps achieving a morphologic characterization of PA6, thanks to ^{13}C and ^{15}N analyzes, as depicted in Figure 16.
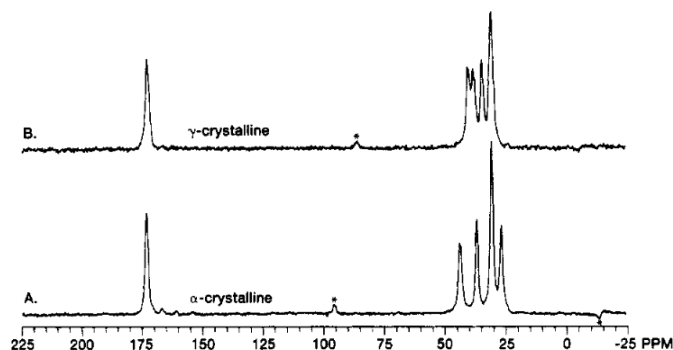
Figure 16: Illustration of the differences between α and γ phases in ^{13}C solid-state NMR [57]

Concerning its chemical properties, PA6 represents a relatively stable aliphatic polymer but potentially reactive amide functions or carboxylic and amine chain-end groups. It is resistant to oils

and fats, however it is sensitive to some chemical substances (water, acids, amines), UV irradiation or heat. PA6 is insoluble in classical organic solvents but is soluble in formic acid, some phenolic solvents or fluorinated alcohols such as 1,1,1,3,3,3-hexafluoropropan-2-ol. Low concentration solutions of mineral acids like hydrochloric, nitric or sulfuric acid weaken nylons, and high concentration solutions hydrolyze them. Exposure to amines and acids results in a decrease of the molecular weight of PA6 **[60]**. Water alone also hydrolyzes PA6 but at higher temperatures and pressures (above 150 °C), whereas PA6 is not affected by moisture up to 80 °C. The processing temperatures being higher, PA6 needs to be dried before use.

Finally, PA6 has good physical and mechanical properties, such as abrasion resistance, low coefficient of friction, high tensile strength and good creep resistance. These properties are maintained in a broad range of temperatures (-50 to 170 °C).

I.1.9   *Thermal decomposition and burning behavior of PA6*

Despite a great number of researches in the field of thermal decomposition of polymers, there is not yet a general accepted mechanism for the decomposition of aliphatic nylons. A variety of experimental conditions can be found in the literature which does not lead to a common decomposition pathway of PA6. Levchik et al. however made a review on this topic **[61]**. Some main mechanisms have been identified, involving the release of ε-caprolactam monomer. The depolymerization (Figure 17) begins at temperatures slightly above 200 °C by intramolecular end-group cyclization (end-biting), main chain cyclization (back-biting) or intermolecular aminolysis **[62]**.
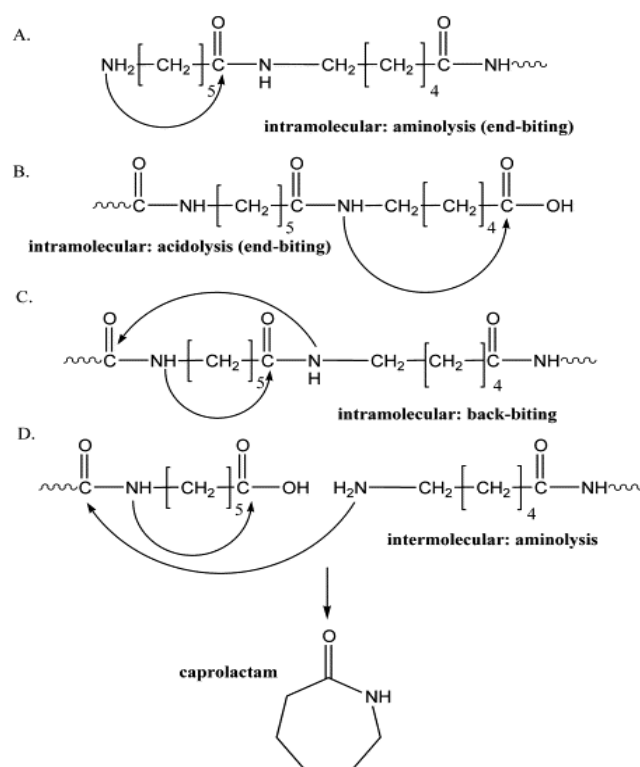
Figure 17: Intra and intermolecular generation of ε-caprolactam during degradation of PA6 [61]

The flammability of aliphatic nylons has been investigated by means of many methods, among which the measurement of LOI. A measurement of LOI for various nylon 6 samples was carried out by

Reimschuessel et al **[63]**. These researchers assumed the flammability of nylon 6 is linked to the production of fuel. A relation between LOI, molecular weight (viscosity η), concentration of amine (a) and carboxylic (c) chain-ends was proposed **[63, 64]** (Equation 1). Thus, due to their low melt viscosity, aliphatic nylons are considered to have an apparent low flammability.

$$LOI = 13.5 \times \left(1 + \frac{1}{\eta}\right) + \frac{2050}{(13.5\,a + ac)}$$

Equation 1

I.1.10   Additives and uses of PA6

Like PBT, PA6 is not often used in its neat form. It is generally compounded with additives that increase its properties. Antioxidazing agents and UV-stabilizers are used to increase its resistance to weathering. Processing agents are sometimes used when PA6 is turned into molded parts. Glass fibers are also classically used in PA6 to improve its mechanical properties such as stiffness, impact resistance or dimensional stability under heat. Masterbatches containing a definite load of glass fibers constitute a class of commercial products (such as BASF Ultramid® for PA6).

PA6 is used in a wide range of applications. In automotive, door handles and radiator grills can be made of PA6. It is also used in E&E parts, like miniature circuit breakers, switches and fuses, contactors and cabinets. PA6 is also sometimes used in sports applications, such as ski bindings or in-line skates, as it presents good fatigue properties and high impact strength. Moreover, it is most of all used to make synthetic fibers.

I.1.11   Conclusion

PBT and PA6 are both engineering polymers that find a great variety of uses in automotive, E&E, building, and packaging industries. Their use developed in the past decades due to their excellent chemical, physical and mechanical resistance, stiffness, and the versatility in their possibilities of use. In that frame, they are generally compounded with reinforcements or stabilizers.

Despite their numerous qualities, PBT and PA6 exhibit one major drawback: they are highly flammable. To be used in applications where the fire risks cannot be neglected (E&E and transportation) and where regulations are growing strict with the years, they need to be flame-retarded. It has been previously shown that when these polymers decompose upon heating, they release in the gas phase flammable compounds such as THF or ε-caprolactam that are sharply flammable.

The next section of this work is thus devoted to the fire retardancy of polymers, with an obvious focus on the flame retardants (FR) classically used in PBT and PA6. A special attention will be given to phosphorus-based flame-retardants and especially phosphinate salts as they represent a broad class of commercial flame-retardants, on which this work is based.

I.2. FIRE RETARDANCY OF ENGINEERING PLASTICS

Because of their organic nature, most polymers are combustible **[8]**. In the past decades, numerous researchers have investigated the fire retardancy of various matrixes in order to minimize the reaction to fire of materials and the resulting hazards to humans **[65]**. In this section, a first part will consider the literature of combustion will be presented. The different mechanisms of action of common FR will be detailed. Then the FR commercially used in PBT and PA6 will be exposed, with a particular focus on phosphorus flame-retardants, mainly phosphinate salts.

I.2.1 *General aspects on combustion*

When exposed to heat, the properties of thermoplastic materials change; they soften and some then melt. There exists a critical temperature above which the energy brought to the material overcomes the energy needed to break bonds inside the molecules and/or to thermo-oxidize the material at its surface. Decomposition products are then released in the gas phase, depending on the material that decomposes. They ignite when mixed with oxygen from the air once a critical concentration is reached. The flame then heats back the material and self-maintains the combustion process. The combustion cycle, as depicted in Figure 18, also called "fire triangle" is then maintained. If any branch of the triangle is suppressed (air source, fuel from polymer degradation etc.), the combustion stops.
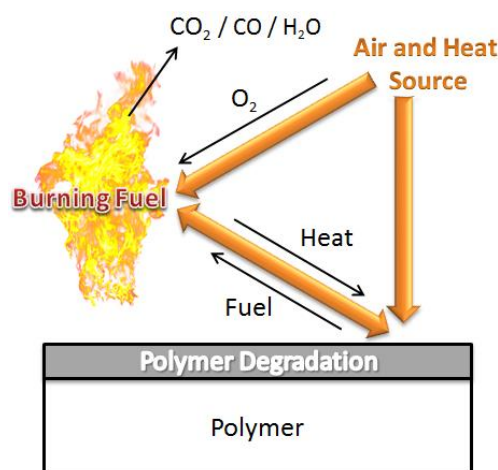
Figure 18: The Combustion Cycle

Upon thermal decomposition, many phenomena can occur in the polymer degradation zone: softening (and also melting for crystalline and semicrystalline polymers), hydrolysis, crosslinking, charring, dripping etc.. Two mechanisms of decomposition can be distinguished, depending on the presence and reaction of oxygen or not **[66]**.

The non-oxidizing thermal degradation, also called pyrolysis, consisting in chain scissions by homolytic or heterolytic cleavages. The chain scission can lead to free radicals which will propagate the decomposition reaction or to the formation of molecules comprising a double bond.

The oxidizing thermal decomposition when the polymer chains or its decomposition products react with oxygen to generate various molecules (carboxylic acids, alcohols, ketones or aldehydes). The oxidation processes also generates radical species due to the formation of peroxides. Crosslinking can also occur through recombination of macromolecular radicals; however bond scission remains the dominant reaction.

I.2.2   Mode of action of flame retardants

Flame retardants are designed to interfere with the combustion cycle. They are intended to stop or inhibit phenomena occurring in the "fire triangle", by acting either chemically or physically either in the gas or in the condensed phase. A representation of the four general ways FR act has been proposed by Price et al. **[67]** and is presented in Figure 19.
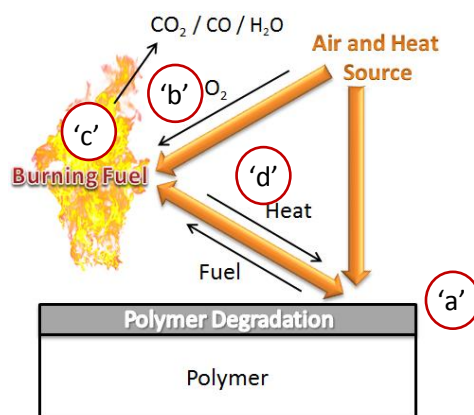
Figure 19: Scheme of the combustion cycle; a-d represent potential modes of action of FR [67]

FR are considered to:

→ 'a' - modify the degradation pathway of the polymer during pyrolysis to either reduce the amount of released flammable gases or to increase the formation of less flammable gases or char.

→ 'b'- *reduce the oxygen supply*. The release of non-flammable species (such as water for instance) results in lowering the concentration of combustibles in the gas phase (dilution effect).

→ 'c' - *introduce flame inhibitors in the matrix.* The FR releases active species, mainly radicals, to poison the flame.

→ 'd' - *reduce the heat flow back from the combustion of gases to the polymer to prevent further pyrolysis.* This can be achieved by using heat-sink compounds (e.g. compounds that decompose endothermically) or compounds that produce a barrier effect when exposed to fire conditions. Intumescent systems are FR combinations that typically work according to this mechanism.

I.2.3   Classes of flame retardants

Flame retardants can be first classified in two categories. *Additive flame retardants* are usually incorporated during the processing of the polymer like other additives or fillers. In this case they have to be thermally stable at the processing temperature of the polymer. *Reactive flame retardants* are incorporated to the polymer during its synthesis or during post reaction processes such as grafting. They are linked to the polymer chains. Additive flame retardants are generally preferred because handling and processing in that case are easier and more cost-effective. This section will review the general families of additive flame retardants.

I.2.3.1 Halogenated flame retardants

Halogenated compounds, especially the brominated ones, are widely used as FR in various matrixes due to their high performances. Chlorinated compounds exhibit lower efficiency **[68]**; iodinated and

fluorinated compounds do not present significant activity in the temperature range which is that of polymer decomposition **[66]**.

These compounds (RX) mainly act by flame inhibition. During their decomposition, they release hydrogen halide species (HX) that scavenge the H° and OH° radicals of the flame (Figure 20). Hydrogen halides also induce the crosslinking of macromolecular fragments (R'H) by transferring radicals on their chains (R'°). This may lead to the formation of a carbonaceous protective shield at the surface of the material. As a consequence, a possible condensed-phase action has also been reported in the literature for some of the halogenated FR **[66]**.

$$RX \rightarrow R° + X°$$
$$X° + R'H \rightarrow R'° + HX$$
$$HX + H° \rightarrow H_2 + X°$$
$$HX + OH° \rightarrow H_2O + X°$$
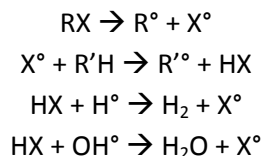
Figure 20: Quenching mode of halogen-based species released in the gas phase

Antimony oxide (Sb_2O_3) is one of the major synergistic agents used with halogenated FR. It interacts with halogens during the combustion, which results in the formation of antimony trihalides or oxyhalides. The latter were found to be more effective in trapping the flame radicals than single hydrogen halides **[68]**.

In the field of E&E (where the requirements in terms of fire safety are severe), tetrabromobisphenol A (TBBPA) and polybromodiphenylethers (PBDE), as illustrated in Figure 21, were the most commercialized FR on the worldwide market **[66]**. A polycarbonate oligomer of TBBPA has been successfully used in glass fiber reinforced PET/PBT blends in combination with antimony oxide **[13, 69]**. Decabromodiphenylether has been used in glass fiber reinforced PBT, reaching a V-0 ranking (0.8 mm thickness) in the UL-94 when used at 10 wt% with 5 wt% antimony oxide **[70]**.
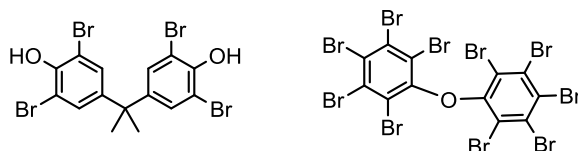
Figure 21: Tetrabromobisphenol A and decabromodiphenylether (example of polybromodiphenylether)

However, since the late 1980s, the United Nations and the European Community have emitted some restrictions concerning the use of some halogenated FR with reference to various studies concerning their negative impact on the environment or health **[71, 72]**. For instance, the annex 17 of REACH lists restrictions of use for Pentabromodiphenylether (PBDE), Octabromodiphenylether (OBDE), or other compounds in specific applications (Tris(2,3-dibromopropyl)phosphate, or TRIS, is not allowed in articles for skin contact, e.g. textiles). Consequently, halogenated systems tend to be banned due to market demand on halogen-free products.

I.2.3.2 Nitrogen-containing flame retardants

Melamine and its derivatives (Figure 22), such as melamine cyanurate, polyphosphate, or pyrophosphate, represent an entire class of flame retardants. Melamine is a thermally stable crystalline compound characterized by a melting point as high as 345 °C, and which contains 67 wt% nitrogen atoms. Melamine sublimates at about 350 °C and cools down the system by endothermic

processes. Melamine molecules can also condensate into melam, melem, or melon (Figure 22), while releasing ammonia (diluting gas).
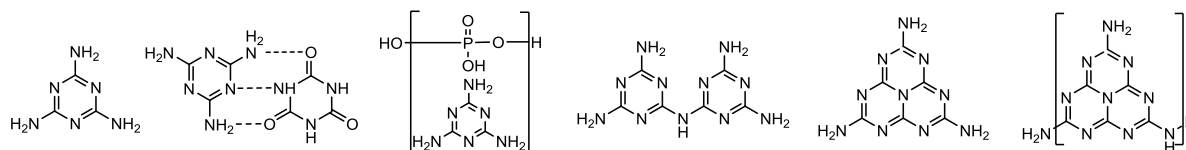
Figure 22: Melamine, melamine cyanurate, melamine polyphosphate, melam, melem, melon

These reactions compete with melamine volatilization and are enhanced if melamine volatilization is hindered. This is the case when a salt of melamine is used causing the formation of a protective layer including melamine. The retention and condensation of melamine-based species in the condensed phase is also effective for flame retardancy.

Melamine shows limited efficiency when used alone in PBT. 40 wt% loading in unreinforced material is required to obtain a V-0 ranking at 2 mm thickness in the UL-94 test. In this case an increase of the LOI from 22 to 26 vol% is observed. The study reported by Balabanovich **[73]** establishes that the condensation of melamine into melem or melon results in the formation of a protective char at high loadings. Moreover, the aminolysis of ester bonds due to the release of ammonia leads to the formation of aromatic amides and nitriles (Figure 23) which act as fuel-diluting and flame-cooling agent.
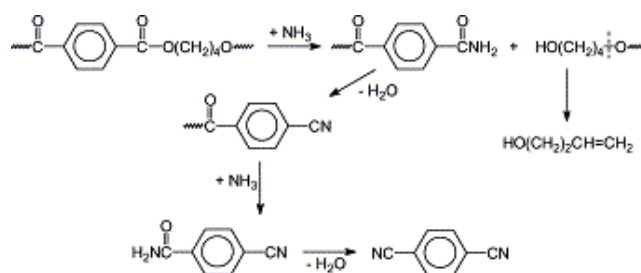
Figure 23: Aminolysis of PBT and formation of aromatic amides and nitriles [73]

In PA6, melamine alone (at 5 to 20 wt% loadings) is sufficient to provide a V-0 performance in UL-94. However combining it with various halogen derivatives, metal oxides, guanidine sulfamate or certain organophosphorus, halogen, or alkaline salts was referenced as advantageous in the literature **[15, 74]**.

Melamine salts are a specific class of commercial products that proved to be efficient in both PBT and PA6 **[75, 76]**. For instance BASF commercializes different grades of melamine cyanurates or melamine polyphosphates (Melapur® grades). They exhibit a higher thermal stability as compared to the pure melamine. Besides releasing melamine in the gas phase, they provide supplementary condensed phase modes of action.

Melamine cyanurate (MCA) is a salt of melamine and cyanuric acid (Figure 22). It exhibits the same endothermic mechanism as melamine (*heat sink effect*). Besides, it decomposes the polymer, thus removing it from the burning zone very rapidly (*runaway effect*) **[77]**. V-0 ranking in UL-94 can be obtained with MCA in unfilled PA6 at 8 to 15 wt% loadings, and at 13 to 16 wt% in mineral filled PA6 formulations **[78]**. In unreinforced PBT, at contents of 20 to 30 wt%, MCA moderately increases LOI value to 26 vol%, however such loadings do not lead to a V-0 ranking in UL-94. MCA is combined with phosphinate salts in most cases of use in PBT **[79]**.

Melamine polyphosphate (MPP) is a salt of melamine and polyphosphoric acid. Again, it releases melamine upon endothermic decomposition. However, phosphoric acid released during the degradation of polyphosphoric acid can react with the polymer, leading to the formation of a char. It thus limits fuel and heat transfers in the decomposition zone of the material [80]. MPP is used as co-additive in most cases of use. In PBT and PA6 for instance, it is generally compounded with phosphinates [81, 82]. A recent study by Coquelle et al. showed that a 50/50 mixture of MPP and guanidine sulfamate was suitable to flame retard PA6 at only 5 wt% loading [83].

I.2.3.3 Mineral flame retardants

This class of flame retardants is mainly composed of inorganic or mineral additives, among which the most common ones are aluminum hydroxide (ATH) and magnesium hydroxide (MDH). These additives mainly act by physical way, through endothermic dehydration and the formation of a ceramic protective layer. Due to the release of water, the flame is diluted, leading to a delayed ignition. A ceramic protective layer composed of metallic oxides is also obtained, characterized by a high heat capacity [84]. ATH and MDH for instance decompose into the corresponding oxides (Al_2O_3 and MgO) releasing water with an enthalpy of 1050 and 1300 kJ/kg respectively. The major drawback of these FR is the high loading needed to comply with the requirement of FR regulations (generally 35 to 65 wt%). As a consequence, plastics loaded with metal hydroxides suffer from a decrease in their mechanical properties such as strength, elongation at break, or impact properties. Among mineral FR, there also exist hydrocarbonates, but with a smaller market volume [85]. Hydromagnesite $Mg_5(CO_3)_4(OH)_2,4\ H_2O$ and the mixture of hydromagnesite and huntite $Mg_3Ca(CO_3)_4$ are reported as efficient FR in the literature [86, 87].

Mineral compounds are widely used in polyolefins, thermoplastic elastomers, poly(vinyl chloride), rubbers even if they can also be used in engineering plastics. As the processing temperature of PA6 and PBT exceeds that of decomposition of ATH, MDH is preferred for the fire retardancy of these matrices. PA6 can be successfully flame retarded to a V-0 ranking in UL-94 (1.6 mm thickness) when about 60 wt% of MDH are used, but this material is difficult to process and is rather stiff. MDH can also be activated with small amounts of metal catalysts, reducing the needed loading to 33 wt% [88]. In PBT, a mixture of $Mg(OH)_2$ and the hydromagnesite/huntite mixture was studied at relatively high loadings (45 to 50 wt%) in unreinforced PBT, leading to a material with V-0 ranking in the UL-94 at 1.6 mm thickness [13].

I.2.3.4 Boron-containing compounds

Boron compounds are a family of inorganic additives with flame retardant properties. Most commercial boron flame retardants are hydrates. Among them, zinc borates such as $2ZnO.3B_2O_3.3.5H_2O$ are the most frequently used. They exhibit an endothermic decomposition (ΔH about 503 kJ/kg) between 290 and 450 °C, releasing water (about 13 to 15 wt%) and resulting in the formation of B_2O_3ZnO.

B_2O_3 forms a protective vitreous layer at the surface of materials above 500 °C. Moreover in the case of oxygen-containing polymers, boric acid causes dehydration of the molecules and thus formation of a carbonized layer [66]. In this case, the dehydration water does not only dilute the flame but also blows the char to foam (phenomenon of *intumescence*) [89]. This foamy layer protects the polymer from the heat and also reduces the release of combustible gases. In parallel, zinc oxide acts as a

smoke suppressor (most of all in PVC, where ZnO is transformed in zinc chloride, a strong Lewis acid) **[90]**.

Ammonium pentaborate has been studied in PA6 and was found to be efficient at 10 to 30 wt% loadings **[15]**. In PBT, the literature also reports the use of borates together with antimony oxide **[91]**.

I.2.3.5 Phosphorus-containing compounds

Phosphorus-based compounds have known a great deal of attention as they represent a serious alternative to halogenated FR. This family of flame retardants is extremely wide, including different oxidation levels of phosphorus, generally from phosphine oxides to phosphates (Figure 24). They are known to be active in gas and/or condensed phase.

Phosphate   Phosphonate   Phosphinate   Phosphine oxide
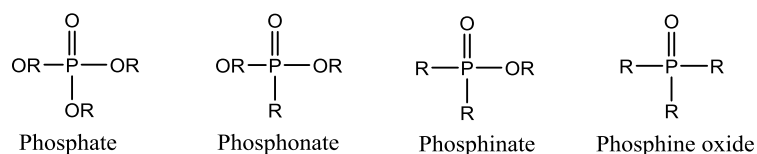
Figure 24: Chemical structure of phosphorus compounds exhibiting different oxidation levels

In the condensed phase, phosphorus species are particularly effective in matrices containing heteroatoms (mainly O and N). Through thermal decomposition and oxidation, they generally release phosphates or phosphoric acid. The latter can condense into pyro-, then meta-, and finally polyphosphoric acids at higher temperatures, thus releasing water. The reactions in the condensed phase lead to the formation of a char (protection from heat, limitation of oxygen and fuel diffusion).

Phosphorus-based FR can also volatilize and act in the gas phase. In that case the volatile species can form active radicals ($HPO_2°$, $PO°$ and $HPO°$), which act as scavengers for the flame radicals $H°$ and $OH°$ and thus quench exothermic combustion reactions.

- *Red phosphorus*

Phosphorus atom is involved in many flame retardants. The simplest form of phosphorus when it is used as FR is red phosphorus. Red phosphorus is effective in presence of oxygen-containing polymers. Red phosphorus is turned into white phosphorus upon heating **[92]**. The latter diffuses to the surface of the polymer and is oxidized into phosphoric acid which helps creating the char barrier as depicted before.

Red phosphorus showed particular efficiency in glass fiber reinforced polyamides, where a V-0 ranking in the UL-94 can be achieved with only 6 to 12 wt% loading. 10 wt% red phosphorus can increase the LOI of unfilled PA6 from 21 to 24 vol%, together with a V-0 classification in UL-94 **[15]**. Balabanovich reported the use of red phosphorus at 12.5 wt% loading in neat PA6 **[93]**. In this study, the aim was to crosslink the PA6 matrix by irradiation with γ-rays. V-0 was obtained when 5 wt% of triallyl cyanurate were added (in order to use lower irradiation doses). Alone in unreinforced PBT, only 5 to 6 wt% of a coated grade of red phosphorus was claimed to provide a V-0 ranking (at 0.8 mm thickness) **[94]**. In glass-fiber reinforced PBT, the combination of 5.5 wt% red phosphorus and 5.5 wt% Novolac (phenol formaldehyde resin) gave a V-0 (0.8 mm) ranking and a LOI of 35 vol% **[95]**.

- *Phosphine oxides*

Among phosphine oxides, triphenylphosphine oxide (TPPO) and 1,4-diisobutylene-2,3,5,6-tetrahydroxy-1,4-diphosphine oxide (Cyagard RF 1204 from Cytec Industries) (Figure 25) are the most common phosphine oxide commercial FR. Glass fiber reinforced PBT achieves a V-2 (1,6 mm) ranking when compounded with 25 wt% TPPO **[96]**; V-0 is reached when 20 wt% of TPPO are combined with 15 wt% MCA **[97]**. Concerning Cyagard, it was reported that it destabilizes PBT and modifies its degradation pathway, leading to marginal V-2 (1,6 mm) ranking **[98]**. The use of such structures in PA6 is not reported in literature though.
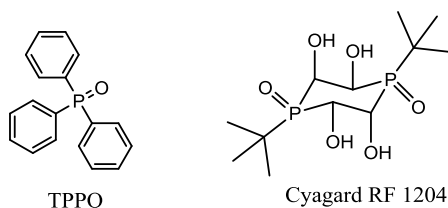
Figure 25: TPPO and Cyagard RF 1204

- *Aromatic phosphates*

Resorcinol bis(diphenyl phosphate) (RDP) and Bisphenol A bis(diphenyl phosphate) (BDP) (Figure 26) are flame retardant plasticizers generally used to flame-retard polycarbonates. They are able to crosslink with phenolic functions and thus have a high propensity to char. They supply an important condensed phase mode of action during the thermal decomposition process. However, they have limited performances in PBT and PA6. Their major drawback is their migration at the surface of the polymer above a certain loading (i.e. 8 wt% and 10 wt% for RDP and BDP respectively) **[99]**. They were in some cases combined with phenolic charring resins such as Novolac to improve their performances. In reinforced PBT, they are less efficient due to the fact that glass fibers prevent the swelling of the char and reduce the effectiveness of the carbonaceous protective shield. In PA6, these aryl phosphates were combined with high loadings of magnesium hydroxide **[100]**. In that case, 5 wt% RDP or BDP together with 50 wt% magnesium hydroxide changes the V-1 classification in UL-94 to a V-0.
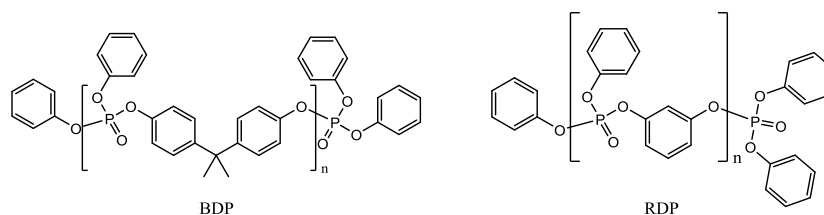
Figure 26: Structure of aromatic phosphates RDP and BDP

- *DOPO compounds and phosphinates*

Aromatic phosphinates based on 9,10-dihydro-9-oxa-10-*phosphaphenathrene*-10-oxide (DOPO) were also widely studied in the past few years, notably by Döring et al. **[101-103]**. Such structures can be categorized as phosphinates, on which the focus will be made hereinafter.

- *Phosphorus-containing structures : miscellaneous*

Recent literature reports the use of special nitrogen-phosphorus based substances such as cyclophosphazenes or polyphosphoramides (Figure 27). These compounds have a high nitrogen and phosphorus content. They were most of all investigated in PBT or PBT/polyamide blends **[104, 105]**. Their major drawback is their cost, so that they only exist at lab scale.

cyclophosphazene   polyphosphoramide
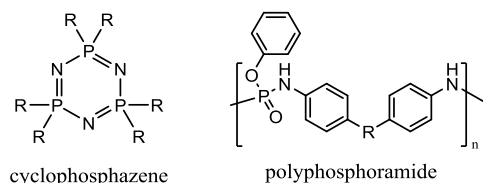
Figure 27: General structure of cyclophosphazenes and example of polyphosphoramide

Other simple structures were also studied or patented, but generally showed poor efficiency compared to widely used FR. Phosphonates for instance (patented by Ciba-Ceigy **[106]**) showed only good performances when used together with ethylmethylphosphinate **[107]**. Other compounds such as Antiblaze 1045 from Rhodia (Figure 28) found commercial applications when compounded with melamine, metal hydroxides, carbonates or other melamine-based FR **[108]**. Hypophosphites count among the most recently developed compounds; however their use is still quite restricted due to the release of toxic phosphine (PH_3) inherent to their processing **[109]**.
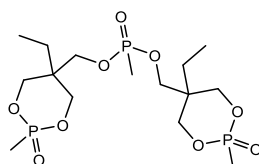
Figure 28: Structure of Antiblaze 1045

I.2.4   Conclusion

This section exposed the multiple ways to flame retard engineering plastics, with a focus on examples of flame retardants studied in PBT and PA6. One has not been exposed yet: the phosphinate salts. Since the 2000s, a huge increase has been observed in the number of publications on the use of phosphinate salts in flame retardancy, as depicted in the bibliometrics in Figure 29. Many patents and papers were in particular applied to PBT and PA6 (and engineering plastics in general). Thus, the next section will focus on the recent literature on phosphinate salts as flame retardants for PBT and PA6.
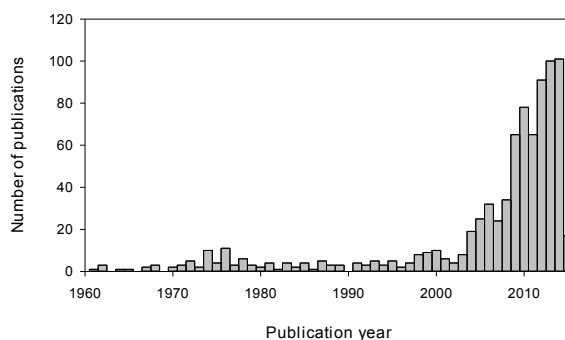
Figure 29: General bibliometrics for the keywords "Flame retardancy" and "phosphinate" (Scifinder, Apr.2015)

I.3. THE USE OF PHOSPHINATE SALTS

The use of phosphinates as flame retardants for textiles was first patented in the 1950s **[110]** by DuPont. Their use in PBT and PA6 was first patented in the 1970s **[111, 112]**. Many phosphinate structures were studied and patented since that time, and their modes of action and mechanisms of decomposition were elucidated for most of them.

In this section, after giving a general review on the use of phosphinates in PBT and PA6 (illustrated by several examples), a focus will be done on the oxaphospholanes. The latter were already studied in the PhD of Dr. Jeremie Louisy, in a previous partnership between BASF SE (Ludwigshafen, Germany) and the Laboratory UMET ISP R2Fire (Lille, France). This section also reviews the synthesis and use of novel phosphinates in PBT and PA6.

I.3.1   *General review on phosphinates*

The synthesis of the first phosphinic acid-based structures was achieved in 1898 by Michaelis and Kaehne, and these works were also reviewed by Arbusow **[113]**. Since this discovery, the studies on phosphinate compounds were not only led in the field of flame retardancy. A variety of other fields such as inorganic chemistry, organometallics, or peptides also report studies on phosphinates. The field of polymers (sections "Plastics Manufacture and Processing", "Plastics Fabrication and Uses", "Chemistry of Synthetic High Polymers" and "Textiles and fibers") only represents about 20% of the publications corresponding to the keyword "phosphinate", as depicted in Table 1. In the field of flame retardancy, as described in the previous section, the use of phosphinates increased since 2000.

Table 1: Bibliometrics on the keyword "phosphinate", refined by Section title, SciFinder, Apr. 2015

Topic	Number of publications	% of publications
Organometallic and Organometalloidal Compounds	1419	32
Plastics Manufacture and Processing	591	13
Inorganic Chemicals and Reactions	301	7
Plastics Fabrication and Uses	143	3
Physical Organic Chemistry	120	3
Enzymes	96	2
Amino Acids, Peptides, and Proteins	91	2
Chemistry of Synthetic High Polymers	89	2
Phase Equilibriums, Chemical Equilibriums, and Solutions	83	2
Synthetic High Polymers	73	2
Carbohydrates	67	1
Textiles and Fibers	62	1
Pharmacology	61	1
Coatings, Inks, and Related Products	53	1
Other subjects	1253	28

The first synthesized phosphinic acids or phosphinates were small organic molecules and as a consequence their use without further modification as FR in polymers was impossible due to their low thermal stability or their volatility. The first papers or patents that report the use of phosphinic acids or phosphinates to obtain self-extinguishing oligomers or polymers were published in the 1960-1970s **[114, 115]**, whether by radical polymerization or polycondensation. Later on, bis(hydroxymethyl)phosphinic acid (Figure 30) was incorporated as diol monomer for the synthesis of flame-retardant polyurethanes **[116]**.

Phosphinate structures were also used to produce phosphorus-containing derivatives of common polymers such as PA6 by polymerizing caprolactam with (N-caprolactam)phosphinates **[117]** (Figure

30). The use of aromatic phosphinate structures to produce epoxy monomers (Figure 30) was also published in the 1990s **[118]**. The latter were the first dihydro-oxa-phosphaphenanthrene-oxide (DOPO) to be reported. It should be highlighted that, recently, numerous studies were led on DOPO structures.

bis(hydroxymethyl)phosphinic acid   2,5-dichlorophenyl-bis(N-caprolactam)phosphinate   10-(2',5'-diglycidyletherphenyl)-9,10-dihydro-9-oxa-10-phosphaphenanthrene-10-oxide
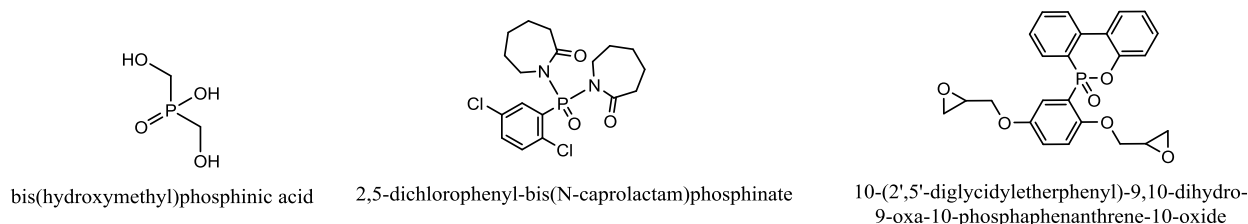
Figure 30: Examples of phosphinate-based monomers

In parallel, other researches were led to allow the use of small phosphinic-based molecules in polymers. As observed in previous investigations, it was shown that phosphorus can act in both condensed and gaseous phase; the aim of the researchers was to find model small molecules that could both volatilize and produce a charring or protective residue.

In 1976, Hoechst patented various formulations based on the use of phosphinate salts of metal cations such as Na$^+$ or Zn^{2+} **[119]**. They were the first phosphinate metal salts to be patented. Nissan Chemical Industries patented in 1977 various diphosphinate structures with higher thermal stability than monophosphinate structures **[120]**. These diphosphinate compounds were claimed to be useful as fireproofing agents. Many patents followed that of Nissan Chemical Industries, concerning the use of various phosphinic ester structures **[121, 122]**.

Between 1980 and 1995, many authors and industrials patented or reported the use of such phosphinic ester structures, but also the use of novel phosphinate-containing polymeric structures. However, in 1996, Hoechst patented the use of Calcium or Aluminum salts of monophosphinic acids as FR for PET and PBT **[123]**. The development of such formulations in polyamide was also patented in 1997 **[124]**. One year later, phosphinate salts were combined with so far well-known nitrogen-containing additives such as melamine **[125]**: the first example of phosphinate salts/nitrogen synergist formulations still used today were born. From the 1990s to nowadays, a competition between phosphinic esters and phosphinate salts is observed in the number of patents filled per year (Figure 31).
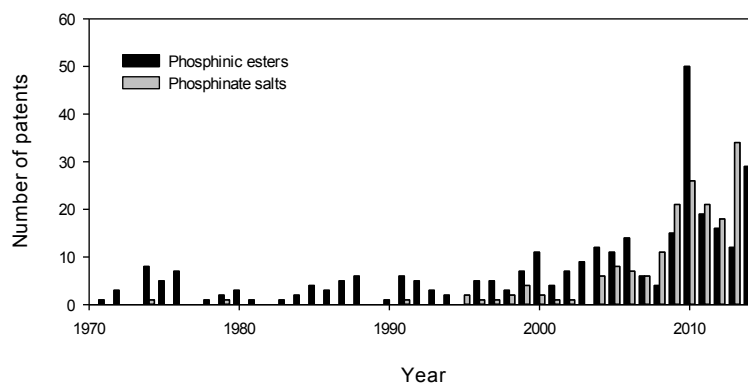
Figure 31: Bibliometrics on the keywords « Phosphinic esters » and « Phosphinate salts », associated to « flame retardancy » and limited to the patents, SciFinder, Apr. 2015

At the beginning of the 2000s, Clariant included phosphinate salts in its brand Exolit®, as new *Exolit OP* compounds, then joining existing polyphosphates based flame-retardant. Thanks to the number of patents involving the various phosphinate structures, many compounds were developed, for specific applications. Sometimes different brand names were created for different grades or particle sizes of a same product. This is for instance the case of OP1230 and OP1240 (Aluminum diethylphosphinate, also referred to as AlPi or DEPAL, Figure 32) which count among the most studied phosphinates. OP13xx products are combination of OP1230 with synergists. The Exolit® OP products commercialized by Clariant are reported in Table 2.
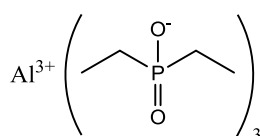
Figure 32: Exolit OP1230/1240 (Aluminium diethylphosphinate)

Table 2: Phosphinate grades commercialized by Clariant

Exolit® grade	Composition and/or application
OP 550/560	Highly effective reactive, non-halogenated phosphorus polyol
OP 950	Phosphinate flame retardant melting at 200 °C, therefore suitable for melt-spinning
OP 930	Fine grained powder Phosphinate especially developed for epoxy laminate systems
OP 935	Finer grained version of OP 930 for adhesive applications
OP 1230	Highly stable phosphinate flame retardant for high temperature nylons
OP 1240	Phosphinate flame retardant for polyester injection moulding applications
OP 1260	Phosphinate flame retardant system for polyester injection moulding applications
OP 1311	Flame retardant system for reinforced PA6 and elastomers
OP 1312/1313/1314	Combination of OP1230 with synergists, systems for reinforced PA6 and PA6.6
OP 1400	Highly stable flame retardant for polyamides

I.3.2   *Phosphinate salts for PBT and PA6 applications*

The most known phosphinate salts used in engineering thermoplastics are the dialkylphosphinate ones, especially the aluminum-based salts. They have proven high level of efficiency in PA6 and PBT. At a content of 20 wt% in glass fiber reinforced PBT, AlPi provides a V-0 (1.6 mm) ranking in UL-94 **[17-19]**, but also a V-0 (0.8 mm) ranking and a LOI of 44 vol% **[37]**. The corresponding Zn salt has however no satisfactory properties in glass fiber reinforced PBT. In glass fiber reinforced PA6, AlPi combined with a polyphosphate (namely *Exolit OP1311*) can obtain a classification of 960 °C/1mm at glow wire flaming index (GWFI, IEC 60695-2-12) and 775 °C for the glow wire ignition temperature (GWIT, IEC 60695-2-13) **[126]**.

The combination of AlPi with MCA **[37]** or MPP **[127]** has been reported by Braun et al.. Some synergistic effect has been highlighted between AlPi and melamine salts. These synergies are reinforced in presence of zinc borate. The use of organo-modified clays as synergists for AlPi can also be found in literature **[128]**. Recently, the combination of AlPi with other mineral particles such as aluminum trihydrate **[129]** was also investigated. As depicted before, aluminum trihydrate is not suitable for extrusion in PA6, however the metal hydrate-AlPi combination could be investigated with magnesium dihydrate.

The multiple combinations of alkylphosphinates with other synergists lead to a variety of possible uses, processing temperature ranges, and synergistic effects (promoting char formation, cooling the matrix in combination with gas-phase activity). It is noteworthy that the combination of diethylphosphinate salts with melamine-based FR in particular has been the subject of numerous researches. For instance, a screening and an optimization on various mixtures of OP1240 with synergists by Louisy [20] led to highlight Resorcinol bis(diphenyl phosphate) (RDP) as a synergist of metal phosphinate salts. OP1240 (20 wt%) and OP1240/RDP (18 wt%/2 wt%) were compared to neat PBTGF (25 wt% fibers) through LOI and Mass Loss Cone calorimeter (MLC). Neat PBT reached a LOI of 19 vol% whereas OP and OP/RDP formulations reached 42 and 41 vol% respectively. In MLC, neat PBT achieved a peak of Heat Released Rate (pHRR) of 332 kW/m² whereas OP and OP/RDP formulations respectively presented a pHRR of 147 kW/m² and 107 kW/m², showing a slight synergistic effect.

I.3.3   Mechanisms of degradation and modes of action of alkylphosphinate salts

Braun et al. investigated the mode of action of Al and Zn diethylphosphinate salts in glass fiber reinforced PBT [79]. The authors reported that phosphinate salts evolved during a main degradation step diethyl phosphinic acid in the gas phase while forming metal terephthalates in the condensed phase. In a second minor decomposition step, the terephthalates evolve into benzene and CO_2 while phosphinates remaining in the condensed phase oxidize releasing ethene (from the cleavage of ethylenic groups attached to phosphorus) and aluminum phosphate (Figure 33).

As a result, metal phosphates and a relatively small amount of carbonaceous char are yielded in the final residue. The char would apparently act as an adhesive for glass fibers and increase the mechanical stability of the residue, providing an additional protection against the transfer of flammable volatiles to the gas phase during combustion.

There exists a slight difference between Zn and Al phosphinate. No carbonaceous char is obtained in the residue with the Zn salt. Thus the residue present poor mechanical properties and does not protect the material as well as it was the case for Al-based systems [37].
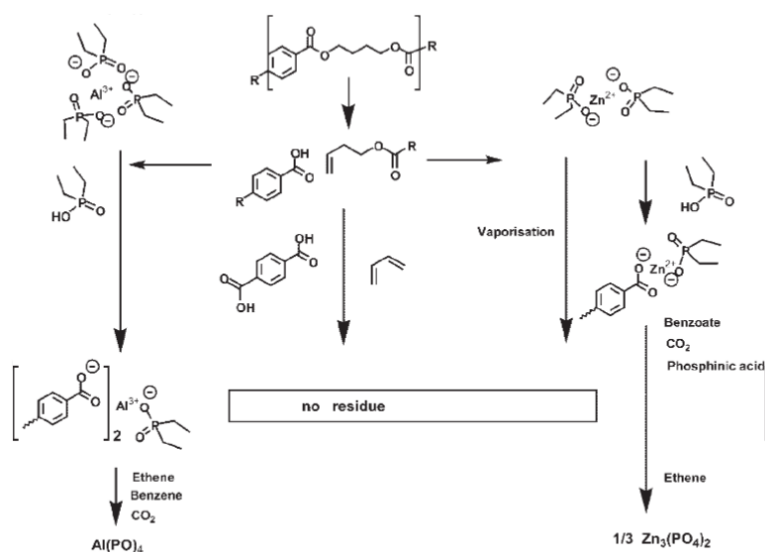
Figure 33: Decomposition pathway of the formulation PBT / Al or Zn phosphinate [37]

In PA6, the mechanisms of action of aluminum diethylphosphinate were also investigated by Braun et al. **[81]**. It was shown that the carbonyl functions of the polymer chains are polarized by the presence of AlPi, which enhances the intramolecular cyclizations and thus the depolymerization of PA6 into ε-caprolactam. The complexation of AlPi by the polymer chains further lead to the formation of a charred structure at the end of the decomposition, comprising aluminum phosphates and carbonaceous residues. The mechanism is illustrated in Figure 34. In this figure, the grey boxes represent the structures identified through various analyses of gas and condensed phase.

In the previously cited studies from Braun et al., aluminum phosphinate was also combined with MPP. In these cases, it was shown that MPP and AlPi exhibit synergistic effects in the gas phase. A strong gas phase action was observed upon fire, combining the effects of melamine and phosphinic acid. However, Samyn et al. demonstrated that no reaction between the constituents was observed in the condensed phase in spite of the char promotion highlighted **[128]**.

As a conclusion, it was shown that the dialkylphosphinates (e.g. diethylphosphinate in the developed case studies) can act in both gas and condensed phase, however a stronger effect in the gas phase (illustrated by high LOI values) was proposed. In PBT and PA6, AlPi was shown to affect the decomposition reactions of the polymer, leading to a stabilization of the residues in the condensed phase.
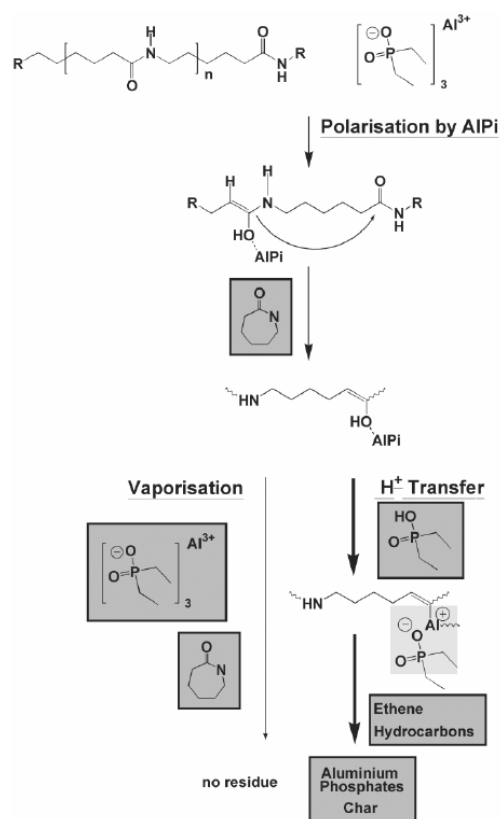
Figure 34: Decomposition pathway of the formulation PA6 / Al phosphinate [81]

I.3.4   *Focus on the previous study by Dr Louisy*

In a previous partnership between the laboratory UMET and BASF SE, Dr Jeremie Louisy studied particular phosphinate structures: the oxaphospholanes. On the basis of a commercial compound, Louisy synthesized various novel nitrogen- and phosphorus-containing flame retardants, and

compared them to Exolit® OP 1240 (a grade of AlPi). This section will consist in a short review on oxapospholanes and on Louisy's work.

I.3.4.1 General overview on oxapospholanes

The synthesis of oxapospholanes originally described by Chajrullin [130], is performed in a two steps process [131] (Scheme 1). In the first step, alkyldichlorophosphine reacts with acrylic acid to yield chloroformylphosphonic acid chloride (acrylation intermediate), which is cyclized in a second step into the oxapospholane using acetic anhydride or water.
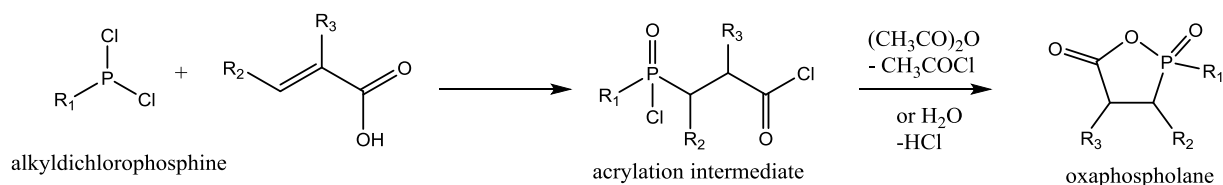
Scheme 1: Synthesis of oxapospholanes

The 2-methyl-1,2-oxaphospholan-5-one 2-oxide (R_1=CH_3, R_2/R_3=H) is already commercially available and known as Exolit PE110 (CAS N°15171-48-9). It was used to produce inherent flame retardant PET fibers commercialized as Trevira CS® fibers or Avora® plus fibers. Balabanovich et al. reported that this oxapospholane (OxP) could allow to reach UL-94 V-0 ranking (2 mm) and a LOI of 28 vol% by incorporating 10 wt% of the OxP with 10 wt% of poly(sulfonyldiphenylene phenylphosphonate) and 10 wt% of polyphenylene oxide in PBT [132]. This OxP was also used with ammonium polyphosphate (APP) (20 wt% of APP and 10 wt% of OxP) to achieve UL-94 V-0 ranking in PBT as well [38].

Few patents refer to OxPs as electrophilic reagents for the synthesis of flame retardant additives [133, 134]. The reactivity of OxPs is different depending on the nucleophilic reagents, as kinetics are different. Hydroxyl-based compounds lead to phosphinic ester derivatives whereas amine-containing substances lead to carboxylic amide derivatives (Scheme 2).
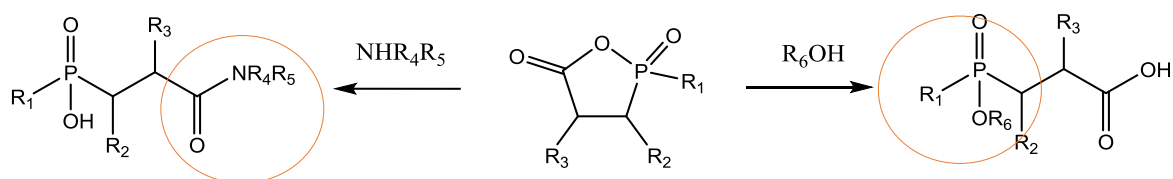
Scheme 2 : reaction of nucleophiles on oxapospholanes

In particular, a patent by Hoechst relates to the synthesis of nitrogen containing diphosphinic acids [135]. PBTGF formulations containing 12 to 15 wt% of these diphosphinic acids and 2 to 9 wt% melamine as synergistic agent exhibit UL-94 V-0 (1.6 mm) ranking. Preparation of the alkali and metal salts of these mono and bifunctional nitrogen-based phosphinic acids was also disclosed in a patent [133].

I.3.4.2 Summary of Louisy's work

The fire performances of Exolit PE110 derivatives were studied during the PhD thesis of J. Louisy [20]. Exolit PE110 was condensed with various nucleophilic alcohol or amine reagents, and the corresponding ester/amides were turned into metal phosphinates (Scheme 3). Some of the reagents, namely piperazine, ethylene diamine and m-phenylenediamine had already been employed for the preparation of nitrogen-containing phosphinic acids [135]. They were claimed to provide V-0 ranking

(1.6mm) to PBTGF at a loading of 11 to 15wt%. These compounds achieve a high thermal stability allowing them to be processed in PBT.

However, it is noteworthy that the acid form and the metal-cationic form have different behaviors. On the one hand, they differ in terms of interaction with PBT chains (the acid form should have a negative impact on a polyester leading to its degradation during the processing step). On the other hand, their thermal stability is different (the salts present a higher thermal stability and are thus less efficient as FR additives). Aluminum was selected as metal cation because it was demonstrated that aluminum phosphinates are the most effective in PBT [79].

Exolit PE110 derivatives as presented in Scheme 3 [20] were compared to well-known commercial additives, namely Exolit OP1240 (Figure 32) and Exolit OP1200 (mixture of AlPi and MCA). The reference materials containing 20 wt% OP1240 or 20 wt% OP1200 achieve a V-1 (0.8 mm) ranking and a V-0 (0.8 mm) ranking respectively. It should be mentioned that a comparison with aged samples (seven days at 70 °C) was also realized and in this case, PBTGF/OP1200 achieves a V-2 ranking after ageing.
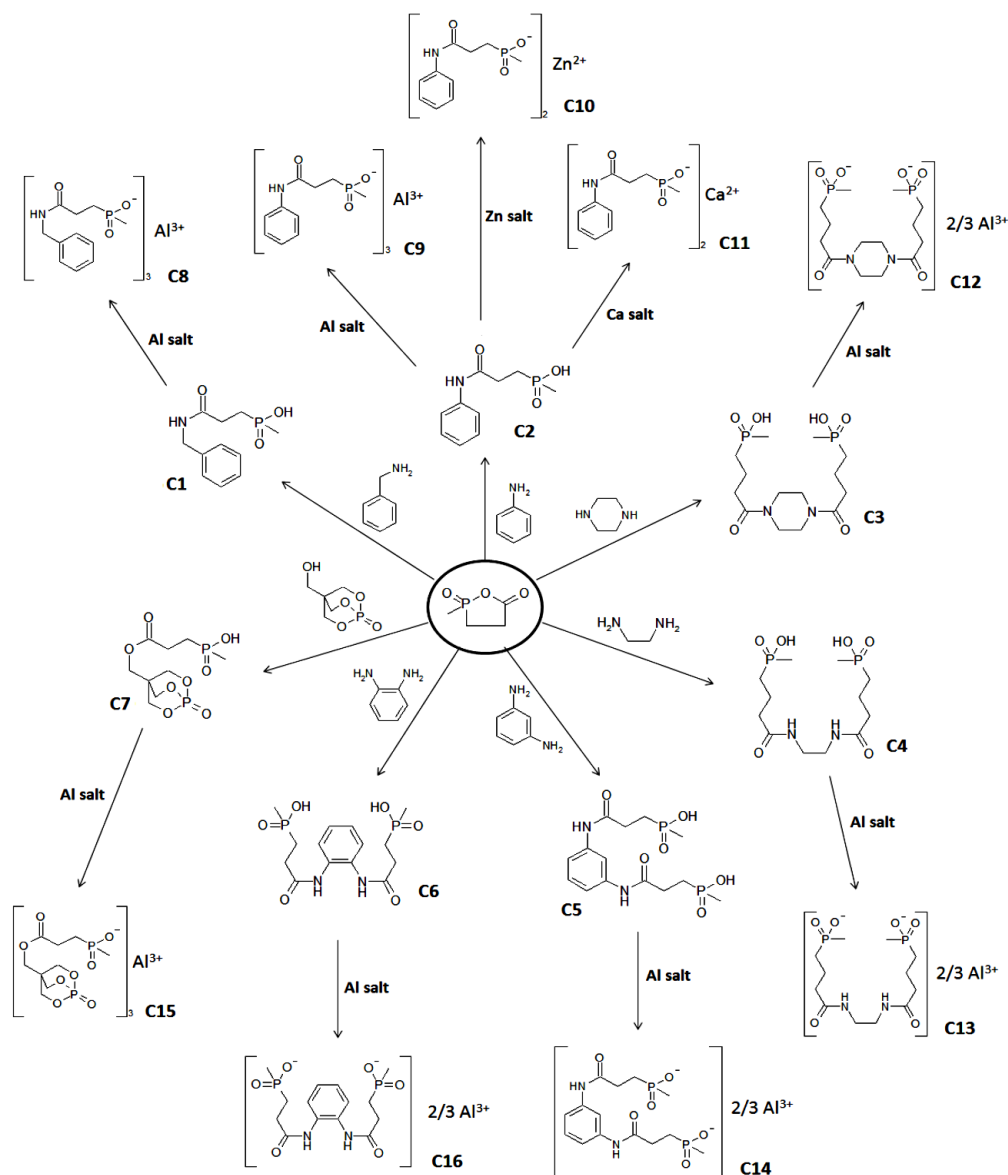
Scheme 3: Synthesis of various phosphinate salts from Exolit PE110 [20]

The results obtained with the synthesized phosphinic acid aluminum salts depended on the structure of the amine. However it is noteworthy that aniline-based phosphinic acid aluminum salt (C9, Scheme 3) achieved a LOI of 50 vol% and a V-0 (1.6 mm) ranking at a loading of 17 wt% in PBTGF (58 wt% PBT, 25 wt% GF).

The mechanisms of action of the additives (synthesized as well as commercial) were studied through TGA-FTIR and Py-GC/MS. As the work was based on the study of fire retarded PBT, its mechanism of degradation was also investigated. Tetrahydrofuran (THF), butadiene, CO_2, H_2O, benzoic acid and various esters (PBT fragments or oligomers) were identified in the gas phase during the decomposition of PBT (evidenced by TGA-FTIR). The PBT ester fragments were further analyzed in Py-GC/MS. Louisy's observations confirmed what was presented in section I.1.4 on the literature of the decomposition of PBT. Concerning the mechanisms of degradation of the synthesized products, they depended on their structure: aniline and benzylamine derivatives for example behaved differently. The main information was that these salts would not react with PBT directly but would interact with the flame during the combustion by releasing phosphorylated fragments. Thus, a gas phase mechanism was proposed.

I.4. CONCLUSION

PBT and PA6 are engineering thermoplastics used in a wide range of applications. Up to the 2000s, they both were most of all flame-retarded with halogenated compounds. However, due to many investigations on the potential impact of halogenated compounds on environment or health, much effort has been made to withdraw them from the market. Phosphinate salts were FR compounds which matured since the 1980s, giving birth to novel structures with high performances and many FR combinations. Various studies on their decomposition and modes of action in PBT and PA6 were also published. Aluminum dialkylphosphinate salts are nowadays known to have a strong effect in the gas phase while leaving an aluminum phosphate-containing charred residue.

However, in spite of the high number of structures covered by the patents, only few of them were investigated and then commercialized. Many formulations in academical or industrial studies involved aluminum diethylphosphinate. Only a few studies report other alkyl chains in the dialkylphosphinate structure.

Oxaphospholanes are a particular branch of alkylphosphinates illustrated by cyclic compounds. These cycles can be opened by reaction with various nucleophiles such as alcohols or amines. In a partnership between BASF SE and UMET, anterior to the present manuscript, Dr. Louisy tried to overcome the classical limits of studies led so far. He carried out reactions of Exolit PE110 (one of the few other dialkylphosphinates commercialized by Clariant) with nucleophiles and investigated the effectiveness of yielded compounds as flame retardants. The modes of action of the designed structures were also discussed. Louisy proposed a gas-phase mode of action, similar to that of AlPi. As a consequence, a hypothesis could be made that dialkylphosphinate with short alkyl chains (C1-C3) would easily decompose and act in the gas phase.

In this context, the main goal of this PhD thesis is to study a different branch of oxaphospholanes which does not correspond anymore to dialkylphosphinates, but to arylalkylphosphinate. Arylphosphinates existing so far were regrouped in the specific class of DOPO derivatives. In our study, the starting material is not Exolit PE110 which was a methylphosphinate, but 2-phenyl-1,2-oxaphospholan-5-one 2-oxide (2-POO, Figure 35) which is a phenylphosphinate. The shift of methyl to phenyl might imply a different thermal behavior and a different flame-retardant mechanism.
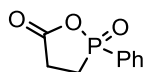
Figure 35: 2-phenyl-1,2-oxaphospholan-5-one 2-oxide (2-POO)

The synthesized FR will be incorporated in glass fiber reinforced PBT and PA6, and their FR performances will be investigated through UL-94, LOI, and Glow Wire. Afterwards, the degradation pathway and modes of action of one of the synthesized compounds (selected for its good FR performances) will be investigated. The design of novel flame retardants cannot be carried out only through synthesizing and screening. A good comprehension of the decomposition pathway of the compounds, the influence of their structure, and the interaction with the matrices is essential before investigating and creating novel structures. The next chapter will be dedicated to the presentation of materials, compounding techniques, and analyses used in this project.

_____

Chapter II. Materials compounding and experimental techniques

_____

This chapter is dedicated to the description of the materials, techniques, and synthesis protocols used in this work.

As the main aim of this project is to investigate the effectiveness of novel compounds as FR, they first need to be synthesized. The procedures of synthesis of the various investigated phosphinates will be described in the first part of this chapter.

Then, the two materials, namely PBT/GF and PA6/GF, which were used in this project will be described, as well as the processing techniques used to prepare the polymer/flame retardant formulations. The different methods used to evaluate the fire behavior of the prepared formulations will be presented. A further investigation of mechanisms will also be presented in this manuscript, through the instrumentation of the UL-94 test to fire. This test is the main test used by BASF to evaluate the reaction of materials to fire. The instrumentation of the test allows coupling understanding and fire testing. This section of the chapter will present the equipment used for this complementary study.

As exposed before, this work is also based on the understanding of the modes of action of the flame retardants. Hence, numerous analyses of gas and condensed phase during the degradation of the materials are needed, and will thus be detailed in the last section of this chapter.

II.1. EXPERIMENTAL PROCEDURES FOR THE SYNTHESIS

In this part, all the procedures used to prepare different phosphinate salts will be depicted. The various salts have been prepared by reaction of amines on 2-POO. The general scheme of reaction is presented in Figure 36. It is mentioned that all reagents comprised in this scheme (aniline, dichlorophenylphosphine…) were obtained from commercial suppliers and used without further purification.

Dimethylformamide (extra dry, for synthesis), Acetonitrile (extra dry, for synthesis), Dichlorophenylphosphine (DPP, 97%), Aniline (99.5%), Benzylamine (99%) and Ethylenediamine (99%) were purchased from Acros Organics (Fischer Scientific). Acrylic acid (anhydrous, 99%), p-phenylene diamine (99%) and piperazine (99%) were obtained from Sigma-Aldrich.

It should be highlighted that in this section, all the results in liquid-state NMR are depicted as δ ppm (number of protons [if ^{1}H analysis], multiplicity [s for singlet, d for doublet, t for triplet and m for multiplet], attribution).
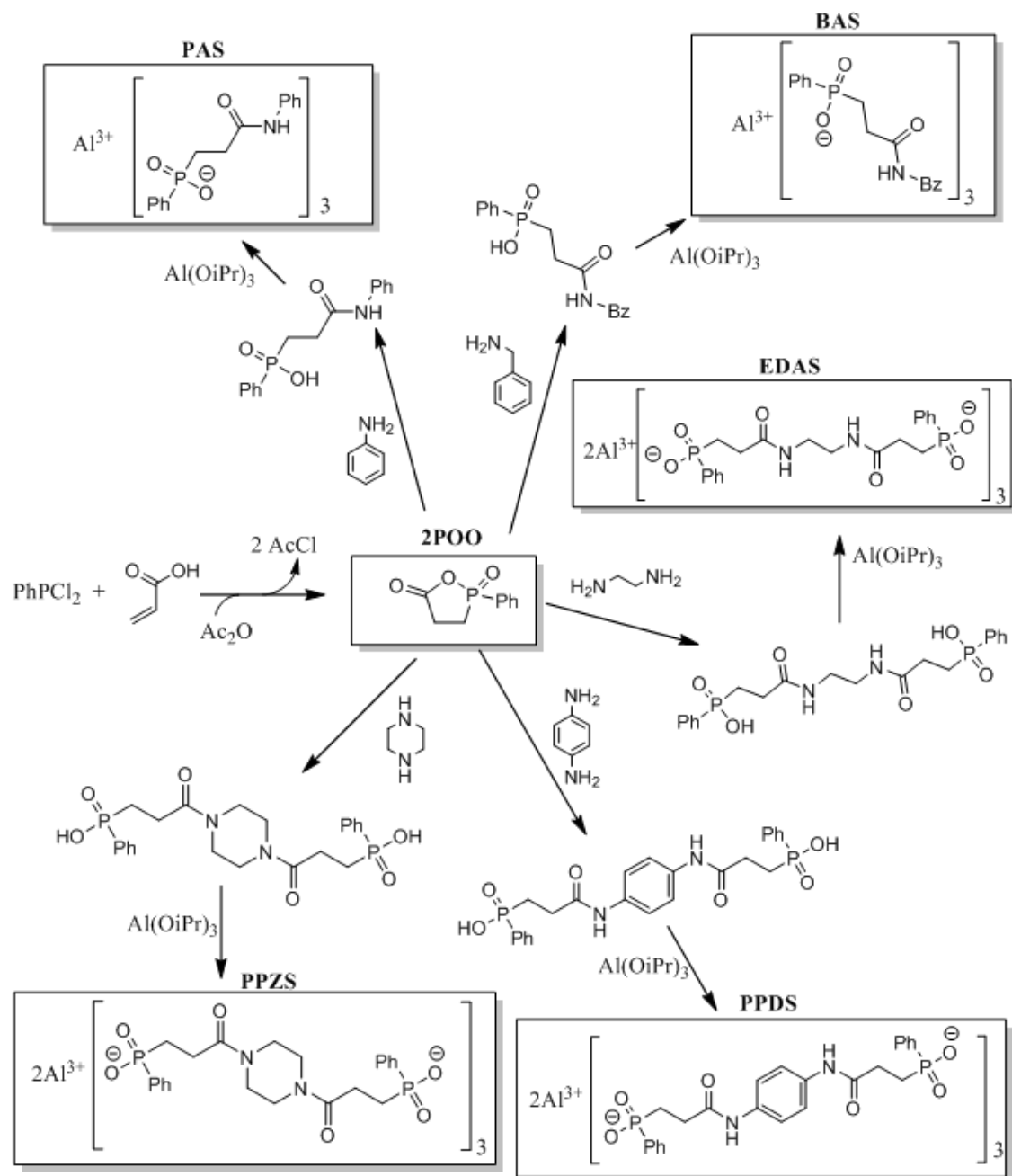
Figure 36: Synthesis scheme of studied phosphinate salts

II.1.1   Synthesis of 2-phenyl-1,2-oxaphospholan-5-one 2-oxide (2-POO)
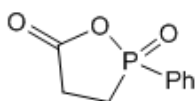
2-POO

- *From Dichlorophenylphosphine (DPP)*

100.0 g DPP (560 mmol) were heated to 65-70 °C under nitrogen. 50 mL (730 mmol) acrylic acid were added dropwise at a temperature lower than 80 °C. After complete addition, the mixture was heated to 125-130 °C for 1 h, then cooled down to 60 °C. 60 mL acetic anhydride (635 mmol) were added dropwise to the mixture. After 5 to 10 % addition, a reflux was observed due to the release of acetyl chloride. The mixture was left at 60 °C for 1.5 hour. Acetyl chloride was distilled under atmospheric pressure (observed temperature 50 ± 1 °C). Acetic anhydride was distilled under reduced pressure (observed at 43 °C in 29 mbar). After cooling down to room temperature, a white solid was obtained. The latter was recrystallized in a $CHCl_3$ / Et_2O 1/1 mixture, to yield around 90.0 g white crystals (80 % yield).

- *From 3-(hydroxy(phenyl)phosphoryl)propanoic acid*

50.0 g 3-HPP (234 mmol) were dissolved in 60 mL acetic anhydride (635 mmol) at reflux temperature. Yielded acetic acid and excess acetic anhydride were removed under reduced pressure. After cooling down to room temperature, a white solid was obtained, and was recrystallized in a $CHCl_3$ / Et_2O 1/1 mixture, to yield around 41.0 g white crystals (90 % yield). NMR results are equal to those previously presented.

^{1}H NMR (CDCl$_3$, stand. TMS): δ (ppm) 2.81 (2H, m, CH$_2$-CO), 2.84 (2H, m, CH$_2$-PO), 7.55 (2H, m, Ph), 7.66 (1H, m, Ph), 7.80 (2H, m, Ph). **^{13}C NMR dec-^{1}H (CDCl$_3$, stand. TMS):** δ (ppm) 24.5 (d, J$_{CP}$=74 Hz, CH$_2$-PO), 29.3 (d, J$_{CP}$=6 Hz, CH$_2$-CO), 127.8 (d, J$_{CP}$=134 Hz, Ph), 129.2 (d, J$_{CP}$=14 Hz, Ph), 131.4 (d, J$_{CP}$=11 Hz, Ph), 134 (d, J$_{CP}$=3 Hz, Ph), 168.5 (2 peaks, CO). **^{31}P NMR (dec-^{1}H, CDCl$_3$):** δ (ppm) 49 (m).

II.1.2   Synthesis of phenyl amide of 3-(hydroxy(phenyl)phosphoryl) propanoic acid (PA-3-HPP)
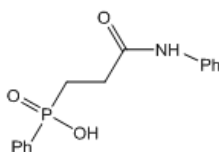
PA-3-HPP

19.0 g (204 mmol) of aniline dissolved in 100 mL Acetonitrile (ACN) were added dropwise for 0.5 h to 40.0 g (204 mmol) 2-POO in 100 mL ACN at 80 °C. At the end of the addition, the mixture was left at 80 °C for 4 h. After cooling, Et$_2$O was added to the mixture and the product precipitated. It was then filtered and washed with Et$_2$O, then re-dissolved in 250 mL NaOH 1 M solution. The solution was extracted with 3x 50 mL Et$_2$O. HCl 1 M was finally added to the aqueous phase and the product precipitated. After filtration and drying overnight under reduced pressure at 60 °C, 53.0 g of white crude product were collected (90 % yield).

^{1}H NMR (DMSO, stand. TMS): δ 2.10 (2H, m, CH$_2$-CO), 2.45 (2H, m, CH$_2$-PO), 7.00 (1H, t, J$_{NPh}$=7 Hz, N-Ph), 7.27 (2H, t, J$_{NPh}$=7 Hz, N-Ph), 7.54 (5H, m, P-Ph/N-Ph), 7.75 (2H, m, P-Ph), 9.93 (1H, s, NH). **^{13}C NMR dec-[1]H (DMSO, stand. TMS):** δ 26.3 (d, J$_{CP}$=98 Hz, CH$_2$-PO), 29.7 (s, CH$_2$-CO), 119.4 (s, N-Ph), 123.5 (s, N-Ar), 128.9 (d, J$_{CP}$=11 Hz, P-Ph), 129.0 (s, N-Ph), 131.3 (d, J$_{CP}$=10 Hz, P-Ph), 132.0 (d, J$_{CP}$<2 Hz, P-Ph), 134.3 (d, J$_{CP}$=126 Hz, P-Ph), 139.6 (s, N-Ph), 170.2 (2 peaks, CO). **^{31}P NMR (^{1}H coupling, DMSO):** δ 36 (m).

II.1.3   Synthesis of benzyl amide of 3-(hydroxy(phenyl)phosphoryl) propanoic acid (BA-3-HPP)
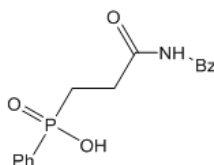
BA-3-HPP

22.0 g (206 mmol) of benzylamine in 100 mL ACN were added dropwise for 0.5 h to 40.0 g (204 mmol) 2-POO in ACN at 80 °C. At the end of the addition, the mixture was left at 80 °C for 4 h. After cooling, Et$_2$O was added to the mixture and the product started to precipitate. It was then filtered and washed with Et$_2$O, then re-dissolved in 150 mL NaOH 1 M solution. The solution was extracted with 3x 30 mL Et$_2$O. HCl 1 M was finally added to the aqueous phase and the product precipitated. After filtration and drying overnight in a vacuum oven at 60 °C, 40.0 g of white crude product were collected (64 % yield).

^{1}H NMR (DMSO, stand. TMS): δ 1.97 (2H, m, CH$_2$-CO), 2.26 (2H, m, CH$_2$-PO), 4,21 (2H, d, J$_{Ph-CH2-NH}$=6 Hz, Ph-CH$_2$-N), 7.22 (3H, m, N-Ph / P-Ph), 7.29 (2H, m, N-Ph / P-Ph), 7.50 (3H, m, N-Ph / P-Ph), 7.71 (2H, m, N-Ph / P-Ph), 8.49 (1H, t, J$_{NH-CH2}$=6 Hz, NH). **^{13}C NMR dec-[1]H (DMSO, stand. TMS):** δ 26.9 (d, J$_{CP}$=99 Hz, CH$_2$-PO), 28.7 (d, J$_{CP}$<2 Hz, CH$_2$-CO), 42.6 (s, CH$_2$-N), 127.0 (s, N-Ph), 127.6 (s, N-Ph), 128.6 (s, N-Ph), 128.7 (d, J$_{CP}$=13 Hz, P-Ph), 131.3 (d, J$_{CP}$=9 Hz, P-Ph), 131.8 (d, J$_{CP}$<2 Hz, P-Ph), 134.9 (d, J$_{CP}$=125 Hz, P-Ph), 139.9 (s, N-Ph), 171.5 (2 peaks, CO). **^{31}P NMR (^{1}H coupling, DMSO):** δ 36 (m).

II.1.4   Synthesis of ethylene diamide of 3-(hydroxy(phenyl)phosphoryl)propanoic acid (EDA-3-HPP)
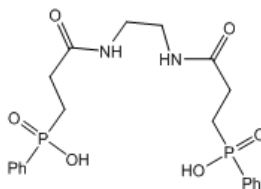
EDA-3-HPP

6.1 g ethylene diamine (102 mmol) dissolved in DMF were added dropwise for 0.5 h to 40.0 g (204 mmol) 2-POO (204 mmol) in DMF at 60 °C. After complete addition, the mixture was then heated at 90 °C for 4 h. After cooling, Et$_2$O was added to the mixture. The white solid obtained after 12 h was filtered and re-dissolved in 150 mL NaOH 1 M solution. The solution was extracted with 3x 30 mL dichloromethane. 300 mL HCl 1 M were finally added to the aqueous phase and the product

precipitates. The solid was filtered and washed with 100 mL distilled water, 100 mL acetone and 50 mL diethyl ether. After drying overnight under reduced pressure at 60 °C, 33.0 g of crude product were collected (72 % yield).

^{1}H NMR (DMSO, stand. TMS): δ (ppm) 1.98 (4H, m, CH$_2$-CO), 2.16 (4H, m, CH$_2$-PO), 3.00 (4H, s, CH$_2$-N), 7.50 (4H, m, Ph), 7.57 (2H, m, Ph), 7.70 (4H, m, Ph), 7.96 (2H, s, NH). **^{13}C NMR dec-^{1}H (DMSO, stand. TMS):** δ (ppm)   26.5 (d, J$_{CP}$=99 Hz, CH$_2$-PO), 28.6 (s, CH$_2$-CO), 38.7 (s, CH$_2$-N), 128.9 (d, J$_{CP}$=11 Hz, Ph), 131.3 (d, J$_{CP}$=8 Hz, Ph), 132 (d, J$_{CP}$=2 Hz, Ph), 134.2 (d, J$_{CP}$=126 Hz, Ph), 171.4 (2 peaks, CO). **^{31}P NMR (^{1}H coupling, DMSO):** δ (ppm) 36 (m).

II.1.5   Synthesis of para-phenylene diamide of 3-(hydroxy(phenyl)phosphoryl) propanoic acid (PPD-3-HPP)
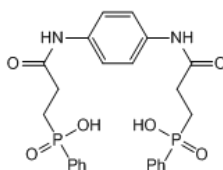
PPD-3-HPP

12.4 g (115 mmol) p-phenylene diamine (PPD) in DMF were added dropwise for 0.5 h to 46.0 g (235 mmol) 2-POO in DMF at 80 °C. The mixture was then heated at 110 °C for 4 h. At the end of the reaction, DMF was removed and the product was recovered and washed with 3x 50 mL methanol. The pale purple solid was filtered and re-dissolved in 150 mL NaOH 1 M solution. The solution was extracted with 3 x 30 mL dichloromethane. 300 mL HCl 1 M were finally added to the aqueous phase and the product precipitated. The solid was filtered and washed with 100 mL distilled water, 100 mL acetone and 50 mL diethyl ether. After drying overnight under reduced pressure at 60 °C, 33.0 g of crude product were collected (60 % yield).

^{1}H NMR (DMSO, stand. TMS): δ 2.06 (4H, m, CH$_2$-CO), 2.4 (4H, m, CH$_2$-PO), 7.42 (4H, s, N-Ph-N), 7.52 (6H, m, Ph), 7.74 (4H, m, Ph), 9.89 (2H, s, NH). **^{13}C NMR dec-^{1}H (DMSO, stand. TMS):** δ 26.3 (d, J$_{CP}$=99 Hz, CH$_2$-PO), 29.6 (d, J$_{CP}$=2 Hz, CH$_2$-CO), 120.0 (s, N-Ph-N), 128.8 (d, J$_{CP}$=12 Hz, P-Ph), 131.3 (d, J$_{CP}$=10 Hz, P-Ph), 132 (d, J$_{CP}$=3 Hz, P-Ph), 134.3 (d, J$_{CP}$=122 Hz, P-Ph), 134,9 (s, C(Ph)-N), 169.8 (2 peaks, CO). **^{31}P NMR (^{1}H coupling, DMSO):** δ 35.6 (m).

II.1.6   Synthesis of piperazine diamide of 3-(hydroxy(phenyl)phosphoryl) propanoic acid (PPZ-3-HPP)
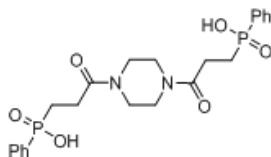
PPZ-3-HPP

8.7 g (101 mmol) of piperazine in DMF were added dropwise for 0.5 h to 40.0 g (204 mmol) 2-POO in DMF at 110 °C. At the end of the addition, the mixture was left at 110 °C for 4 h. DMF was then evaporated, and the resulting product was dissolved in 150 mL NaOH 1 M solution. The solution was extracted with 3x 30 mL dichloromethane. HCl 1 M was finally added to the aqueous phase. The
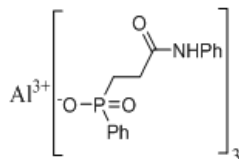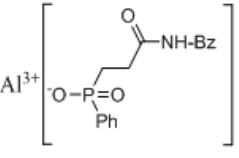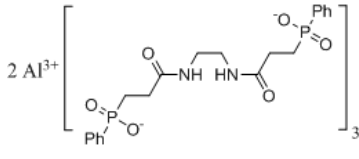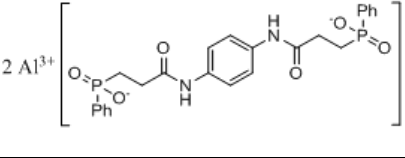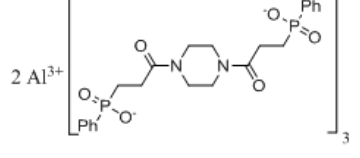
solution was held overnight and crystals started to appear. Crystals were filtered and washed with Et$_2$O. After drying overnight in a vacuum oven at 60 °C, 15.9 g of crude product were collected (33 % yield).

¹H NMR (DMSO, stand. TMS): δ 2.04 (4H, m, CH$_2$-CO), 2.48 (4H, m, CH$_2$-PO), 3.37 (8H, m, CH$_2$-N), 7.29 (4H, m, P-Ph), 7.53 (6H, m, P-Ph). **¹³C NMR dec-¹H (DMSO, stand. TMS):** δ 26.2 (d, J$_{CP}$=99 Hz, CH$_2$-PO), 31.1 (d, J$_{CP}$<2 Hz, CH$_2$-CO), 43.2 (4 peaks, 2 splittings, CH$_2$-N), 128.8 (d, J$_{CP}$=13 Hz, P-Ph), 131.3 (d, J$_{CP}$=9 Hz, P-Ph), 132 (d, J$_{CP}$<2 Hz, P-Ph), 134.4 (d, J$_{CP}$=126 Hz, P-Ph), 170 (2 peaks, CO). **³¹P NMR (¹H coupling, DMSO):** δ 36 (m).

II.1.7   General procedure for the conversion of phosphinic acids into salts

About 30.0 g of phosphinic acid derivative and 1/3 or 2/3 equivalent of aluminum isopropoxide (dependent on the acid functionality of phosphinic derivatives) were dispersed in a mixture of Ethanol / Water (50/50). The mixture was heated to 80 °C for 8-9 h, then cooled down to room temperature. The precipitate was filtered and washed with 200 mL distilled water and then with 200 mL ethanol. After drying two days under reduced pressure at 80 °C, the products were recovered: in the case of ethylene diamide, piperazine diamide, phenyl amide, and benzyl amide, the yields were close to 55 % while in the case of p-phenylene diamide, the yield was about 90 %. In the next chapters, the aluminum salts PA-3-HPP, BA-3-HPP, EDA-3-HPP, PPD-3-HPP and PPZ-3-HPP will be named PAS, BAS, EDAS, PPDS and PPZS respectively as depicted in Table 3.

Table 3 : abbreviations used in the next chapters for the phosphinate salts

Abbreviated name	Aluminum salt abbreviated name	Structure
PA-3-HPP	PAS	
BA-3-HPP	BAS	
EDA-3-HPP	EDAS	
PPD-3-HPP	PPDS	
PPZ-3-HPP	PPZS	

_____

PAS
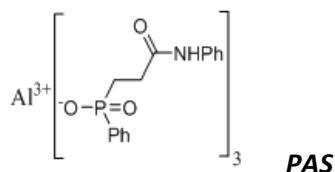
Table 4: Elemental analysis of PAS - calculated for C$_{45}$H$_{45}$N$_3$O$_9$P$_3$Al

Atom	Al	P	C	H	N	O
Calculated wt%	3.03	10.42	60.61	5.09	4.71	16.15
Found wt%	4.29	9.68	56.71	5.1	4.21	20.01*

calculated by difference to 100 wt%

^{13}C solid-state NMR – CP/MAS dec-^{1}H: δ (ppm) 26, 31, 120, 123, 128, 132, 138, 171. **^{31}P solid-state NMR - CP/MAS dec-^{1}H:** δ (ppm) 24, 35. **^{27}Al solid-state NMR:** δ (ppm) -16, 6.

_____

BAS
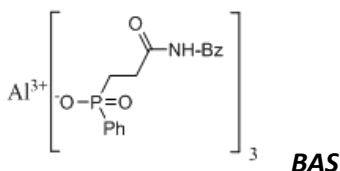
Table 5: Elemental analysis of BAS - calculated for C$_{48}$H$_{51}$N$_3$O$_9$P$_3$Al

Atom	Al	P	C	H	N	O
Calculated wt%	2.89	9.95	61.74	5.5	4.5	15.42
Found wt%	3.59	9.52	59.06	5.54	4.33	17.96*

calculated by difference to 100 wt%

^{13}C solid-state NMR – CP/MAS dec-^{1}H: δ (ppm) 28, 43, 128, 134, 139, 172. **^{31}P solid-state NMR - CP/MAS dec-^{1}H:** δ (ppm) 25, 33. **^{27}Al solid-state NMR:** δ (ppm) -16, 6.

_____
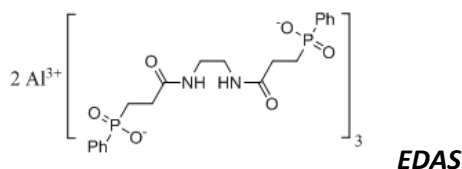
EDAS

Table 6: Elemental analysis of EDAS - calculated for C$_{60}$H$_{72}$N$_6$O$_{18}$P$_6$Al$_2$

Atom	Al	P	C	H	N	O
Calculated wt%	3.84	13.23	51.29	5.17	5.98	20.50
Found wt%	6.58	10.83	42.15	5.06	4.58	30.80*

calculated by difference to 100 wt%

13C solid-state NMR – CP/MAS dec-1H: δ (ppm) 29, 39, 128, 132, 172. **31P solid-state NMR - CP/MAS dec-1H:** δ (ppm) 24, 35. **27Al solid-state NMR:** δ (ppm) -16, 6.

_____
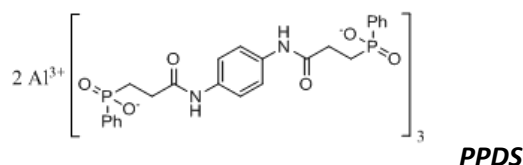
PPDS

Table 7: Elemental analysis of PPDS - calculated for $C_{72}H_{72}N_6O_{18}P_6Al_2$

Atom	Al	P	C	H	N	O
Calculated wt%	3.48	12.00	55.82	4.68	5.42	18.59
Found wt%	4.15	10.38	48.45	4.95	4.58	27.49*

*calculated by difference to 100 wt%

13C solid-state NMR – CP/MAS dec-1H: δ (ppm) 29, 120, 122, 129, 131.3, 131.8, 133, 136, 136.5. **31P solid-state NMR - CP/MAS dec-1H:** δ (ppm) 26, 38. **27Al solid-state NMR:** δ (ppm) -16, 6.

_____
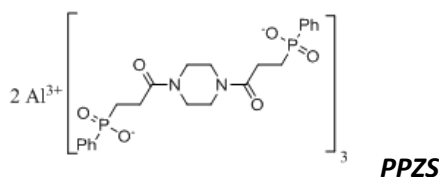
PPZS

Table 8: Elemental analysis of PPZS - calculated for $C_{66}H_{78}N_6O_{18}P_6Al_2$

Atom	Al	P	C	H	N	O
Calculated wt%	3.64	12.53	53.45	5.30	5.67	19.42
Found wt%	4.72	11.27	46.25	5.37	4.58	27.81*

*calculated by difference to 100 wt%

13C solid-state NMR – CP/MAS dec-1H: δ (ppm) 28, 42, 129, 132, 171. **31P solid-state NMR - CP/MAS dec-1H:** δ (ppm) 24, 38. **27Al solid-state NMR:** δ (ppm) -16, 6.

II.1.8   *Evaluation of the pH of the salts in deionized water*

1.0 g of the aluminum phosphinates was dissolved in 100 mL deionized water (pH: 5.5-5.6), and stirred for 10 min. pH was then measured with a Mettler Toledo MP 220 device equipped with a KCl probe. For the neutralization of the salts depicted in Chapter III, two protocols were applied to PAS:

→ 2 g PAS dispersed in 100 mL deionized water and stirred for 4 h
→ 2 g PAS and 0.5 g $NaHCO_3$ dispersed in 100 mL deionized water and stirred for 4 h

Both dispersions were filtered and rinsed with 50 mL deionized water, 50 mL ethanol and 50 mL acetone. The solid was dried for 24 h in drying oven at 80 °C.

II.2. MATERIALS AND COMPOUNDING

II.2.1   Materials used for the screening

The PBT used in this work is the grade Ultradur® B4520 which was provided by BASF SE (Ludwigshafen, Germany). This grade exhibits a medium viscosity and rapid freezing injection molding properties. Its properties are reported in Table 9. Two batches of PBT were provided: the "classical" B4520, and a masterbatch containing 30 wt% glass fibers.

Table 9: Properties of Ultradur® B4520

PHYSICAL	ASTM Test Method	Property Value
Specific Gravity	D-792	1.3
Mold Shrinkage (1/8" bar, in/in)		0.015
Moisture, %	D-570	
(50% RH)		0.25
(Saturation)		0.5
MECHANICAL	**ASTM Test Method**	**Property Value**
Tensile Strength, Yield, MPa (psi)	D-638	
23C (73F)		60 (8,700)
Elongation, Yield, %	D-638	
23C (73F)		3.7
Flexural Modulus, MPa (psi)	D-790	
23C (73F)		2,300 (334,000)
IMPACT	**ASTM Test Method**	**Property Value**
Notched Izod Impact, J/M (ft-lbs/in)	D-256	
-40C (-40F)		37 (0.7)
23C (73F)		43 (0.8)
THERMAL	**ASTM Test Method**	**Property Value**
Melting Point, C(F)	D-3418	223 (433)
Heat Deflection @ 264 psi (1.8 MPa) C(F)	D-648	60 (140)
Heat Deflection @ 66 psi (.45 MPa) C(F)	D-648	163 (325)

The PA6 used for the screening of the additives was Ultramid® B3EG6, also supplied by BASF SE. This grade is a masterbatch already containing 30 wt% glass fibers. The properties of this polymer are reported in Table 10.

Table 10: Properties of Ultramid® B3EG6

PHYSICAL	ISO Test Method	Property Value	
Density, g/cm	1183	1.36	
Moisture, %	62		
(50% RH)		2.1	
(Saturation)		6.6	
RHEOLOGICAL	**ISO Test Method**	**Dry**	**Conditioned**
Melt Volume Rate (275 C/5 Kg), cc/10min.	1133	50	-
MECHANICAL	**ISO Test Method**	**Dry**	**Conditioned**
Tensile Modulus, MPa	527		
23C		9,500	6,200
Tensile stress at break, MPa	527		
23C		185	115
Tensile strain at break, %	527		
23C		3.5	8
Flexural Strength, MPa	178		
23C		270	180
Flexural Modulus, MPa	178		
23C		8,600	5,000
IMPACT	**ISO Test Method**	**Dry**	**Conditioned**
Izod Notched Impact, kJ/m^2	180		
23C		15	20
Charpy Notched, kJ/m^2	179		
23C		15	30
-30C		11	-
Charpy Unnotched, kJ/m^2	179		
23C		95	110
-30C		80	-
THERMAL	**ISO Test Method**	**Dry**	**Conditioned**
Melting Point, C	3146	220	-

Aluminum diethylphosphinate (referred to as AlPi) Exolit®OP1240, purchased from Clariant was used to prepare formulations containing a reference phosphinate.

II.2.2   Compounding and processing

The formulations were prepared using a DSM Xplore Micro15 twin screw micro-extruder (Figure 37) having a volume of 15 cm^3. Glass fiber reinforced PA6 or PBT (PA6GF or PBTGF) and additives were melt mixed in nitrogen flow at 250 °C for 3 minutes with a screw speed of 80 rpm. Raw materials were dried at least for one night at 80 °C before use. The torque and extrusion parameters can be followed and recorded via computer thanks to the software MidiExtruder.

All the formulations in the screening contain 20 wt% additive and 80 wt% glass fiber reinforced polymer, that is, 56 wt% polymer / 24 wt% glass fibers / 20 wt% additive.

Bar specimens of 0.8 and 1.6 mm thickness used to carry out the UL-94 tests have been prepared with a DSM Xplore small scale injection molding machine (Figure 37). The molten formulations were directly collected from the micro-extruder by means of the injection unit and maintained at 260 °C for 1 minute before injection. The injection molding was performed in a conical shaped mould heated at 120 °C with a pressure of 6 bars for 1.6 mm thickness bars and 14 bars for 0.8 mm thickness bars. Samples needed to perform the LOI tests as well as UL-94 bar specimens of 1.6 mm thickness were also obtained using a Darragon press (Figure 37) at 250 °C with a pressure of 40 MPa applied for 8 minutes.

DSM microextruder   **DSM injection moulding press**   **Darragon press**

Figure 37: Picture of the polymer processing techniques

II.3. FIRE TESTING METHODS

Fire behavior can be described through three major parameters: the ignition, the contribution to flame spread and the heat release. Depending on the material application fields, some specific tests can be implemented to simulate specific fire scenarios. The UL-94, the Limiting Oxygen Index (LOI), the Glow Wire test (GWIT and GWFI), and the Mass Loss Calorimeter (MLC) test simulate the three parameters above-mentioned. In this manuscript, MLC will only be used as a characterization tool. BASF (and in general E&E industry) wished to focus on the UL-94 results.

II.3.1   UL-94 vertical burning test

The UL-94 tests were realized on a Fire Testing Technology Limited equipment on bars 127.0x12.7x0.8 mm^3 and 127.0x12.7x1.6 mm^3 in accordance with the recommendations of the standard (ASTM D3801, IEC 707 or ISO 1210) (Figure 38). This small-scale test determines the tendency of a material either to extinguish or to spread the flame once the specimen has been ignited [136]. Specimens are clamped vertically and exposed to a defined flame ignition source from the bottom for 10 sec. The flame is applied twice if the sample self-extinguished after the first ignition. Cotton is also placed below the sample to evaluate the presence or not of flaming drops.
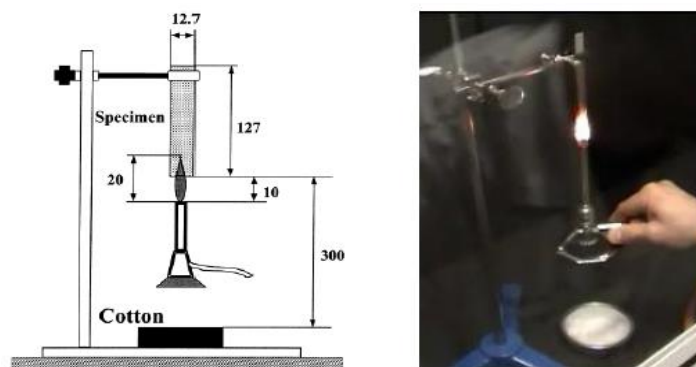
Figure 38: Description of the vertical burning test UL-94

The bars are ignited by a blue flame (without cone) of 20 mm. The flame is generated by a methane-burner having a gas flow rate of 105 mL/min with a back pressure less than 10 mm of water. Three classifications are assigned to materials based on their behavior regarding burning, flame propagation and dripping: V-2, V-1 and V-0, V-0 being the best ranking. If the material does not meet the criteria, it is non-classified at the UL-94 test (NC). The criteria required for the ratings are presented in Table 11.

Table 11: Criteria for UL-94 classifications

Criteria	V-0	V-1	V-2
Afterflame time for each individual flaming	≤10s	≤30s	≤30s
Afterflame+afterglow time for each individual specimen, after second flaming	≤30s	≤60s	≤60s
Total afterflame time for any condition set (5 flamings)	≤50s	≤250s	≤250s
Cotton indicator ignited by flaming drops	No	No	Yes
Afterflame or afterglow of any specimen up to the holding clamp	No	No	No

II.3.2   Instrumentation of the UL-94 test

In this manuscript, new data were collected from the UL-94 test through various instrumentations. A similar approach was proposed previously by Kandola et al. who already developed a method to quantify the melt dripping of a sample while exposing it to a given temperature [137]. In our study, thermocouples embedded in the bar allow measuring the temperatures at different locations in the polymer bar as a function of time leading to temperature profiles. The weight measurement of the bar and of the melting drops during the test allows quantifying in the same time the dripping behavior and the thermal degradation of the material (volatilization and material remaining in the condensed phase). These data provide information on the behavior of the material during the test and so, lead to more than a simple classification.

Two setups were designed as reported in Figure 39. The first one aims at measuring temperature gradients inside the bar during the test (Figure 39a) whereas the second one aims at measuring the mass of both bar and flaming drops released during the test (Figure 39b). A complete frame was designed, made of aluminum, but with a support on the top and a possibility to adapt a clamp, so that the two configurations (hanging the bar under the balance or holding it with a clamp with embedded thermocouples) are possible.
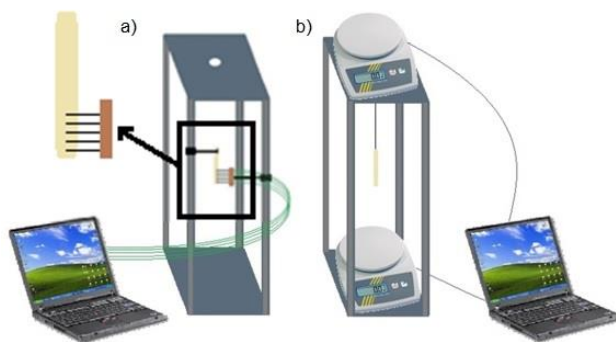
Figure 39: Scheme of UL-94 instrumented test; a) measurement of temperature gradients (TC mode) b) quantification of dripping (WM mode)

In the "thermocouples" configuration (TC mode), a "brush" made of five thermocouples purchased from Omega (TJC100, K-type, 0.5 mm diameter) was connected to a Graphtek midi Logger GL220. The thermocouples were embedded every 15 mm in the bar after drilling and a measurement of temperature was carried out every 100 ms. As a matter of simplification, the temperature measured by the different thermocouples will be referred T1 to T5 and will be numbered as described in Figure 40. The measurement of temperatures was carried out in standard UL-94 conditions. In case of dripping, the temperature curve is drawn until the thermocouple is not embedded anymore in the material.

Figure 40: scheme of the numbering of thermocouples in the UL-94 bar

Measurements were carried out four times in order to evaluate the repeatability of experiments as illustrated in Figure 41 for FR-PA6 as an example concerning T1. The four curves illustrate the good repeatability obtained in the measurements: the profiles are very close and the peak temperatures achieved are within a margin of ±10% in temperatures and ±2 s in time. It is noteworthy that in the case of materials that are burning up to the clamp, a higher error margin was found, due to the burning behavior. Indeed, when a sample burns fast, flame spread cannot be a controlled parameter.
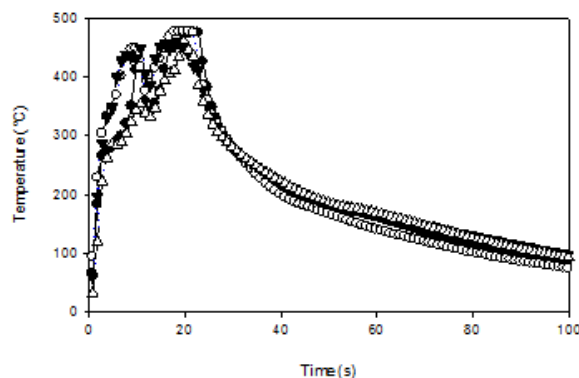
Figure 41: Repeatability study for the measurement of temperature, example with T1 testing FR-PA6

In the second configuration (Weight Measurement, WM mode), a dynamic recording of masses was made by two digital balances (PL-602L purchased from Mettler Toledo). They were installed on the top and on the bottom. The balance located on the top was used to measure the weight of the bar during the test. The sample was linked to the hook of the balance with a copper wire.

A long wire (200 mm) was necessary to minimize the effects of convection due to the combustion of the sample during the test (which could interfere with the hook system). The bottom balance was used to measure the mass of the molten droplets. Both mass data were real-time recorded, with a margin of error of ±0.01g. Masses were converted into weight rates (per cent) with respect to the initial bar weight. The rate of sample transferred to the gas phase can be deduced by the following calculation:

$$wt\%_{gas\ phase} = 100 - wt\%_{bar} - wt\%_{droplets}$$

Mass measurements were carried out three times to evaluate their repeatability, as illustrated in Figure 42. This figure illustrates the good repeatability in the measurement of masses. The margin of error is about ±3 %. During flaming, a slight destabilization of the mass can however be observed which leads to a more important margin of error for the calculation of proportion of evolved gases.
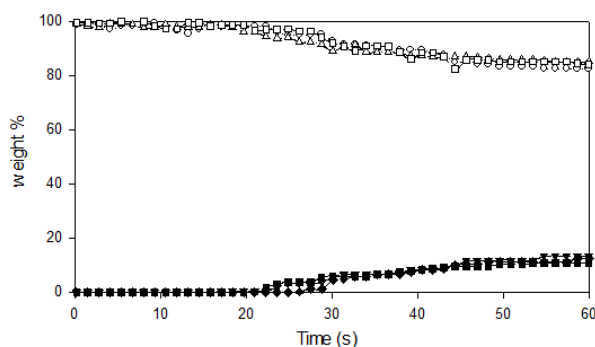
Figure 42: Repeatability study for the measurement of masses, example with PA6

It is noteworthy that the shape of drops is not observed nor investigated as it was done in the work of Kandola et al. **[137]**. The results presented in this manuscript will show the mass and temperature instrumented tests for each formulation. The curves are calibrated so that the zero in time corresponds to the first ignition of 10 s. The second ignition is only applied if required by the standard, that is to say when the bar flames out after first ignition.

II.3.3   Glow wire

Glow wire test (Figure 43), described by IEC 60695-2-12, is widely used to evaluate the flammability of materials used for electrical parts. A sample (100 x 100 x 1.2 mm^3) is fixed vertically on a trolley loaded with a 1N weight. The sample moves towards the glowing wire, settled to a determined temperature (from 550 to 960 °C), until they are in contact. After 30 s of contact, the trolley goes back to its initial position. The time of ignition (t_i) is determined together with the time of extinguishment (t_e).

The test is successful when two conditions are fulfilled simultaneously:

→ The time of extinguishment must be lower than 30 s after the removal of the glow wire.
→ The cotton placed below the sample must not ignite.
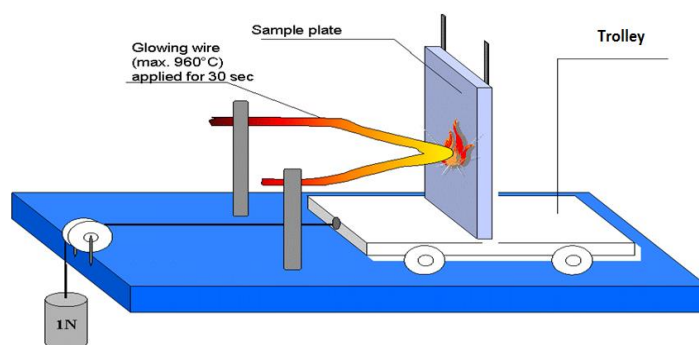
Figure 43: Glow wire test scheme

The highest temperature at which the test is successful is called the glow wire flammability index (GWFI). To determine the GWFI, the wire is heated at a temperature comprised between 550 and 960 °C as reported in Table 12.

The glow wire ignition temperature (GWIT) is the temperature which is 25 K (30 K between 900 °C and 960 °C) higher than the maximum temperature of the tip of the glow-wire which does not cause ignition of a test specimen of given thickness during three subsequent tests. To evaluate the GWIT, the wire is heated from 550 to 960 °C every 25 °C.

Table 12: Test temperatures to evaluate the GWFI

Test temperature (°C)	Tolerances (K)
550	±10
600	±10
650	±10
700	±10
750	±10
800	±15
850	±15
900	±15
950	±15

There are no publications available to describe the phenomena involved in this test, except the one from Acquasanta et al **[138]**, which suggested a simplified scheme of glow wire test described in Figure 44. They supposed that for the part of the specimen in contact with the wire, three zones could be identified (Figure 44):

→   The pyrolysis zone: the temperature is above the decomposition temperature.
→   The melting zone: the material melts and the degradation is slow.
→   The softening zone: the temperature is not high enough to melt the polymer but the material is deformed by heat distortion.

It should be highlighted that in the case of thermosetting polymers, no melting of the polymer is observed. As a consequence, this simplified scheme proposed by Acquasanta et al. cannot be transposed to all the polymers.

Acquasanta et al. suggested that GWIT is led by heat transfer, pyrolysis and ignition, while GWFI result depends also on the combustion and the fire propagation. But they supposed that the processes occurring in the pyrolysis zone mainly determine the test result of GWIT, and that rheological and mechanical properties have a huge importance too.
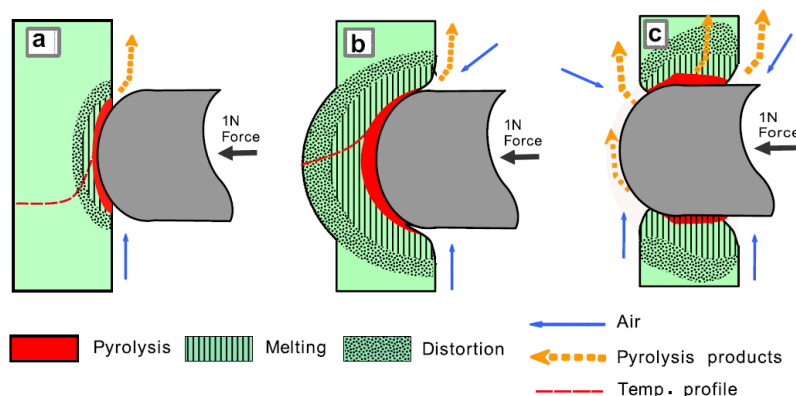
Figure 44: Scheme showing the three stages of a glow wire test [138]

II.3.4   *Limiting Oxygen Index*

The LOI fire test is a standardized test (ISO 4589), which allows determining the minimum concentration of oxygen (in Vol%) in a nitrogen/oxygen mixture that is required for the combustion of a material in vertical position ignited by the top **[139]**. For a given concentration, the combustion time and the burnt part of the bar are measured. The concentration in oxygen has to be increased if the combustion time is lower than 3 minutes and if the flame does not spread beyond 50 mm along the sample. The testing specimen is fixed from the bottom in a N_2/O_2 gas circulating chamber where it is ignited by a butane/propane flame for a maximum period of time of 10s. Measurements were carried out with a Fire Testing Technology apparatus on bars of 100 x 10 x 3 mm^3 (Figure 45). The margin of error of the obtained results is estimated at ± 1 vol%.
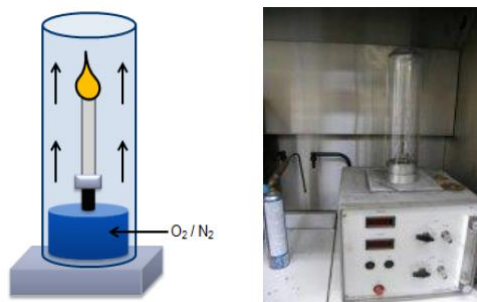
Figure 45: Schematic representation of the LOI test

II.3.5   Mass loss cone calorimeter (MLC)

Mass loss cone calorimeter experiments were performed using 10 x 10 x 0.3 cm^3 plates of material, in a Fire Testing Technology apparatus (Figure 46). Materials were tested under a heat flux of 35 kW/m² at a given distance from the resistance of the cone (25 mm), and Heat Released Rate (in kW/m²) was measured as a function of time, after calibrating using a burning methane flow. HRR measurement allows as well measuring the Total Teat Release (MJ/m²) of the sample. HRR indicates heat released from the sample during the experiment and THR is the total energy over time. At the beginning of the test, the plate is exposed to an igniter. This one is removed after ignition. Each formulation is exposed to heat a same time of 10 minutes corresponding to around 2 minutes after the flameout of the virgin polymer, so as to get comparable mass loss in time.
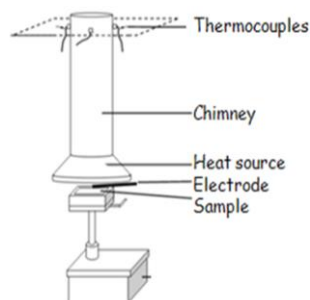
Figure 46: Scheme of the mass loss cone calorimeter

II.3.6   Pyrolysis-Combustion Flow Calorimeter (PCFC)

Another way to evaluate the fire-retardant capability is the pyrolysis combustion flow calorimeter (Figure 47). This device was supplied by Fire Testing Technology. PCFC was developed by Lyon **[140]** from FAA and allows measuring the flammability of small powder samples.
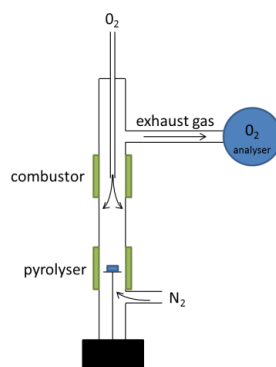
Figure 47: Schematic representation of the PCFC

Samples were placed in open alumina pans, and were degraded in nitrogen atmosphere ("pyrolyzer") at a heating rate of 1 °C/s with a nitrogen flow of 80 mL/min. The decomposition gases were then burnt in a nitrogen/oxygen mixture ("combustor") at 900 °C with 80 mL/min and 20 mL/min flows respectively. The heat release is measured as a function of the temperature using an oxygen analyzer, according to the Hugget relation **[141]**. With the use of a heating ramp of 1 °C/s, pHRR value in W/g equals heat release capacity (HRC) in J/(g.K). The determination of an optimal sample mass was performed by testing different amounts of powder in the PCFC pan. The maximum oxygen consumption should reach around 50% of total O_2 in the N_2/O_2 mixture in order to get the most repeatable measurements, that is to say the peak of consumption should reach $10\pm3\%$ O_2. The adequate mass determined after optimization was 5 ± 0.5 mg.

II.4. ANALYTICAL TECHNIQUES

Fire retardancy can take place in the gas phase, in the condensed phase or both. It might modify (or not) the decomposition pathway of the polymer (or of the flame retardant). It thus results in the release of specific gaseous degradation products. To elucidate these mechanisms, it is hereinafter proposed to investigate the thermal decomposition of the formulations as well as their ingredients (polymer, flame retardant systems).

First the thermal decomposition of materials was characterized by thermogravimetric analysis. Through this technique, the characteristic temperatures of decomposition of materials are determined. Materials were heat treated at those temperatures and characterized. Residues were thus collected and then analyzed using adapted techniques in order to be able to propose the mechanisms occurring in condensed phase. As a complement, evolved gas analysis techniques were used to determine the nature of gaseous degradation products released by the materials.

In the following section, the methods implemented to understand the modes of action of flame retardant systems are presented. The end of this section will also describe the analytical techniques used to characterize the synthesized products.

II.4.1 ThermoGravimetric Analysis (TGA)

TGA measurements were carried out on two instruments: a TA Instruments (TGA Q5000IR with alumina crucibles) and a Setaram (TG92-16 with quartz crucibles). Balance and purge flow rates were set at 15 and 100 mL/min respectively in the TA device, and sample flow rate was set at 100 mL/min in the Setaram device. For all experiments, nitrogen was chosen as purge gas in the Q5000, and argon was chosen as furnace gas in the Setaram. The samples of about 10 mg were submitted to an isotherm at 50 °C for 10 minutes then followed by a heating ramp of 10 °C/min up to 800 °C.

TG curves allow determining characteristic points. The derivative of the TG curve (dTG) allows finding the mass loss rate at given temperature and ramp, and so identify the main steps of the decomposition. One of the characteristic points is the onset temperature of degradation **[142]**. The onset temperature is determined as follows. The abscissa of the intersection of the two slopes of the TGA curve before and during a degradation step corresponds to the onset temperature (Figure 48). The second point that will be presented hereafter is the "max" point, which corresponds to a maximum loss rate in the dTG.
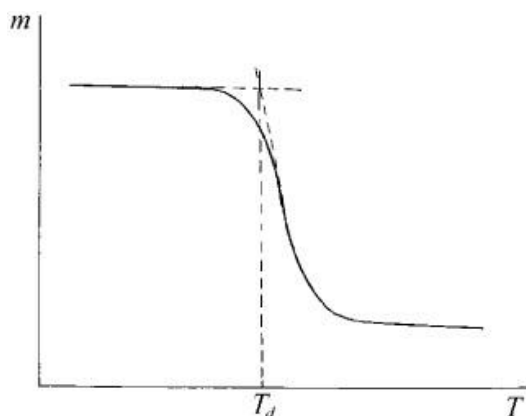
Figure 48: determination of an onset temperature

→ *Comparison between experimental and calculated TGA curves:*

In order to determine potential interactions between a polymer and flame retardant additives during the thermal degradation, a comparison between the experimental and a calculated TGA curve was performed. The calculated curve is obtained by linear combination of the TGA curves of each single component (polymer, additives) weighted by their respective mass fractions in the formulation. The interaction between components can be illustrated by the difference weight loss curve ΔM (Equation 2).

$$\Delta M = M_{exp} - M_{calc}, \text{ with } M_{calc} = \Sigma x_i M_i$$

with M_i the mass of the constituent i at given temperature and x_i the fraction of i in the formulation.

Equation 2

The ΔM curve allows pointing out a potential increase or decrease in the thermal stability of the polymeric matrix related to the presence of one or several additives. When the experimental curve is higher than the calculated one (or when the ΔM curve is positive), the weight loss is lower than expected, showing that the interaction between the polymer and the additives leads to a thermal stabilization of the material. On the opposite, if the experimental curve is lower than the calculated one (or when the ΔM curve is negative), a thermal destabilization occurs.

II.4.2   *ThermoGravimetric Analysis (TGA) coupled with FTIR*

In this technique, the FTIR spectrometer is connected to the TGA device via a heated transfer line. As gases evolve during the TGA experiment, they pass through the flow cell of the FTIR spectrometer where the infrared spectra are collected. The FTIR flow cell is compatible with all types of evolved gases and materials. Additionally, the large flow cell diameter provides high throughput and prevents spectral interference caused by deposits on the walls.

The experiments have been performed on the TA instruments TGA Q5000IR previously described coupled with a Nicolet FTIR spectrometer from ThermoFischer. Parameters used to carry out the experiments are those described previously. The heat transfer line temperature is set at 225 °C to avoid condensation of the evolved gases. The IR spectra were recorded in the 400-4000 cm^{-1} spectral range through the OMNIC software. The obtained spectra correspond to the accumulation of 8 scans with a resolution of 4 cm^{-1}.

The attribution of each band was carried out through the use of databases and the limits of integration of the definite bands are reported in Table 13.

Table 13: integration limits for definite IR bands

Function or group	Integration limits (cm^{-1})
H-C=	3150 - 3000
THF	3020 - 2935
H-C-	3000 - 2820
CO_2	2400 - 2280
-N=C=O	2300 - 2260
NH_2 / NH	1660 - 1560
NH_3	990 - 906

II.4.3   ThermoGravimetric Analysis (TGA) coupled with DSC (SDT)

The measurement of heat flows during the decomposition was achieved with a TA Instruments SDT-Q600. Balance and purge flow rates were set at 15 and 100 mL/min respectively. Measurements were carried out in N_2 atmosphere to avoid exothermic oxidation reactions occurring in air. The 100 mL/min purge flow was maintained for two hours with the furnace closed to purge the furnace from air in that case. Alumina sample cups foiled with gold foil were used, to prevent the reaction of decomposing material with alumina. A blank was measured on the foiled cup. The integration of the experimental curve (after subtraction of the blank) thanks to the TA Analysis software led to the decomposition Enthalpy.

II.4.4   Pyrolysis - Gas Chromatography/Mass Spectrometry analysis

Pyrolysis-GC/MS was used in complement to the TGA-FTIR analyses. This technique provides an extremely sensitive tool to determine the nature of gases evolved during the thermal decomposition of a material.

The Pyrolysis-GC/MS measuring system was provided by Shimadzu. An illustration of this system is found in Figure 49. A micro-furnace pyrolyzer (Frontier Lab PY-2020iD), a gas chromatograph equipped with a capillary column and a quadrupole mass spectrometer equipped with an Electron-Impact (EI) ionization source (Shimadzu GC/MS QP2010 SE) are directly connected in series. Two analyzes are available: py-GC/MS and EGA/MS (Evolved Gas Analysis).

In py-GC/MS, analysis is performed through a thermal desorption mode which consists in heating the sample at a defined temperature ramp in the pyrolyzer furnace while heavy evolved gases condensate at the beginning of the GC column and volatile fragments are detected after ionization. Right after reaching the desired temperature in the pyrolyzer furnace, condensed products are desorbed and separated in the GC column to finally be observed in the mass spectrometer.
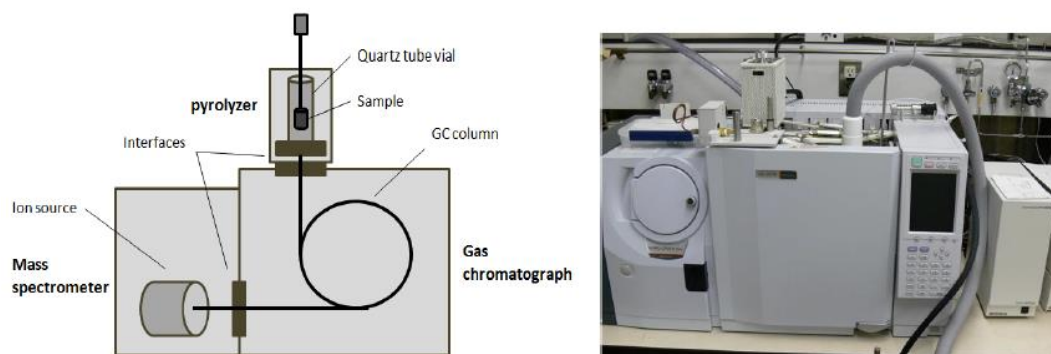
Figure 49: Schematic representation and picture of the Pyrolysis-GC/MS measuring system

About 0.2 mg of the samples is added in a stainless steel sample cup. The latter is first placed at the upper position of the pyrolyzer, and then introduced into the center of the furnace (inside a quartz tube vial) under a helium gas flow. In the pyrolyzer furnace, the temperature was initially set at 50 °C and then raised to a defined temperature with a selected heating rate (generally 10 °C/min). The temperature of the interface between the pyrolyzer and the GC injection port and the injection port were respectively set at 320 °C and 280 °C.

A part of the carrier gas flow is reduced by a splitter so as to prevent clogging of the GC column as well as to prevent saturation of the signal during the detection of gases. Split parameters (50, 100 or

200) were empirically determined depending on the heat treatment temperature in the pyrolyzer. A fused silica capillary column (30 m x 0.25 mm x 0.25 μm film thickness) was used and the linear velocity of helium as a carrier gas was 40 cm/s.

The GC column temperature was maintained at 35 °C during the whole temperature ramp of samples in the pyrolyzer (whether programmed ramp or flash pyrolysis) and then programmed up to 300 °C at the rate of 5 °C/min, followed by an isotherm of at least 10 min at 300 °C (Figure 50). Electron-Impact spectra were recorded at 85eV with a mass scan rate of 2 scan/s. Pyrograms and mass spectra were treated using a GC/MS post-run analysis program (Shimadzu). The NIST and FSearch mass spectral databases were used for the identification of products. MSFragmenter tool, from ACDlabs, was used to help identifying synthesis molecules (not belonging to databases).

In EGA/MS, the analysis differs in the nature and temperature of the column. An Ultra ALLOY®-DTM non-polar column (2.5 m x 0.15 mm x 0.47 mm) is used, and heated at 300 °C from the beginning of the experiment. The sample is treated in the same way as in py-GC/MS, but the evolved gases directly go through the column, then are ionized and observed (Figure 51). The chromatograms depend on the degradation steps and do not show separated products, so that this technique is complementary to py-GC/MS to help attributing the degradation temperature of definite fragments (previously separated in py-GC/MS).
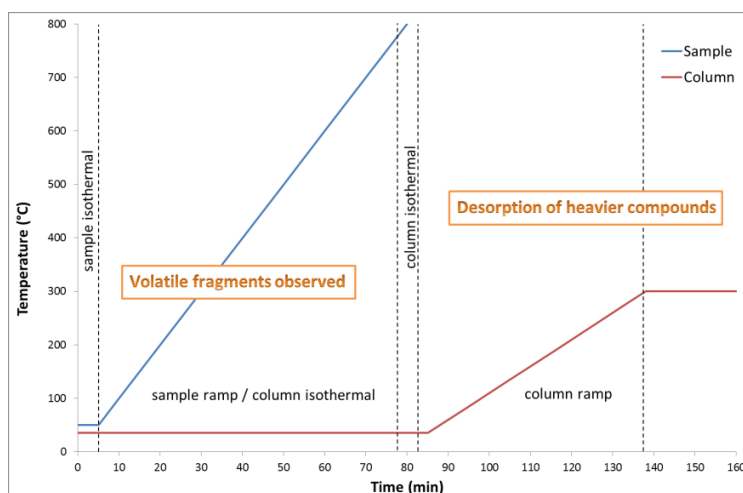
Figure 50: Scheme of the py-GC/MS procedure of use
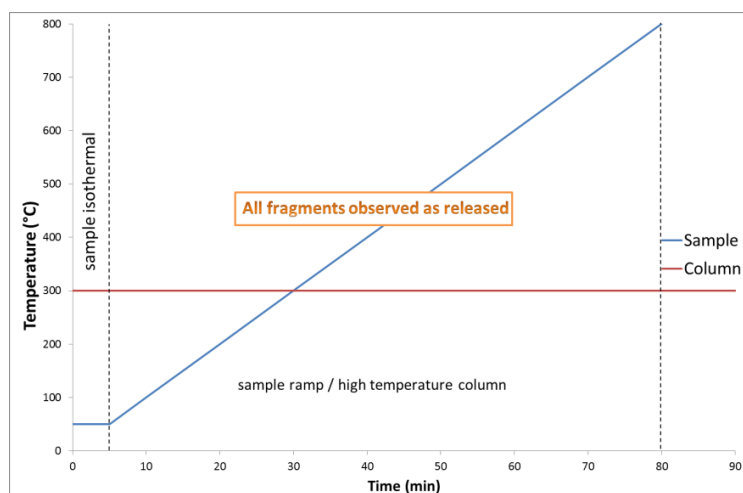
Figure 51: Scheme of the EGA/MS procedure of use

II.4.5   Thermal treatment

Thermal treatments consist in heating a sample in a furnace (Figure 52) at a defined temperature (Heat Treatment Temperature; HTT). The treatment temperatures were determined according to TGA curves as they correspond to the characteristic degradation steps of the systems. Samples were heat treated under air at a heating rate of 10 °C/min (similar to that used for the TGA measurements) from ambient to the HTT followed by an isotherm of 1 hours. The samples were then cooled to ambient temperature before being collected. The residues obtained after thermal treatments were stored in a desiccators to avoid hydrolysis of the residues and then analyzed by solid state NMR.
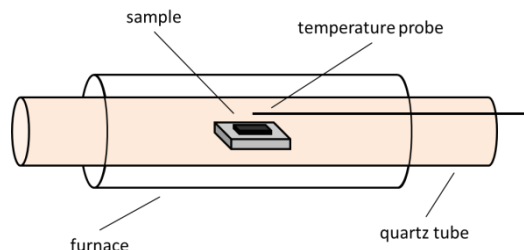
Figure 52: Tubular furnace used for thermal treatments

II.4.6   Solid-state NMR

The solid-state nuclear magnetic resonance (NMR) is an effective tool to analyze the changes in the chemical environment of an atom inside a material. In the solid state (on the contrary to liquid state), the chemical shift anisotropy (anisotropy of magnetic moment, CSA), has a strong effect on the spectra, by broadening peaks. Through a tensoral analysis of the magnetic moments in a molecule, it is possible to demonstrate that there exists a "Magic Angle" with respect to the applied magnetic field at which the spinning of the sample leads to a minimization of absorption line broadening due to CSA. This method of analysis is so called "Magic Angle Spinning" (MAS).

In the case of carbon, the resonance of atoms is only possible in their isotopic form (^{13}C). However their low abundance leads to poor signal. This poor signal can be overcome by an excitation of protons in the sample and have them resonate at the same frequency than that of target atom (Hartman-Hahn condition). This process is called cross-polarization (CP), and the time of polarization is also called contact time. CP leads to a high enhancement of the excitation of studied nuclei. However there exists an interference of the large number of protons on the decay of isolated nuclei, due to weak spin interactions. In this case, the dampening of the signal can be removed with a strong radiofrequency signal which holds the protons in a high resonance state so that they do not absorb resonance from the nuclei. This is called ^1H decoupling.

All measurements were carried out on a Bruker Advance II 400 (B_0=9.4 T) with a probe head of 4 mm and a MAS of 10 kHz.

^{27}Al NMR measurements
The repetition time (D1) was fixed at 1 s and 512 scans were performed to obtain a satisfactory signal to noise ratio. Al aqueous solution was used as a reference.

^{31}P NMR measurements
^1H decoupling was used because of the high relaxation time of phosphorus nuclei (10 to 500 s), and 16 scans were carried out. A repetition time of 120 s was applied, and H_3PO_4 aqueous solution (85%) was used as reference.

^{13}C NMR measurements

High power ^{1}H decoupling and ^{1}H-^{13}C CP (with a contact time of 2 ms and a recycle delay of 5 s) were used. 1024 scans were performed. Glycine was used as a reference.

Two-dimensional ^{27}Al-^{31}P D-HMQC

The spatial proximity between phosphorus and aluminum sites was investigated with a 2D MAS-NMR D-HMQC (Dipolar Heteronuclear Multiple Quantum Coherence) sequence **[143]**. This NMR experiment uses the standard HMQC pulse sequence to produce heteronuclear coherences but an additional pulse scheme allows creating through-space coherences in place of the standard through-bonds signals obtained with the basic HMQC sequence. As a consequence, the 2D spectrum displays correlation signals between spatially close atoms. The ^{27}Al D-HMQC spectrum has been obtained with a 4 mm triple channel probe at 9.4 T ($_{vL}(^{27}$Al) = 104.2 MHz and $_{vL}(^{31}$P) = 161.9 MHz) and with a spinning frequency of 10 kHz. The through-space correlations were created by a scheme pulse based on the SR4 (symmetry-based radio-frequency pulse sequence) **[144]** technique applied for 1 ms. The 2D spectrum was recorded with 1536 scans and a recycle delay of 1 s.

II.4.7   *Laser Flash Analysis (LFA)*

Flash method, or Laser Flash Analysis, is commonly used to measure the thermal diffusivity of homogeneous and isotropic materials. In its first version, this method is built upon the analysis of the back face temperature rise of a plate whose front face is submitted to an energy pulse of short time compared to the observed phenomenon. The speed of the temperature propagation through the sample is directly linked to the thermal diffusivity of the material and to its geometrical characteristics **[145]**. The thermal diffusivity was measured using the NETZSCH laser flash apparatus LFA 467 HyperFlash®. The unit is equipped with a furnace which is capable for operation from -100 °C to 500 °C. The front surface of the sample is heated by a Xenon flash lamp with variation of energy by voltage and pulse-length. The resulting temperature increase on the rear face is measured using an IR-detector (InSb or MCT).

II.4.8   *Microscopies*

II.4.8.1 Scanning electron microscopy

Scanning electron microscopy (SEM) is a technique that uses the interactions occurring between electrons and matter. An electron beam is sent on the sample, leading among other things to the emission of secondary electrons and backscattered electrons, which are then used to obtain topographic and chemical information respectively. The SEM analyses were carried out using an Hitachi S4700 at 6 kV. All the samples were microtomed with a diamond knife on a Leica UltraCut microtome at cryogenic temperature (-120 °C) to obtain smooth surfaces.

II.4.8.2 Electron-probe micro-analysis

Electron probe microanalysis (EPMA) is an analytical technique that is used to establish the composition of small areas on specimens. A beam of accelerated electrons is focused on the surface of a specimen using a series of electromagnetic lenses, and these energetic electrons produce characteristic X-rays within a small volume (typically 1 to 9 µm^3) of the specimen. These X-rays are detected at particular wavelengths, and their intensities are measured to determine concentrations. All elements (except H, He, and Li) can be detected. This analytical technique has a high spatial resolution and sensitivity. Additionally, the electron microprobe obtaining highly magnified

secondary- and backscattered-electron images of a sample. In this work EPMA (Cameca – SX 100) was used to characterize the dispersion of FR into the fibers and to get back-scattering electron pictures of the samples.

II.4.9 *Specific analytical techniques for the synthesis*

II.4.9.1 Liquid-state NMR

^{31}P, ^{13}C and ^{1}H NMR measurements were performed on a Bruker Advance 300 (magnetic field B_0=7 T). Tetramethylsilane was used as a reference. ^{1}H measurements were done with a pulse of 30° and 16 scans. ^{13}C measurements were done with a proton-decoupling method, a pulse of 30° and 1024 scans. ^{31}P measurements were done with a proton-decoupling method and 32 scans.

II.4.9.2 Chemical analysis

Elemental analyses for carbon, hydrogen and nitrogen were performed with an Elementar micro cube CHN analyzer. The sample is weighed in a tin capsule and burned with O_2 under Helium atmosphere. Different catalysts are used to convert the elements into specific compounds (C to CO_2, H to H_2O and N to various nitrogen oxides) which are detected by a thermal conductivity detector (TCD). The initial weight of the sample is $1 – 10$ mg. The quantification limit is 0.5 g / 100 g and the measuring accuracy is ±0.1 g / 100 g.

Elemental analyses for aluminum and phosphorus were performed with a Vista pro spectrometer system. The experiments are conducted as follows: 0.1 g of the sample is added to a solution of Cs_2SO_4 as well as to a mixture of concentrated sulfuric and nitric acids. After solubilizing the sample with the oxidizing acids, the mixture is vaporized and the residue is dissolved in hypochloric acid. The relative percentages of Al and P of this solution are determined by means of atomic emission spectroscopy with inductive coupled plasma (ICP-AES). The standard deviation of the method is inferior to 2 %.

II.5. CONCLUSION

This chapter defined the materials, techniques and protocols used to develop novel phosphinate flame retardants for PBT and PA6 and to investigate their mode of action and mechanism of degradation. The protocols of synthesis of the phosphinate salts (from the synthesis of 2-POO to the preparation of the aluminum salts from phosphinic acids) were described. The basic polymers and compounding techniques used to prepare the engineering plastics formulations (based on the phosphinate salts) for the screening phase of Chapter IV were presented. The fire tests on which this study is based were also exposed. Finally, the analytical techniques and instrumentation used to investigate the mechanisms of fire retardancy of the phosphinate salts in Chapters V and VI were detailed.

The next step, Chapter III, will further detail the different challenges and adaptations of protocols encountered during the syntheses. The thermal behavior of the products will also be investigated. Thermal stability is a key parameter to investigate before any compounding in Chapter IV, so as to make sure the compounds are stable enough at the processing temperature.

Chapter III.   Synthesis and characterization of novel phosphinate salts

The first chapter of this manuscript highlighted the fact that phosphinate salts remain nowadays a valuable choice for the fire retardancy of PBT and PA6. It has been shown that various structures of phosphinates lead to different results in different matrices. However, there are still unexplored routes in the research of efficient flame retardants of this type for PBT and PA6.

The collaboration between UMET-R2F and BASF SE aims at finding novel appropriated phosphinates able to give flame retardant properties to PBT and PA6. Interestingly, arylphosphinates were not fully explored for flame retardant applications in PBT and PA6. The use of this aromatic ring bonded to the phosphorus atom raises obvious questions: would such phosphinate salts behave differently to alkyl ones? What would be the mode of action in that case? Does the addition of various amine building blocks sharply change the thermal behavior of arylphosphinates? To answer those questions, various structures have been synthesized and carefully examined in that work.

The first part of this chapter describes the preparation of the phosphinate salts. Different synthesis protocols were used. The complete synthesis of the salts can be split into three parts: the preparation of 2-POO, the ring-opening reaction with amines and the conversion of phosphinic acids into metal salts. The protocols of analysis of the obtained products are also depicted.

The second part aims at investigating the thermal stability of the products. As they should be processed in PBT and PA6, the compounds should achieve appropriate thermal stabilities before any screening for their FR properties which will be presented in Chapter IV.

III.1.   SYNTHESIS OF NOVEL PHOSPHINATE SALTS

III.1.1   Strategy

The use of the phosphinate salts obtained from the ring-opening reaction of oxaphospholanes with classical alcohols was lately patented by Clariant [146] (case of Exolit PE110). These compounds were proved to be effective in PBT at between 15 and 20 wt% loadings. However, no reaction between PE110 and non-halogenated amines was reported.

In this context, a first partnership between UMET and BASF SE was created, and reactions between PE110 and six different amines were undertaken. Most elected amines had already been employed for the preparation of nitrogen-containing diphosphinic acids, namely piperazine, ethylene diamine and m-phenylene diamine. In fact, these disubstituted structures should achieve a high thermal stability. Other amines such as o-phenylene diamine, aniline or benzyl amine were also selected for the sake of comparison. Amines were selected because it was shown that nitrogen can participate in the flame retardancy mechanism. The decomposition of amine structures induces two principal effects. In the gas phase, the release of ammonia dilutes the combustion gases. In the condensed phase, nitrogen atoms tend to stabilize the residue.

However, the considered phosphinic acids, when used in polyesters or polyamides, should have a negative impact on the integrity of the polymer chains. This effect could be overcome by neutralization of the acid, that is why a focus was made on metal salts of the phosphinic acids. Moreover, metal-phosphinate salts achieve a higher thermal stability, which is required for their processing. Aluminum was selected as main metal cation, based on the previous studies led by Braun et al. already exposed in this manuscript [79].

The phosphinates discussed above are still derivatives of well-known products: alkylphosphinates. The aim of this project is to investigate another category of products: the arylphosphinates,

represented in their category by DOPO compounds. Thus, another starting material was proposed by BASF SE: 2-phenyl-1,2-oxaphospholan-5-one 2-oxide (2-POO).

The strategies of synthesis would be similar, however the presence of an aromatic ring bonded to the phosphinate O-P=O group implies a difference of reactivity and stability of the structure (due to electron delocalization). Arylphosphinic acid should be a stronger acid than alkylphosphinic acid, if compared to carboxylic acids (benzoic acid, pka=4.2 > acetic acid, pka=4.76; the pKa of methylphenylphosphinic acid calculated using Advanced Chemistry Development Software V11.02 is equal to 2.43). The presence of aromatic rings may also have an impact on the stability of corresponding salts. In the case of fire science, the presence of the aromatic ring induces charring in many cases, which is an interesting parameter. These two points give clues on the use of such compounds as flame retardants, that is why they need to be investigated.

Five amine building-blocks will be used in this study: aniline (as the corresponding product proved effective in the study on alkylphosphinates), benzyl amine, ethylene diamine, p-phenylene diamine, and piperazine. Aluminum will be used as metal cation.

III.1.2   Synthesis of the electrophile: 2-POO

The synthesis of 2-POO was achieved following three different protocols.

First, 3-(hydroxy(phenyl)phosphoryl)propanoic acid (3-HPP), provided by BASF SE, was converted into 2-POO using acetic anhydride or thionyl chloride (Scheme 4). In both cases, long white crystals were recovered when crystallizing in a chloroform/Et$_2$O mixture, with a yield of 90 %.
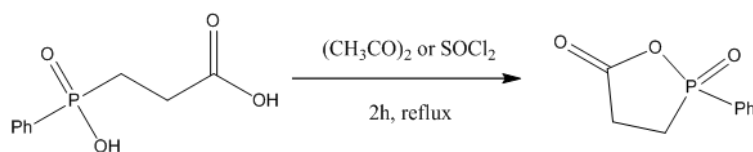
Scheme 4 : synthesis of 2-POO from 3-HPP

The second protocol corresponds to the patent from Solutia Inc. **[147]**. The addition of the acrylic building-block to a chlorinated phenyl-phosphine leads to the phosphinic/carboxylic chloride (acrylation intermediate, AI) which can be cyclized using acetic anhydride (Scheme 5). A yield of 90 % is obtained in this case.
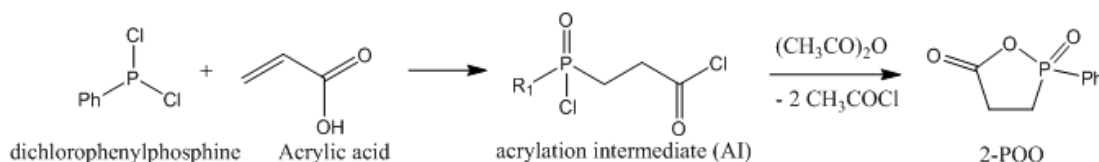
Scheme 5 : synthesis of 2-POO from DPP and acrylic acid

The reaction of dichlorophenylphosphine (DPP) with acrylic acid was followed by ^{31}P liquid-state NMR (Figure 53): the conversion of DPP into the AI leads to a very distinct form of phosphorus. DPP is a P(III) with a chemical shift of 36 ppm while the phosphinyl chloride is a P(V) with a chemical shift of 52 ppm.

Other forms of phosphorus were observed which correspond to oxidation or hydrolysis of PPhCl$_2$ during handling (39.5 ppm, 40.0 ppm and 50.5 ppm). These byproducts represent integrals of 0.05, 0.07 and 0.12 respectively when the main peak at 52 ppm is calibrated to 1.0.

It is noteworthy that the reactions based on the DPP are very sensitive and lead to impurities in the first steps and so lower final yields. The 2-POO was also harder to recover or crystallize due to the amount of impurities.
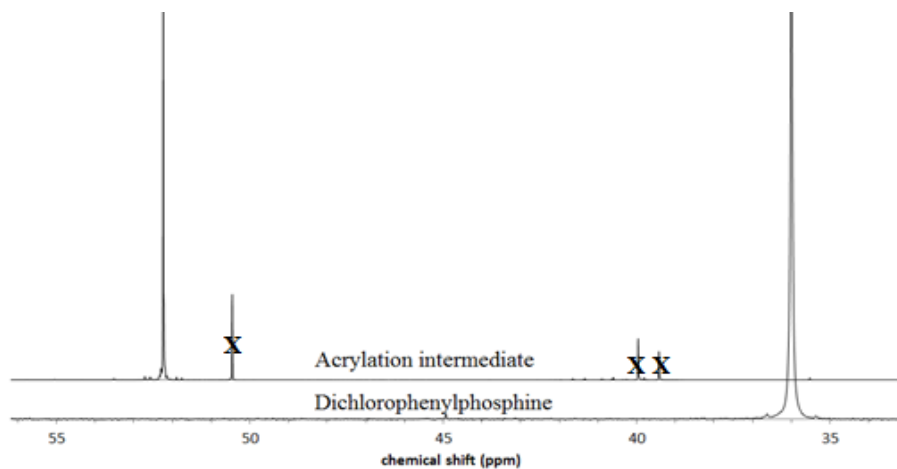
Figure 53: ^{31}P NMR spectrum (CDCl$_3$ of the conversion of DPP (t=0h) into acrylation intermediate (t=1h30)

Another way to synthesize the 2-POO from DPP is to hydrolyze the acrylation intermediate using one equivalent water (Scheme 6). The problem encountered in this case is that the "equivalent" is dependent on the purity of the DPP at the beginning of the reaction. If a part of DPP is already hydrolyzed through handling, it is difficult to determine the necessary amount of water. In the case of an excess of water, a mixture of 2-POO and 3-HPP is obtained (2-POO is itself sensitive to water and ring-opens in that case). Moreover, the release of hydrochloric acid in the presence of water leads to H$_3$O$^+$Cl$^-$ salts that remain in the mixture. The latter does not permit the crystallization of 2-POO in chloroform/Et$_2$O mixture, or leads to brown crystals. These H$_3$O$^+$Cl$^-$ salts can be identified in ^{1}H liquid-state NMR as a fine peak with high chemical shift (around 11 ppm).
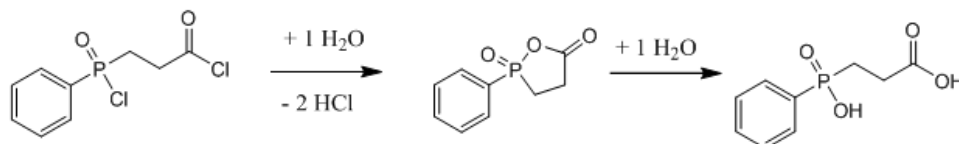
Scheme 6: hyrolysis of the acrylation intermdiate into 2-POO and into 3-HPP

A complete hydrolysis of the acrylation intermediate was however possible, leading to 3-HPP. In this case, water is slowly added to the acrylation intermediate (dropwise in a first step because of the very exothermic release of hydrochloric acid). After the complete hydrolysis, a large excess of water was added and the reactor was cooled down to 5 °C. After a couple of hours, 3-HPP precipitated. Following reaction depicted in Scheme 4 , 2-POO could then be obtained.

Liquid-state ^{13}C and ^{1}H NMR can be useful tools to achieve more than substance identification via report of chemical shifts and integrals. In the liquid state, molecules are generally in a dynamic state, and they adopt various conformations which are summed into one spectrum. When an atom cannot adopt various configurations (nonequivalent or locked configuration), this leads to a different multiplicity of the signals. In the case of 2-POO, this specific asymmetry is observed in the P-CH$_2$-CH$_2$-C structure. The protons of the CH$_2$ center are not equivalent due to the 3D structure of the molecule (Figure 54) and the possible asymmetric center on the phosphorus atom (sp^3). The corresponding ^{1}H NMR spectrum (Figure 55) shows a particular second order coupling structure, with

high multiplicity. The "twin" protons of the CH_2 in fact couple with each other, then with the other close CH_2 and finally with phosphorus, which leads to this particular multiplicity.
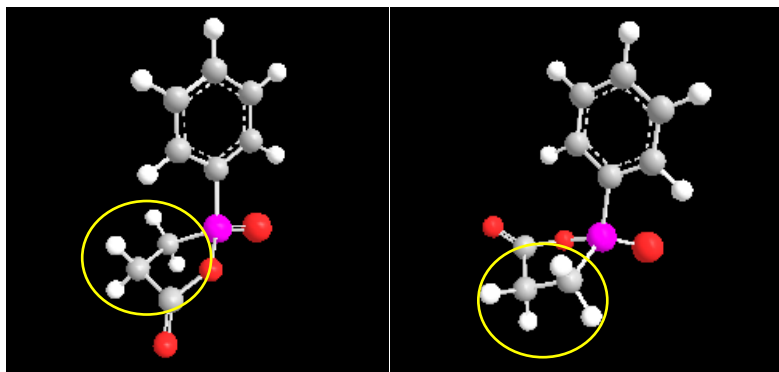
Figure 54: 3D view of possible configurations of 2-POO molecule
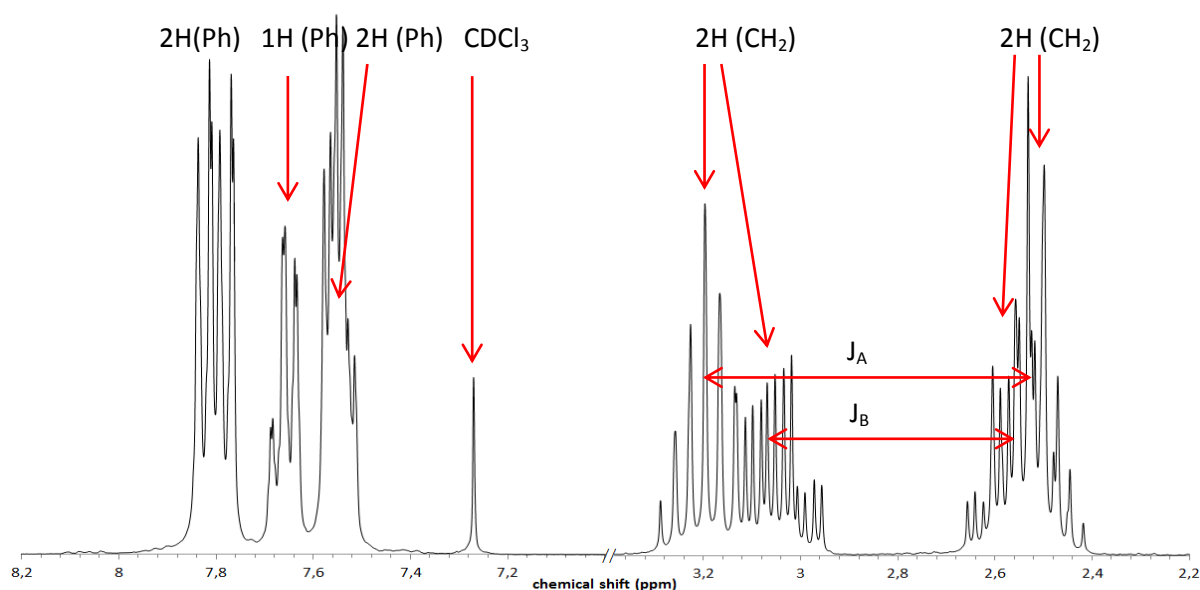
Figure 55: ^{1}H liquid-state NMR spectrum of 2-POO

III.1.3   Synthesis of Blöcker's amides

The studied phosphinate salts are first synthesized by the condensation of amines with 2-POO to yield amides of 3-(hydroxy(phenyl)phosphoryl) propanoic acid, with which aluminum salts are synthesized in a second reaction. These syntheses were based on Blöcker's procedures [135] as considered in the previous partnership with BASF SE. However, procedures need to be adapted in order to precipitate or crystallize the expected products.

Acetonitrile (ACN) was used as solvent for the syntheses based on mono-amines. As in the case of Louisy's work [20], dimethylformamide (DMF) was convenient for the reactions with diamines, in spite of its relatively high toxicity. A lower temperature was needed for the reaction with ethylene diamine due to its lower boiling point (116 °C) compared to other diamine reagents.

In the first steps of the project, it was observed that the evaporation of the solvent did not lead to a solid but to a viscous residue. ^{1}H NMR analyses of the latter showed the products still contained unreacted starting materials and potentially the ammonium salt of the corresponding phosphinic

acid (Scheme 7). Washing the residue with methanol did not lead to crystallization nor to precipitation of the product. Another purification method was thus developed.
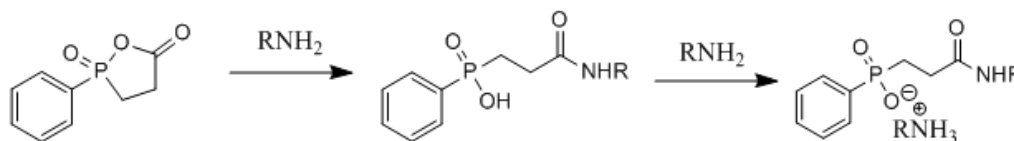
Scheme 7: Formation of Ammonium salt of Phosphinic acid after reaction of 2-POO with and excess of amine

As the products are phosphinic acid derivatives, they are soluble in basic water. This property allowed their easy purification by extraction as many solvents of the reagents are not miscible with water, mainly Et$_2$O and dichloromethane (DCM). A summary of the procedures used to prepare the amine-based phosphinic acids is reported in Table 14.

Table 14: Summary of the protocoles of synthesis of amine-based phosphinic acids

Reagent	Solvent	Temp. (°C)	Time (h)	Purification	Yield (%)
aniline	ACN	80	4	Extraction with Et$_2$O in NaOH 1M	90
benzyl amine	ACN	80	4	Extraction with Et$_2$O in NaOH 1M	64
ethylene diamine	DMF	90	3	Extraction with DCM in NaOH 1M	72
p-phenylene diamine	DMF	110	3	Extraction with DCM in NaOH 1M	60
piperazine	DMF	110	4	Extraction with DCM in NaOH 1M	33

The reaction of aniline with 2-POO in ACN at 80 °C allowed obtaining the phenyl amide of 3-(hydroxy(phenyl)phosphoryl) propanoic acid (PA-3-HPP) following the procedure used by Louisy (Scheme 8). The product precipitates after reaction. A purification was performed with Et$_2$O after dissolving PA-3-HPP in basic water and re-acidificating led to a yield of 90%.
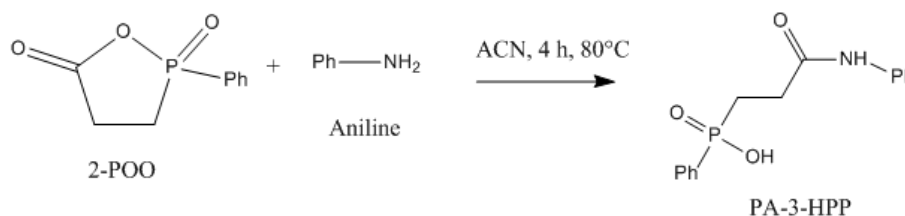
Scheme 8 : Synthesis of phenyl amide of 3-(hydroxy(phenyl)phosphoryl) propanoic acid (PA-3-HPP)

It should be highlighted that the oxaphospholane structure in 2-POO can present two reactive centers: the phosphoryl and the carbonyl structures. In the case of a reaction of the amine on the phosphoryl center, a phosphamide can be formed. This reaction induces much more complex ^{31}P NMR spectra.

An additional splitting of the peak due to the coupling between phosphorus atom and N-H proton would have been observed in the case of primary amines. The observation of this phenomenon in ^{13}C or ^{1}H NMR would be trickier. In our case, ^{31}P spectra (illustrated by an example with PA-3-HPP in Figure 56) show a specific multiplicity due to spin-spin coupling (J_{PCH}=11 Hz) with CH$_2$ and Ph protons (-CH$_2$-P(O)OH-Ph) which indicates the reaction occurs on the carbonyl center.
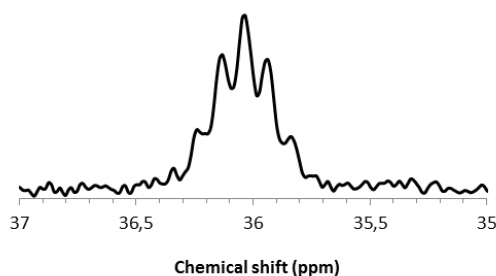
Figure 56: 31P liquid-state NMR spectrum of PA-3-HPP, DMSO, no decoupling

The synthesis of benzyl amide of 3-(hydroxy(phenyl)phosphoryl) propanoic acid (BA-3-HPP) was achieved by reacting benzyl amine with 2-POO in ACN at 80 °C (Scheme 9). The procedure used by Louisy needed to be adapted as the product did not precipitate in ACN. The addition of Et$_2$O at room temperature however allowed precipitating the BA-3-HPP. Again, a further purification with Et$_2$O in basic medium led to the re-precipitation (back to acidic medium) of the purified product. The yield was 64%.
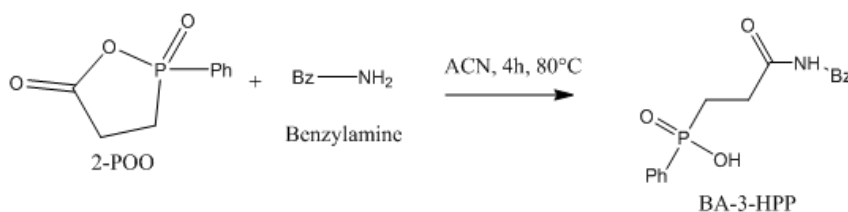
Scheme 9 : Synthesis of benzyl amide of 3-(hydroxy(phenyl)phosphoryl) propanoic acid (BA-3-HPP)

The use of ethylene diamine as nucleophilic reagent to open the ring of 2-POO led to the crude ethylene diamide of 3-(hydroxy(phenyl)phosphoryl) propanoic acid (EDA-3-HPP, Scheme 10) with a yield of 72%. The reaction needed dimethylformamide (DMF) as a solvent and Et$_2$O was used as co-solvent in order to precipitate EDA-3-HPP. In Louisy's work, DMF was evaporated and methanol was used to wash the product but in our case, EDA-3-HPP was soluble in methanol and not recovered once the DMF was eliminated. Impurities were then removed by extraction with dichloromethane, after dissolving the crude product in basic water. Re-acidification led to the precipitation of EDA-3-HPP.
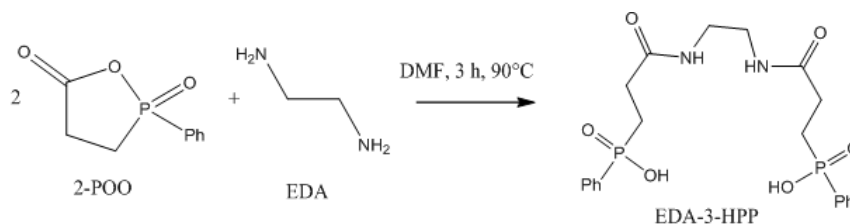
Scheme 10: Synthesis of ethylene diamide of 3-(hydroxy(phenyl)phosphoryl) propanoic acid (EDA-3-HPP)

When p-phenylene diamine was added to 2-POO in DMF at 110 °C, p-phenylene diamide of 3-(hydroxy(phenyl)phosphoryl) propanoic acid (PPD-3-HPP, Scheme 11) was obtained after evaporation of the DMF, extraction of impurities with dichloromethane (using basic water as described previously). Again, this method was needed as the product did not precipitate as in Louisy's work. The product was recovered by turning back to acidic medium. The yield was 60%.
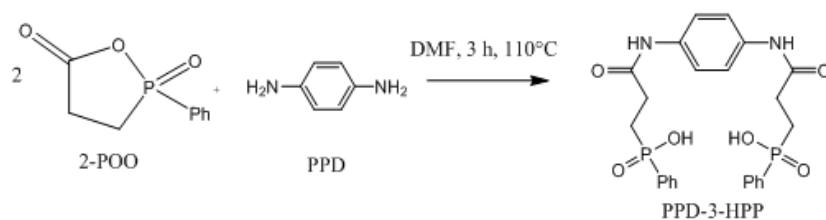
Scheme 11 : Synthesis of p-phenylene diamide of 3-(hydroxy(phenyl)phosphoryl) propanoic acid (PPD-3-HPP)

The reaction of piperazine with 2-POO following Blöcker's procedures **[135]** (Scheme 12) did not yield piperazine diamide of 3-(hydroxy(phenyl)phosphoryl) propanoic acid as expected but led to a mixture of reactants and mono- and diamide products (observed in ^{1}H NMR). A change of solvents (DMF or ACN) or the use of a catalyst (triethylamine) did not permit to obtain the expected diamide alone. Thus, a purification step was necessary, using the same method of extraction as above, with dichloromethane in basic medium. The re-precipitation in acidic medium led only to 33% yield, illustrating the incomplete disubstitution reaction. This fact is easily explained by the steric congestion of piperazine, which is the only secondary amine used in this study. The attack of a cyclic secondary amine on a structure with steric congestion logically leads to a lower yield and incomplete substitution.
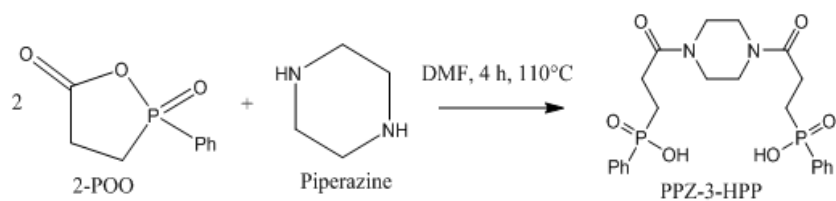
Scheme 12: Synthesis of piperazine diamide of 3-(hydroxy(phenyl)phosphoryl) propanoic acid (PPZ-3-HPP)

In ^{13}C proton decoupled NMR, the carbon of the carbonyl of amides shows up as a doublet, as depicted in the example in Figure 58. As there is no other possible coupling in the molecule, this multiplicity should be attributed to asymmetric environments of this carbon. Indeed, carbonyls generally belong to structures that cannot rotate freely **[148, 149]**. This implies the molecules could adopt two specific configurations in solution, probably due to hydrogen bonds (illustrated in yellow in Figure 57). Favored configurations are a fact which should be highlighted as it can have an influence on the thermal behavior of the products. Afterwards, the phosphinic acids need to be transformed into salts. This undoubtedly changes the configurations of the molecules.
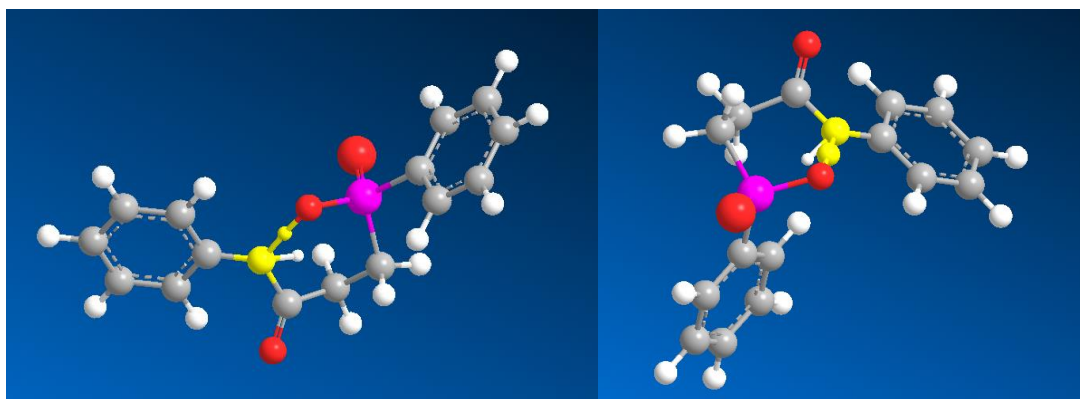
Figure 57: Possible configurations of PA-3-HPP after intramolecular hydrogen bonding
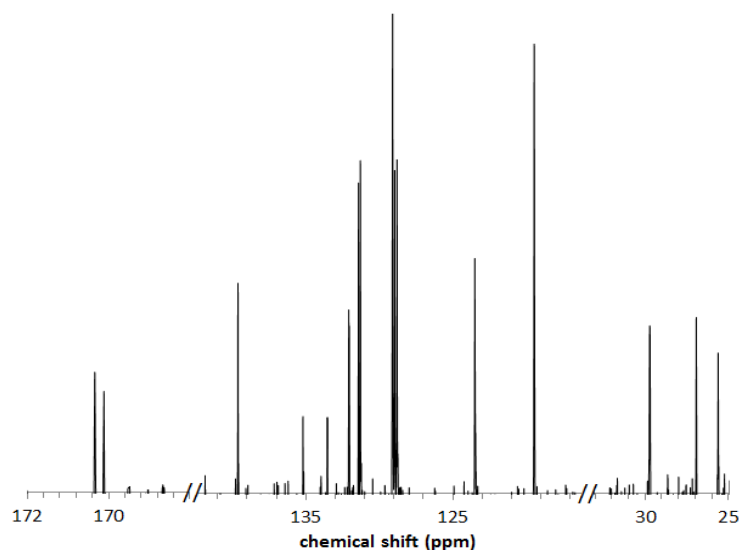
Figure 58: 13C liquid-state NMR spectrum of BA-3-HPP

III.1.4 Synthesis of phosphinate salts

PA-3-HPP, BA-3-HPP, EDA-3-HPP, PPD-3-HPP and PPZ-3-HPP were treated with aluminum isopropoxide in an ethanol/water mixture at 80 °C for 8h (Scheme 13). The corresponding aluminum salts precipitate after the reaction, yielding 55% product in the case of PA-3-HPP, BA-3-HPP, EDA-3-HPP and PPZ-3-HPP, and 90% in the case of PPD-3-HPP.
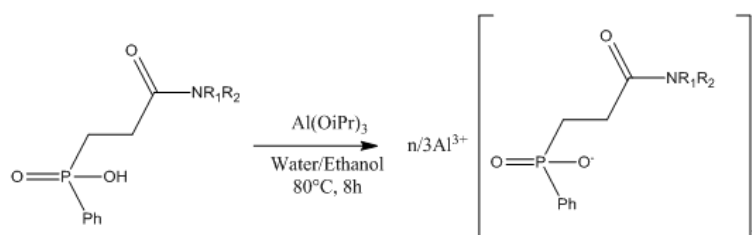
Scheme 13: General synthesis of aluminium phosphinate salts from amides of 3-HPP

Each product was then characterized by elemental analysis. The experimental mass fractions in % compared to the theoretical mass fractions (Theo. MF, calculated by Equation 3, where *N theo$_i$* represents the number of atoms i in the theoretical neutral molecule and Ma$_i$ the atomic mass of i) are reported in Figure 59. It should be highlighted that the values for Oxygen atoms are calculated as the difference of other results to 100% (100 - $\sum_i$ Exp MF$_i$).
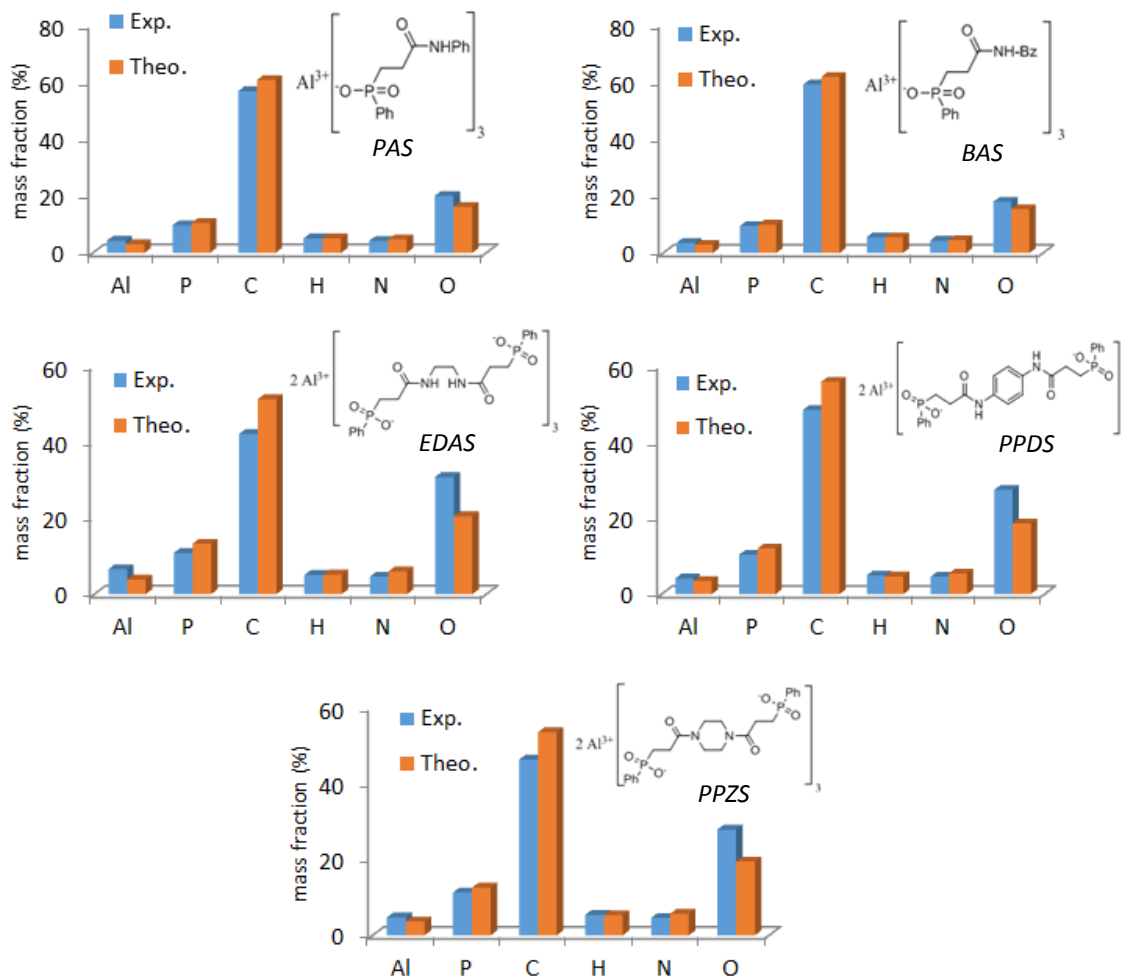
Figure 59: Experimental and theoretical mass fractions of atoms in elemental analysis of phosphinate salts

$$Theo\ MF_i = \frac{N\ theo_i\ \times\ Ma_i}{\sum(N\ theo_i\ \times\ Ma_i)} \times 100$$

Equation 3

The mass fractions do not report significant differences between experimental and theoretical results. Actually, aluminum, phosphorus and nitrogen atoms represent a very small fraction of the mass of the molecule, so that a significant defect or excess of the atom is not easily observed through mass fractions.

To overcome this problem, on the basis of experimental mass fractions (Exp MF), the experimental number of atoms (N exp_i) can be obtained by a rationalization to the fraction of phosphorus; phosphorus is in fact the only atom which should be found in known number in first reactant (2-POO) and is not added through reactions. That is the reason why it was chosen as reference. The way to obtain N exp_i is reported in Equation 4, and can be compared to the number of atoms in the neutral expected molecule (N $theo_i$). The ratio between N exp_i and N $theo_i$ indicates the correlation between theoretical and experimental values and was equal to 100 % in the case of phosphorus. The results are summarized in Table 15.

$$N\ exp_i\ =\ \frac{Exp\ MF_i\ \times\ Theo\ MF\ (P)}{M_i \times Exp\ MF\ (P)}$$

Equation 4

Table 15: elemental analysis of synthesized phosphinate salts

		Al	P	C	H	N	O
PAS	N exp	1.5	3.0	45.4	49.0	2.9	12.0
	N theo	1	3	45	45	3	9
	N exp / N theo (%)	152.7	100.0	100.9	108.9	96.3	133.5
BAS	N exp	1.3	3.0	48.1	54.1	3.0	11.0
	N theo	1	3	48	51	3	9
	N exp / N theo (%)	129.9	100.0	100.2	106.1	100.7	121.8
EDAS	N exp	4.2	6.0	60.3	86.9	5.6	33.1
	N theo	2	6	60	72	6	18
	N exp / N theo (%)	209.3	100.0	100.5	120.7	93.6	183.7
PPDS	N exp	2.8	6.0	72.3	88.7	5.9	30.8
	N theo	2	6	72	72	6	18
	N exp / N theo (%)	137.7	100.0	100.5	123.2	97.7	171.0
PPZS	N exp	2.9	6.0	63.6	88.6	5.4	28.7
	N theo	2	6	66	78	6	18
	N exp / N theo (%)	144.3	100.0	96.4	113.6	90.0	159.4

In Table 15, it is noteworthy that there is an excess of Al (30 to 110%) compared to our calculation, probably due to the presence of Al-O-Al bonds in the solid network or of aluminum-hydrate terminations whatever the salts. The possible presence of Al-OH groups would also be correlated with the excess of Oxygen (20 to 80%) and Hydrogen (6 to 20%) in the elemental analysis of the products. However, the quantification and identification of such groups is quite hazardous since on the one hand values for O atoms are obtained by difference, and on the other hand moisture can also contribute to the excess of O and H. Another hypothesis in this case is a partial substitution of the phosphinic acid. The formation of P-OH terminations and Al-OH terminations instead of the P-O-Al group would explain an excess of O and H atoms, but also a possible excess of Al. This particular case of partial substitution can be highlighted by solid-state NMR, which will be presented hereafter. Carbon and nitrogen in any case show good correlation (up to 4% difference for C, 1 to 10% for N, knowing that only 3 or 6 N atoms are expected in the molecules, which implies a higher relative error on calculations).

The phosphinate salts were also analyzed by ^{13}C, ^{31}P and ^{27}Al solid-state NMR. In solid-state, NMR brings information on the chemical environment of atoms, but also on the global structure of the solid. Since carbon nuclei are not affected by homonuclear (dipolar) or quadrupolar couplings, the variations in the shape of the peaks shall be explained by a modification of the chemical environment. Sharp peaks generally indicate an ordered (crystalline) structure, whereas broader peaks suggest disordered (amorphous) structures.

The ^{13}C NMR spectra of PAS (Figure 60.a), BAS, EDAS and PPZS exhibit chemical shifts close to those measured in liquid-state NMR for the phosphinic acid. The peaks are broad which indicates the

products do not crystallize in a given form. On the contrary, the spectrum of PPDS (reported in Figure 60.b) exhibits sharp peaks, illustrating a more crystalline structure. A hypothesis in this case is that the compound is mainly under its unsubstituted phosphinic acid form, which is probably more crystalline than the salt form due to hydrogen bonding and stacking of aromatic structures. The other solid-state NMR analyses should confirm this hypothesis.

a)

b)
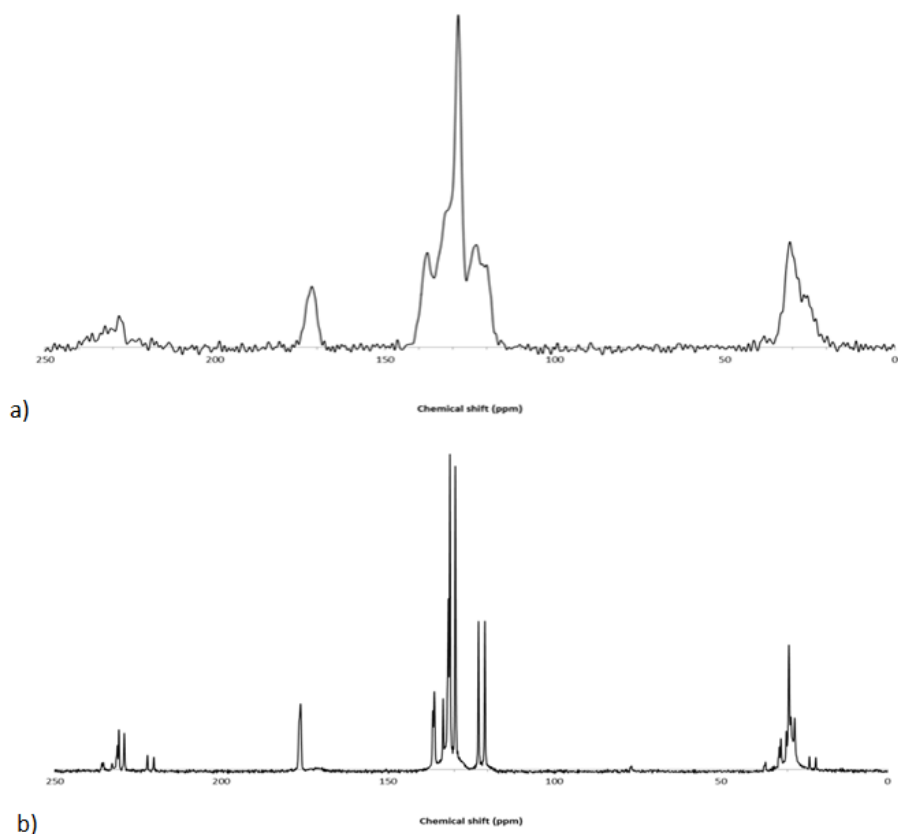
Figure 60: ^{13}C solid-state NMR of a) PAS and b) PPDS

The ^{31}P solid-state NMR spectra of the salts exhibit the typical ^{31}P resonance of aluminum phosphinates centered around 24-26 ppm (Figure 61.a). However, the bands spread out over a relatively wide range of frequencies, up to that of phenylphosphinic acid **[150]**, with a shoulder centered around 36 ppm. This suggests the presence of residual phosphinic acids in the salt. The width of the bands confirms the assumption of a disordered structure for the salts. PPDS exhibits a sharp ^{31}P band at 35 ppm (Figure 62.a), showing on the contrary a crystalline character, and the presence of phosphinic acid mainly.

a)

b)
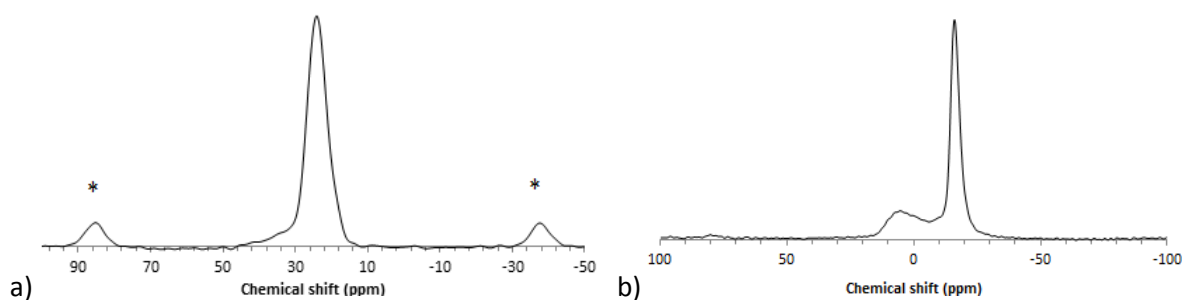
* denotes spinning side bands
Figure 61: a) ^{31}P and b) ^{27}Al solid-state NMR of PAS

The ^{27}Al solid-state NMR analyses confirm most of the observations made by ^{13}C and ^{31}P NMR. The salts exhibit a main signal centered around -16 ppm (Figure 61.b), corresponding to the typical chemical shift of octahedral Al atoms coordinated to eight framework oxygen atoms with phosphorus in their second coordination sphere **[84, 151]**. In all spectra, another band with a chemical shift around 6 ppm can be seen as a broad shoulder downfield from the site at -16 ppm Figure 61.b).

a)

b)

* denotes spinning side bands
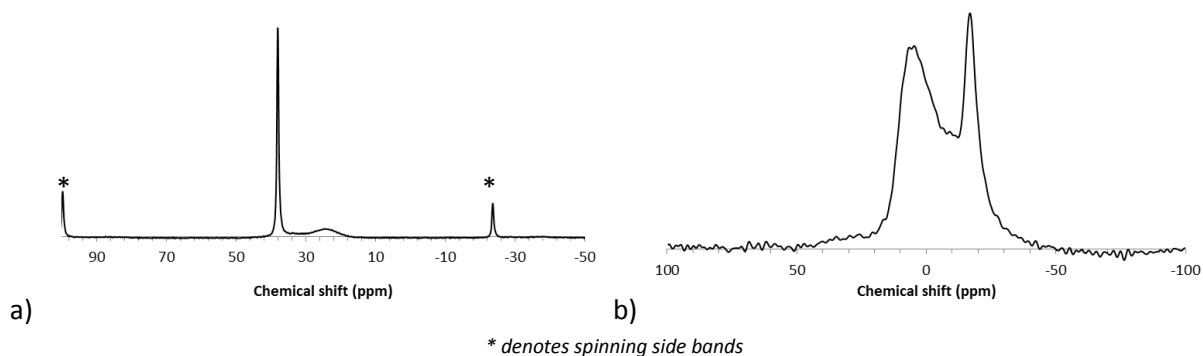
Figure 62: a) 31P and b) 27Al solid-state NMR of PPDS

In the literature **[151, 152]**, this kind of band at 6 ppm is attributed to aluminate-hydrate complexes (possibly containing hydroxo groups). The presence of such bands in the spectrum of aluminum phosphinates would indicate whether an excess of aluminum atoms (under the form of aluminum hydrates) or an incomplete substitution of the phosphinic acid. Regarding the results obtained in ^{31}P solid-state NMR and elemental analyses, both hypotheses seem to be realistic (presence of phosphinic acid and significant Al-hydrate band).

In the [27]Al spectrum PPDS, the signal at 6 ppm is superimposed with the signal of the site at -16 ppm (Figure 62.b). The surface area of this second site is very important demonstrating that in that case, a large amount of aluminum hydrates is present. In the three-dimensional structure, both phosphinic acid (P-OH) and Al-OH groups may replace Al-O-P coordinates and lead to the large excess of O and H, which is consistent with previous elemental analyses.

In order to confirm previous assumptions and to check the coordination of Al atoms by P-O terminations, two-dimensional solid-state NMR was carried out. [27]Al-[31]P D-HMQC was carried out on the samples, and the 2D HMQC spectrum of PAS is reported in Figure 63. In this spectrum, the resonance located at the intersection of the ^{31}P and the [27]Al band illustrates the spatial proximity of Al and P atoms. This experiment confirms what is observed through interpretation of chemical shifts: the salts are composed of octahedral aluminum-oxygen framework with phosphorus close in the coordination sphere. The HMQC resonance is centered on the ^{31}P band at 24 ppm, and no resonance is observed at 36 ppm for the potentially "unsubstituted" phosphinic acid shoulder peak.
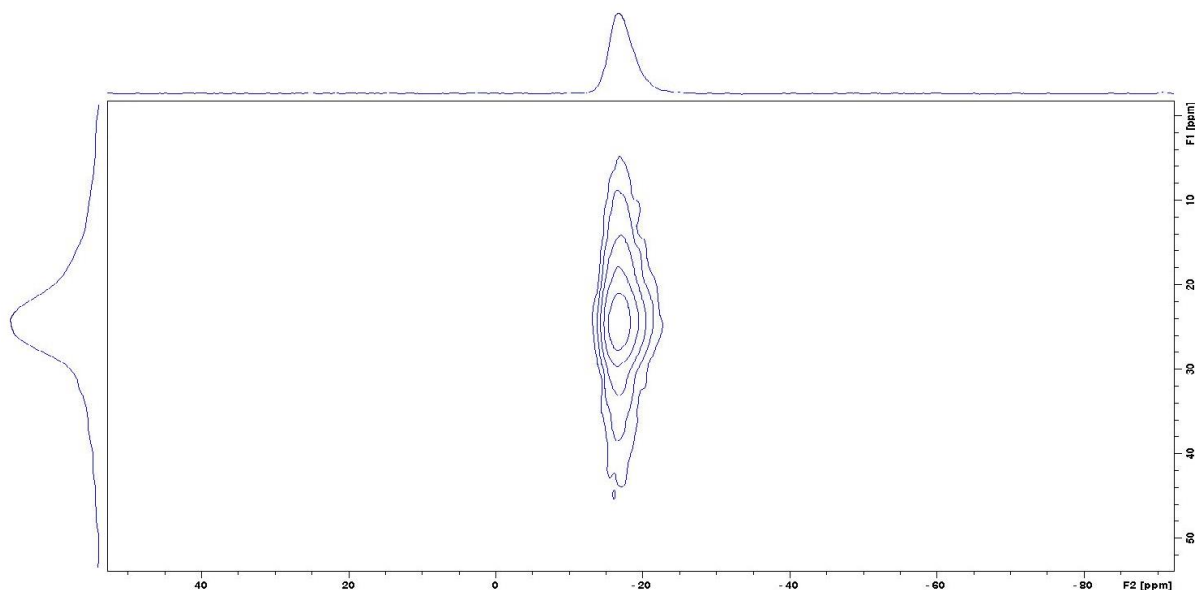
Figure 63: Two dimensional ^{27}Al - ^{31}P D-HMQC of PAS

Solid-state NMR and elemental analyses reported a potential presence of unsubstituted phosphinic acid molecules. Their potential impact on the matrix in which they can be incorporated should be taken into account. As a consequence, the salts were dispersed in deionized water to measure their pH. The results are reported in Table 16.

Table 16: measure pH of the phosphinate salts in water

Salt	PAS	BAS	EDAS	PPDS	PPZS	*Deionized water*
pH	4.7	2.1	3.1	3.1	3.2	5.5

All the salts are acidic, possibly due to the phosphinic acids or the presence of Al-OH groups, which under the form of aluminum trihydrate acts as amphoteric specie **[153]**. However there is no correlation between the aluminum excess in elemental analysis and pH measurements. PAS exhibits a pH of 4.7, really close to that of deionized water. EDAS and PPDS exhibit a pH of 3.1 and PPZS exhibits a pH of 3.2 which already represents a strong acidity. Finally BAS exhibits a pH of 2.1 which is the most acidic of the salts.

According to the solid-state NMR results, it was expected that PPDS should be the most acidic compound. Indeed, the solid-state NMR spectra demonstrated that this phosphinate is for its major part composed of unsubstituted phosphinic acid. This specie should have an important impact on pH measurements. However, it is not the case and it seems that there is no correlation between acidity and aluminum substitution. Possibly, the aluminum hydrate excess moieties could absorb acidity as they are amphoteric.

In most cases, industrial and commercial products are neutralized before use, to avoid any negative interaction with sensitive matrices. As a consequence, a neutralization of the synthesized phosphinate salts was carried out. Two different protocols were applied to PAS, depicted in Chapter II.

Both residues were analyzed in solid-state NMR and compared to PAS without further neutralization. The obtained spectra are reported in Figure 64. When PAS is washed with water, no significant

change is observed in the spectrum compared to non-washed PAS, and the mass of collected residue nearly equals the mass of PAS before washing (1.92 g collected, 96 wt% of starting material). The small amount lost should be due to handling the product through the washing protocol.

When it is washed with sodium carbonate, more mass is lost and only 1.43 g (71.5 wt%) residue are recovered. A decrease in the intensity of the peak of aluminum phosphinate (24 ppm) is observed in ^{31}P NMR, and the AlO$_4$ site (6 ppm) in ^{27}Al NMR is sharply increased. This implies a change in the structure of the salt after washing with sodium carbonate. The hypothesis in this case is that sodium carbonate replaces aluminum with sodium in the phosphinate salt, making the latter soluble in water, and leaving the aluminum as metal hydrate. As a conclusion, washing the salts would not improve their properties, so that they will be used in their post-synthesis form (without neutralization) in the formulations.
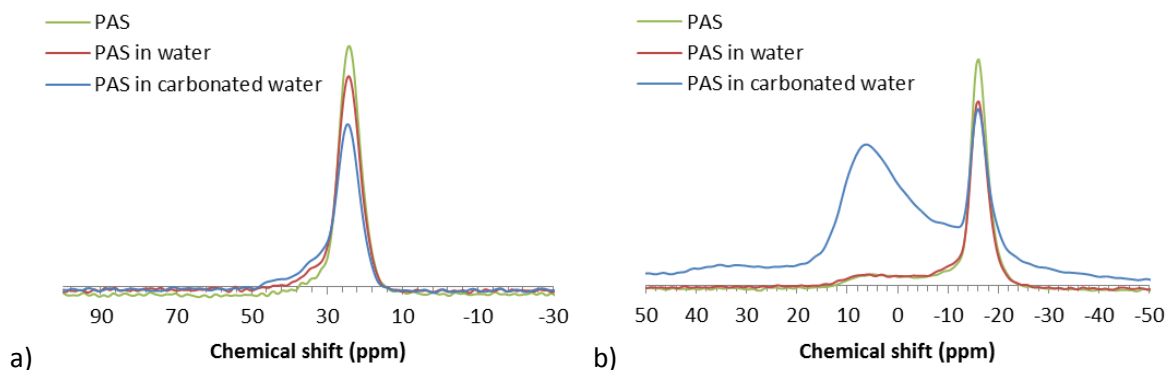
Figure 64: a) ^{31}P and b) ^{27}Al solid-state NMR of PAS, PAS washed in water, and PAS washed with sodium carbonate

III.2.   THERMAL BEHAVIOR OF THE SALTS

Before any use in targeted polymeric matrices, the thermal stability of the phosphinate salts has to be investigated. Each of the prepared phosphinate salts was exposed to a temperature ramp of 10 °C/min in air atmosphere. The curves are reported in Figure 65 and the characteristic temperatures and weight losses are reported in Table 17. As the main line of this work is to use the previously synthesized phosphinates in PBT and PA6, they need to be compounded in the matrices and thus stable at the processing temperatures. In the TGA presented hereafter, the processing temperature of PBT and PA6 will be illustrated by a dotted line.
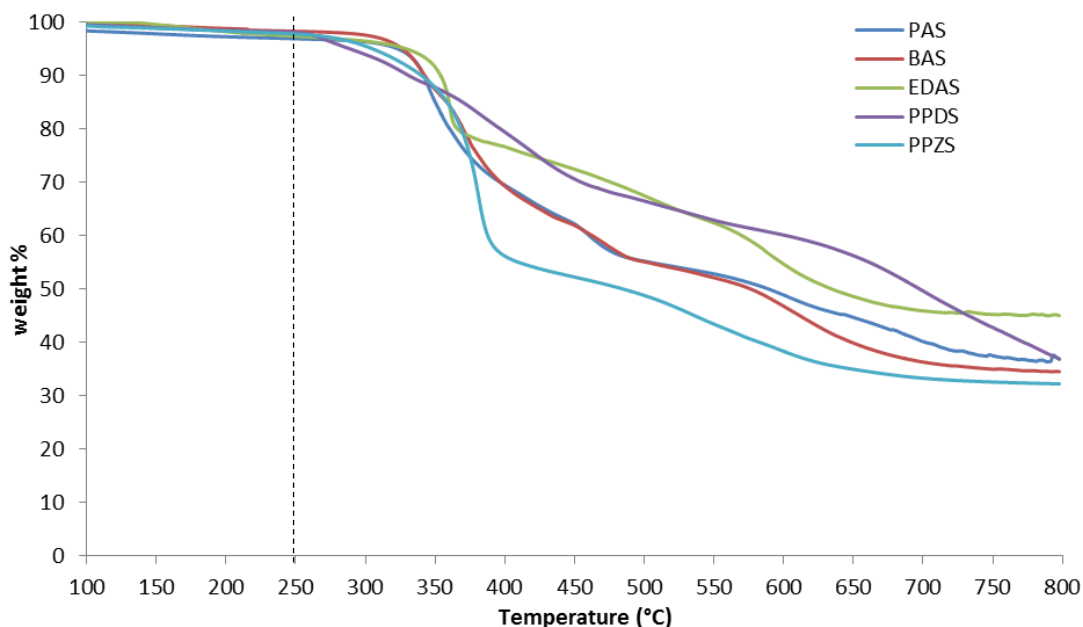
Figure 65: TGA curves of synthesized phosphinate salts, in air, 10 °C/min

It should be highlighted that Table 17 only reports up to three degradation steps. However, in air, regarding the complex shape of the TG curves, many thermo-oxidation reactions should occur that lead to multiple weight loss stages. Only the most important steps (corresponding to the main peaks in dTG) are reported in this study.

Table 17: TGA (10 °C/min in air) data for phosphinate salts

Product	Onset 1 (°C)	Max 1 (°C)	Residue 1 (wt%)	Onset 2 (°C)	Max 2 (°C)	Residue 2 (wt%)	Onset 3 (°C)	Max 3 (°C)	wt% at 800 °C
PAS	320	344	66	449	456	56	540	600	36
BAS	310	374	66	440	470	56	552	605	34
EDAS	327	360	78	550	590	-	-	-	45
PPDS	250	413	70	455	522	60	588	692	37
PPZS	300	380	55	470	550	-		-	32

PAS and BAS behave quite similarly and degrade in three main steps. The first onset is observed at 320 °C and 310 °C respectively and the first degradation steps show a maximum degradation at 344 °C and 374 °C, leading to 66 wt% residue in both cases. The second step starts at 449 and 440 °C respectively, with maxima at 456 and 470 °C, leaving 56 wt% residue in both cases. The last step starts at 540 and 552 °C, reaching maximum loss rates at 600 and 605 °C respectively. The final residue yields are 36 and 34 wt%.

EDAS degrades in two main steps. The first onset is observed at 327 °C and this step presents a maximum of degradation at 360 °C, leaving 78 wt% residue. The second step starts at 550 °C and reaches its maximum degradation at 590 °C. The product yields 45 wt% residue at 800 °C.

PPDS degrades following three main steps. The first step shows an onset in the earliest stages of the ramp at 250 °C, and shows a peak of loss rate at 413 °C leading to 70 wt% residue. The second step starts at 455 °C and reaches a maximum of degradation at 522 °C. The last steps onsets at 588 °C and reaches a maximum of degradation at 692 °C. It is noteworthy that even if three main steps are identified, the product keeps degrading quite constantly upon heating. Moreover, it has to be noticed that at 800 °C, the degradation still occur. The residue yield at 800 °C is 37 wt%.

Finally, PPZS degrades following two main steps. The first step starts at 300 °C, and shows a maximum of degradation at 380 °C leading to 55 wt% residue. The second step starts at 470 °C and reaches a maximum of degradation at 550 °C. The residue yield at 800 °C is 32 wt%.

In the TGA under air atmosphere, the five salts are divided in three groups. PPZS exhibits the highest degradation among the salts at 400 °C (45 wt% loss) and also the lowest residue at 800 °C. PAS and BAS behave similarly and correspond to an "intermediate" degradation (34 wt% loss at 400 °C). EDAS and PPDS achieve the highest stability at 400 °C (22 and 30 wt% loss respectively), and even above, the TG profiles of these two salts remain higher than for the other salts. From these first results, a relation can be made between structure and thermal stability. PPZS is the only secondary diamide among the five salts, which was also difficult to prepare. It is reasonable to assume that this product could thus be less stable due to the absence of hydrogen bonding specific to primary amides. However it is not consistent with the fact that it is a diamide, which should exhibit a higher thermal stability, at least higher than mono-amides. Again, PAS and BAS achieve intermediate and similar thermal stabilities since they are both mono-amide and aromatic-based with very close structures (aniline and benzylamine). The higher thermal stability achieved by EDAS and PPDS would be explained by the fact that these salts are diamides. The first step of degradation of PPDS leads to the lowest stability among the salts however, which should be due to the wrong substitution of the phosphinic acid. Whatever the salt, the thermal stability at the processing temperature is suitable for extrusion, as less than 3 wt% are lost at 250 °C.

The phosphinate salts were submitted to the same 10 °C/min ramp but using N_2 as carrier gas. The curves are reported in Figure 66 and the characteristic degradation temperatures are reported in Table 18. Similarly to what was observed under air, EDAS and PPZS degrade following two steps and PAS, BAS and PPDS degrade in three steps. However, it can be observed that whereas under air, the maximum degradation temperature of the first step is observed in the same temperature range whatever the salts (340-400 °C except for PPDS), it is not the case when the TGA are carried out under N_2. The maximum degradation temperature of the first degradation step is indeed observed in a larger range (from 360 to 479 °C) if we do not consider the low first step of PPDS.

The first degradation step of PAS starts at 346 °C and the maximum of degradation is observed at 360 °C, with a residue of 67 wt%. The second step presents an onset temperature of 430 °C and rapidly reaches its maximum at 440 °C. Before the third step, the residue is equal to 45 wt%. This last step onsets at 623 °C and reaches its maximum at 646 °C. The final residue at 800 °C is 35 wt%.

BAS behaves quite similarly to PAS as observed under air. Its first degradation step is observed at 357 °C with a maximum loss rate at 381 °C leading to a residue of 67 wt%. The second step starts at

462 °C and reaches a maximum at 479 °C, leaving 45 wt% residue. The final step starts at 656 °C with a maximum at 675 °C. The residue at 800 °C is 38 wt%. The thermal behavior of BAS and PAS are thus very close which can be reasonably explained by the fact that their structures are very close.
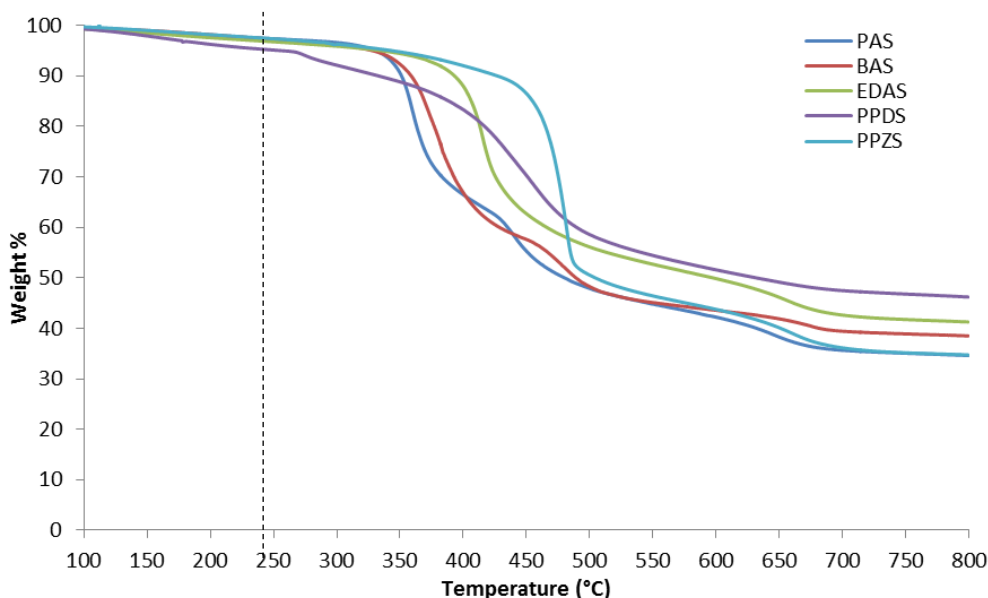
Figure 66: TGA curves of synthesized phosphinate salts, in N$_2$, 10 °C/min

EDAS degrades first with an onset temperature at 399 °C and a maximum loss rate at 416 °C. Before the second step, starting at 630 °C and with a maximum at 656 °C, the residue is equal to 56 wt%. The final residue at 800 °C is 41 wt%.

Again and as observed when the TGA are carried out under air atmosphere, PPDS degrades at lower temperatures. A first pre-degradation step can be observed from 267 °C. The first maximum loss rate is observed at 276 °C and the residue after this step is 92 wt%. This is consistent with the partial substitution of the phosphinic acid likewise under air. The second step of degradation of PPDS starts at 406 °C and reaches its maximum at 455 °C, with a residue of 63 wt%. The additive then degrades slowly up to 800 °C leading to a residue of 46 wt%.

Finally, PPZS degrades with a first step presenting an onset temperature at 464 °C and a maximum loss rate at 479 °C. The residue before the second degradation step is 51 wt%. The second step starts at 637 °C and exhibits a maximum loss rate at 661 °C. The final residue yield is 35 wt% at 800 °C.

Table 18: TGA (10 °C/min in N$_2$) data for phosphinate salts

Product	Onset 1 (°C)	Max 1 (°C)	Residue 1 (wt%)	Onset 2 (°C)	Max 2 (°C)	Residue 2 (wt%)	Onset 3 (°C)	Max 3 (°C)	wt% at 800 °C
PAS	346	360	67	430	440	46	623	646	35
BAS	357	381	67	462	479	45	656	675	38
EDAS	399	416	56	630	656	-	-	-	41
PPDS	267	276	92	406	455	63	-	-	46
PPZS	464	479	51	637	661	-	-	-	35

In the TGA under N$_2$ atmosphere, the behavior of the salts is similar to that achieved under air atmosphere, except for PPZS, and the same three categories drawn before cannot be drawn again. In these conditions, PAS and BAS achieve equivalent thermal stabilities and their first degradation step

occurs at lower temperatures than the other salts. This is consistent with their similar mono-amide structure, as depicted before. It should however be highlighted that PPDS exhibits a "pre-degradation step" (about 10 wt% loss) which occurs before the first degradation of these salts. EDAS and PPDS achieve in these conditions "intermediate" thermal stabilities, higher than PAS and BAS, correlated to their diamide structure. PPDS is still degrading quite constantly upon heating and should be considered as particular case, even if its stability is close to that of EDAS between 450 and 800 °C. On the opposite to the TGA carried out under air atmosphere, PPZS achieves the highest thermal stability concerning its first degradation step, but the residue is the lowest among the salts at 800 °C. This difference of behavior between air and N_2 suggests that PPZS is more sensitive to thermo-oxidation than the other salts. Under nitrogen atmosphere, the thermal stability of the salts at 250 °C is suitable for extrusion. All salts exhibit a weight loss of 2 % except PPDS which exhibits 5 wt% loss.

It is well established that in the case of aluminum phosphinates, aluminum can react with phosphorus oxidized species to form aluminophosphonates and then aluminophosphates [154]. In order to evaluate the yield of residue out of Al-P species, the maximum theoretical weight % of aluminophosphates ($AlPO_4$ that could be obtained from Al and P atoms, considering a complete oxidation without formation of aluminophosphonates) is compared to the experimental residue yield (Table 19). Average molecular masses are calculated for a neutral molecule. For example, it is considered that EDAS corresponds to $(EDA-3-HPP^{2-})_3 * 2\ Al^{3+}$ which can yield 2 x $AlPO_4$.

In all cases, the residue yield (35 to 46 wt%) is sharply higher than that calculated for the content in phosphorus and aluminium leading to aluminophosphates (13 to 17 wt% residue). That means these additives may yield char in addition to mineral parts such as $AlPO_4$. The char yield is also a key factor in fire retardancy, as the char would produce a barrier effect. However, its role in the mechanism of action of the various salts should be further confirmed. Indeed, the direct correlation between TGA residue and flame-retardant performance is debated in literature. Some authors observe a strong correlation between char yield and fire resistance [155]; this should be highlighted in the case of intumescent formulations, where char yield is capital. On the contrary, the results for phosphinates in LOI or UL-94 in the case of Louisy were not dependent on the TGA residues [20].

Table 19: Comparison between P and Al contents and residue yields in TGA

Product	Molecular mass (g/mol)	Expected yield $AlPO_4$ (wt%)	Residue yield (wt%)
PAS	891	13.7	35
BAS	933	13.1	38
EDAS	1404	17.4	41
PPDS	1548	15.8	46
PPZS	1482	16.5	35

In some cases, TGA analyses prove to be a valuable method to evaluate the possible interaction of an additive with a matrix for flame retardancy purposes. A degradation of the additive in the temperature range close to that of the matrix can be a key asset for the flame retardancy of the polymer [156]. Therefore, TGA was also carried out on PBTGF and PA6GF. The TGA curves are reported in Figure 67, and corresponding characteristic data are reported in Table 20.

Both matrices decompose in one step under nitrogen whereas under air, a second step corresponding to the thermo-oxidation of transient char appears at high temperature. The onset and the maximum of degradation of PBTGF and PA6GF occur in a range of 350-360 °C and 400-420 °C respectively. PAS and BAS exhibit a degradation onset in the range of that of matrices, particularly in N_2 (320 and 310 °C in air, 346 and 357 °C in N_2 respectively), but they reach their maximum of degradation at lower temperatures (344 and 374 °C in air, 360 and 381 °C in N_2 respectively). EDAS reaches its maximum degradation in the proper range (360 °C in air and 416 °C in nitrogen) but the degradation starts at higher temperature. Same considerations could be done with PPDS and PPZS, but indeed, no salt reaches both proper temperature ranges.
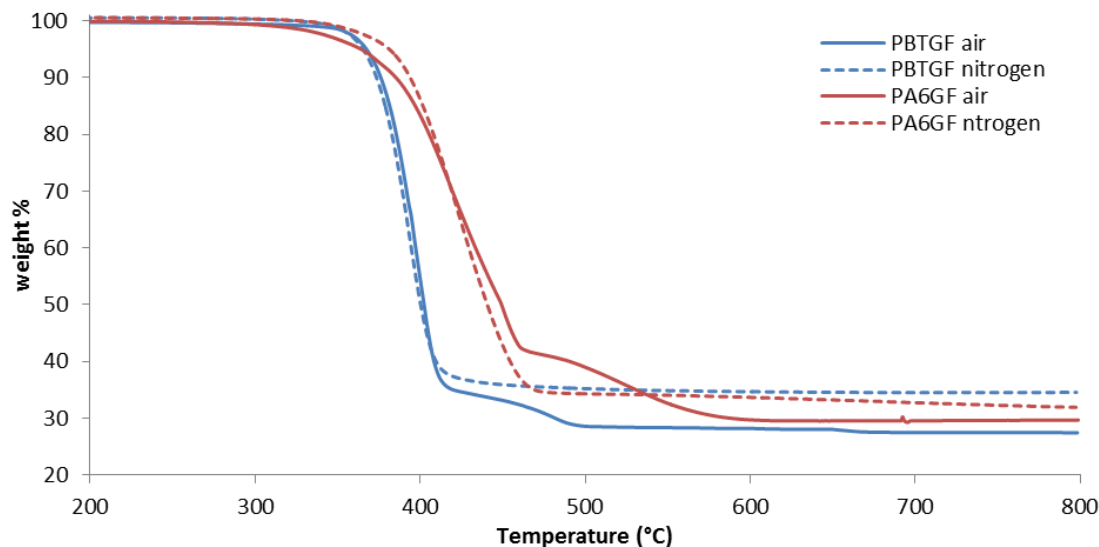
Figure 67: TGA curves of PBTGF and PA6GF in air and nitrogen at 10 °C/min

Table 20: TGA (10 °C/min in air or N_2) of PBTGF and PA6GF

Matrix	Atmosphere	Onset 1 (°C)	Max 1 (°C)	Residue 1 (wt%)	Onset 2 (°C)	Max 2 (°C)	wt% at 800 °C
PBTGF	air	362	399	35	461	480	28
PBTGF	N_2	352	401	34	-	-	34
PA6GF	air	360	420	42	490	525	32
PA6GF	N_2	365	420	35	-	-	34

Interestingly, as the temperatures of degradation of PA6 are slightly higher than those of PBT, and as four of the salts exhibit temperatures of decomposition that are lower than PBT, more interactions should be expected between PBT and the salts than between PA6 and the salts. This assumption is particularly true for PAS and BAS which present a first step of degradation in the onset of degradation of PBT. On the contrary, EDAS would present more interactions with PA6.

III.3. THERMAL BEHAVIOR OF THE FORMULATIONS: FR POTENTIAL

In the field of flame retardancy, interactions between additives and matrix generally give clues on the potential action of the additives. Stabilization or destabilization of the residue at given temperatures could indicate potential condensed-phase actions.

To properly evaluate the interactions between the additive and the matrix, TGA was first carried out on the formulated systems. For the sake of this manuscript, only PBTGF filled with phosphinate salts was studied under air atmosphere to eventually observe differences on the transient char. The formulations were cryo-grinded analyzed in TGA. The characteristic temperatures and weight losses obtained from the TG curves in Figure 68 are reported in Table 21.

Table 21: TGA (10 °C/min, air) data for PBTGF formulated with phosphinate salts

Product	Onset 1 (°C)	Max 1 (°C)	Residue 1 (wt%)	Onset 2 (°C)	Max 2 (°C)	wt% at 800 °C
PBTGF	362	399	35	461	480	28
PBTGF 20 wt% PAS	340	390	42	509	548	29
PBTGF 20 wt% BAS	350	394	46	526	539	29
PBTGF 20 wt% EDAS	343	379	52	480	530	31
PBTGF 20 wt% PPDS	332	395	45	499	545	27
PBTGF 20 wt% PPZS	340	380	44	435	535	30
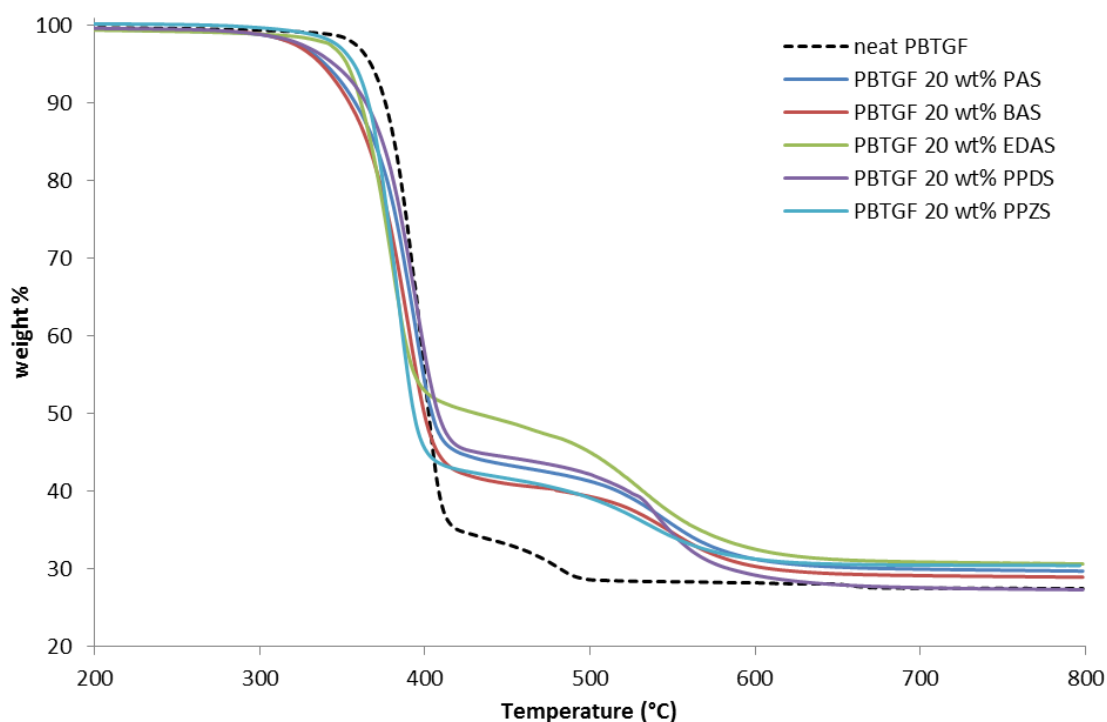
Figure 68: Thermogravimetric analysis of PBTGF with or without 20 wt% of designed phosphinate salts, 10 °C/min, air

Whether PBTGF contains or not phosphinate salts, it shows a similar thermal behavior presenting two steps of degradation. The virgin matrix shows a final residue yield is 28 wt% at 800 °C, corresponding to the effective loading of glass fibers, since PBTGF yields no carbonaceous char at 800 °C in air as it is a non-charring polymer **[140]**.

PBTGF loaded with 20 wt% PAS has a first step of degradation which starts at 340 °C and presents a maximum of degradation at 390 °C, yielding 42 wt% residue. The second step has an onset

temperature at 509 °C and reaches a maximum of degradation at 548 °C. The residue yield at 800 °C is 29 wt%.

PBTGF containing 20wt% BAS has a first step of degradation with an onset temperature of 350 °C and a maximum degradation temperature of 394 °C, yielding 46 wt% residue. The second step onsets at 526 °C and reaches a maximum of degradation at 539 °C. The residue yield at 800 °C is 29 wt%. Similarly to what was observed for pure additive, the thermal stability of both formulations (PBTGF loaded with 20 wt% PAS and BAS) are quite similar.

PBTGF flame retarded with 20 wt% EDAS has its first step starting at 343 °C for a maximum of degradation at 379 °C, yielding 52 wt% residue. Then, the second step starts at 480 °C for a maximum at 530 °C. The residue yield at 800 °C is 31wt%. It can be noted that the amount of transient char is the highest when EDAS is used as FR additive with PBT. This is consistent with the thermal stability of pure additive that is rather high in that range of temperatures.

The formulation PBTGF with 20 wt% PPDS has a first step of degradation starting at 332 °C to reach a maximum at 395 °C, yielding 45 wt% residue. The second step begins at 499 °C and reaches a maximum at 545 °C. The residue yield at 800 °C is 27 wt%.

Finally, PBTGF loaded with 20wt% PPZS has a first step of degradation starting at 340 °C and a maximum degradation at 380 °C, yielding 44 wt% residue. The second step starts at 435 °C and reaches a maximum degradation at 535 °C. The residue yield at 800 °C is 30 wt%.

These results allow drawing some general facts. EDAS and PPZS achieve a similar behavior in PBTGF (onset, maximum and residue), except the weight achieved in the transient char zone between 400 and 550 °C. This is consistent with the residue obtained in the first step of degradation of the salts studied alone. PAS, BAS and PPDS exhibit a similar behavior, which is unexpected considering the TG curves of PPDS alone. In this case, a possible hypothesis is to draw a relation between structure of the additive and properties. Aromatic-based additives (aniline, benzyl amine and phenylene diamine) would decompose and act the same way and aliphatic-based additives (piperazine and ethylene diamine) another way. It is well-known that additives containing aromatic rings tend to enhance the formation of a char, while it is not always the case of aliphatic ones.

The addition of salts (whatever among all the studied ones) has an influence on the yield of transient char, and also its thermal stability regarding oxidation. Indeed, the maximum degradation of second step is shifted to higher temperatures (530-550 °C) than PBTGF (480 °C), and the residue yield in this second step is about 10 to 15 wt% higher in the presence of phosphinate salts. These observations suggest an action in the condensed phase, which should be considered in further investigations.

Finally, it is possible to compare the residue yields of the neat components of the matrix and the loaded polymer calculating the difference mass loss curve (as described in the experimental part) and considering its value at 800 °C. The data are reported in Table 22.

The expected values for the residue yield are in accordance with experimental residues (around 0.5 to 2% difference, which is in the margin of error). The additive does not seem to enhance the stability of the final residue at high temperature. The amounts of residue are consistent with those drawn in Table 19, which indicates that the salts leave a residue. Without residue, the GF content should be

24 wt% (30 wt% x 0.8 parts in the formulation), so that there is around 6 wt% more corresponding to the residue for 20 wt% additive content.

Table 22: Comparison between expected residue yield and experimental residue yield at 800 °C

Formulation	Expected residue (wt%)	Experimental residue (wt%)	ΔM at 800 °C (%)
PBTGF 20wt% PAS	29.6	29.0	0.6
PBTGF 20wt% BAS	29.2	27.0	2.2
PBTGF 20wt% EDAS	31.4	31.0	0.4
PBTGF 20wt% PPDS	29.6	30.0	0.4
PBTGF 20wt% PPZS	28.8	30.0	1.2

Difference weight loss curve (ΔM) also permits to highlight the interactions between the components of the formulation but in the whole range of temperatures (from ambient to 800 °C). Figure 69 clearly shows some interactions between the components of the mixture. It is observed that all the additives behave in a similar way. Between 350 and 410 °C, a strong destabilization (-5 to -17 wt%) is observed, whereas between 410 and 600 °C, a stabilization of the system occurs (+5 to +10 wt%). The PPZS achieves the strongest destabilization at 400 °C, and EDAS achieves the strongest stabilization at 500 °C. Over 550 °C, PPDS achieves another destabilization steps, different from the behavior of other salts.
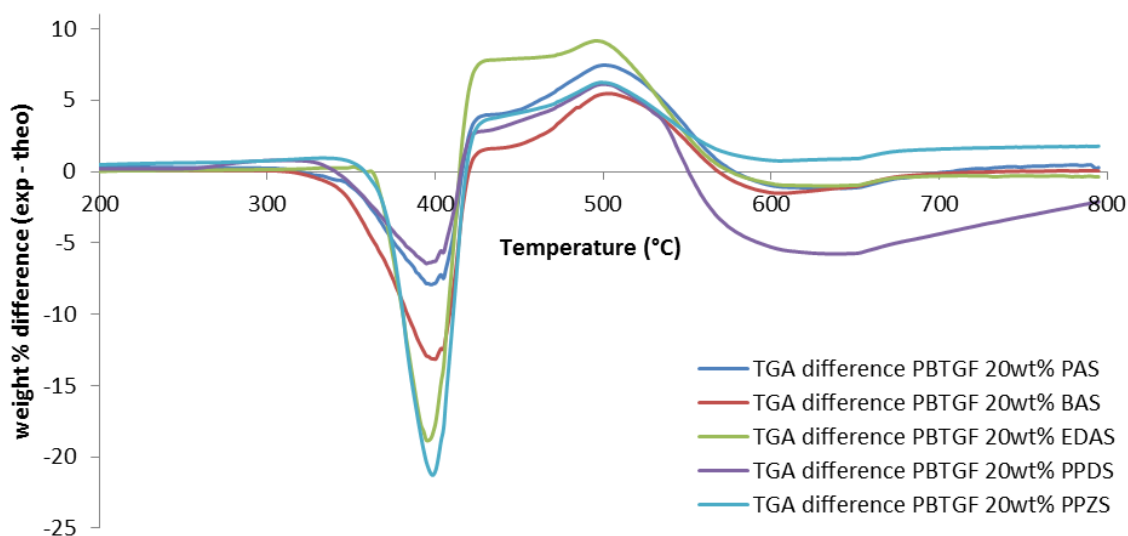
Figure 69: TGA difference curves for PBTGF flame retarded with the designed phosphinate salts

III.4.   CONCLUSION

This chapter has described the synthesis and then conversion into aluminum salts of novel phosphinic acids, obtained by grafting amine building blocks on the phenyl oxaphospholane oxide 2-POO. Indeed, unlike the case of Louisy and Exolit® PE110, the raw material was not commercial. The dehydration-cyclization of 3-HPP was the best way to obtain 2-POO, but 3-HPP was not a commercial substance either. The equimolar hydrolysis of the dichloride derivative of 3-HPP obtained from dichlorophenylphosphine led to a product which was harder to recrystallize. The method of full hydrolysis and dehydration (compilation of the two other methods) from commercial substances was then chosen to prepare 2-POO.

Two types of salts were synthesized: mono-amine based structures and diamine-based structures, leading then to two different aluminum substitutions. The reactions needed different conditions from those used with the methyl oxaphospholane oxide. The prepared products have been thoroughly characterized by liquid and solid-state NMR and elemental analysis. In spite of using defined literature protocols, it was not possible to obtain the expected Al/P ratio in the salts. Moreover, they exhibit an acidic character and should not be washed with a base. This was not the case of the products prepared in the previous partnership with BASF SE, which suggests that replacing the methyl group attached to phosphorus by a phenyl group has an influence on the structure or stability of the salt. However, as no relationship was established between acidity and Al/P ratio, it was decided nevertheless to incorporate these salts as FR in PBT and PA6.

Before compounding, the thermal stability of the salts was evaluated in thermogravimetric analysis. All the salts were suitable for extrusion in PBT and PA6. The TG measurements allowed obtaining first information on the potential action of the salts as FR. The latter yield more residue at 800 °C than the minimum aluminophosphate residue that could be expected from the Al and P content. It is well known that many FR additives act by stabilizing the char, thus a potential carbonaceous residue is a key parameter. The salts do not degrade in the exact temperature range the polymers do. A study of the potential interactions between additives and matrix during the degradation was thus carried out on the formulations.

It appeared that all formulations achieve a higher residue yield in the transient char zone between 400 and 550 °C in air compared to the neat matrix, which indicates a stabilizing effect of the salts. However at 800 °C, no enhancement of the charring was observed. On the other hand, clear interactions between the additives and the matrix between 350 and 600 °C, which can be a clue of a potential FR effect, were observed considering the TGA difference curves. However, only a screening in UL-94 will give appropriate information on the effectiveness of the salts as flame-retardants. This will be done in the next chapter that investigates the FR properties of the salts when mixed with PBT and PA6.

Chapter IV.   Evaluation of flame-retardant efficiency of phosphinate salts: fire testing

This chapter aims at investigating the flame retardant performances of the synthesized phosphinate salts in PBT and PA6. Fire tests were performed (mainly the UL-94 test since a focus was made on E&E applications). Other flame retardant properties were investigated using Glow Wire, LOI and mass loss cone calorimeter.

The first part of this chapter will show the UL-94 classification of formulations containing the phosphinate salts in PBTGF first and then in PA6GF. The results will be further commented in terms of fire behavior. In a second part, LOI, Glow Wire, cone calorimeter and PCFC will be used to characterize the potential FR effect of the salts. The fire performances of the materials formulated with unreinforced PBT will also be investigated in order to investigate the role of GF.

IV.1.   FLAME RETARDANCY OF PHOSPHINATE SALTS - SCREENING

The five previously synthesized salts were first incorporated at 20 wt% in the PBT masterbatch containing 30 wt% glass fibers. The resulting formulations contain 56 wt% PBT, 20 wt% phosphinate salts and 24 wt% glass fibers, and will be hereafter referred as PBTGF-salt. The screening was performed using the UL-94 fire test. According to the standard, the bar specimen were tested after 2 days at 25 °C (2d-25 °C, unaltered state) and bars of 0.8 and 1.6 mm thickness were tested.

Two preparation methods were investigated:

→ The bars were molded in injection molding (IM) directly after extrusion (no cooling)
→ The bars were molded using a hot press (HP), in a classical way (materials are cooled and pelletized prior to molding).

Indeed, hot press was first used as it allows preparing up to eight UL-94 bars at once, which simplifies the process. However, injection-molding remains in the industry the main way to produce many parts of various shapes.

IV.1.1   Evaluation of the flame retardancy in PBTGF by UL-94 at 1.6 mm

The efficiency of the phosphinate salts is first investigated using 1.6 mm thickness bars. The results are summarized in Table 23. The times t1 and t2 are the average of burning times after ignition corresponding respectively to the first and the second ignition. The dripping or burning up to the clamp are also indicated in the legend of the table.

When the HP process is used, PBTGF-PAS achieves a V-2 rating, as the burning times are short (21 s considering both flaming times) and around half of the bar is burnt. However, PBTGF-BAS burns up to the clamp and is not classified in spite of the short burning times (14 s for both flaming times) since its burning is very fast. PBTGF-EDAS is non-classified as it drips and burns very fast up to the clamp. As in the case of PBTGF-BAS, the use of PPDS allows achieving a borderline result, between V-2 and not classified, as two of the five samples burn up to the clamp. The use of PPZS as FR additive for PBTGF will not be investigated using HP process.

When the IM process is used, PBTGF-PAS achieves a V-1 rating. Even though, in terms of average burning times, the material is close to fulfill the conditions to reach a V-0 classification, two specimens burnt above 10s which justifies the V-1 ranking. PBTGF-BAS is classified V-2 in this case, as it drips after a second ignition and ignites cotton, leading to self-extinguishment. PBTGF-EDAS leads to a constant combustion after first ignition and thus is not classified since the bar burns up to the clamp. PPDS is again not classified; the formulation strongly drips during combustion and burns

totally. Finally, PBTGF-PPZS is not classified in spite of no dripping and no burning to the clamp, as its combustion is slow and burning times exceed 30 s.

Out of this first screening, only PAS and BAS pass the UL-94 classification when the IM process is used. When HP and IM processes are compared, it is clearly observed that the HP process reduces the fire performances of the additives. PAS- and BAS-based formulations are V-1 and V-2 respectively in IM while they are V-2 and NC in HP. It is reasonable to assume that the materials degrade (visible on the bars which are a bit porous and yellowish) in hot press because of the time of exposure to temperature in the press (8 min in the case of HP vs 2 min in the case of IM). Moreover, the materials are exposed two times to a heating ramp when HP is used whereas in the case of IM, the materials are directly molded after extrusion without a cooling step. The higher mechanical constrains due to the pressure (40 kN in HP versus 6 bars in IM) should also have an influence on degradation of the polymer. As a consequence, IM will be used for the next screenings depicted in this chapter.

Table 23: UL-94 (1.6 mm) results for synthesized salts in PBTGF
Y for yes, N for No if the bar drips or burns up to the clamp, (i) if the cotton is ignited
HP for hot press process, IM for injection molding process

Additive	Method	t1 / t2(s)	Drip	Clamp	Ranking	Observation
PAS	HP	12 / 9	Y (i)	N	V-2	1st ignition leads to dripping, 2nd self-extinguishes
	IM	4 / 9	N	N	V-1	No dripping, variation of the second burning time, borderline V-0
BAS	HP	12 / 2	Y (i)	Y	NC	Burns at 1st ignition, up to the clamp 2nd ignition
	IM	8 / 4	Y (i)	N	V-2	Dripping at second ignition, cotton is ignited
EDAS	HP	14 / 9	Y (i)	Y	NC	Burns up to the clamp after a 2nd ignition, half is burnt at 1st ignition
	IM	47 / -	Y (i)	Y	NC	Burns up to the clamp at first ignition
PPDS	HP	14 / 2	Y (i)	Y	NC	Borderline V-2 result for "burning up to the clamp" depending on the bar
	IM	35 / 19	Y (i)	Y	NC	Burns up to the clamp at second ignition, degraded formulation
PPZS	IM	32 / 7	N	N	NC	No dripping, but slow combustion (flaming >30s)

These first results show that PAS is the only salt presenting interesting performance in PBTGF. On the other hand, it was shown in the first chapter that phosphinate salts like AlPi exhibit a synergistic effect when used together with melamine cyanurate (MCA) or melamine polyphosphate (MPP). MCA exhibits a gas phase and cooling mode of action, and MPP a charring effect. The objective of this section is thus to evaluate the potential synergistic effect of the previously synthesized additives with both co-additives (MCA and MPP).

In order to do so, formulations containing 15 wt% salts and 5 wt% MCA or MPP were prepared (20 wt% additives to be comparable to the previous results), 1.6 mm thickness bars were molded using IM and evaluated through UL-94 standard. The results are reported in Table 24 and Table 25.

Table 24: UL-94 (1.6 mm) results for formulations with synthesized salts and MPP as co-additive in PBTGF
Y for yes, N for No if the bar drips or burns up to the clamp, (i) if the cotton is ignited

Additive (3/1 ratio)	t1 / t2(s)	Drip	Clamp	Ranking	Comment	Ranking of the salt without MPP
PAS/MPP	2 / 5	N	N	V-0	-	V-1
BAS/MPP	3 / 5	Y (i)	N	V-2	V-2 because of dripping, but not all bars are dripping (borderline V-0)	V-2
EDAS/MPP	58 / -	Y (i)	Y	NC	Burns to the clamp at first ignition	NC
PPDS/MPP	17 / 6	Y (i)	Y	NC	Borderline V-2	NC
PPZS/MPP	30 / 12	Y (i)	Y	NC	Long burning times	NC

When PAS is mixed with MPP, the performances of PBTGF-PAS-MPP turn from V-1 to V-0: burning times are really short and the formulation self-extinguishes. On the other hand, its performances are lower when MCA is used as co-additive: the burning time is longer at first ignition, and the flame nearly reaches the clamp. Whether used with MPP or MCA, PBTGF-BAS keeps a V-2 rating. However, the result is borderline V-0 when MPP is used, as only two bars among the five tested ignited the cotton. PBTGF-EDAS is not classified neither in the presence of co-additives or not: the formulations burn up to the clamp at first ignition. The use of PPDS leads to intense dripping without auto-extinction, even with the use of co-additives. When used together with MPP, the formulation is not classified but borderline V-2, and with MCA, a V-2 ranking is reached since strong dripping enhances self-extinction. PBTGF-PPZS is not classified even with the use of synergists, and the combustion times remain high after the first ignition.

Table 25: UL-94 (1.6 mm) results for formulations with synthesized salts and MCA as c-additive in PBTGF
Y for yes, N for No if the bar drips or burns up to the clamp, (i) if the cotton is ignited

Additive (3/1 ratio)	t1 / t2(s)	Drip	Clamp	Ranking	Comment	Ranking of the salt without MCA
PAS/MCA	24 / 6	Y (i)	Y	NC	Borderline V-2 as not all the bars are dripping	V-1
BAS/MCA	9 / 2	Y (i)	N	V-2	V-2 because of dripping	V-2
EDAS/MCA	70 / -	Y (i)	Y	NC	Drip of the entire bar	NC
PPDS/MCA	15 / 1	Y (i)	N	V-2	Self-extinguishing because of dripping	NC
PPZS/MCA	19 / 10	Y (i)	Y	NC	Two bars tested : first is V-1, second is NC	NC

The screening of the synthesized flame-retardants in PBTGF and their potential synergies with classical co-additives to phosphinates showed that among the five prepared salts, only PBTGF-PAS (V-1), PBTGF-BAS (V-2), and PBTGF-PAS-MPP (V-0) pass the UL-94 test. The addition of MPP to PAS increases the V-1 ranking of its formulation to V-0, while the use of co-additives does not change the

classification of formulations containing BAS. The same method of investigation (salts used alone and with co-additives) was carried out in PA6.

IV.1.2   Evaluation of the flame retardancy in PA6GF by UL-94 at 1.6 mm

The use of synthesized phosphinate salts as FR in PA6GF was investigated in UL-94. MCA and MPP were also investigated as co-additives. The results are reported in Table 26 for the salts used alone, in Table 27 with MPP and in Table 28 with MCA.

Table 26: UL-94 (1.6 mm) results for synthesized salts in PA6GF
Y for yes, N for No if the bar drips or burns up to the clamp, (i) if the cotton is ignited

Additive	t1 / t2 (s)	Drip	Clamp	Ranking	Comment
PAS	12 / 20	Y (i)	Y	NC	No self-extinguishment
BAS	22 / 48	Y (i)	Y	NC	Constant burning, up to the clamp at second ignition
EDAS	30 / 21	Y (i)	Y	NC	Constant burning up to the clamp, self-extinguishment while dripping at first ignition
PPDS	23 / 3	Y (i)	Y	NC	Long burning a first ignition
PPZS	17 / 2	Y (i)	N	V-2	Extinguishment due to dripping in both ignitions

Table 27: UL-94 (1.6 mm) results for formulations with synthesized salts and MPP as co-additive in PA6GF
Y for yes, N for No if the bar drips or burns up to the clamp, (i) if the cotton is ignited

Additive (3/1 ratio)	t1 / t2 (s)	Drip	Clamp	Ranking	Comment
PAS/MPP	25 / 7	Y (i)	Y	NC	No self-extinguishment, long burning at first ignition
BAS/MPP	35 / -	Y (i)	Y	NC	Constant burning up to the clamp at first ignition
EDAS/MPP	35 / 10	Y (i)	Y	NC	Visible glowing during the test but self-extinguishment not reached
PPDS/MPP	13 / 8	Y (i)	Y	NC	Borderline V-2
PPZS/MPP	30 / 12	Y (i)	Y	NC	No self-extinguishment, long burning at first ignition

What should be highlighted is that no salt proved a real efficiency as flame retardant for PA6GF. In most cases, no flameout is observed and thus a constant burning up to the clamp occurs. When the additive is used with MCA, PA6GF-PPDS reaches a V-2 classification since the material auto-extinguishes due to dripping.

It has also to be noted that as in the case of PBTGF, the bars of this formulation are brownish and probably already degraded during processing, which induces dripping, self-extinguishment and in

some cases classification. On the other hand, PA6GF-PPZS reaches a V-2 ranking, with a flameout due to dripping. It is the only formulation in PA6GF which exhibits a ranking.

Table 28: UL-94 (1.6 mm) results for formulations with synthesized salts and MCA as co-additive in PA6GF
Y for yes, N for No if the bar drips or burns up to the clamp, (i) if the cotton is ignited

Additive (3/1 ratio)	t1 / t2 (s)	Drip	Clamp	Ranking	Comment
PAS/MCA	20 / 21	Y (i)	Y	NC	No self-extinguishment, long burning at first ignition
BAS/MCA	25 / 8	Y (i)	Y	NC	No self-extinguishment, long burning at first ignition
EDAS/MCA	26 / 14	Y (i)	Y	NC	Constant burning up to the clamp, self-extinguishment while dripping at first ignition
PPDS/MCA	17 / 1	Y (i)	N	V-2	Self-extinguishment due to dripping
PPZS/MCA	40 / 10	Y (i)	Y	NC	Two bars tested, borderline V-1

IV.1.3   Conclusion of the screenings in UL-94 (1.6 mm)

The screening on the synthesized phosphinate salts as well as the investigation of potential synergisms allowed demonstrating that EDAS, PPDS and PPZS are not effective as flame retardants in PBTGF, with or without the use of co-additives. It should be highlighted that the formulations containing PPDS look clearly degraded after extrusion. The molten formulation exhibits a low viscosity and is brownish. This is consistent with the dripping character of the formulation during the fire tests. PBTGF-BAS reaches a V-2 classification, with or without co-additives. A synergistic effect between PAS and MPP is observed, as PAS reaches a V-0 ranking with the co-additive compared to a V-2 ranking when used alone. MCA leads to an antagonistic effect with PAS; indeed, PBTGF-PAS-MCA is not classified.

In PA6, nearly all formulations do not meet the criteria of the UL-94. The burning times are long and self-extinguishment is barely observed. PPDS, which probably degrades PA6GF during processing, achieves a ranking when used with MCA but only due to enhanced dripping. PA6GF-PPZS reaches a V-2 ranking and is the only formulation classified in PA6GF, again because of strong dripping.

Out of the TGA results, not all the results achieved in the UL-94 were expected. On the one hand, EDAS exhibited a degradation temperature suitable for interactions with PA6GF but does not lead to a real FR effect at UL-94 of PA6GF-EDAS. In the case of PAS and BAS, the corresponding formulations in PBTGF meet the criteria of the UL-94, which was one of the formulated hypotheses. Indeed the onset of degradation of PAS and BAS is the closest to that of PBT, which suggested a potential effect for these compounds in PBT. These results show that a general case cannot be drawn thanks to TGA results only.

As a consequence, as a main conclusion of this first screening, PAS is the only additive leading to satisfying FR properties for PBTGF. A focus will thus be made in the next sections and chapters on the use of PAS in PBT.

IV.2.　　THE USE OF PAS AS FLAME RETARDANT FOR PBT

The section IV.1 of this chapter showed the good performances of PAS in PBTGF. The latter achieves a V-1 classification when used alone and a V-0 classification together with MPP in a ratio 3/1. These classifications are achieved with bars of 1.6 mm thickness in UL-94. Moreover, it was shown that depending on the process used to prepare the materials, the FR properties are different. If an industrial application is expected, it is thus essential to understand the effect of the processing conditions on the structure and thus properties of the materials. Moreover, main applications considered so far are E&E, however, if we want to evaluate potential application of our additives in other sectors, other FR properties than UL-94 have to be investigated. Thus, the first part of this section deals with the investigation of the influence of the processing conditions on the FR properties of the materials while the second investigates the FR performance of PBT-PAS according to MLC, LOI and PCFC.

IV.2.1　　Optimization of the formulation

In the previous sections, the influence of the preparation methods of the sample has been demonstrated. In the literature, the effect of the dispersion of additives on the fire properties has been extensively studied **[66]**. Many studies were carried out on nanocomposites; however these studies also investigate the case of additives. The impact of the processing parameters on dispersion and the related fire properties is thus of prime interest. Moreover, it has been shown that the phosphinate salts, including PAS, are acidic. It is thus needed to investigate the potential degradation of the formulation during its processing.

In order to investigate the effect of the processing parameters on the properties of FR-PBTGF, different residence times were used. Indeed, the extrusion time is a key parameter which could have an effect both on dispersion of the additive and on the degradation of the matrix. There exists a competition between the effects of the shear stress, on the one hand leading to higher dispersion and on the other hand leading to the faster degradation of the material. Three processing methods were studied: PBTGF was extruded for two minutes, then PAS was added and the mixture was extruded for 1(a), 2(b) or 4(c) min. UL-94 bars were then molded by IM and a transversal cut was made. The cross-sections were observed in scanning electron microscopy (Figure 70) and electron-probe micro analysis (Figure 71).

The SEM clearly illustrates two facts. Firstly, there is a slight improvement of the dispersion with the extrusion time, which was expected. Smaller PAS aggregates (circled in red) are observed when the extrusion time increases. Secondly, there is a clear orientation of the glass fibers (regular white spots) due to the injection.

The EPMA mapping confirms the previous results obtained according to SEM analysis. The Al and P mappings show a slight improvement of dispersion with extrusion time. Al aggregates are still observed after 1 min extrusion, which is not the case after 2 min extrusion. Si mapping only shows glass fibers.

Another potential effect of the residence time is the degradation of the polymeric matrix. Corresponding bars (1, 2 and 4 min extrusion after addition of PAS) were tested in UL-94, to evaluate the impact of the extrusion time on the classification. The results are reported in Table 29, and it has to be noticed that only 2 bars were evaluated for each experimental condition whereas five are

required by the standard. The results highlight the fact that the extrusion time has a negative impact on the classification, as the bar shifts from V-0 to V-1 because the burning times increase. Over 2 minutes extrusion, t1 is crossing the limit of 10 s burning which is required for the V-0 ranking.

Two antagonistic effects can occur while increasing the residence time during extrusion. It has first been shown that the dispersion of the additives is improved when the extrusion time increases. On the other hand, increasing the extrusion time would affect the degradation of the polymeric matrix. Whereas a better dispersion is in general linked to an improvement of the FR properties (most of all in nanocomposites **[157]**), the UL-94 ranking usually decreases when the polymeric matrix is degraded. Indeed, if the polymer degrades, the molecular weight of the chains decrease, which induces a lower melt viscosity in the case of thermoplastic polymers, which has a dramatic impact on the behavior of the formulation in UL-94 **[158]**, both in terms of flaming and dripping. As a conclusion, a balance has to be determined.

a)   b)   c)
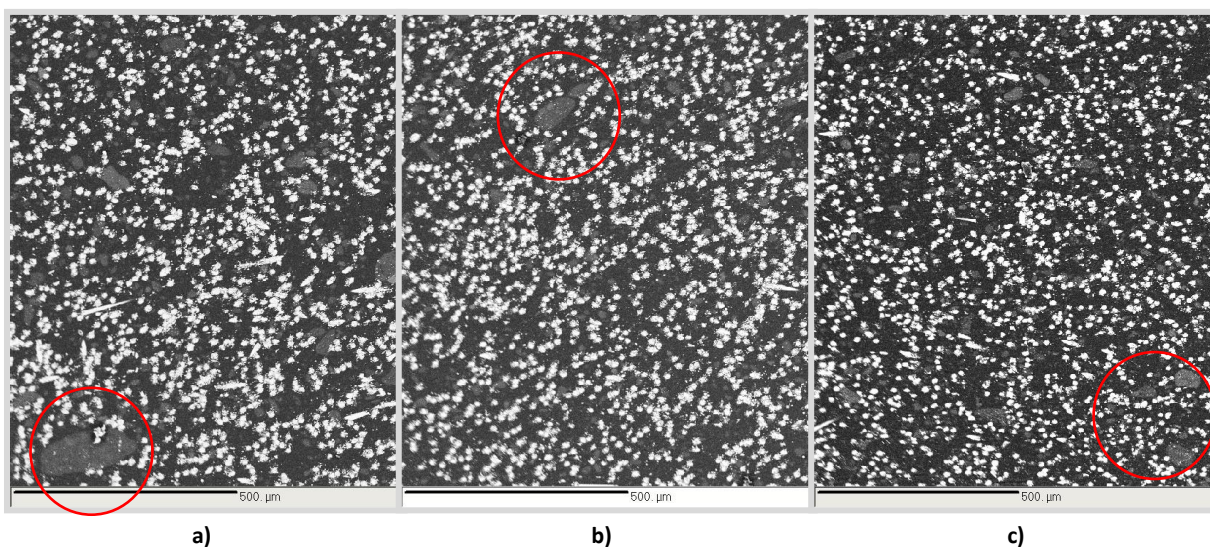
Figure 70: SEM pictures of PBTGF-PAS (500 µm);
1 min (a), 2 min (b) and 4 min (c) extrusion after addition of PAS.

a)   b)   c)
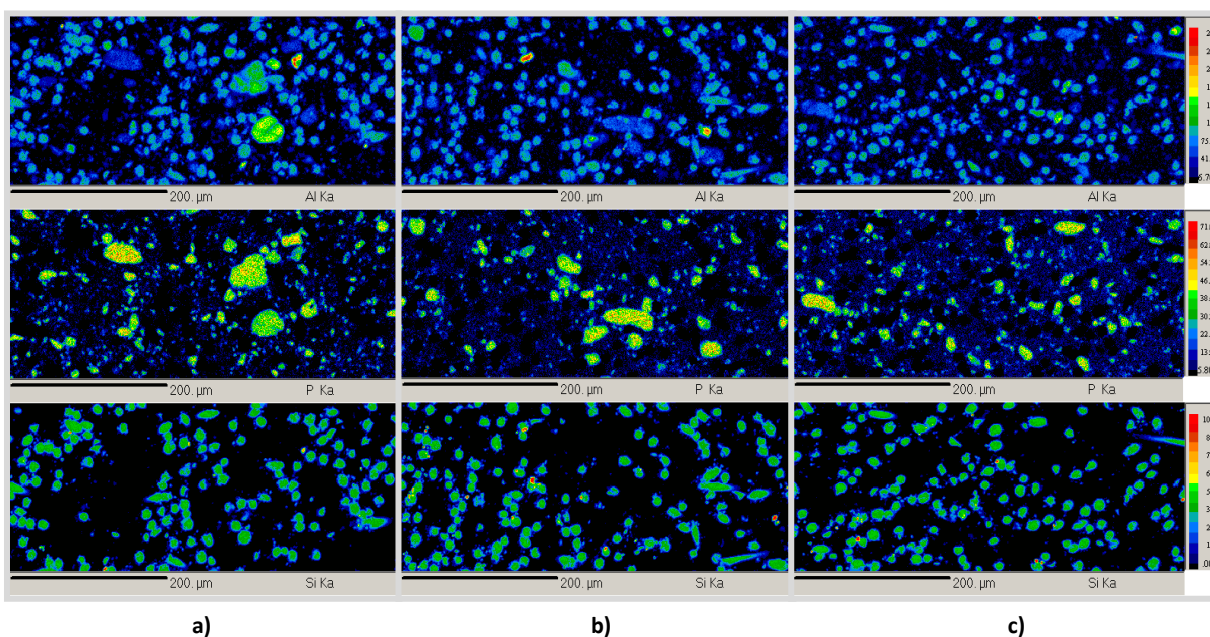
Figure 71: EPMA mapping of Al, P and Si at 200 µm;
1 min (a), 2 min (b) and 4 min (c) extrusion after addition of PAS

Table 29: UL-94 data for the PBTGF-PAS system with different extrusion times after addition of PAS
***ranking obtained with two bars**

Extrusion time	t1 / t2 (s)	Drip	Clamp	Ranking*
1 min	3 / 1	N	N	V-0
2 min	2 / 6	N	N	V-0
4 min	12 / 6	N	N	V-1

The degradation of PBTGF in the presence of PAS was evaluated through the measure of torque in the microextruder. The torque is directly related to the melt viscosity of the mixture which is extruded, generally with a power law **[159]**. PBTGF and PBTGF-PAS were then extruded following the second extrusion protocol (2 min extrusion after addition of PAS). The measurement of torque is reported in Figure 72. In this figure, two tangents, before and after addition of the additive are drawn in orange dotted line.
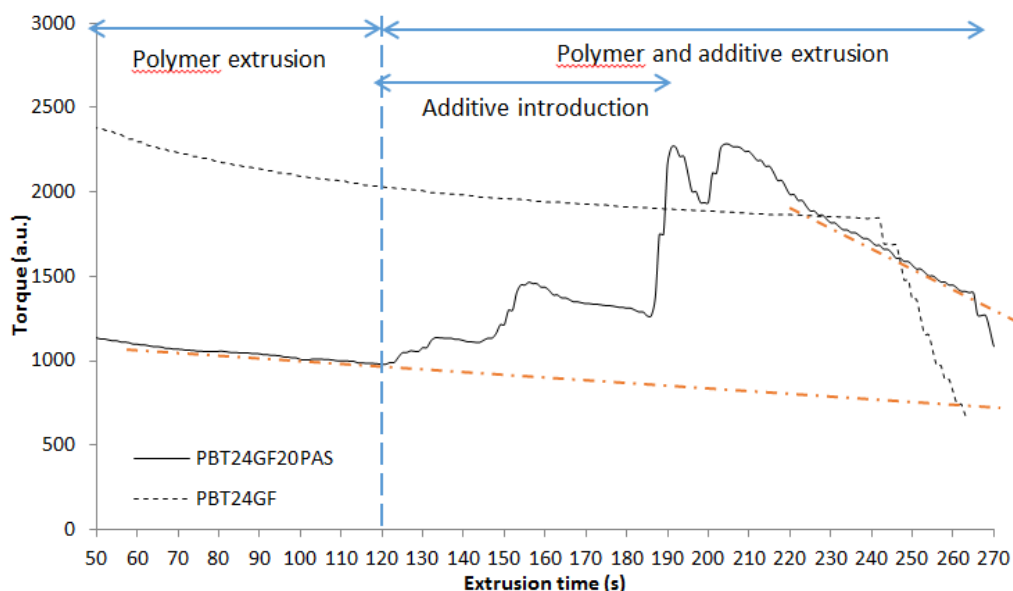
Figure 72: Measurement of the torque during extrusion of PBTGF and PBTGF-PAS

The torque decreases from 2000 to 1900 (a.u.) within 2 minutes without PAS, and from 2500 to 1500 within 2 min after addition of PAS. A higher slope is achieved when PAS is added, and the torque (and so the viscosity and molecular mass of PBT) decrease faster. As a conclusion, PAS degrades the matrix. Therefore regarding the results of dispersion and torque studies, limiting the extrusion time to 2 min is a good compromise between dispersion and degradation.

Studies on the degradation of matrices with residence time in an extruder have already been carried out multiple times in the literature **[160, 161]**. Alexy et al. notably report that in the case of poly(vinyl alcohols), the degradation mechanism is autocatalytic, as the release of acetic acid through extrusion degrades the polymer chains. In the case of PBT, random chain scissions or acidic attack of PAS can exponentially decrease the molecular mass of the matrix due to the formation of acid-containing chain ends. However, it should be highlighted that this consideration is only valuable for this particular screening process. In an industrial twin-screw extruder, the processing conditions are

sensibly different, which implies a different degradation. Limiting the residence time to 2 min is rather impossible in the real industrial process.

IV.2.2   Full characterization of FR performances in PBTGF

As previously described, the first targeted application concerned E&E, so UL-94 1.6 mm was the first requirement. However, in order to widen the application field of the developed FR materials, other properties such as UL-94 0.8 mm, LOI or HRR have to be evaluated.

PBTGF-PAS was tested at 0.8 mm thickness to evaluate its performances in stricter conditions. The results are summarized in Table 30. It should be underlined that the bars were prepared only by IM.

In the 0.8 mm thickness conditions, PBTGF-PAS exhibits a V-2 ranking. After the second ignition, the low viscosity of the materials leads to dripping and extinguishment of the bar, but also to the ignition of the cotton.

Table 30 : UL-94 (0.8 mm) results for PBTGF-PAS
Y for yes, N for No if the bar drips or burns up to the clamp, (i) if the cotton is ignited

Additive	t1 / t2 (s)	Drip	Clamp	Rating	Observation
PAS	4 / 1	Y (i)	N	V-2	The surface of the polymer is bubbling

The LOI of the PBTGF-PAS formulation was measured, and also compared to the LOI of all salts formulations. The results are summarized in Table 31.

Table 31: Limiting Oxygen Index results in PBTGF

Additive	neat	PAS	BAS	EDAS	PPDS	PPZS
LOI (vol % O$_2$)	20	30	23	23	25	24

PBTGF exhibits a LOI of 20 wt%. When added to PBTGF, EDAS and BAS lead to a material with a LOI of 23 vol%. PPZS based formulation reaches a LOI of 24 vol%. PPDS reaches a LOI of 25 vol%. The highest LOI is obtained for PAS leading to a LOI of 30 vol%. Only PAS reaches a high LOI while the other products lead to values from 23 to 25, which are only 2 to 4% higher than the O$_2$ content of ambient atmosphere. It should also be highlighted that these values are taken on bars obtained in HP.

As PAS showed good results in UL-94, the LOI of its formulation in PBTGF was also evaluated on UL-94 1.6 mm thickness bars made by injection-molding process. In this case, the measured LOI reached 37 vol% O$_2$. This result highlights again the degradation of the formulation during the HP process. A pre-degraded formulation generally needs less energy and less O$_2$ to be burnt, which induces a lower LOI. Processing has thus a strong influence on the results of any test.

Other tests used by industrials in E&E industries but also in railway are the Glow Wire (IEC 60695-2-12) and the Cone Calorimeter (ISO 5660-1, ASTM 1354). PBTGF-PAS was evaluated in both tests. First, results for the Glow Wire test are reported in Table 32. Data were also collected for PBTGF as a matter of comparison. It should be noticed that the regulation IEC 60335-1 ed. 4 **[162]** has been recently applied, taking into account the "safety of household and similar electrical

appliances" and establishing the suitability criteria from the point of view of electric, mechanical, thermal, fire and radiation hazard. In this regulation, the GWIT of parts exposed to electrical hazard should be at least 775 °C.

PBTGF achieves a GWFI lower than 800 °C, and a GWIT of 750 °C. The addition of PAS in the matrix lowers the GWIT to 725 °C (even if this difference if small and within the margin of error) but it has to be noted it increases the GWFI to 960 °C which is the highest classification and the level usually required by the end users. In the presence of the flame retardant, the ignition occurs earlier, but the resistance of the material to propagate the heat and its self-extinguishing behavior are enhanced. Nevertheless, the GWIT performances do not meet the IEC 60335-1 criteria.

Table 32: Results of glow wire test for PBTGF/PAS

Formulation	GWIT (°C)	GWFI (°C)
PBTGF	750	<800
PBTGF-PAS	725	960

Secondly, the results for the mass loss calorimeter test are reported in Table 33 and the corresponding curves of HRR versus time are reported in Figure 73.

Table 33: Mass loss calorimeter (35 kW/m²) data for PBTGF and PBTGF 20 wt% PAS
ti: time to ignition, tf: time to flameout

Formulation	ti (s)	tf (s)	pHRR (kW/m²)	t pHRR (s)	THR (MJ/m²)	Residual mass (wt %)
PBTGF	58	390	254	107	38	33
PBTGF - PAS	49	289	139 *(-45 %)*	135	25 *(-33 %)*	42
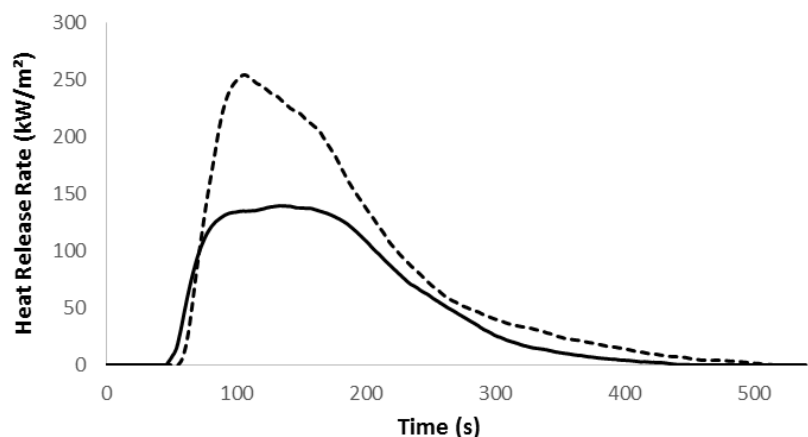
Figure 73: HRR vs time for PBTGF (dotted line) and PBTGF 20 wt% PAS (full line) in mass loss cone calorimeter, 35 kW/m²

In mass loss calorimeter test, when exposed to a heat flux of 35 kW/m², PBTGF ignites after 58 s of exposition and shows a peak of heat release (pHRR) of 254 kW/m² after 107 s. The sample flames out after 390 s, corresponding to a flaming time of 332 s. When PAS is added to the PBTGF, the ignition occurs at lower time (49 s). The formulation shows a peak of heat release of 139 kW/m² at 135 s (a plateau is reached which lasts about 100 s). The sample flames out at 289 s. Reductions of 45% the pHRR and of 33% of the Total Heat Release (THR) are thus observed. The residual mass also increases in presence of PAS, as the final residue after 600 s equals 33 wt% (corresponding to the glass fibers content) in the case of PBTGF whereas it increases to 42 wt% in the case of PBTGF-PAS. This value is

higher than the residual mass after the TG measurement (29 %), which can be expected as the testing conditions are significantly different (MLC sample is thermally thick whereas TGA sample is a thermally thin powder). A higher char residue in the case of a real fire testing compared to the ex-situ analyses is a clue of the efficiency of the additive.

Pyrolysis combustion flow calorimetry (PCFC) was finally used to evaluate the FR properties of materials on milligram-scale samples. In this test, the conditions are different, since the test is small-scale and the sample is not exposed to "direct" burning conditions (as it was in cone calorimeter). The sample is pyrolyzed at a fixed heating rate. Heat transfers are not the same (likewise TGA, material is thermally thin in PCFC but thermally thick in MLC) and thermo-oxidation of the sample at its surface is not taken into account. Several effects determining the fire behavior such as wicking, dripping, intumescence, etc. are not covered by mg-based methods such as PCFC **[163, 164]**. However, this tool allows investigating quickly the interaction of pyrolysis gases with the flame on small powder samples, which is interesting compared to cone calorimeter plates.

PBTGF, PAS and PBTGF 20wt% PAS were thus analyzed using PCFC. Corresponding data are reported in Table 34 and the heat release rate (HRR) curves are reported in Figure 74.

Table 34: PCFC data of PBTGF, PAS, and their corresponding formulation

Formulation	HRC (J/g.K)	THR (kJ/g)	pHRR (W/g)
PBTGF	391	16	378
PAS	143	19	137
PBTGF - PAS	284 *(-27%)*	15 *(-7%)*	275 *(-27%)*
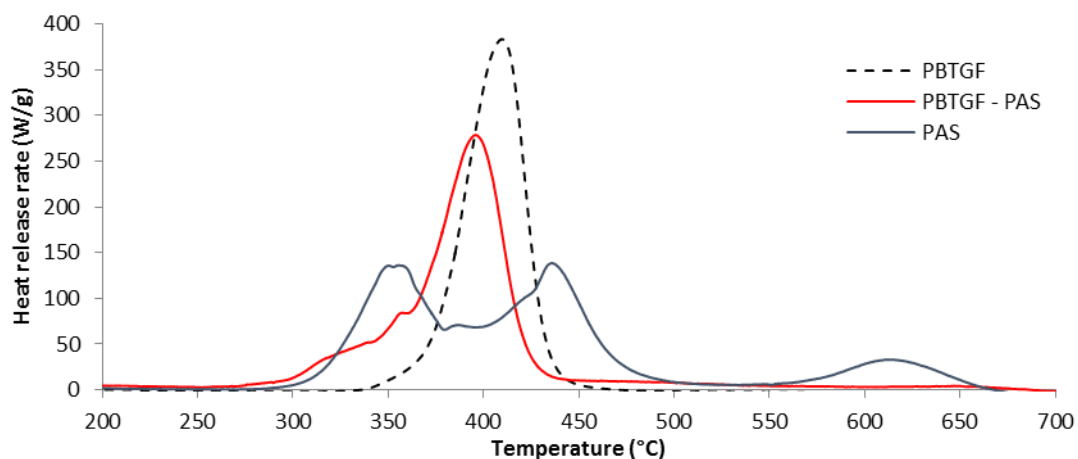
Figure 74: HRR curves of PBTGF, PAS and PBTGF - PAS

PBTGF exhibits a heat release capacity (HRC) of 391 J/g.K, a total heat release (THR) of 16 kJ/g, and a peak of heat release rate (pHRR) of 378 W/g.

PAS exhibits a HRC of 143 J/g.K, a THR of 19 kJ/g and a pHRR of 137 W/g. PBTGF-PAS exhibits a HRC of 284 J/g.K (which represents a reduction of 27% compared to neat PBTGF), a THR of 15 kJ/g (7% reduction) and a pHRR of 275 W/g (27% reduction). The reductions are lower than those measured in the MLC experiments (33 % reduction of the THR and 45% reduction of the pHRR). According to Sonnier et al. **[165]**, who established empirical relations between HRR in MLC and PCFC, a more

important reduction of HRR in the MLC experiment compared to PCFC should indicate that PAS exhibits an action more pronounced in the condensed phase.

In the literature, no study reports the use of PCFC on additives only, out of their formulations. PCFC has been used however to evaluate the contribution of particular molecular groups to the flame **[166]**. The measurement of the HRR of an additive in the PCFC conditions allow drawing the "HRR difference" curve (Figure 75), which corresponds to the difference between the experimental PCFC curve for the formulation and the sum of the curves of the separated components weighted by their corresponding ratio. The interactions between the components in the formulation are illustrated in this kind of study, likewise the TGdifference presented in Chapter III.
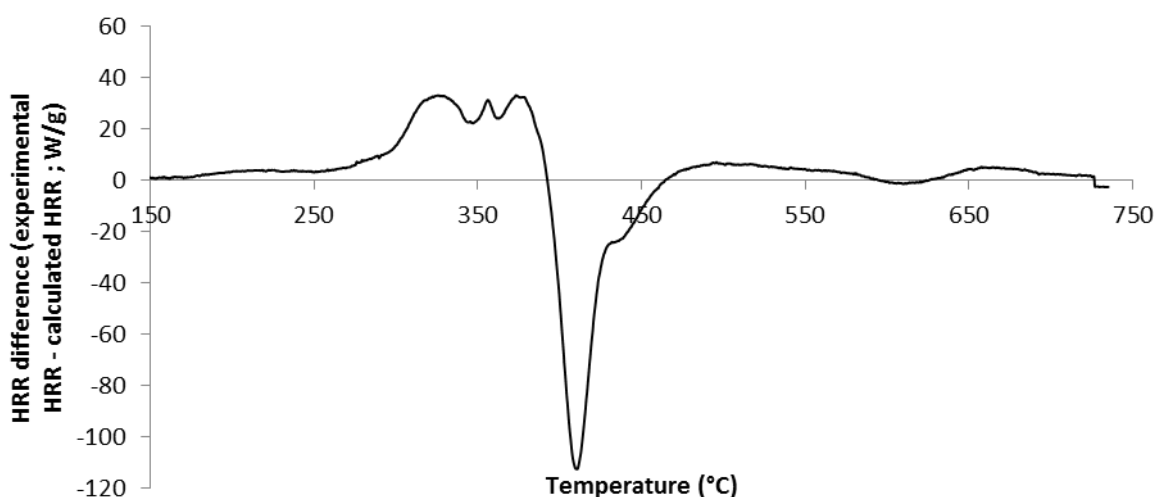

Figure 75: HRR difference curve for PBTGF-PAS

The HRR difference curve of PBTGF 20 wt% PAS reveals two different behaviors: an increase of HRR between 300 and 400 °C, and a reduction of HRR between 400 and 450 °C. This means there is first a negative interaction and then a positive interaction between PAS and PBTGF in term of flammability.

This negative interaction could be correlated with both the decrease in GWIT and the TGdiff curves established in the previous chapter. The destabilization of the formulation observed in Figure 69 (pp.90) leads to a higher HRR, indicating more combustible fragments are released. More combustible released in this step induces the easier ignition during the glow wire test and thus the lower GWIT.

These assumptions are also consistent with an action of PAS more pronounced in the condensed phase. Indeed, according to Acquasanta et al. **[138]**, the GWIT does not take into account the formation of a char or a protective layer as the wire keeps penetrating the material and breaks the potentially forming char. In that case, GWIT is not improved by the presence of a flame retardant acting such a way.

IV.2.3   Evaluation of FR performances in unreinforced PBT

It is well known that the behavior of polymers regarding fire is different whether they are reinforced or not. As PAS showed interesting results in glass-fiber reinforced PBT, 20 wt% of the additive were also used in unreinforced PBT. The corresponding formulation will be hereafter called PBT-PAS. Same UL-94 bars and glow wire samples as before were prepared and tested.

PBT-PAS achieves a V-0 ranking in the UL-94. During both exposures to the burner, the bar does not ignite, giving null flaming times. However, at second exposure, the bar melts and drips without igniting cotton. The V-0 ranking is clear, unlike in PBTGF, where flaming times varied. PBT-PAS achieves a LOI of 37 vol% O_2, and GWFI/GWIT of 960/725 °C respectively. 5 wt% MPP were also used as synergist together with 15 wt% PAS. In this case, the UL-94 ranking drops to V-2 as the dripping ignites cotton though flaming times are very short (3 s total).

Table 35: Summary of the results of fire tests for PBT-PAS and PBT-PAS-MPP

Test	Result for PBT-PAS	Result for PBT-PAS-MPP
UL-94 (1.6 mm) ranking	V-0	V-2
GWFI (°C)	960	
GWIT (°C)	725	
LOI (vol% O_2)	37	

All properties are enhanced in unreinforced PBT compared to the glass-fiber reinforced PBT, which is an unexpected fact, at least in UL-94 since unreinforced PBT should be more sensitive to dripping. The use of MPP gives an opposite trend, leading to a decrease in the ranking. In the case of such differences in the presence or not of glass fibers, two properties may be affected: mechanical properties and thermal properties.

In PBTGF, the addition of MPP decreases the flaming time. This effect could be due to the melamine released by MPP which would help blowing the flame (or prevent ignition). MPP also enhances the production of a char, which would protect the inner material from the flame, also decreasing flaming. This char, reinforced by glass fibers, would exhibit excellent properties. Without glass fibers, the classification is lower when MPP is added to PAS; in the case of unreinforced PBT, heat is evacuated from the flaming zone thanks to dripping. The presence of MPP, promoting the mechanical resistance with char, would prevent dripping, leading to lower the classification. These previous observations would lead to a global hypothesis: PAS would essentially act by cooling. Without GF, evacuation of heat by dripping is sustaining the effect of PAS. On the contrary, with GF, the heat would not be efficiently evacuated, and above a given temperature, self-extinguishing character would not be sufficient.

IV.3.   CONCLUSION

In this chapter, the efficiency of the synthesized phosphinate salts prepared in Chapter III as FR for PBTGF and PA6GF was evaluated. After a first screening carried out according to UL-94 standard (1.6 mm), it appeared that only PAS exhibited a classification which should be satisfying regarding industrial requirements. The salt allows achieving a V-1 classification when used alone in PBTGF and V-0 when MPP is used as co-additive. In PA6GF though, no satisfying result was achieved. PAS was thus selected for complementary studies.

First, a difference was observed in the classification of bars prepared by injection molding and hot press. It was shown that a good dispersion is achieved when the residence time in the extruder increases whereas it also leads to a degradation of the PBT matrix. Thus, in order to optimize the FR properties of PBTGF-PAS, the processing parameters have to be investigated. 2 min of mixture for PBTGF and PAS appears to be a good compromise for a microextruder screening.

Then, the FR properties of PBTGF-PAS according to LOI, UL-94 0.8 mm, glow wire test, MLC and PCFC were evaluated. The formulation achieved a LOI of 30 vol% O_2 when bars were obtained by hot press and 37 vol% O_2 when the injection molding was used, confirming the influence of the processing method. The LOI results highlight the self-extinguishing character of PBTGF-PAS. The formulation also reached the highest GWFI (960 °C) in glow wire testing (in spite of not meeting the GWIT standard), and shows a reduction of 45% in pHRR and of 33% in THR measured in mass loss calorimeter test compared to PBTGF. Clear interactions were underlined between PAS and PBTGF according to PCFC experiments.

Compared to the molecules synthesized by Louisy (methyl instead of phenyl in our salts), the results are sensibly different. The methyl derivatives achieved higher LOI and were classified V-0 when used alone. One of the objectives of this project was to look for the influence of the phenyl replacing methyl in the phosphinate structure. *A priori*, PAS has less influence on the gas phase (combustion time, LOI) than the corresponding methyl derivative.

Most results in this chapter were based on the UL-94 testing. However, the main conclusions of this test are "pass or fail". On the other hand, studies of mechanisms are led usually without considering the real conditions of fire testing, most of all temperature conditions. Since PAS presents an interesting efficiency in PBT, it is of interest to investigate its role when the material burns. It was shown in UL-94 test that the behavior of the materials should be improved if dripping occurs during the test.

As a consequence, in order to better understand the behavior of PBTGF-PAS in a real fire scenario, instrumentations were set up to obtain more information from the UL-94 test. The next chapter will present a study based on this instrumentation. Information on the temperature profiles in the bars during the test and quantification of dripping of well-known formulations will allow using a new method of analysis of new formulations.

_____

Chapter V. Instrumentation of the UL-94 test: understanding of mechanisms involved in the fire retardancy of polymers in real fire scenario

_____

V.1.INTRODUCTION

In the previous chapter, the synthesized phosphinate salts were evaluated in the UL-94 test. UL-94 test is one of the main tests required in the Electrical and Electronic equipment industry (E&E), and it is used worldwide. Simple bibliometrics using "UL-94" **[167]** (Figure 76) as keyword show the number of studies (papers and patents) related to this test. The analysis of the plot shows that it keeps growing since it was created by Underwriters Laboratories in 1972.
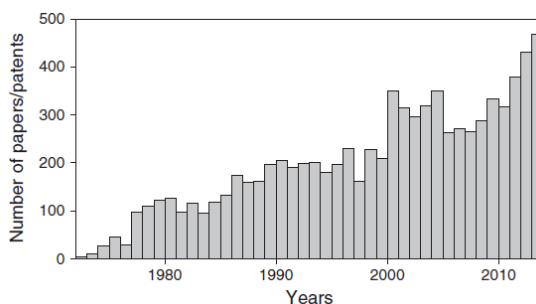
Figure 76: Bibliometrics on the keyword "UL-94"

It is noteworthy that this test takes into account the melt dripping behavior of samples whereas it is not the case in many other conventional tests. The melt dripping of plastics is one of the most important issues in the UL-94 classification **[158, 168]**. The burning time, another main parameter to classify materials according to the UL-94 standard, should also be linked with the melt dripping behavior. Indeed, in case of dripping, heat could be evacuated from the bar which stops burning. However, in case of flaming drops, in spite of removing the polymer fuel from the burning region, dripping can also contribute to propagate the fire. The effect of dripping is thus complex considering the flame retardant properties of materials and thus needs to be further investigated.

Although it is easy to observe, melt dripping is not really understood and is difficult to predict. Most of the time, the UL-94 leads to a classification but no "scientific" information (quantification of dripping, temperature gradients reached inside the bar) is obtained. On the other hand, classical analytical tools like thermogravimetric analysis (TGA) or pyrolysis-gas chromatography-mass spectroscopy (py-GC/MS) cannot give an appropriate decomposition pathway that could be related to the UL-94 conditions.

Among the five salts tested in the previous chapter, PAS showed a good efficiency in PBT. Unexpected results were achieved in the unreinforced material compared to glass-fiber reinforced material, due to flame-dripping. Out of the achieved screening, no clear explanation could be found to this phenomenon. This chapter thus investigates new data obtained during UL-94 tests through various instrumentations set up on the test. A similar approach was proposed previously by Kandola *et al*. who already developed a method to quantify the melt dripping of a sample while exposing it to a defined temperature **[137]**. In the present study, thermocouples embedded in the bar allow measuring the temperatures at different locations in the polymer sample as a function of time leading to temperature profiles. The weight measurement of the bar and of the melting drops during the test allows quantifying in the same time the dripping behavior and the thermal degradation of the material (volatilization and material remaining in the condensed phase). These data provide information on the behavior of the material during the test and so, lead to more than a simple classification. A better comparison of different materials can also be achieved, because a V-0 ranking

material can produce non-flaming drops or no drops; with complementary information, the understanding of phenomena should be easier.

The first part of this chapter focuses on the results given by the instrumented UL-94 on three "model" flame-retarded PA6 formulations as PA6 is a polymer which is widely used in E&E applications, a polymer which presents some dripping issues, and also one of the polymers this manuscript focuses on.

Three different flame retardants were chosen: a gas-phase and condensed-phase active additive (melamine cyanurate), an intumescent additive (melamine pyrophosphate) and a system efficient at very low loadings (guanidine sulfamate/melamine polyphosphate). All systems were investigated through a measurement of masses and temperatures, and corresponding data were linked to the thermal diffusivity of materials, obtained through Laser Flash Analysis. This first part has the objective to validate the methodology.

In a second part, the previously validated methodology will be used to better understand the mechanisms of action of PAS in reinforced and unreinforced PBT. PAS will also be compared to Exolit® OP1240 from Clariant, which is also an aluminum phosphinate and whose mechanism of action is well established as described in Chapter 1.

V.2. PRELIMINARY SETUP ON SELECTED KNOWN FORMULATIONS

V.2.1   Selection of materials

In this setup, PA6 was selected as polymeric matrix. This polymer is well-known for its dripping behavior in UL-94, dripping which can evacuate the heat from the burning zone. In the literature **[169-171]**, neat PA6 is generally not classified at UL-94 vertical test. For various applications, PA6 can be reinforced with glass fibers (GF) to enhance its mechanical properties. These glass fibers can also modify the thermal properties such as thermal conductivity leading to modify the burning behavior **[172]**. As a consequence, in this study, formulations of PA6 will be compared to the same formulation containing 20 wt% glass fibers. Three non-halogenated flame retardant systems were selected: melamine cyanurate, melamine pyrophosphate, and guanidine sulfamate/melamine polyphosphate.

Melamine cyanurate (MCA) was patented as flame retardant in the early 1990s **[173]**, and its mode of action was established later on **[77, 174, 175]**. It is generally accepted that MCA experiences an endothermic decomposition into melamine and cyanuric acid at 350 °C, which decreases the temperature of the burning material. Meanwhile, MCA enhances the decomposition of PA6 to non-flaming drips forming oligomers. This leads to self-extinguishment of the burning material in UL-94 leading to V-0 ranking. On the other hand, it was shown that the effect of MCA is disrupted when it is used in glass-fiber reinforced PA6 **[176]**.

Melamine pyrophosphate (Budit®311, referred hereafter as MPY) was patented as flame retardant in the lately 1990s **[177, 178]**. According to Levchik *et al*. **[174]**, melamine pyrophosphate is efficient at high concentration leading to the formation of an intumescent char which provides a shielding effect for the underlying polymer and prevents the melt flowing.

Finally, the combination of guanidine sulfamate (GAS) and melamine polyphosphate (MPP) in a ratio 50/50 GAS+MPP (hereafter referred as GSMP) was recently studied by Coquelle *et al*. **[83, 179, 180]** in PA6. It was shown that this combination acts both in the gas and condensed phases during the degradation of PA6 by modifying the degradation pathway of the polymer. It was reported that GAS leads to the release of heavier oligomers of PA6 decreasing the flammability while the presence of MPP enhances the charring process. The main advantage of this system is that it is efficient at low loadings (around 5 wt%) compared to the other systems.

These additives or combination of additives were selected in order to compare different modes of action in terms of heat propagation and dripping behavior. MCA provides a flame retardant effect because of evacuation of heat by dripping. MPY exhibits an intumescent effect (condensed phase). Finally, GSMP has its mode of action involving a combination of heat sink and charring effect. MCA was used at 12.5 wt%, MPY was used at 18 wt% and GSMP was used at 5 wt%. The corresponding formulations reinforced with glass fibers contained the same ratio of flame retardants but combined with 20 wt% glass fibers. The studied formulations and their corresponding ranking in the UL-94 test are summarized in Table 36.

Table 36: Loading of different components in studied formulations

	PA6	GAS	MPP	MCA	MPY	GF	UL-94 ranking
PA6	100	—	—	—	—	—	V-2
PA6-MCA	87.5	—	—	12.5	—	—	V-0
PA6-MPY	82	—	—	—	18	—	V-2
PA6-GSMP	95	2.5	2.5	—	—	—	V-0
PA6GF	80	—	—	—	—	20	NC
PA6GF-MCA	67.5	—	—	12.5	—	20	V-2
PA6GF-MPY	62	—	—	—	18	20	NC
PA6GF-GSMP	75	2.5	2.5	—	—	20	NC

The instrumentation of the UL-94 test was set up with the eight formulations of PA6. In this study, PA6 Technyl S27 BL (without glass fibers) and PA6 C216 V30 (30 wt% glass fibers masterbatch) from Solvay were mixed to obtain definite glass fibers contents. Four supplementary additives were needed to complete this study:

→ Melamine cyanurate (referred to as MCA) Melapur® MC15, provided by BASF SE
→ Melamine pyrophosphate (referred to as MPY) Budit® 311, purchased from Budenheim
→ Melamine polyphosphate Melapur® 200, supplied by BASF SE, and Guanidine sulfamate, purchased from Sigma-Aldrich, as a 50/50 mixture (referred to as GSMP)

Those formulations based on PA6 will be used to validate the methodology developed in this study. It will then further be used to investigate the fire behavior of the FR formulations of PBT previously developed.

V.2.2   Results with neat matrices

Before investigating the effects of flame retardants on the behavior of unreinforced and glass-fiber reinforced PA6, the neat matrices were first evaluated. The weight loss, mass of drops, as well as the temperature profiles for PA6 and PA6GF are reported in Figure 77 and Figure 78 respectively.
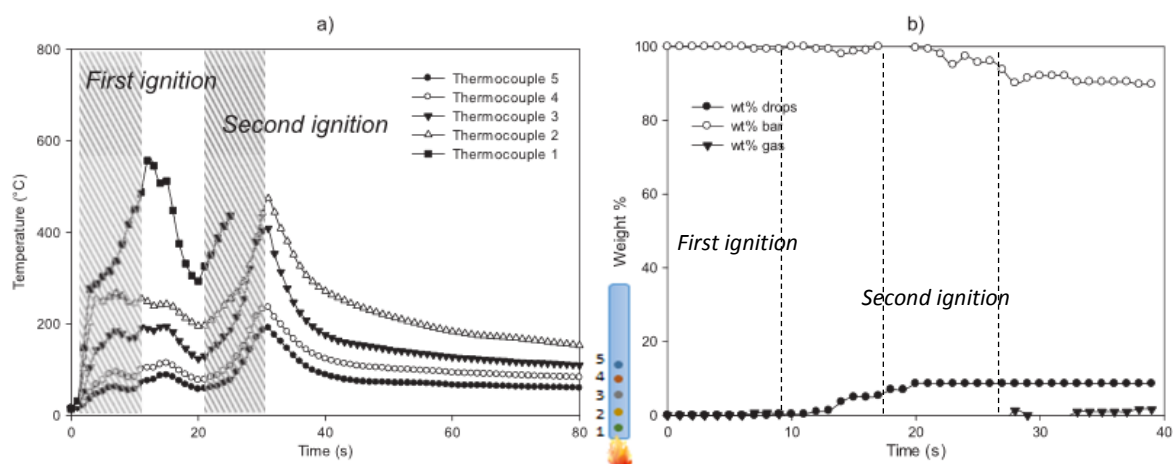

Figure 77: Measurement of a) temperatures and b) masses during the UL-94 test of PA6

In the case of PA6, at first ignition (after 10 sec), T1 reaches a temperature of 560 °C, T2 a temperature of 270 °C, T3 a temperature of 195 °C, T4 a temperature of 115 °C and T5 a temperature of 105 °C. At second ignition, the polymer drips and T1 is not embedded anymore in the matrix. T2

reaches a temperature of 475 °C, T3 a temperature of 415 °C, T4 a temperature of 235 °C and T5 a temperature of 190 °C. It is noteworthy that the dripping at second ignition ignites the cotton leading to a V-2 ranking. After the end of flaming, it is observed that only 1% of PA6 is evolved in the gas phase when since 99% are maintained in the condensed phase (~10% for the drops and 89% remaining in the bar, see Figure 77-b). It thus demonstrates that dripping governs the behavior of PA6 when evaluated according to UL-94.
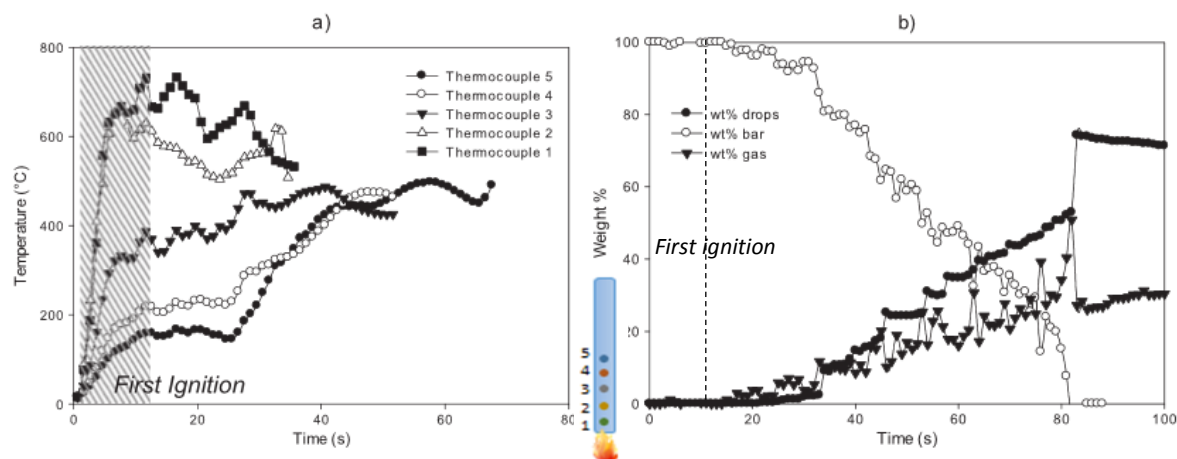

Figure 78: Measurement of a) temperatures and b) masses during the UL-94 test of PA6GF.

In the case of PA6GF and at first ignition, T1 to T5 respectively reach temperatures of 745 °C, 655 °C, 400 °C, 255 °C and 165 °C (Figure 78-a). After burning and at 40, 48 and 57 s respectively, T3, T4 and T5 reach a similar temperature of about 480 °C. PA6GF burns up to the clamp after the first ignition and thus is not classified. Mass measurement reveals a weight loss of 100 wt% of the bar corresponding to 73 wt% of drops and 27 wt% of evolved gases (Figure 78-b).

These measurements emphasize the significant influence of glass fibers on the behavior of PA6 in UL-94 conditions. The temperatures reached by PA6GF are much higher (about 200 °C higher) than in the case of neat PA6, and heat is no longer evacuated because temperatures remain high for about 30 s. Indeed, in that case dripping occurs at longer time when compared with neat PA6 (t=10 s compared to 32 s). The degradation of the bar is complete, and a high rate of polymer is volatilized (27 wt% volatiles are obtained from 80 wt% matrix in the bar, corresponding to 33 wt% of material "evolved" in the gas phase). As shown in a previous work **[172]**, it is assumed this behavior is assigned to the changes of the thermal properties of the material (higher heat conductivity of PA6GF versus PA6 because of the incorporation of GF). This aspect will be further detailed in the following section.

V.2.3   Results with flame-retarded matrices

PA6 and PA6GF were first flame-retarded with 12.5 wt% MCA. The weight loss curve, weight of drops and temperature profiles versus time of PA6-MCA are reported in Figure 79 and in Figure 80 for the glass-fiber reinforced material.

In the case of PA6-MCA, at first ignition, T1 reaches a temperature of 420 °C, T2 a temperature of 325 °C, T3 a temperature of 250 °C, T4 a temperature of 114 °C and T5 a temperature of 64 °C. At second ignition, T1 to T5 respectively reach temperatures of 480 °C, 460 °C, 360 °C, 200 °C and 120 °C. PA6-MCA does not ignite nor at first nor at second ignition, and drops are non-flaming leading to a V-0 ranking. This result is illustrated by the weight loss which is null in first ignition. The

bar releases a drop at 27 s. The weight loss at the end of the test is about 7 wt%, which corresponds to 6 wt% drops and 1 wt% volatiles. The results are similar to what was observed for neat PA6. The main difference is that the drops do not ignite the cotton in the case of PA6-MCA.
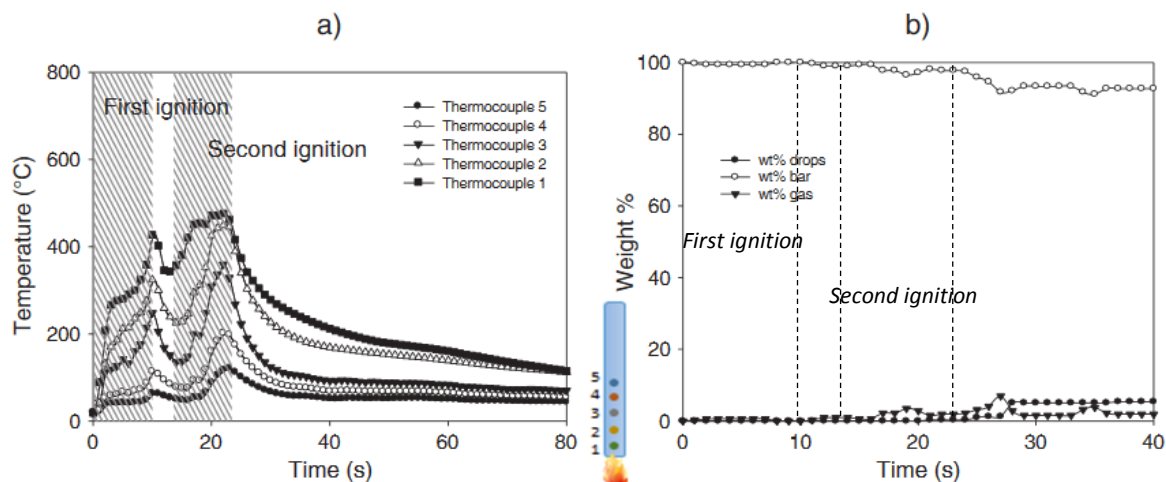

Figure 79: Measurement of a) temperatures and b) masses during the UL-94 test of PA6-MCA

In the case of PA6GF-MCA, at first ignition, T1 to T5, respectively, reach temperatures of 590 °C, 410 °C, 325 °C, 170 °C and 115 °C. At second ignition, T1 reaches a temperature of 550 °C, T2 a temperature of 475 °C, T3 a temperature of 420 °C, T4 a temperature of 295 °C and T5 a temperature of 230 °C. PA6GF-MCA does not ignite at first ignition but does at second ignition. The flaming time is very short (about 1 s) and the bar flames out thanks to a flaming drop permitting heat evacuation but leading to a V-2 ranking. The weight loss is very similar to what was observed in the case of the unreinforced system. The total weight loss is equal to 6 wt% corresponding to 3 wt% drops and 3 wt% volatiles (4 wt% of combustible material).
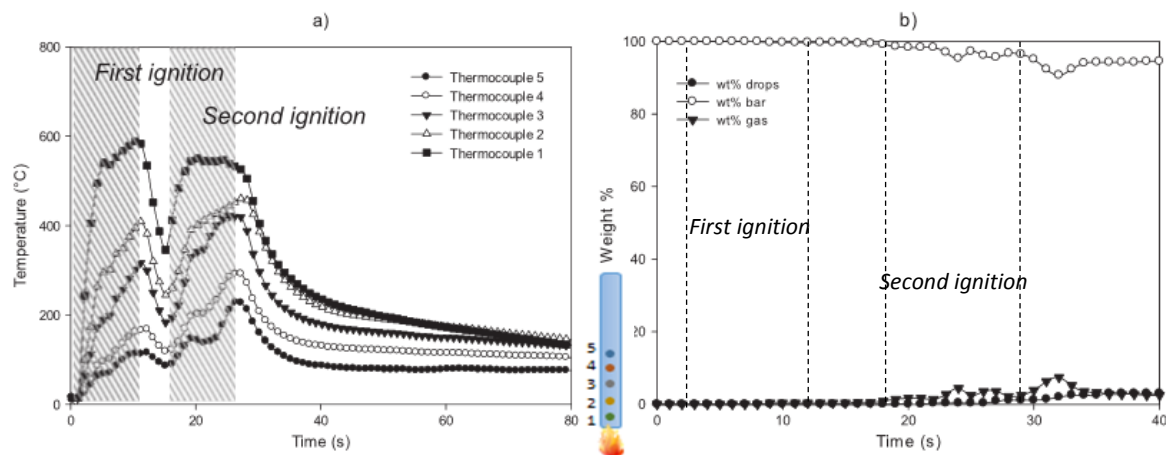

Figure 80: Measurement of a) temperatures and b) masses during the UL-94 test of PA6GF-MCA.

When MCA is used, the difference observed between reinforced and unreinforced material is mainly observed in the temperature profile. The temperatures reached by the reinforced material are higher (40 °C up to 170 °C higher) than those reached by the unreinforced system. The same assumption formulated in the case of PA6 given above (higher heat conductivity of the material because of the incorporation of GF) is proposed.

A second difference is observed in the classification PA6GF-MCA versus PA6-MCA because drops of PA6GF-MCA ignite the cotton while PA6-MCA does not. It is noteworthy the weight of drops slightly changes between those two materials, as more material is evolved to the gas phase in the case of PA6GF-MCA. It suggests the physico-chemical properties of the drop may change. The presence of glass fibers may have an effect on the flaming of drops. If we assume that the presence of GF increases the thermal diffusivity of the material then the heat is better distributed in the drops (lower heat gradients). The higher temperature inside the drop promotes the decomposition of the material and hence it sustains flame on the drop. Another hypothesis is also to consider *a priori* that the temperature of the drop is equivalent to the temperature of the bottom of the bar just before dripping. In that case, the temperature of the drop for PA6GF-MCA should be higher, it would decompose faster (leading to more volatiles) and the drop would not cool down fast enough to self-extinguish before reaching cotton. This hypothesis should be confirmed by the observation of the drop with an IR camera.

PA6 and PA6GF were also flame retarded with 18 wt% MPY. The weight loss curve, weight of drops and the temperature profiles and mass measurements of PA6-MPY and PA6GF-MPY are reported in Figure 81 and Figure 82, respectively.

In the case of PA6-MPY, at first ignition, T1 reaches a temperature of 560 °C, T2 a temperature of 605 °C, T3 a temperature of 320 °C, T4 a temperature of 155 °C and T5 a temperature of 110 °C. At second ignition, T1 reaches a temperature of 405 °C, T2 a temperature of 455 °C, T3 a temperature of 455 °C, T4 a temperature of 265 °C and T5 a temperature of 195 °C. PA6-MPY flames out 2 s after first ignition but keeps burning for 5 s after second ignition. Flameout occurs because of the dripping of a flaming chunk leading to a V-2 ranking. This result is consistent with the weight loss curve. The mass of the bar decreases after 20 s (during second ignition) and reaches 20 wt% loss corresponding to 15 wt% drops (charred bar chunk) and 5 wt% volatiles.
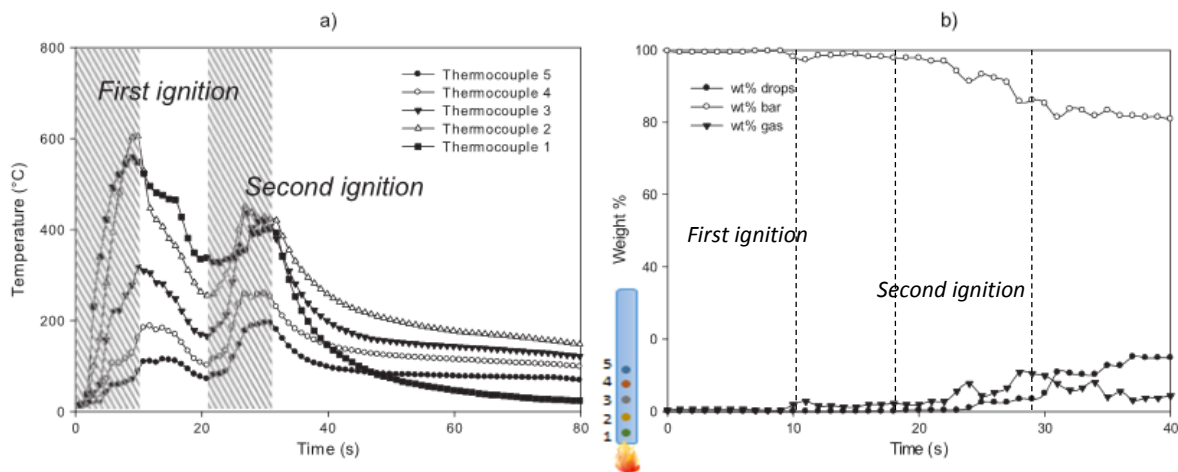

Figure 81: Measurement of a) temperatures and b) masses during the UL-94 test of PA6-MPY

In the case of PA6GF-MPY, at first ignition, the thermocouples (from T1 to T5), respectively, reach 470 °C, 530 °C, 355 °C, 240 °C and 150 °C. The bar flames out 5 s after the end of first ignition because of the fall of a chunk, and T1 is no more embedded. At second ignition, the thermocouples T2 to T5, respectively, reach 485 °C, 390 °C, 370 °C and 305 °C. After the second flame application, the bar keeps burning up to the clamp releasing two big chunks at 40 and 55 s. The formulation is thus not classified. The temperatures reached by T3, T4 and T5 during this second flaming step are,

respectively, 640 °C, 450 °C and 430 °C. Complementary information is obtained comparing the weight loss, the weight of drops and the weight of volatiles. There are 10 wt% loss before the first drip. Then, the weight loss is equal to 35 wt% corresponding to 20 wt% drops and 15 wt% volatiles. At the end of the test, 100 wt% weight loss is observed, corresponding to 83 wt% drops and 17 wt% volatiles.

The results obtained in the case of reinforced material are sharply different to those observed for the unreinforced material, as previously observed and discussed for other studied materials. Although the temperatures reached at first ignition are 100 °C higher for T1 and T2 in the case of unreinforced material, the effect of the intumescent shielding is clearly observed at second ignition. Indeed T1 to T3 are not higher than 400 °C, and they reach a steady state while exposed to the flame. The dripping of a small chunk leads to the flameout. In the case of glass fiber reinforced material, in spite of lower temperatures achieved at first ignition, the bar does not flame out after second ignition. No small chunk is dripping, and this difference could be linked to the presence of the glass fibers. The latter are known to improve the mechanical resistance of intumescent chars. A rigid char (illustrated by the big chunk observed at 40 sec) prevents the bar from dripping and then accumulates and propagates heat causing the complete combustion of the bar. This result show that the intumescent shield formed in presence of GF is not efficient enough to stop the fire triangle. Indeed, it is already reported that glass fibers can also show antagonistic effect with intumescent formulations. In his PhD work, Dabrowski showed that the presence of glass fibers led to a lower swelling of the intumescent shield **[176]**. This effect could thus contribute to a lower efficiency of MPY in the case of PA6GF-MPY.
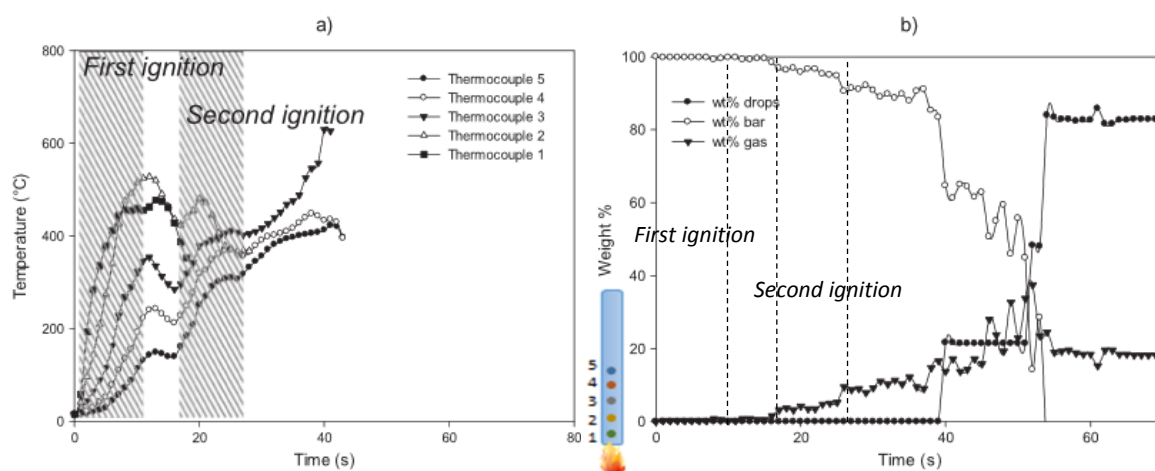

Figure 82: Measurement of a) temperatures and b) masses during the UL-94 test of PA6GF-MPY

Finally, PA6 and PA6GF were flame retarded with 5 wt% of GSMP. The weight measurements (bar, drops and volatiles) and temperature profiles of PA6-GSMP and PA6GF-GSMP are reported in Figure 83 and Figure 84, respectively.

In the case of PA6-GSMP, at first ignition, the five thermocouples T1 to T5, respectively, reach temperatures of 455 °C, 250 °C, 140 °C, 95 °C and 50 °C. At second ignition, T1 reaches a temperature of 615 °C, T2 a temperature of 325 °C, T3 a temperature of 215 °C, T4 a temperature of 150 °C and T5 a temperature of 105 °C. PA6-GSMP does not ignite when applying flame twice. Drop falls off at second ignition but without igniting the cotton leading to a V-0 ranking. During the second ignition, the material slowly releases volatiles (from 15 to 20 s testing) and then melts and releases a heavy

non-flaming drop which represents 5 wt% of the bar. The total weight loss is 13 wt% after 30 s, among which 8 wt% volatiles.
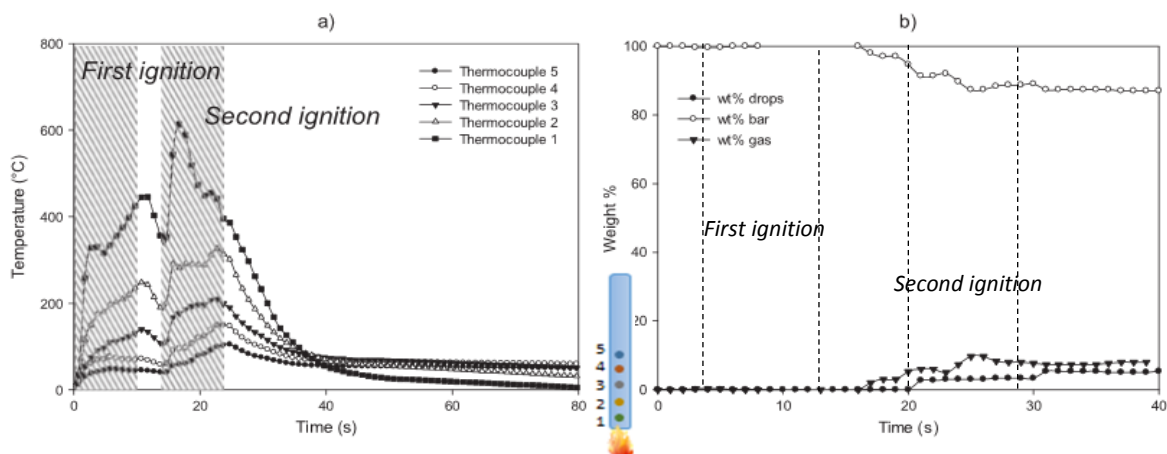

Figure 83: Measurement of a) temperatures and b) masses during the UL-94 test of PA6-GSMP

In the case of PA6GF-GSMP, the five thermocouples from T1 to T5, respectively, reach temperatures of 375 °C, 405 °C, 310 °C, 205 °C and 110 °C. The bar ignites and keeps burning up to the clamp in 55 s. The material is thus not classified. The temperatures reached by each thermocouple are around 420–430 °C. Volatiles are released after the ignition, and the mass loss corresponding to volatiles constantly increases from 10 to 50 s and reach 29 wt% (36 wt% of combustible material). The increase of the mass of drops is not constant because the bar progressively releases 5 chunks of about 10 to 20 wt%, to reach 71 wt% drops, and a total loss of 100 wt%.
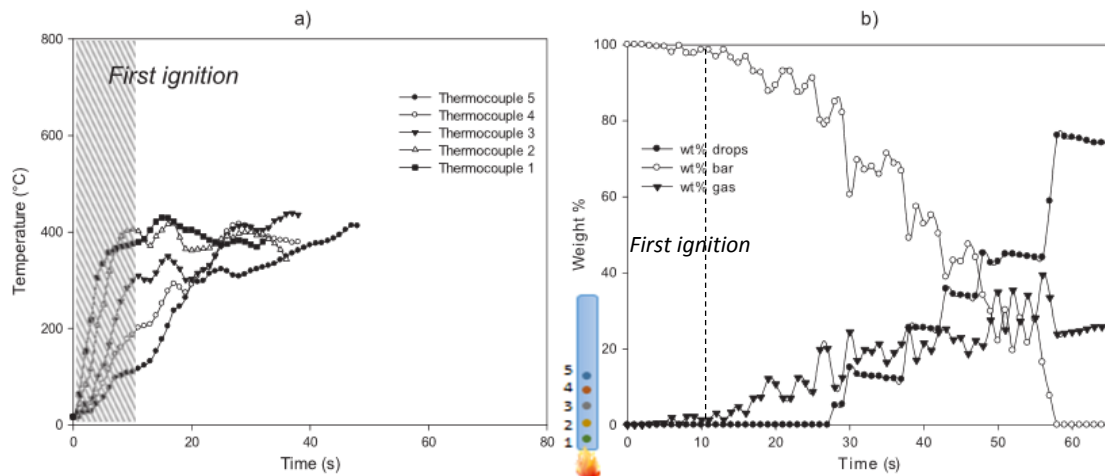

Figure 84: Measurement of a) temperatures and b) masses during the UL-94 test of PA6GF-GSMP

When GSMP is used as flame retardant, different behaviors depending upon the material is reinforced or not reinforced is observed. Even if the temperatures reached in the case of unreinforced material are higher, the material self-extinguishes because of the heat-sink effect (non-flaming dripping); thus, it is classified. As in the case of PA6GF-MPY, glass fibers prevent the material from dripping which causes an accumulation of heat and a continuous combustion of the material. This suggests that GSMP is more effective when dripping could occur. It is reasonable to assume that the mode of action of GSMP in the case of UL-94 is rather because of the modification of PA6 degradation pathway than to the formation of a charred material.

V.2.4   General discussion

Among the eight studied PA6 formulations, a general trend is observed: when glass fibers are incorporated into the formulation, the fire properties dramatically decrease according to UL-94. Unreinforced materials that are classified lose their ranking when reinforced. The two specific measurements provide understanding on the mode of action of the flame retardants and on the effects of GF.

The temperature profiles allow observing clear differences in the behavior of materials when they are exposed to the flame. The temperature profiles of T5 for the eight formulations and during the first ignition are reported in Figure 85. T5 was selected because it is the furthest from the flame and so the contribution of the flame should be minimized. These measurements are not directly affected by any decomposition process or mechanical change (char structure for example).

In these different profiles, the temperature reached by glass fiber reinforced materials is clearly higher (100–200 °C compared to 50–100 °C for unreinforced materials), and the slopes of curves at shorter times are also higher. It strongly suggests that the thermal diffusivity of glass fiber reinforced materials should be higher than that of unreinforced material. To confirm this hypothesis, thermal diffusivity measurements were carried out by Laser Flash Analysis. The corresponding results are reported in Figure 86. The measured thermal diffusivities are consistent with the previous observations: all the reinforced formulations show higher diffusivities (0.21–0.25 mm^2/s for the reinforced materials compared to 0.17–0.20 mm^2/s in the case of unreinforced materials between room temperature and 100 °C).
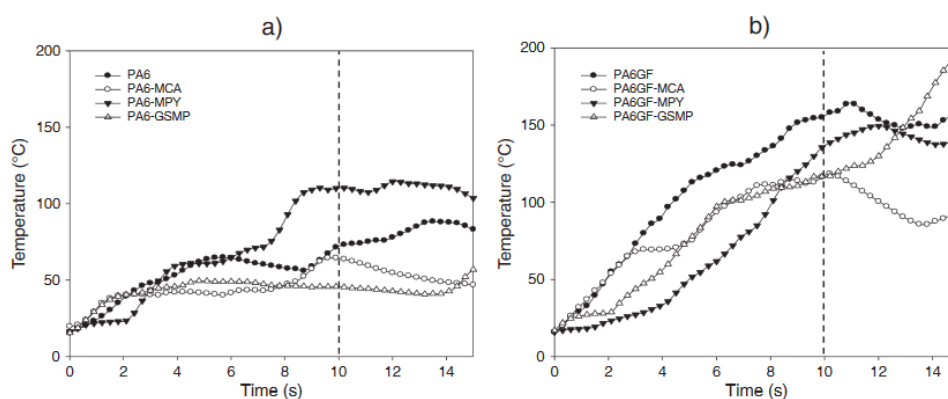

Figure 85: Temperature profiles of T5 during first ignition for: a) unreinforced materials, and b) GF reinforced materials
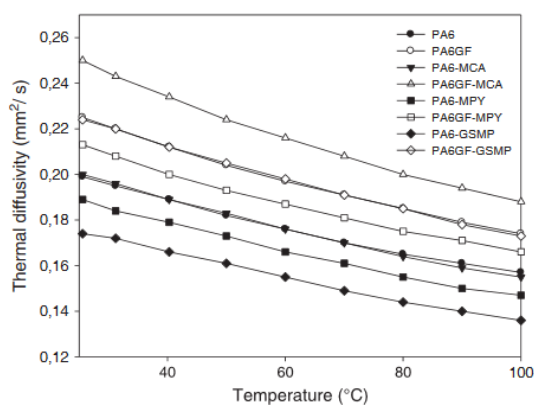

Figure 86: Thermal diffusivity of studied formulations measured by Laser Flash Analysis

The T5 temperature profiles during ignition also allow comparing the effect of the different additives in unreinforced materials, and their corresponding efficiency in reinforced materials. PA6 shows a plateau between 4 and 8 sec of ignition, which can be attributed to the endothermic melting of the polymer. Compared to neat PA6, PA6-MCA and PA6-GSMP show a heat sink effect. T5 remains at 50 °C after 3 sec of ignition in the case of PA6-GSMP and increases again between 8 and 10 sec up to 70 °C in the case of PA6-MCA. The endothermic decomposition of additives can thus be evidenced in these cases. Concerning PA6-MPY, T5 reaches 100 °C and stabilizes after 8 sec of ignition. It is assumed that the development of the intumescent shield is slower than the decomposition of cooling additives such as MCA or GSMP and hence, the protection occurs at longer time. It is also generally accepted that in the case of intumescent formulations, the thermal destabilization (illustrated by an increase of temperature) is necessary to the formation of the intumescent shield which then stabilizes the temperatures. These results are consistent with the UL-94 ranking as MPY only leads to a V-2 whereas MCA and GSMP lead to a V-0. It thus demonstrates that the decomposition kinetic of materials is a crucial parameter considering UL-94 tests.

In the glass fiber reinforced materials, the previous effects appear to be disrupted. Only MCA still shows its cooling effect at 3 and 7 sec (T5 reaching a plateau at 100 °C from 7 to 10 sec). No effect is detected in the formulations containing MPY and GSMP as the temperature keeps increasing up to 150 °C during the 10 sec of ignition. It is assumed a change in the rheological and mechanical properties of the matrix could also interfere with the additives (worse diffusion of substances diluting the flame in the case of MCA or GSMP, interactions of fibers with the intumescent shield in the case of MPY).

The measurement of weight losses also highlights differences in the mode of action of the additives, most of all in the case of unreinforced materials. For instance, PA6 and PA6-MCA release about 1 wt% volatiles whereas PA6-MPY releases 5 wt% and PA6-GSMP releases 8 wt%. This means the mechanisms of PA6 and PA6-MCA mainly occur in the condensed phase. In that case, flame stops because of dripping (8 wt% for neat PA6 and 6 wt% for PA6-MCA) and in the case of FR formulation the drops do not ignite cotton. As far as MCA is concerned, it leads to PA6 chain scission thus to a decrease of its molecular weight and viscosity, leading to dripping. However, combustion times also need to be considered. In the case of MPY, the formation of the intumescent structure is required to protect the material and stop the flame. The formation of this structure is linked to chemical decomposition and reaction of both the additive and of the decomposition products of the polymer and thus the formation of volatiles is expected. Last, if we consider PA6-GSMP, "dripping" effect linked to a modification of the decomposition pathway of PA6 occurs, and thus it reasonably explains the formation of 8 wt% volatiles.

Concerning reinforced materials, the mass measurement also gives trends on the effect of glass fibers on the formulations. For instance, the release of heavy char chunks in the case of PA6GF-MPY indicates a change in the rheological, mechanical and thermal properties of the material. Indeed, a higher weight of char is needed to induce the fall of a chunk, so that the mechanical resistance is increased, and also the thermal diffusion inside the bar leads to the propagation of the flame. The progressive release of heavy drops in the case of PA6GF-GSMP suggests that the evacuation of heat by dripping is not as efficient as in the unreinforced formulation. A longer delay between drips could induce a stronger degradation and hence, leads to the propagation of combustion. PA6GF-MCA shows the effect of the flame retardant is only disrupted in terms of flaming of the drop though.

V.2.5   Conclusion

In this section, instrumentation was set up on the UL-94 standard vertical test to provide better understanding of the mechanisms occurring in the materials during the test. It was shown that, it is easy to observe at which levels different additives can participate in the fire retardancy of materials and in their classification in UL-94. The measurement of the mass of bar and drops also permits to quantify the volatiles released during the test. This instrumentation should help to better understand the mechanisms of action of various FR, including PAS, the previously prepared novel phosphinate salt. In the next sections, the methodology hereinbefore developed will be applied to FR PBT and PBTGF including PAS and Exolit® OP1240 (a commercial flame retardant for PBT for which the mechanism of action was elucidated).

V.3. STUDY OF PBT-GF-PAS SYSTEM

In Chapter IV, it has been shown that the addition of 20 wt% PAS allows the development of a flame retardant formulation for PBTGF (PBTGF-PAS; V-1 ranking). The efficiency of this self-prepared additive is even higher in unreinforced PBT (PBT-PAS; V-0 ranking), at least in terms of UL-94 classification. This trend is in good correlation with the previously reported results: UL-94 ranking decreases when FRPBT is reinforced with GF. To better understand the difference of behavior between PBTGF-PAS and PBT-PAS, the instrumentation previously designed on the UL-94 was applied to the four components: PBT, PBT-PAS, PBTGF and PBTGF-PAS.

First, the weight loss, mass of drops, as well as the temperature profiles for neat PBT and GF-reinforced PBT are reported in Figure 87 and Figure 88 respectively. It should be highlighted that the burner was applied only once as the bar burns up to the clamp at first ignition. The neat matrices are thus NC.
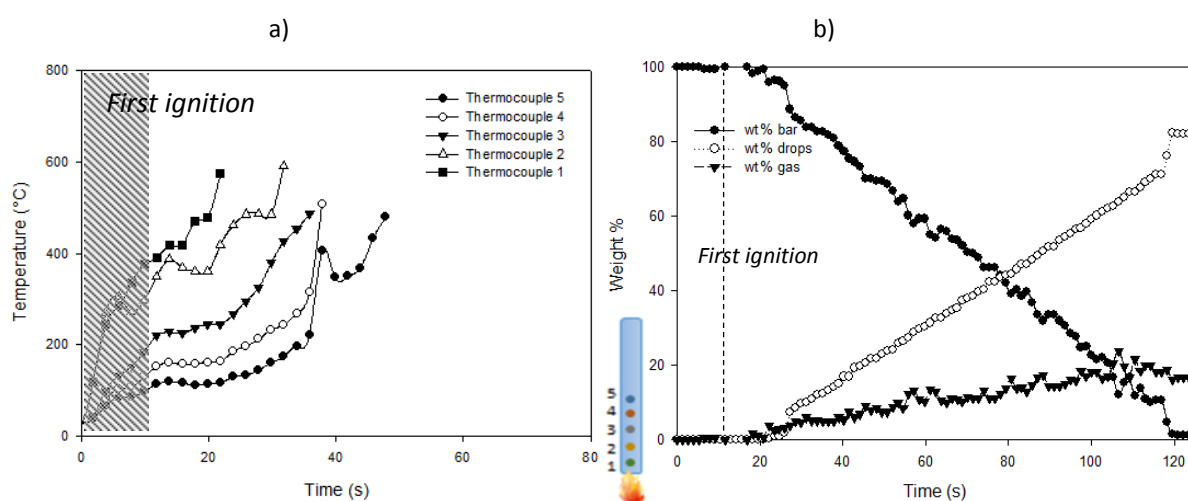

Figure 87: Measurement of a) temperatures and b) masses during the UL-94 test of PBT
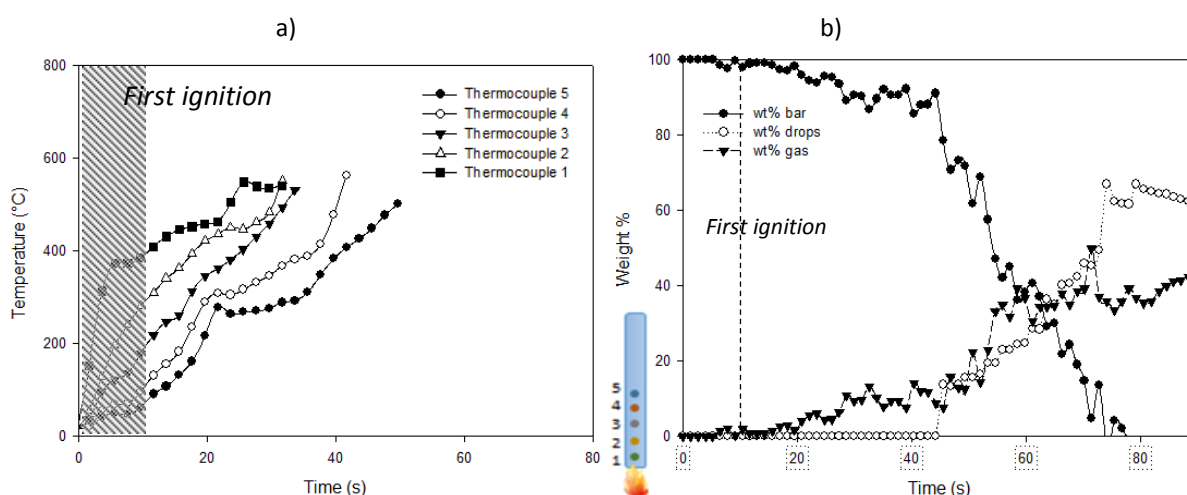

Figure 88: Measurement of a) temperatures and b) masses during the UL-94 test of PBTGF

In the case of PBT, after ignition, the five thermocouples from T1 to T5 reach temperatures of 385, 310, 200, 105 and 85 °C respectively. While the bar burns up to the clamp, each thermocouple reaches maximum temperatures of 585, 580, 485, 505 and 480 °C respectively before the thermocouple gets out of the matrix. The polymer progressively releases molten droplets up to

120 s. Mass loss measurements reveal a constant weight loss corresponding at the end of the test to 82 wt% of drops and 18 wt% of evolved gases (Figure 87-b).

Concerning PBTGF, T1 to T5 reach temperatures of 395, 295, 205, 110 and 75 °C respectively after 10 s ignition. The five thermocouples reach maximum temperatures of 550, 550, 550, 560 and 510 °C respectively, when parts of the bar fall and thermocouples are no more embedded in the matrix. The measurement of mass loss reveals a weight loss of 100 wt% at the end of the test corresponding to 65 wt% drops and 45 wt% volatiles (Figure 88-b).

In term of temperature profiles, PBT and PBTGF behave quite similarly in the UL-94. This fact is unexpected regarding the observations made on PA6 about thermal diffusivities. Temperature profiles are not affected by the presence of GF. This can easily be explained by the fact that the temperatures reached are limited by dripping. Above a given temperature, the matrix decomposes and drips, which gives no more information on the temperature. This should be related with the thermal characterization of PBT (carried out previously, Figure 67), which decomposes around 400 °C and is known to volatilize.

However, the GF clearly affect the degradation of PBT. This effect is particularly observed in the measurement of masses: about three times more volatiles are released in the case of PBTGF compared to unreinforced PBT this is not consistent with the lower content of combustible in PBTGF due to the presence of GF. It is observed that the dripping occurs at longer time in presence of GF (t=45s for PBTGF compared to 20 sec for PBT). At that time, the weight loss due to gas release is around 15 wt%. it could thus be assumed that in presence of GF, dripping is limited or at least delayed and thus the material is longer exposed to the flame and further degraded. In the case of unreinforced PBT, the lower melt viscosity enhances dripping, evacuation of heat, and then slows down the combustion.

Knowing the behavior of neat PBT in this test, it is now possible to investigate the flame-retarded formulation containing PAS. The weight loss curve, weight of drops and temperature profiles versus time of PBT-PAS are reported in Figure 89 and in Figure 90 for the glass-fiber reinforced material.
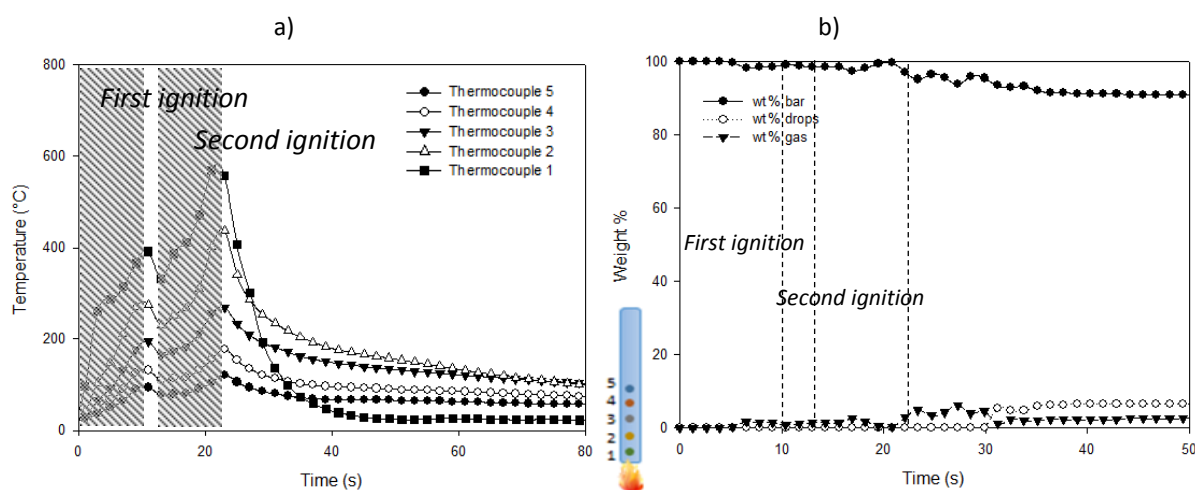

Figure 89: Measurement of a) temperatures and b) masses during the UL-94 test of PBT-PAS

In the case of PBT-PAS, after first ignition, T1 to T5 reach temperatures of 395, 275, 195, 125 and 95 °C respectively. After second ignition, the five thermocouples reach temperatures of 585, 440, 270, 175 and 120 °C. The mass loss measurements reveal a weight loss of 8 wt% corresponding to

6 wt% drops and 2 wt% evolved gases. Only one drop falls from the bar after second ignition, around 25s, leading to a V-0 ranking.

In the case of PBTGF-PAS, the five thermocouples reach temperatures of 520, 330, 260, 185 and 115 °C respectively, after first ignition. The temperatures reached after second ignition are 550, 405, 315, 240 and 205 °C respectively. The bar releases one small char chunk after 50s. The weight loss is 7 wt%, corresponding to 5 wt% drops and 2 wt% evolved gases. PBTGF-PAS reaches a V-1 classification due to combustion time.

Neat matrices exhibited a similar behavior in terms of temperature profiles. On the contrary, flame-retarded matrices do not. PBTGF-PAS reaches higher temperatures at first ignition compared to PBT-PAS. In the case of reinforced system the temperature does not increase at second ignition whereas in PBT-PAS, the maximum temperature for T1 is about 200 °C higher in second ignition than in first ignition. The temperature decreases faster after flameout in the case of PBT-PAS.
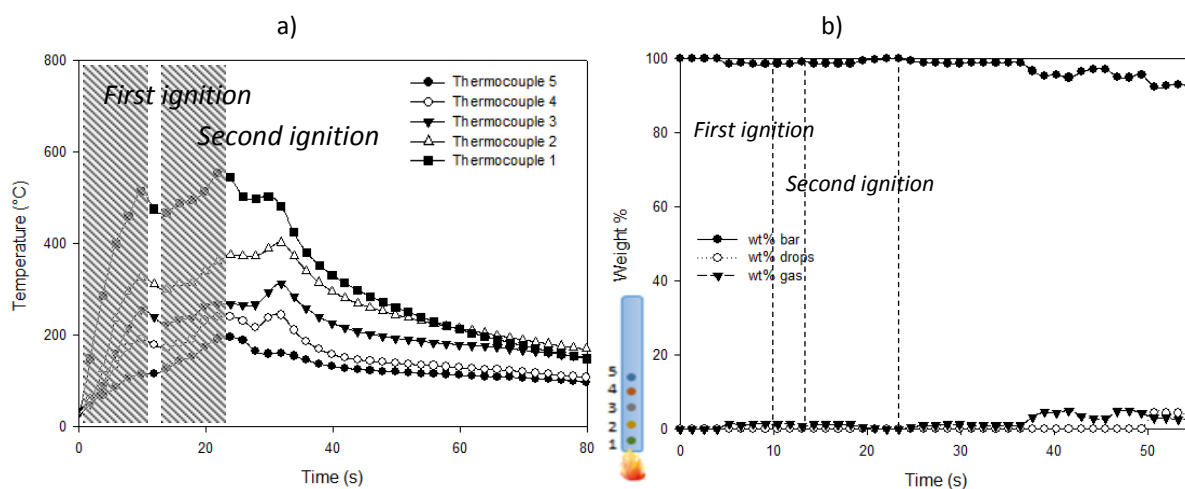

Figure 90: Measurement of a) temperatures and b) masses during the UL-94 test of PBTGF-PAS

It can thus be assumed that the presence of glass fibers promotes heat conduction into the bar (wick effect already illustrated in the previous sections). GF also decrease the cooling speed after flameout, as if they "stored" the heat inside the bar. A measurement of ρ and C_p (to reach the $\rho \times C_p$) would confirm this hypothesis of heat storage.

In both cases, the mass losses are equivalent. As a conclusion, the difference of classification between PBTGF-PAS (V-1) and PBT-PAS (V-0) can be reasonably attributed to the fact that the heat is efficiently evacuated by dripping in the unreinforced material, leading to flameout.

Interestingly, as PAS could be a potential new commercial FR, it should be compared with another well-known FR: Exolit® OP 1240. As it was previously described, OP1240 is also an aluminum phosphinate designed for polyester injection-molding applications, and most of all, the mode of action of this FR has been elucidated. The next section will describe the results of PBT/GF/OP1240 formulations in the instrumented UL-94, which will help understanding the modes of action of PAS and the role of GF in these formulations.

V.4. COMPARISON WITH THE PBT-GF-OP1240 SYSTEM

In the literature, the mode of action of OP1240 was proposed notably by Braun and Schartel, in different matrices and together with various co-additives or not **[37, 81, 127, 181]**. In PBT, the authors showed that OP1240 releases diethylphosphinic acid upon decomposition, which acts as flame poison and radical scavenger under the form of PO°. The formation of a char was also underlined. This charring process was caused simply by the "loss of hydrogen for the formation of volatile hydrocarbon compounds"; consequently carbon-rich derivates remained in residue, together with aluminum phosphates.

PBT and PBTGF were compounded with 20 wt% OP1240, and the corresponding formulations were analyzed in the instrumented UL-94. The results for the unreinforced matrix are reported in Figure 91, and in Figure 92 for PBTGF-OP1240.
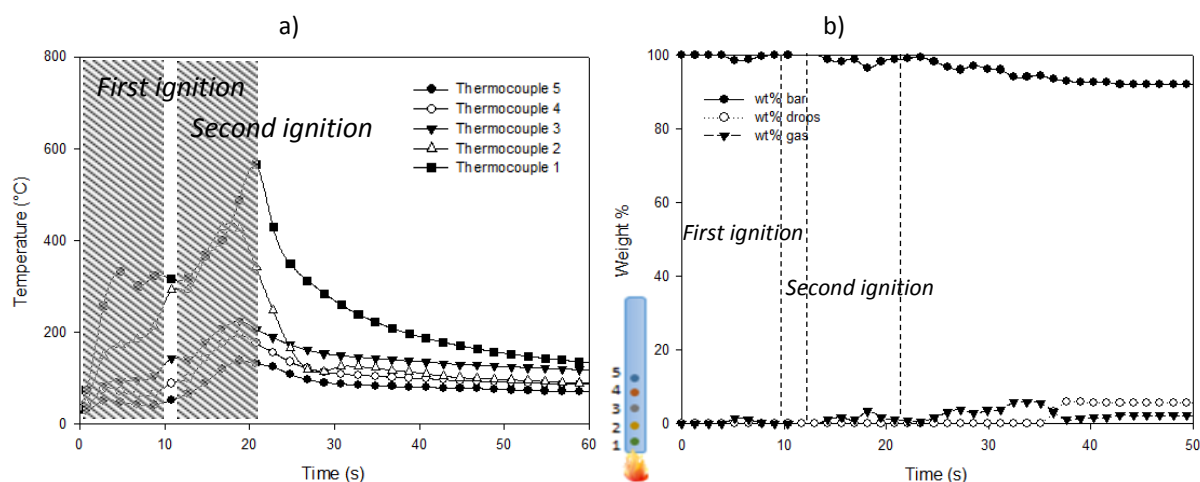

Figure 91: Measurement of a) temperatures and b) masses during the UL-94 test of PBT-OP1240
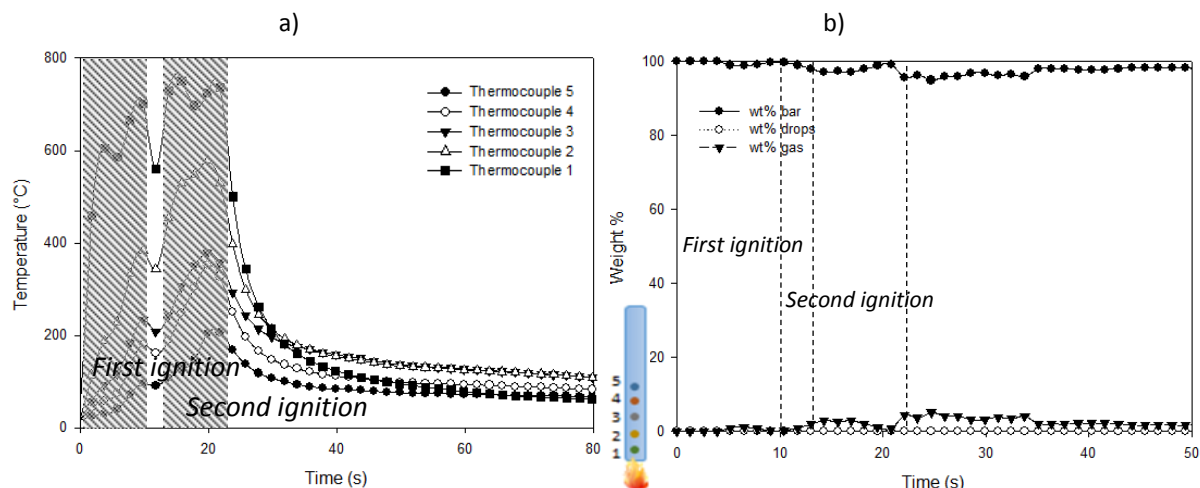

Figure 92: Measurement of a) temperatures and b) masses during the UL-94 test of PBTGF-OP1240

In the case of PBT-OP1240, the five thermocouples reach temperatures of 320, 285, 140, 90 and 55 °C respectively after first ignition. After second ignition, T1 to T5 reach temperatures of 565, 435, 220, 195 and 135 °C respectively. The measurement of mass loss reveals a loss of 8 wt%, corresponding to 6 wt% drops (one heavy drop is released at 35 s) and 2 wt% volatiles. The bar flames out while dripping, leading to a V-0 classification.

Concerning PBTGF-OP1240, T1 to T5 reach temperatures of 710, 390, 230, 180 and 100 °C respectively after first ignition. At second ignition, the thermocouples reach temperatures of 760, 580, 380, 350 and 220 °C. The weight loss of this formulation is very low: no drop is released and only 2 wt% of the bar degrades as evolved gases. The formulation is classified V-0.

The temperatures reached by PBTGF-OP1240 are sensibly higher than those obtained for PBT-OP1240. Again, this should illustrate the "heat-accumulation" effect due to glass fibers. PBTGF-OP1240 does not show any dripping after second ignition compared to PBT-OP1240 which releases a non-flaming drop.

To achieve a better comparison of PAS and OP1240 in PBT and PBTGF, the temperature profiles were overlaid in Figure 93 for PBT and Figure 94 for PBTGF.
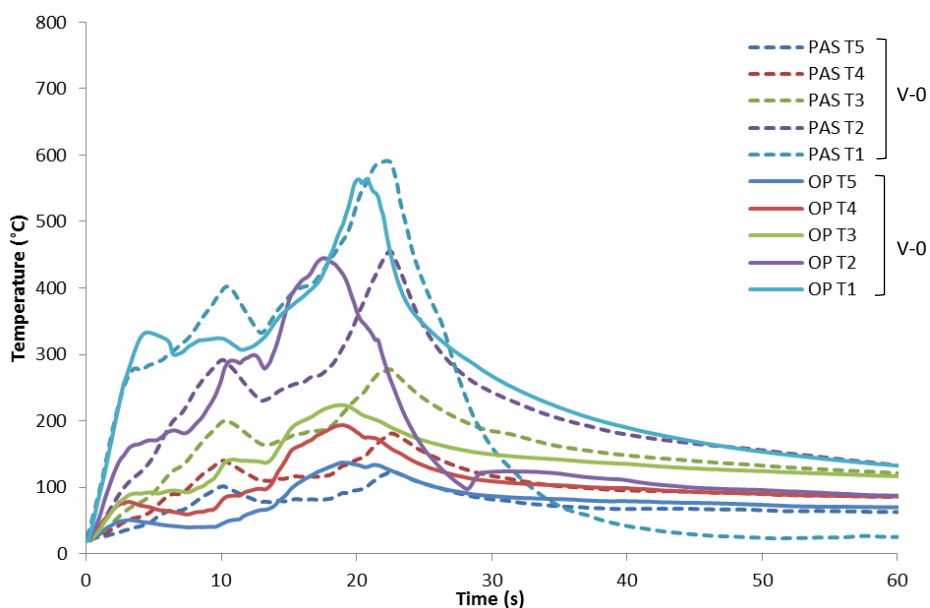

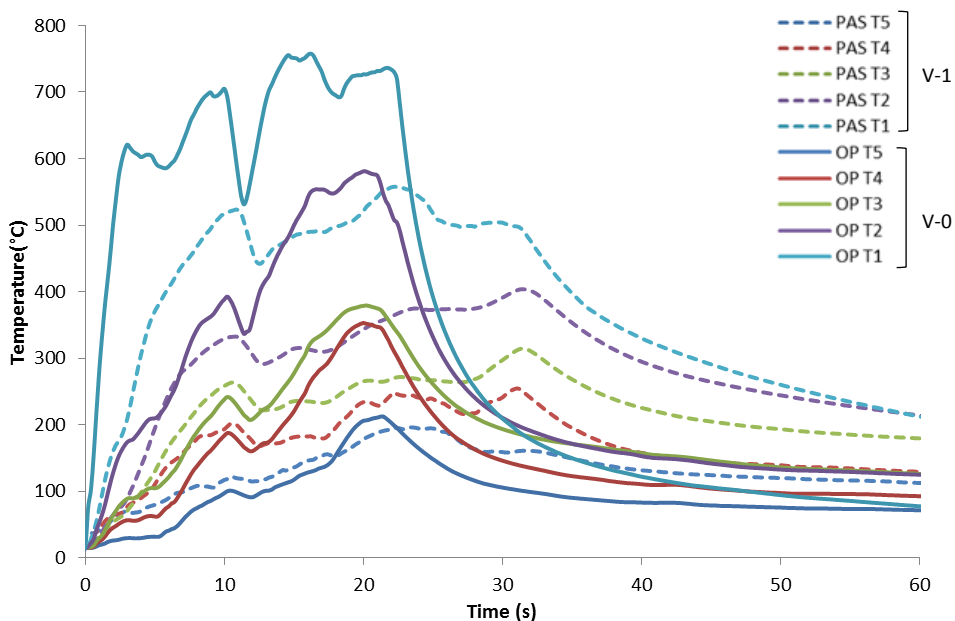**Figure 93: Overlay of temperature profiles of PBT-PAS and PBT-OP1240**

Figure 94: Overlay of temperature profiles of PBTGF-PAS and PBTGF-OP1240

Two different cases are observed in Figure 93 and Figure 94. PBT-PAS and PBT-OP1240 exhibit a comparable behavior (temperatures are within a margin of ±50 °C for each thermocouple). However, it is observed that the highest temperature after second ignition is reached later in the case of PBT-PAS.

In the reinforced matrix, the behavior of the two additives is different. The heating rate at first ignition is slower in the case of PBTGF-PAS, which achieves much lower temperatures in the zone exposed to the flame (T1 and T2). This clearly indicates an endothermic effect in the condensed phase in the case of PBTGF-PAS. However, the temperature decrease after second ignition occurs over a longer period of time in PBTGF-PAS compared to PBTGF-OP1240. After second ignition (after 23 s) the temperature is maintained up to 35 s and then decreases when PAS is used. With OP1240, the temperature directly decreases after 20 s. In fact PBTGF-PAS keeps burning for 10 s after second ignition while PBTGF-OP1240 flames out. This second observation suggests that PAS releases fragments that are less reactive than those of OP1240, and probably has less effect in the gas phase.

From these observations, it is clearly shown that the mode of action of the two additives is rather different. The literature exposes OP1240 as acting mainly in the gas phase. The measurement carried out in unreinforced PBT would lead to the hypothesis that both additives act in the gas phase. However, in that case, dripping is the driving phenomena, and heat is efficiently evacuated by dripping, leading to self-extinguishment. In the reinforced material, PAS reaches lower temperatures but longer flaming times. Two hypotheses can be formulated in this case. First, if the enthalpy of decomposition of PAS was higher than that of OP1240, that would simply explain the lower temperatures achieved during the test. Else, the formation of a charred barrier could occur, which would explain the stabilization of temperatures at lower values; this effect would not be observed in the unreinforced material. Indeed, due to dripping, no efficient shield can be formed. Glass fibers would contribute to the formation of this barrier, likewise an intumescent shield. This barrier will not be efficient enough to stop the fire and would limit the diffusion of the gas phase-active species to the flame.

Thanks to the coupling of TGA and DSC, the decomposition enthalpy of PAS and OP1240 was measured during the TGA (ramp of 10 °C/min in N_2). The results are reported in Figure 95 and Figure 96 respectively.
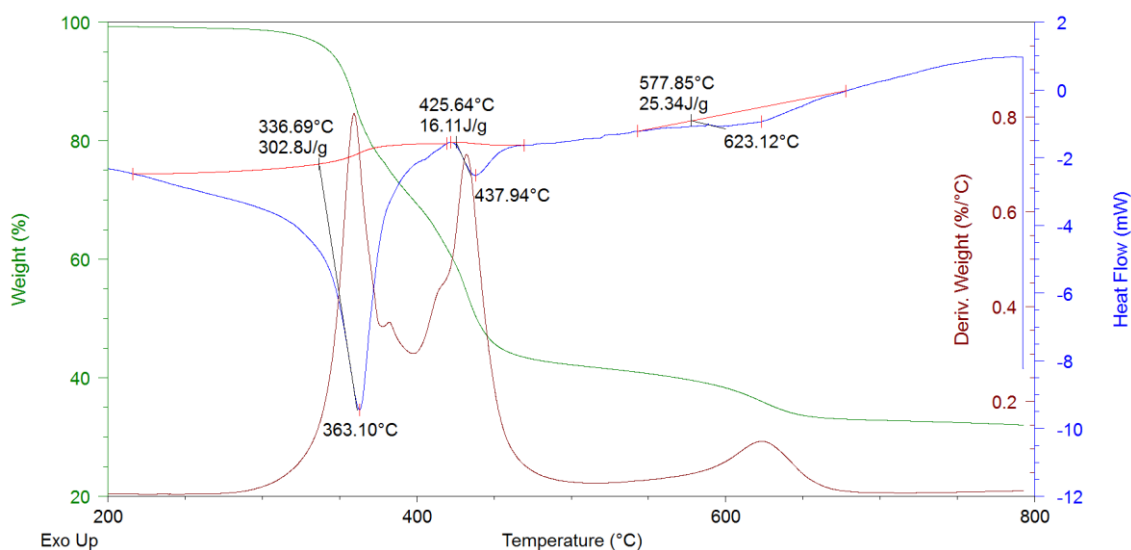

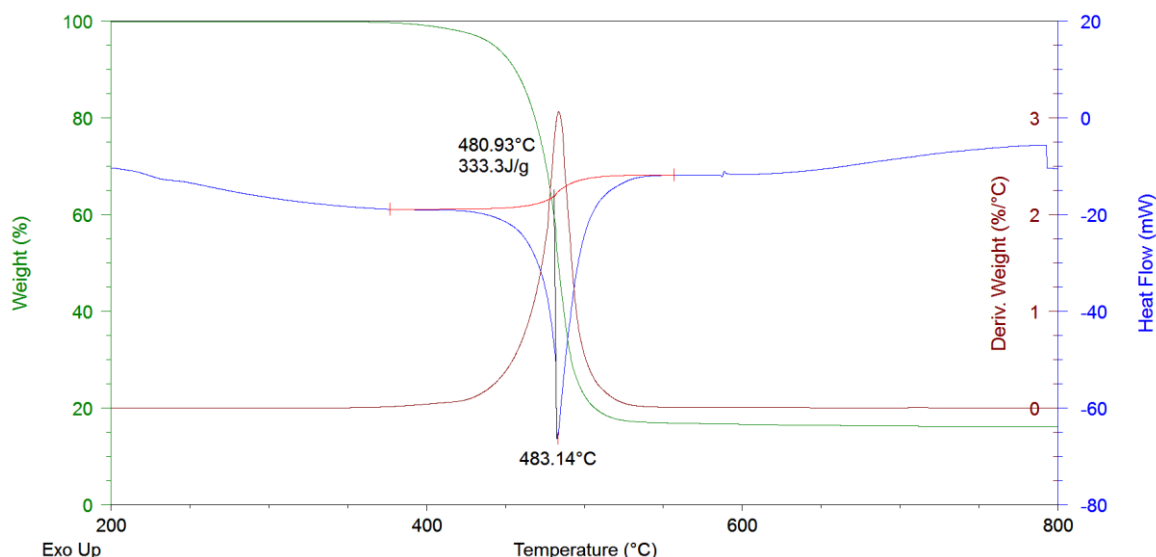**Figure 95: Measurement of the decomposition enthalpy of PAS**

Figure 96: Measurement of the decomposition enthalpy of OP1240

OP1240 decomposes in one step with an enthalpy of 333 J/g, whereas PAS decomposes in three steps with enthalpies of 302, 16 and 25 J/g (global enthalpy of decomposition of 343 J/g). The two additives exhibit similar enthalpies of decomposition. Consequently, the first hypothesis on the enhanced cooling effect of PAS cannot be validated. However, it should be highlighted that these measurements also show that OP1240 decomposes at higher temperatures compared to PAS, which can be linked with the higher temperature achieved by the PBTGF-OP1240 formulation.

On the other hand, the formation of a reinforced shield was observed in SEM pictures on the burnt part of a PBTGF-PAS bar after the UL-94 test (Figure 97). These pictures highlight the presence of glass fibers in a charred structure. The previous results confirm the second hypothesis, according to which PAS degrades during the UL-94 test by forming a charred barrier in which the glass fibers are involved.
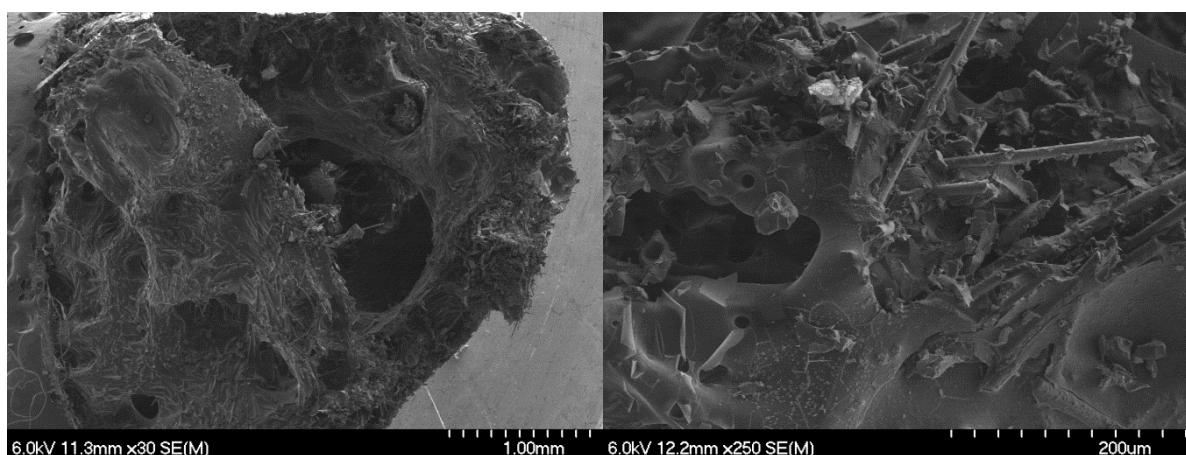
Figure 97: SEM pictures of the burnt part of a PBTGF-PAS bar after UL-94 test

Consequently, the difference of classification between PBT-PAS (V-0) and PBTGF-PAS (V-1) is due to the formation of a protective structure in the reinforced material. Though this structure protects the material from the heat of ignition, the absence of dripping in the reinforced material causes a longer burning as heat is less efficiently evacuated. A longer burning time leads to a worse classification.

V.5.CONCLUSION

In this chapter, a new way to investigate the fire retardancy of materials has been developed. Novel data could be obtained from the UL-94 testing (main test in the E&E industry) thanks to the design of various instrumentations. The temperature gradients inside the materials during the test were measured using thermocouples. A measurement of the mass loss of the bar and of the drops was carried out also during the test, leading to the measurement of the proportion of released evolved gases.

The instrumentation was set up with eight formulations of PA6. Various effects were identified in the temperature profiles and mass measurements: endothermic effects, formation of a char, mechanical reinforcement, and enhancement of dripping. The methodology was then applied on the formulations previously identified in chapter IV: PBT/GF/PAS. Key factors on the classification of these formulations were listed (dripping, cooling effects, or auto-extinguishment), and compared to those of the well-known Exolit® OP 1240.

OP1240 mainly acts in the gas phase. The comparison of PBT-PAS and PBT-OP1240 was not sufficient to explain the mode of action of PAS as the main driving phenomena in the two unreinforced formulation is dripping. However, the lower temperatures achieved by PBTGF-PAS suggested an action in the condensed phase for PAS. The measurement of enthalpies of decomposition and the observation of the burnt bar of PBTGF-PAS in SEM validates the hypothesis of the formation of a protective shield when PAS is used as additive.

This hypothesis still needs to be proven. In many cases, ex-situ analyses do not correspond to real fire scenario. The instrumentation of the UL-94 allowed measuring novel parameters in "real" fire testing conditions. The temperature profiles indicate at which temperature and with which ramp a formulation or an additive should be analyzed for example in TGA or py-GC/MS. The hypothesis of the formation of a protective structure in the condensed phase should be investigated through analyses on residues after thermal treatments. Even if it occurs after longer times compared to PBTGF-OP1240, the self-extinguishment of PBTGF-PAS still indicates a potential action in the gas phase, even if the contribution is not as important as in the case of OP1240. The analysis of the gas phase should thus also give clues on such an action.

In the next chapter, a complete mechanism of chemical decomposition of PAS and of its formulation with PBT and the corresponding physical parameters will thus be investigated.

_____

Chapter VI.   Comprehension of the mechanisms of decomposition of a novel phosphinate salt

_____

VI.1. INTRODUCTION

In the previous chapters, five different novel phosphinate salts were synthesized and tested as FR for PBT and PA6. Among them, one salt showed outstanding flame-retardant properties in PBT: the aluminum salt of phenyl amide of 3-(hydroxy(phenyl)phosphoryl) propanoic acid (PAS). In the previous chapter, it has been shown that this salt exhibits a potential condensed-phase activity. However, the low flammability of PBT-PAS materials and its self-extinguishing properties also suggested a gas-phase activity. This chapter aims at investigating the mechanisms of decomposition of PAS and its interactions with PBTGF by means of various analytical techniques.

TGA-FTIR will allow determining the main degradation products released during a slow heating ramp treatment (in the range of 10 °C/min). This slow heating ramp, as previously shown in the measurement of temperatures in UL-94, does not correspond to the main testing conditions. In case of a fire, only the parts of the polymeric materials which are not directly exposed to the flame may reach this heating ramp. TGA-FTIR will thus simulate at microscale this kind of incident, and will allow a first approach of the decomposition pathway of the additive. The comparison of PAS with two other salts (PPDS and EDAS) will be achieved, to both help elucidating the degradation pathway by analogies and better understand the singularity of PAS. On the other hand, samples will be heat-treated in similar conditions and the residues will be collected. They will be analyzed using carbon, phosphorus and aluminum solid-state NMR. Thanks to such analyses, gas- and condensed-phase activity can be related.

Py-GC/MS is another powerful tool to investigate the degradation pathway of various substances. Compared to TGA-FTIR, this technique brings two advantages. Firstly, it allows applying a flash pyrolysis treatment, which better corresponds to the part of the material exposed directly to the flame in a UL-94 test even if it is at a microscale. In addition, the identification of degradation products is easier in gas chromatography and mass spectroscopy as they are separated by the GC and can be identified through database search in MS, which also allows a relative quantification of detected substances. EGA/MS will also be used to validate the degradation pathway proposed previously.

The combination of all these techniques, applied to PAS, PBTGF, and their formulation, will allow drawing a complete degradation mechanism of PAS and its interactions with PBTGF, thus helping to understand the modes of action of this new additive.

VI.2. ANALYSIS OF EVOLVED GASES

VI.2.1 TGA-FTIR

VI.2.1.1 TGA-FTIR of the phosphinate salts

In this section, the FTIR spectra of evolved gases recorded during the TGA experiment of the phosphinate salts will be presented. For the sake of comprehension, only three salts will be investigated. Interestingly, PAS will be compared to PPDS and EDAS. PPDS exhibits a structure close to that of PAS as it is the corresponding dimer (symmetric aromatic diamide). EDAS exhibits a different structure as it is based on a linear aliphatic structure. Possible differences in terms of decomposition could give trends on the reasons why they are or not effective as FR. It should be highlighted that only FTIR spectra corresponding to the evolved gases at 400, 450, 500 and 550 °C will be presented. These temperatures were chosen regarding the spectra of PAS and its

characteristic TGA data. As a matter of comparison same temperatures will be presented for the other salts. It is also necessary to underline the fact that in the profiles presented hereinafter, the results are not quantitative. However they allow determining the range of temperature in which some of the characteristic band of given species are released.

The TGA-FTIR of PAS (TGA is presented in Figure 98, FTIR Spectra in Figure 99) reveals the presence of characteristic bands of isocyanates (-N=C=O, 2280 cm^{-1}), aniline (=C-H, 3044, 744 cm^{-1}; NH_2, C=C and C-N, 1621, 1502, and 1271 cm^{-1} respectively) and also CO_2 (2382, 2306 cm^{-1}). The presence of the sharp peak at 674 cm^{-1} together with the =C-H over 3000 cm^{-1} also suggests the presence of benzene. Finally, water (3500-3600 cm^{-1}) is also released upon the degradation of PAS.
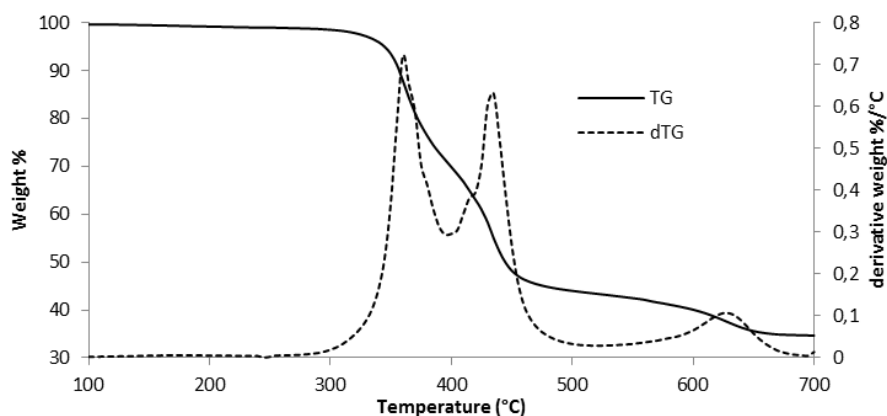

Figure 98: TGA of PAS, 10 °C/min, in N_2
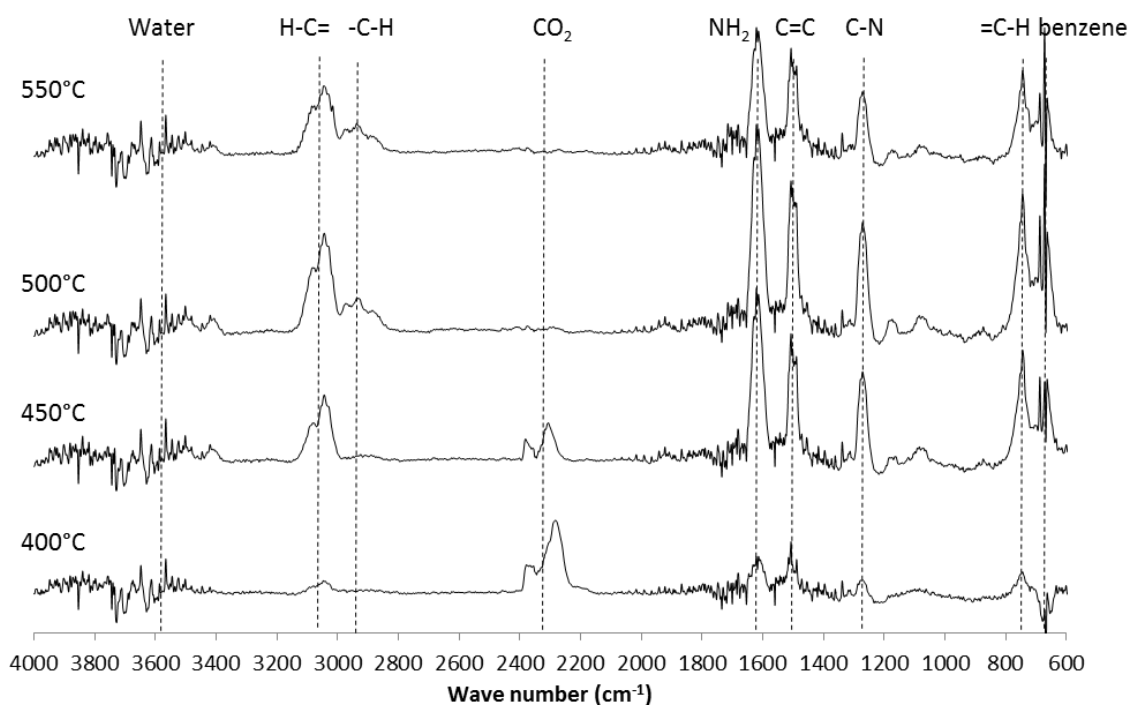
Figure 99: FTIR spectra of the degradation gases collected during TGA of PAS, 10 °C/min, in N_2

The presence of CO_2 was previously explained by Louisy [20]. It was attributed to the evolution of isocyanates (formed upon decomposition of amides) into amine and CO_2. The isocyanate N=C=O asymmetric stretch is observed around 2280 cm^{-1}, that is to say it is shouldering CO_2, and thus giving a profile of these two species is hazardous. In the present case, the profiles indicate isocyanates and

CO_2 are released over the same temperature range. It is reasonable to assume that isocyanates could be formed but hydrolyzed through the FTIR transfer line into phenylamide and CO_2.

The temperature profile of each main band is presented in Figure 100 (temperatures corresponding to the previously depicted spectra are illustrated by dotted lines). It is observed that CO_2 is released between 350 and 500 °C with a maximum intensity at 400 °C. Aliphatic structures are released between 500 °C and 600 °C, and aromatic structures are released from 400 °C to 700 °C with two maxima at 500 °C and 700 °C. Aniline is released from 400 °C to 700 °C but with a broad maximum between 450 and 550 °C.

Figure 100: Area/temperature profile of the different functions identified in TGA-FTIR of PAS (10 °C/min, in N_2)

The TGA-FTIR of PPDS (TGA is presented in Figure 101, FTIR spectra in Figure 102) reveals the presence of CO_2 (2382, 2306 cm^{-1}), aliphatic (3000-2870 cm^{-1}, and bands in the 1300-1600 cm^{-1} region) and aromatic or vinylic structures (3071, 3039, 728 cm^{-1}). Very weak bands can also be found in the same regions as aniline that may correspond to phenylenediamine (NH_2, C=C and C-N, 1621, 1502, and 1271 cm^{-1} respectively). Two small peaks are also observed at 965 and 930 cm^{-1}, and are generally identified as ammonia. Benzene (674 cm^{-1}) and water (3500-3600 cm^{-1}) can also be observed. Finally, two weak peaks attributed to CH_4 (3016 cm^{-1}, C-H stretch, and 1305 cm^{-1}, CH_4 asymmetric bend) are also observed. The formation of methane during the decomposition of the salts is not easily explained though. It might be produced by the rupture of the $P-CH_2-CH_2-$ group.
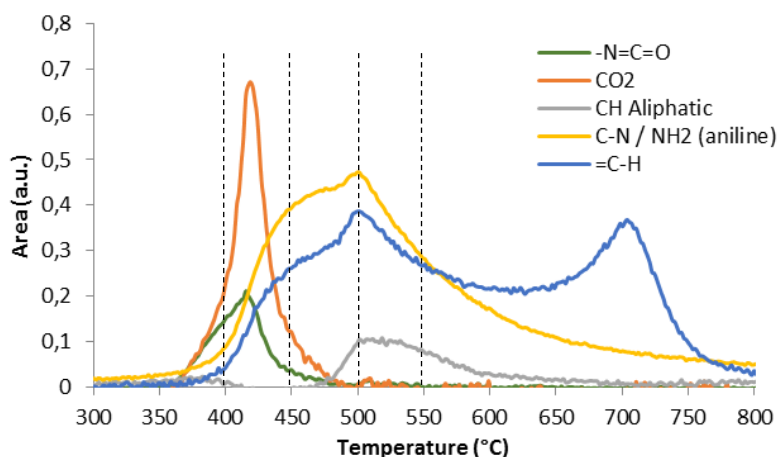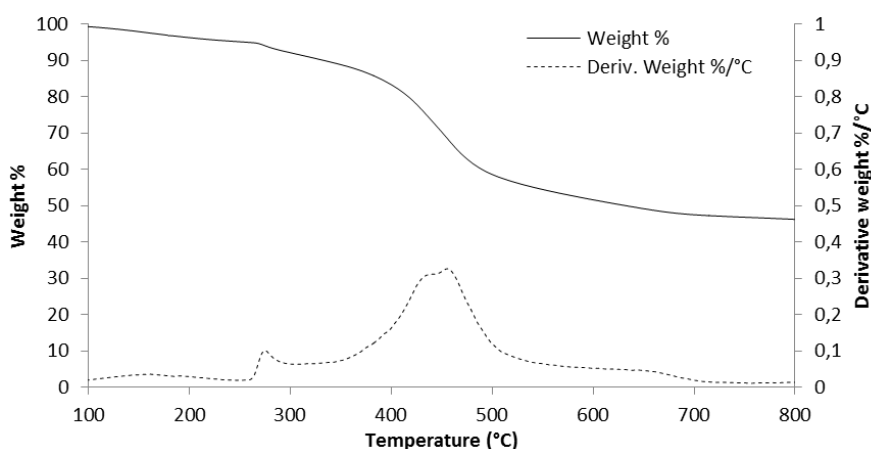

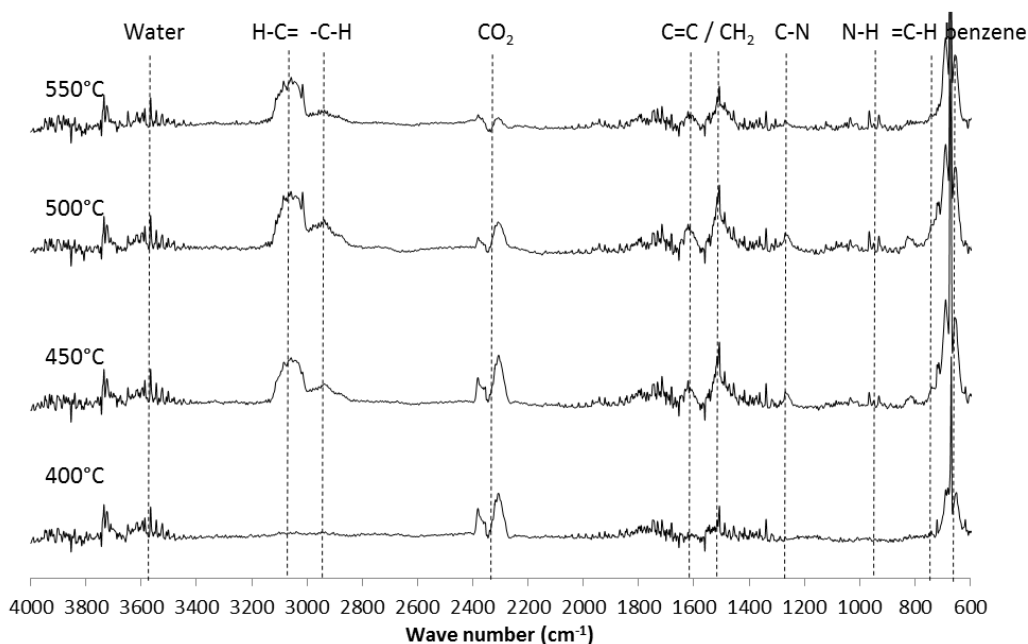Figure 101: TGA of PPDS, 10 °C/min, in N2

Figure 102: FTIR spectra of the degradation gases collected during TGA of PPDS, 10 °C/min, in N$_2$

The profile of the different functions or bonds identified as a function of temperature is presented in Figure 103 (temperatures corresponding to the previously depicted spectra are illustrated by dotted lines). In these profiles, an early release of CO$_2$ can be observed (from 350 to 550 °C with a maximum at 430 °C) similarly to what was observed in the case of PAS but over a longer temperature range. Aliphatic fragments are released in one step (between 400 and 600 °C with a maximum at 500 °C) whereas the release of aromatic fragments occurs in two steps (from 400 to 700 °C with a maximum at 450 °C and a constant release between 500 and 650 °C).
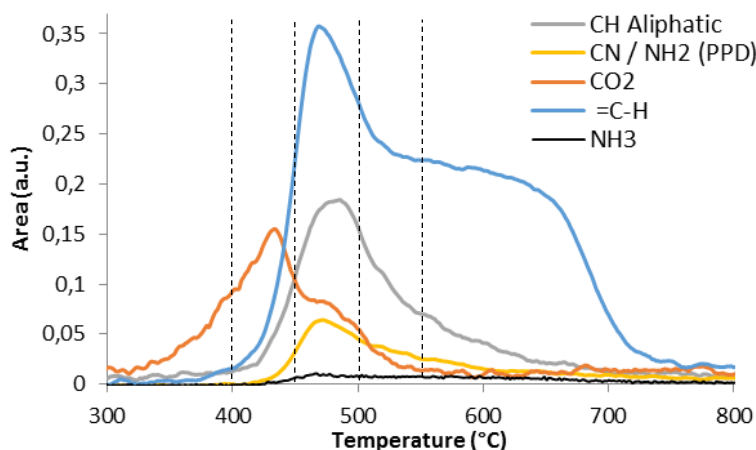
Figure 103: Area/temperature profile of the different functions identified in TGA-FTIR of PPDS (10 °C/min, in N$_2$)

Though PAS and PPDS exhibit a similar structure, the FTIR spectra of evolved gases released during their decomposition at 10 °C/min in nitrogen are different. Compared to PAS and regarding the FTIR spectra, the NH$_2$-Ar bands released in the case of PPDS are much weaker (they were sharp in the case of PAS). This observation, in relation with the effectiveness of PAS compared to PPDS, could highlight the influence of the release of aniline in the mode of action of PAS.

The TGA-FTIR of EDAS (TGA is reported in Figure 104 and FTIR spectra in Figure 105) reveals the presence of CO_2 (2382, 2306 cm^{-1}), aliphatic (2935, 2876, 1500 cm^{-1}) and aromatic or vinylic structures (3071, 3039, 728 cm^{-1}), and also N-H bonds (ammonia, 3333, 965/930 cm^{-1}).

The profile of the different functions or bonds identified as a function of temperature is presented in Figure 106 (temperatures corresponding to the previously depicted spectra are illustrated by dotted lines). It is observed that the release of aromatic fragments occurs from 400 to 750 °C with two maxima at 450 and 700 °C. The release of aliphatic structures occurs from 400 to 600 °C with a maximum at 450 °C.
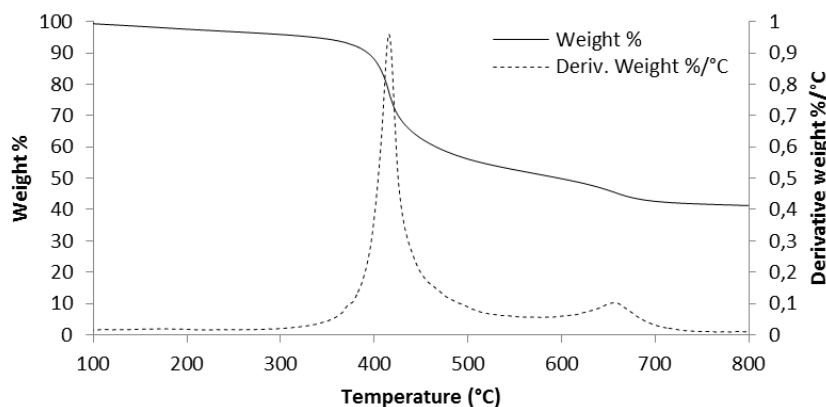
Figure 104: TGA of EDAS, 10 °C/min in N$_2$
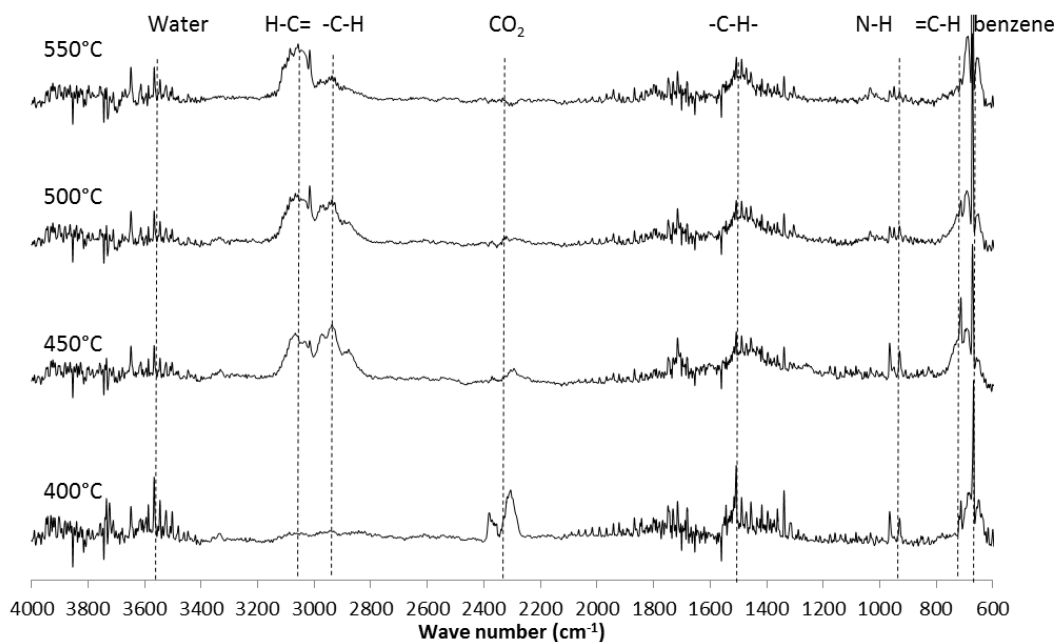
Figure 105: FTIR spectra of the degradation gases collected during TGA of EDAS, 10 °C/min, in N$_2$

The spectra of the evolved gases collected when EDAS degrades are different from those obtained with PPDS. The difference in terms of C-H vibrations (aliphatic as well as aromatic) could be expected as the amine on which EDAS is based is aliphatic whereas PPDS is based on an aromatic core. CO_2 is released later in the case of EDAS compared to PPDS, and more ammonia is released. No isocyanate is observed in EDAS and PPDS, which underlines again the singularity of PAS.

133

Figure 106: Area/temperature profile of the different functions identified in TGA-FTIR of EDAS (10 °C/min, in N$_2$)

One should notice there still can be degradation products released over 600 °C as the dTG of the three salts is not null between 600 and 800 °C. In the figures presented hereinbefore, no focus was done at such temperatures but it should be highlighted that only benzene and water are released (together with a CO$_2$ tailing in the case of PPDS), as depicted in the profiles taken at 650°C (Figure 107).

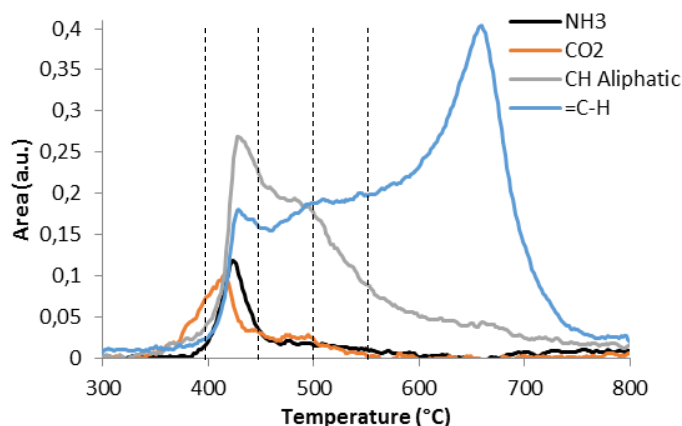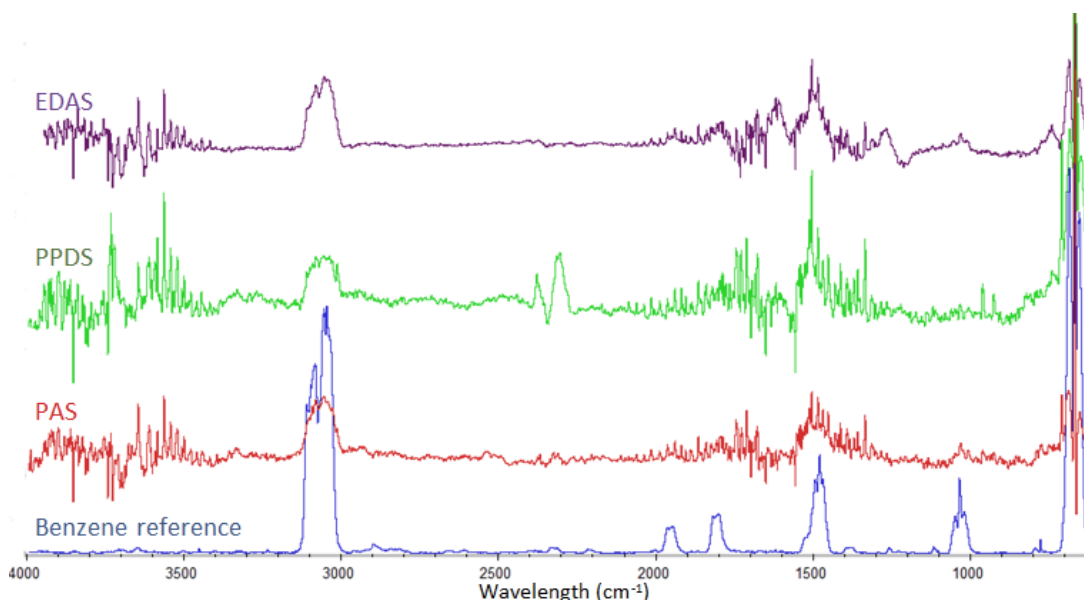**Figure 107: FTIR spectra of the gases collected at 650°C during TGA of PAS, EDAS and PPDS (10 °C/min, in N$_2$)**

VI.2.1.2   TGA-FTIR of PBTGF formulations

Studying the degradation pathway of the phosphinate salts alone does not give information on the way they interact with the matrix they are incorporated in. As a consequence, it is also interesting to investigate the decomposition of PBTGF containing the phosphinate salts. For the sake of this manuscript, a comparison was established between two of the flame retarded materials (PBTGF-EDAS, which did not give satisfactory results in the UL-94 and PBTGF-PAS which exhibited a V-1 classification). Since PBTGF-PPDS TGA-FTIR spectra are similar to those of PBTGF-EDAS, only the latter will be described. It was previously shown that interactions occur between the salts and PBTGF leading to a destabilization between 350 and 410 °C followed by a stabilization between 410 and 500 °C (Figure 69, pp.90).

First, the degradation of PBTGF was studied. In that case (Figure 108), the expected gaseous products from the decomposition pathway proposed in the literature for PBT **[182]** (Figure 6, reported once more hereafter) were observed. However, it should be highlighted that this degradation pathway might be altered by the presence of GF.
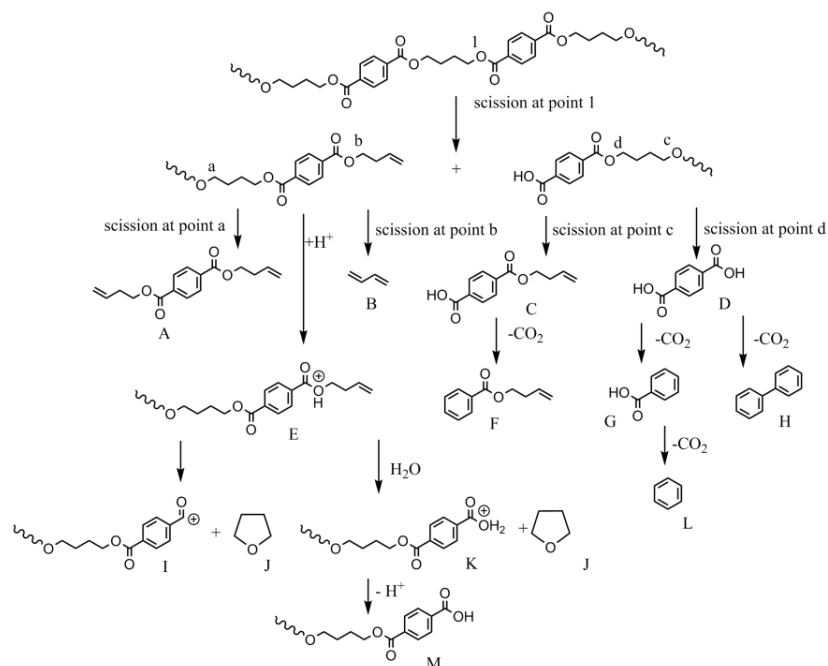
At 400 °C, the degradation is low and peaks of low intensity are observed and attributed to butadiene (908 cm^{-1}) and CO_2 (2370/2300 cm^{-1}). At 450 °C, CO, CO_2, butadiene and esters (1021, 1100, 1180, 1270, and 1740 cm^{-1}) can be observed. At 500 and 550 °C, mainly CO_2 and CO are observed but low intensity bands from esters can still be also be distinguished.
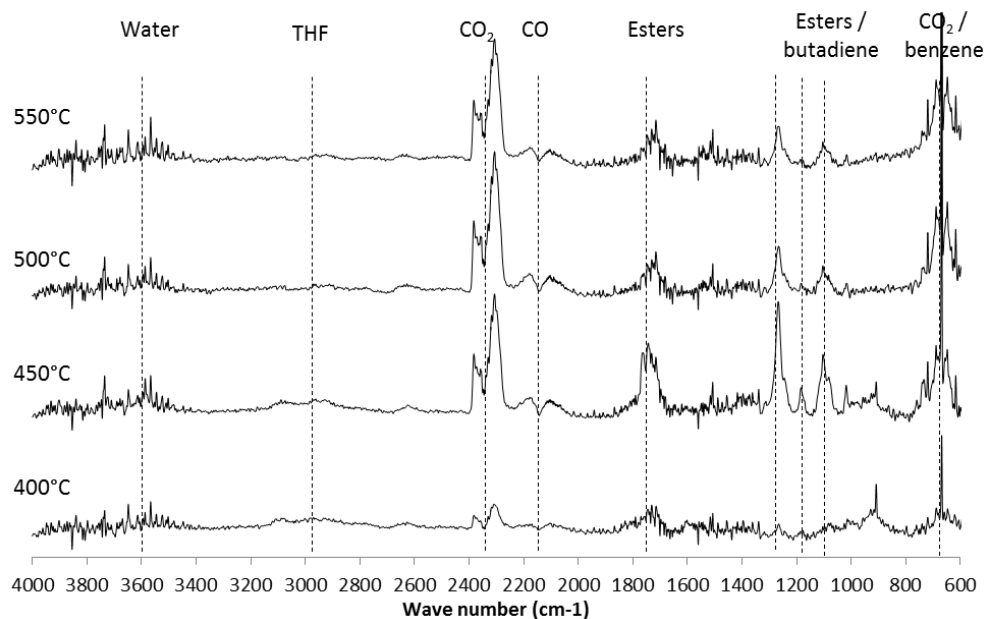
Figure 108: FTIR spectra of the degradation gases collected during TGA of PBTGF, 10 °C/min, in N$_2$

In the case of PBTGF formulated with 20 wt% PAS (Figure 109), a slight difference is observed compared to neat PBTGF. At 400 °C, some peaks of low intensity are observed in the range of 1300

1000 cm^{-1}. Moreover, characteristic peaks corresponding to THF (2980 cm^{-1}, -CH$_2$- , 1070 cm^{-1}, C-O; this second peak is observed in the shoulder of the band at 1740 cm^{-1} and was not marked by a dotted line on the spectra) are clearly observed. Esters are thus released at this temperature, illustrating that the degradation of the matrix occurs at lower temperature in presence of the salt. At 450 °C, water, CO, CO$_2$ and esters are identified. At 500 °C, CO, CO$_2$ and esters are still detected. At 550 °C, again mainly CO$_2$ and CO are observed with weak ester bands.
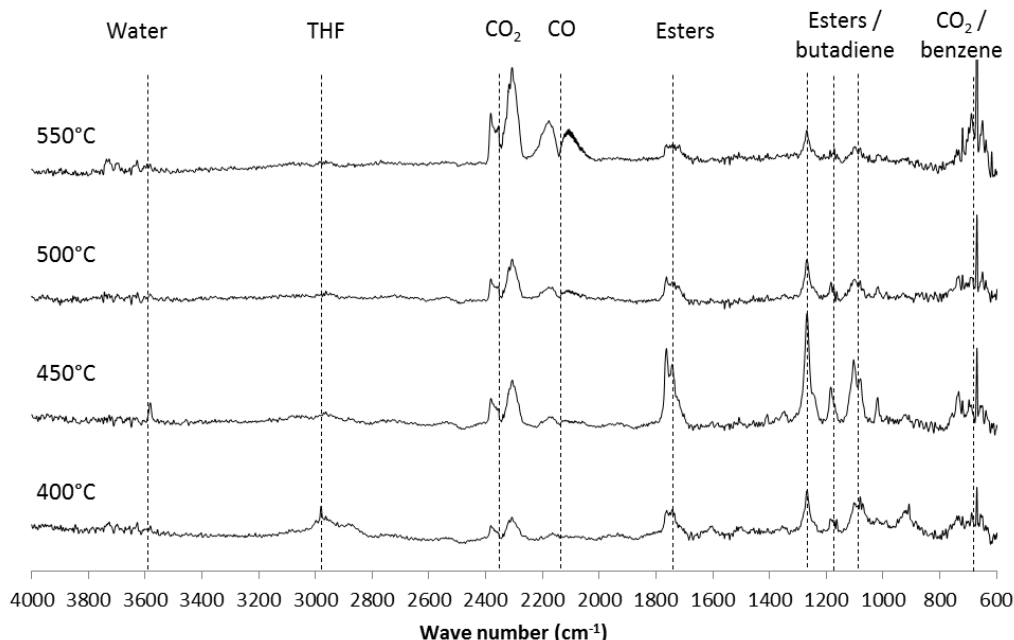
Figure 109: FTIR spectra of the degradation gases collected during TGA of PBTGF 20wt% PAS, 10 °C/min, in N$_2$

In the case of PBTGF flame retarded with 20 wt% EDAS (Figure 110), the pattern is quite similar to that of PBTGF-PAS. At 400 °C, THF is observed as well as weak peaks of CO, CO$_2$ and esters. At 450 °C, the release of THF is still visible, combined with the release of CO, CO$_2$ and esters. At 500 °C and 550 °C, mainly CO and CO$_2$ are identified with weak ester bands.
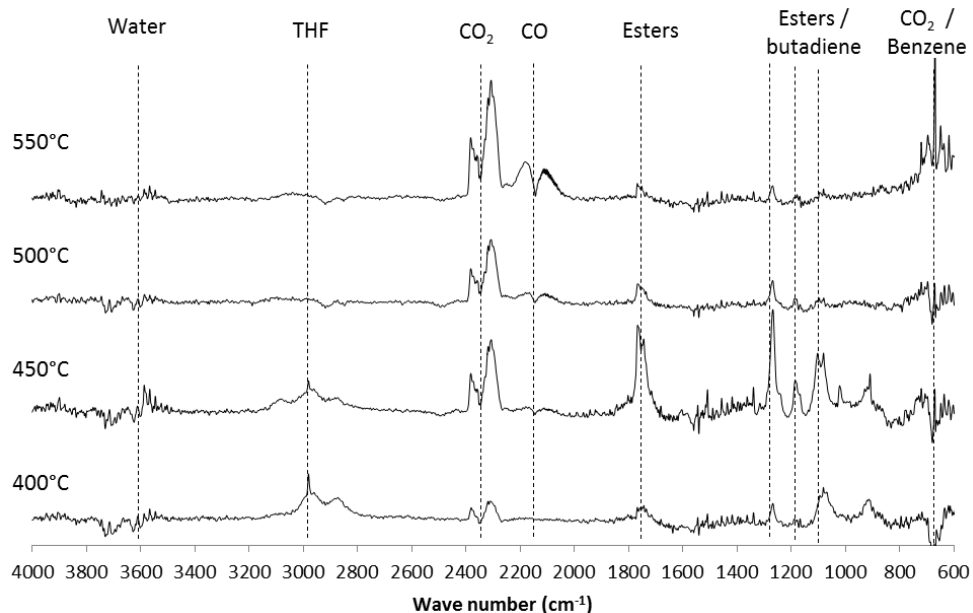

Figure 110 : FTIR spectra of the degradation gases collected during TGA of PBTGF 20wt% EDAS, 10 °C/min, in N$_2$

These results allow illustrating the slight modification of the degradation kinetics of PBT in presence of the phosphinic acid salts. THF is observed during the degradation of the flame retarded PBT and below 450 °C. The interaction observed in the TGdifference curve (Figure 69, pp.90, 360-410 °C) demonstrating a destabilization could, at least partially, be explained by a catalysis of the degradation of PBT leading to more end groups and thus an enhance of the backbiting reaction of PBT leading to the release of THF (Figure 111).
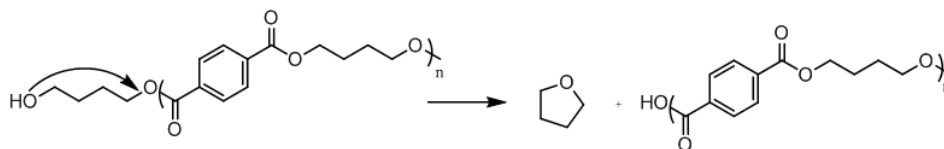

Figure 111: Backbiting reaction of PBT

VI.2.1.3   FTIR of evolved gases: conclusion

The analysis of the gases evolved during the degradation of the salts under inert atmosphere gave a first approach on their mechanism of decomposition. Focusing on a few characteristic bands allow drawing temperature profiles which illustrate the decomposition steps observed in TGA.

The first general conclusion is that the salts probably start to decompose from their amide group, releasing the corresponding amine, CO_2 and isocyanate. Methane or saturated carbonaceous structures are observed in the first stages of decomposition while unsaturated species (that could correspond to the release of aniline or benzene) are released in a large temperature range and at high temperatures.

Concerning the formulations of the salts in PBTGF, the release of THF needs to be highlighted. In the case of pristine PBTGF, THF is barely observed. In the formulations containing the salts, the release of THF is clearly observed at low temperatures (between 350 and 450 °C). This release is stronger in the case of EDAS. I can be assumed that EDAS degrades more PBT during the ramp, causing an increase of backbiting reactions. This result is consistent with its UL-94 classification (NC) and the previously drawn TGA difference curve.

FTIR analysis of evolved gases is a powerful tool to identify many groups released during the thermal degradation of any compound. However, the possible overlay of many functional bands sometimes makes this technique hazardous for drawing complete chemical mechanisms of decomposition. As a consequence, another tool was used to further complete the first hypotheses on degradation pathway of the self-synthesized salts: pyrolysis coupled with gas chromatography-mass spectrometry (py-GC/MS).

VI.2.2   Py-GC/MS

The gas chromatography-mass spectroscopy coupling technique is a powerful tool to allow identifying properly the structure of the molecules that are released in the gas phase when a material degrades. Moreover, as shown in the instrumentation of the UL-94, the degradation of the formulations in the real testing conditions correspond to a flash pyrolysis more than a linear heating ramp as it was done in TGA. As a consequence, py-GC/MS appears as a good complementary technique.

VI.2.2.1   Analysis of the phosphinate salts

The phosphinate salts previously studied in TGA-FTIR were thus submitted to a flash pyrolysis (600 °C for 30s). The evolved gases were collected and separated with the GC leading to a chromatogram. Each peak was attributed according to the MS spectrum. The results obtained for the three salts will be presented, to allow comparing the degradation pathway of the salts and to find the singularities in the case of PAS. Concerning the PBTGF formulations, this section will only focus on PBTGF-PAS to help better understanding the interactions with the matrix in the case of this efficient additive.

It is noteworthy that some products were not directly identified through databases search (FSearch or NIST). In those cases, the spectra were manually interpreted and potential structures were designed regarding the starting material. The designed structures were finally fragmented with the ACDlabs MSFragmenter tool. This software allows choosing fragmentation conditions (number of steps, voltage) and applies the classical rules of fragmentation in mass spectroscopy to reproduce the mass spectrum and compare it to the experimental spectrum.

The chromatogram obtained for the pyrolysis of the PAS is reported in Figure 112, and the most relevant substances are reported in Table 37. Water is released in the earliest steps of the degradation. Benzene and toluene come among aromatic identified structures, that may come from the release of the phenyl group linked to the phosphorus (followed by a radical recombination for toluene). Fragments from the decomposition of the phenyl amide group are also observed: aniline, acrylanilide.
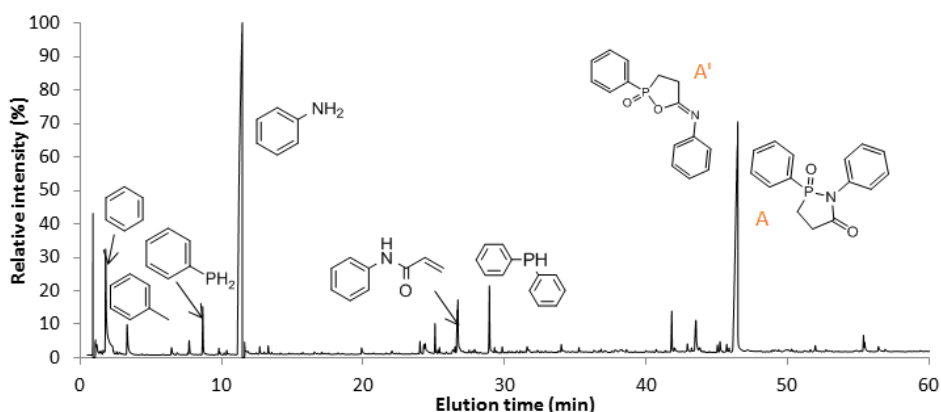
Figure 112: py-GC/MS chromatogram obtained for the pyrolysis of PAS (flash-pyrolysis)

Table 37: Quantification calculations for most relevant fragments in py-GC/MS of PAS

Retention time	% Area auto integrated	% Area recalculated	% Match	Database	Compound
1.798	5,8	7,0	99	FSearch	Benzene
3.320	1,5	1,8	99	FSearch	Toluene
8.663	1,7	2,0	97	NIST	Phenylphosphine
11.454	43,6	51,9	96	FSearch	Aniline
26.699	3	3,6	97	NIST	Acrylanilide
28.928	2,2	2,6	97	NIST	Diphenylphosphine
46.479	26,2	31,2	96	ACD MSFragmenter	A or A' (Figure 112)
Total %	84,0	100,0			

One of the most relevant peaks is attributed to the release of diphenylphosphine. The mechanism explaining the release of this phosphine might be an oxidoreduction reaction of the corresponding phosphinic acid: the same phenomenon was previously observed studying phosphonic acids [183]. In that case, it was proposed that the rupture of the P-Alkyl bond into P-H (phosphite specie) leads to the reaction of disproportionation of the compound into phosphine and phosphate:

$$4\ H_2PO_3^- + H^+ \rightarrow PH_3 + 3\ H_2PO_4^-$$

The same concept could then be applied to phosphinic acids, replacing phosphite with hypophosphite and following twice the previous scheme.

Finally, the higher boiling point molecules are not clearly identified. In the chromatogram, it corresponds to a mass of 271 g.mol^{-1}. The phosphinic acid corresponding to PAS (PA-3-HPP) presents a mass of 289 g.mol^{-1}, that is, a 18 g.mol^{-1} difference. It is proposed that a product could be formed from an intramolecular cyclization of the phosphinic acid with elimination of water (this case can be transposed to the Al-substituted molecule). Two ways of cyclization (N→P or O→P, Figure 113) lead to two possible and potentially stable structures for the corresponding spectrum: *1,2-diphenyl-1,2-azaphospholidin-5-one 2-oxide* (A, resulting from the attack of nitrogen on phosphorus) or *2-phenyl-5-(phenylimino)-1,2-oxaphospholane 2-oxide* (A', resulting from the attack of oxygen atom on the phosphorus). The use of MSFragmenter leads to an equivalent match.
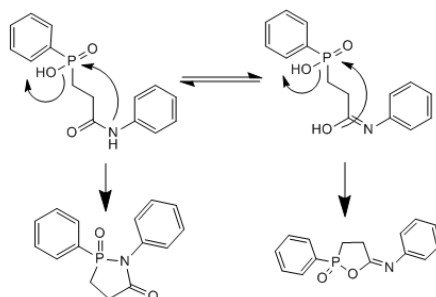
Figure 113: Scheme of intramolecular cyclization during the pyrolysis of PAS for the formation of A and A'

The chromatogram obtained for PPDS is reported in Figure 114 and the corresponding relevant fragments are listed in Table 38 showing the presence of benzene and toluene. The mono- and diamine fragments (aniline and p-phenylene diamine), phenylphosphine and diphenylphosphine are also observed.
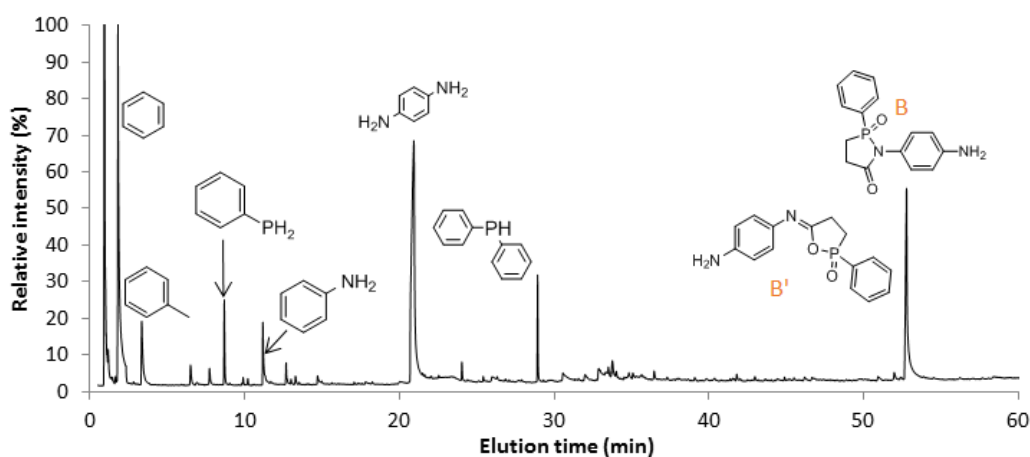
Figure 114: py-GC/MS chromatogram obtained for the pyrolysis of PPDS (flash-pyrolysis)

Finally, the "cyclization product" (*1-(4-aminophenyl)-2-phenyl-1,2-azaphospholidin-5-one 2-oxide* (B) or *5-((4-aminophenyl)imino)-2-phenyl-1,2-oxaphospholane 2-oxide* (B')) as observed in the case of PAS are identified thanks to the MSFragmenter. It should be highlighted that no product resulting from a cyclization on both amide centers is observed.

The chromatogram obtained for EDAS is reported in Figure 115 and the corresponding relevant fragments are listed in Table 39. Different degradation products are found compared to PAS and PPDS, which is consistent with the structure of EDAS (aliphatic ethylene diamine building-block).

Table 38: Quantification calculations for most relevant fragments in py-GC/MS of PPDS

| Retention time	% Area auto integrated	% Area recalculated	% Match	Database	Compound
1.802	18,4	27,8	99	FSearch	Benzene
3.335	3,4	5,1	99	FSearch	Toluene
8.673	2,2	3,3	97	NIST	Phenylphosphine
11.169	1,9	2,9	99	FSearch	Aniline
20.929	26,1	39,5	99	FSearch	p-phenylendiamine
28.934	2,3	3,4	97	NIST	Diphenylphosphine
52.789	11,9	18,0	90	ACD MSFragmenter	B or B' (Figure 114)
Total %	66,1	100,0			

Propenenitrile is identified among the volatiles, in the same retention range as benzene and toluene. It can be produced by the decomposition of the ethylene-diamide fragment upon strong dehydration. A novel phosphine, exhibiting a methyl group (methylphenylphosphine) is also identified. Again, heavy unidentified products are observed, which can correspond to four different cyclization/degradation mechanisms (two pairs of products: *1-(2-oxido-2-phenyl-5-hydro-1,3,2-diazaphosphol-1-yl) prop-2-en-1-one* (C) and *2-((2-oxido-2-phenyl-1,2-oxaphospholan-5-ylidene)amino)acetonitrile* (C'), *2-phenyl-1-vinyl-1,2-azaphospholidin-5-one 2-oxide* (D), and *2-phenyl-5-(vinylimino)-1,2-oxaphospholane 2-oxide* (D')), whose mechanism is proposed in Figure 116.
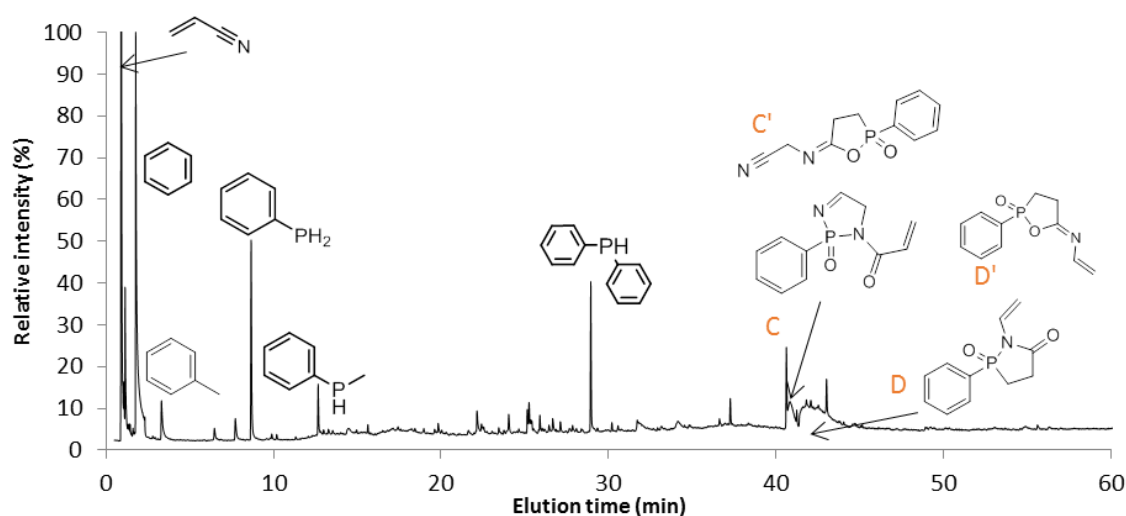

Figure 115: py-GC/MS chromatogram obtained for the pyrolysis of EDAS (flash-pyrolysis)

Table 39: Quantification calculations for most relevant fragments in py-GC/MS of EDAS

Retention time	% Area auto integrated	% Area recalculated	% Match	Database	Compound
1.145	5,3	6,5	96	NIST	2-Propenenitrile
1.782	28,2	34,4	99	FSearch	Benzene
3.316	2,5	3,0	99	FSearch	Toluene
8.668	7,6	9,2	97	NIST	Phenylphosphine
12.666	1,8	2,2	94	ACD MSFragmenter	MethylphenylPhosphine
28.934	4,7	5,7	95	NIST	Diphenylphosphine
40.609	9,5	11,6	90	ACD MSFragmenter	C or C' (Figure 115)
43.002	22,5	27,4	90	ACD MSFragmenter	D or D' (Figure 115)
Total %	82,1	100,0			
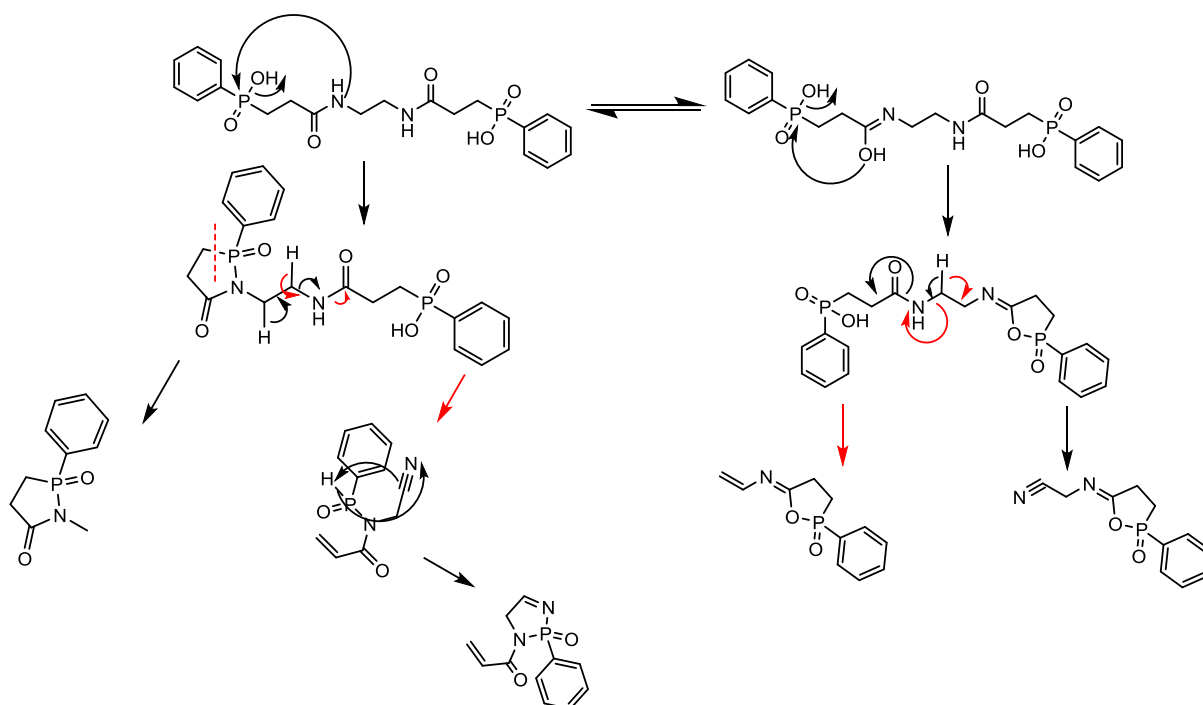
Figure 116: Proposed mechanism of decomposition of EDAS into four cyclization products

The molecules identified through py-GC/MS upon the degradation of PAS (aniline, benzene and acrylanilide) are consistent with what was observed in TGA-FTIR analyses. The identification of phosphines and intramolecular cyclization products brings novel information on the degradation pathway of the salt. The identification of phenylene diamine in the evolved gases of PPDS confirms the observations in TGA-FTIR (the FTIR bands are different but still can be attributed to the NH_2-Ar structure). The py-GC/MS analysis of EDAS reveals the same kind of fragmentation as observed in the case of PAS and PPDS, but different recombinations occur around the ethylene diamine core, leading to complex intramolecular cyclizations. The similitudes in the behavior of PPDS and EDAS that were observed in TGA-FTIR are further observed in py-GC/MS: the diamide salts tend to behave in a different way compared to the mono-amide salt (PAS).

VI.2.2.2   Focus study on PAS: py-GC/MS and EGA/MS

The py-GC/MS can also be used in different conditions: heating ramp py-GC/MS or EGA/MS. Following the TGA conditions used in the TGA-FTIR part, PAS was first heated at 10 °C / min up to

800 °C (with a so-called "desorption" method, maintaining the column at 35 °C during the ramp to observe volatile fragments). The column ramp was then fixed at 10 °C / min, and the non-volatile fragments were then observed. The py/GC-MS desorption spectrum is reported in Figure 117.

Some identified products differ from those obtained with flash pyrolysis (Figure 112). Phenylisocyanate is observed in the case of desorption, whereas phenylphosphine is no longer observed. However, the major fragments (aniline and the cyclization product) are the same, and benzene and diphenylphosphine are still clearly observed.
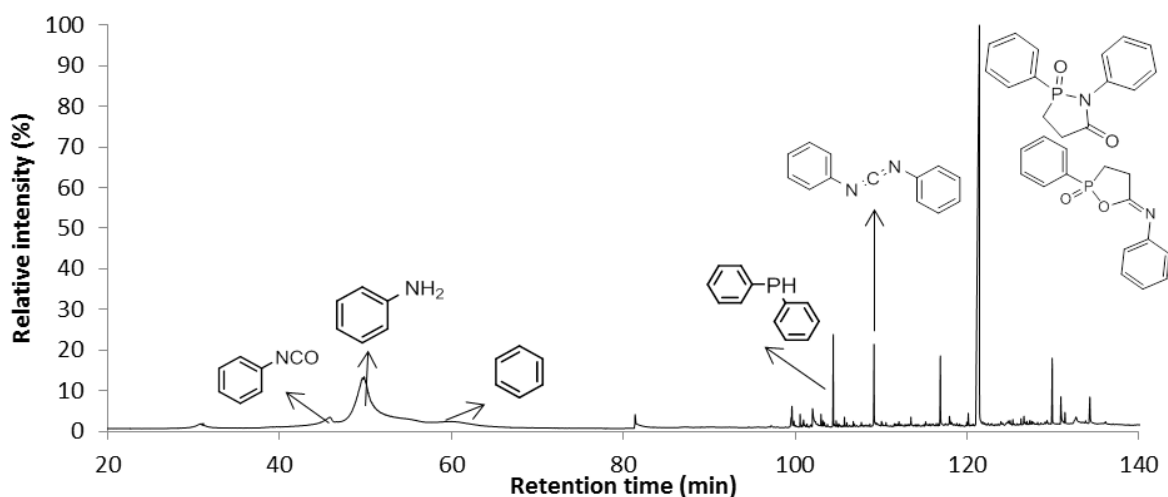
Figure 117: py-GC/MS chromatogram of PAS, desorption mode at 10 °C/min

The identification of the various products released by PAS when heated with a ramp of 10 °C / min in py-GC/MS allowed using the EGA/MS method. For that, PAS was heated again at 10 °C / min up to 800 °C, but the silica column was replaced with an UltraALLOY® non polar column. As a consequence, products were observed as released upon decomposition, which allows attributing a release temperature to each product. The main drawback of this method is that similarly to what was observed for TGA-FTIR, the degradation products are not or less separated. The corresponding EGA/MS chromatogram is reported in Figure 118. The intensity of the characteristic peak corresponding to the mass of each product (previously identified) as a function of temperature is reported in Figure 119. For example, the profile benzene is corresponding to the peak at m/z=78.
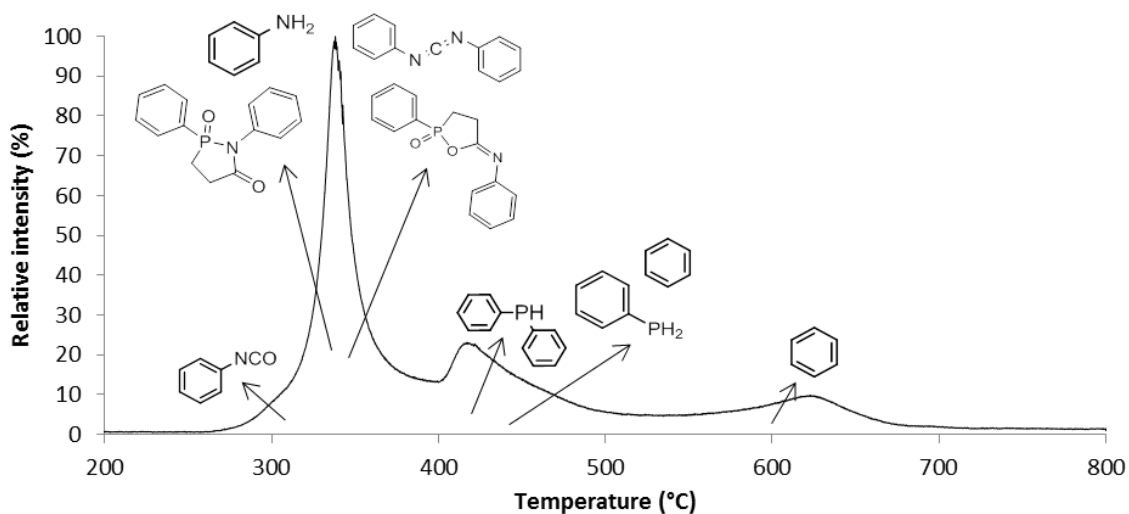
Figure 118: EGA/MS chromatogram of PAS, 10 °C/min

The EGA/MS chromatogram of PAS shows three main groups of products released. Between 250 and 400 °C, phenylisocyanate, aniline, low amounts of benzene and diphenylmethanediimine, and the cyclization products are released. Between 400 and 500 °C, benzene and phosphines are released. Between 500 and 700°, only benzene and low amounts of CO_2 are still released.
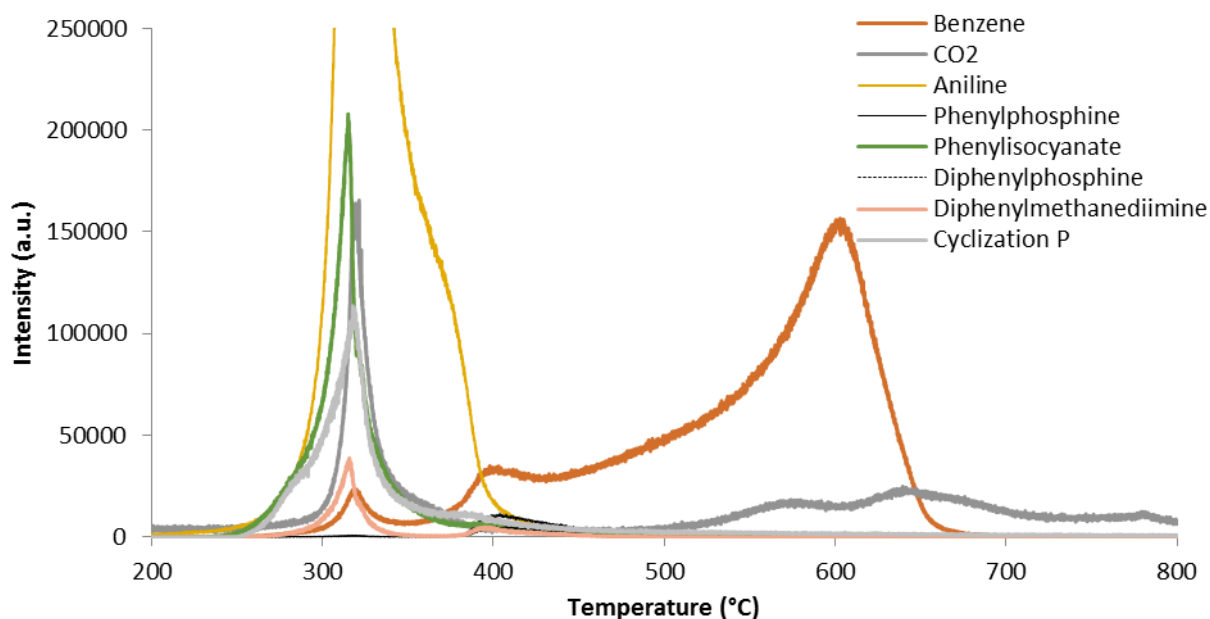
Figure 119: Attribution of each product's characteristic mass in EGA/MS of PAS, 10 °C/min

Compared to the TGA-FTIR analysis in the same conditions, the EGA/MS confirms some of the previous observations and hypotheses. The release of phenylisocyanate at low temperature (320 °C) confirms the hypothesis of the hydrolysis or decomposition of this product in the FTIR transfer line, leading to aniline and CO_2. The release of benzene occurs at higher temperatures (400-700 °C). The observation of aniline in a higher temperature range in TGA-FTIR is not consistent with the EGA/MS observations. The hypothesis in that case is that aniline could condense in the FTIR transfer line, being released over a larger range of temperatures compared to EGA/MS.

As a conclusion, after compiling EGA/MS and TGA-FTIR data, it can be shown that in the lower temperatures (250-450 °C), PAS mainly decomposes into phenylisocyanate, aniline, a cyclization product and CO_2. In higher temperature ranges (450-700 °C), the residues of PAS mainly release benzene.

VI.2.2.3   Analysis of PBTGF-PAS

To further investigate the degradation mechanisms of PAS and to understand its potential interactions with PBT, its formulation in PBTGF was also studied in py-GCMS. First, neat PBTGF was submitted to the flash pyrolysis at 600 °C, so as to identify its decomposition fragments and to work easier on the formulation with PAS. The py-GC/MS chromatogram of PBTGF is reported in Figure 120.
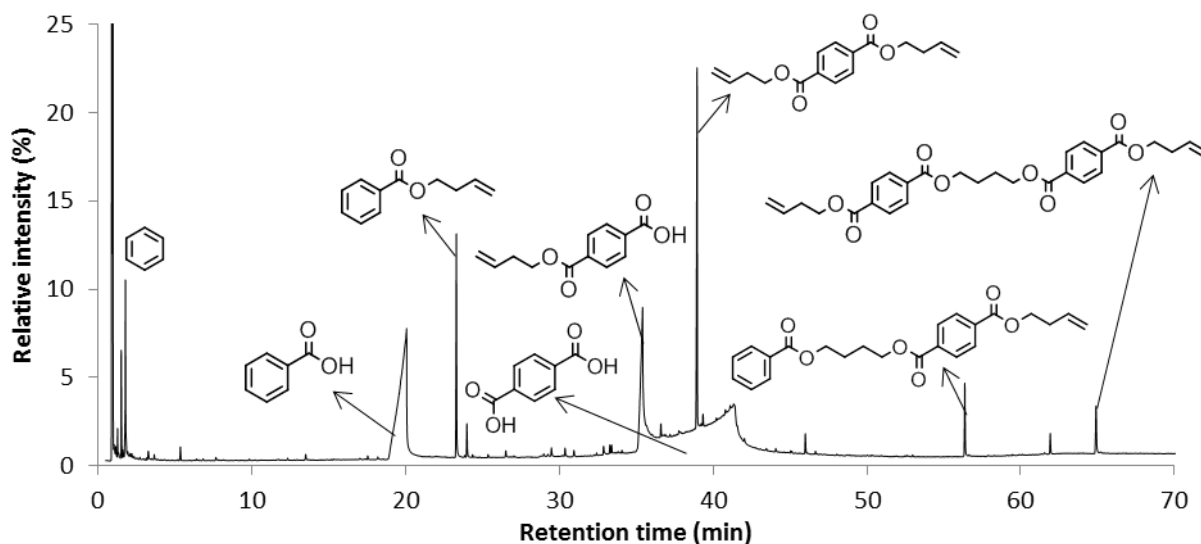
Figure 120: py-GC/MS chromatogram obtained for the pyrolysis of PBTGF (flash-pyrolysis)

The chromatogram of PBTGF only reveals the presence of expected fragments of PBT, with a rupture at the sensitive ester bond: benzoic and terephthalic acid, *but-3-en-1-yl benzoate*, *4-((but-3-en-1-yloxy)carbonyl)benzoic acid*, *di(but-3-en-1-yl) terephthalate* etc. Other larger fragments involving two aromatic rings are also identified. In the low retention times, species such as CO_2, THF and butadiene can be observed. Comments on these low molecular weight evolved gases will be given hereinafter.

PBTGF-PAS was then submitted to the pyrolysis treatment. The obtained chromatogram is reported in Figure 121, where an overlay with the separated components of the formulation is presented. This overlay allows proving that there exist interactions between PAS and PBTGF during degradation, as previously suggested. Fragments such as isocyanate, that are not relevant in the pyrolysis chromatogram of the pure additive, appear with a non-negligible intensity (compared to the rate of additive in the matrix and so in the chromatogram) when the FR formulation is considered.

On another way, fragments such as *N-phenylbenzylamide* or the *but-3-en-1-yl 4-(phenylcarbamoyl)benzoate* show there is a recombination between anilin and the decomposition fragments of PBT during the degradation. Since this recombination occurs, it reduces the release of corresponding separated fragments (benzoic acid, benzoic butenyl ester, aniline…).

On the other hand, the release of potentially gas-phase active fragments such as phosphines does not occur in the case of the formulation, which could have an effect on the fire retardant properties.

Finally, as it was shown in TGA-FTIR that the PBTGF-PAS formulation releases more THF than neat PBTGF, the same comparison was carried out in py-GC/MS. The chromatograms are reported in Figure 122. In this chromatogram, it is clearly shown that PAS enhances the release of THF in formulated PBT, while the release of butadiene and CO_2 is equivalent in both cases. However, it should be highlighted that this kind of presentation is based only on semi-quantitative measurements (based on relative intensities in scaled chromatograms).
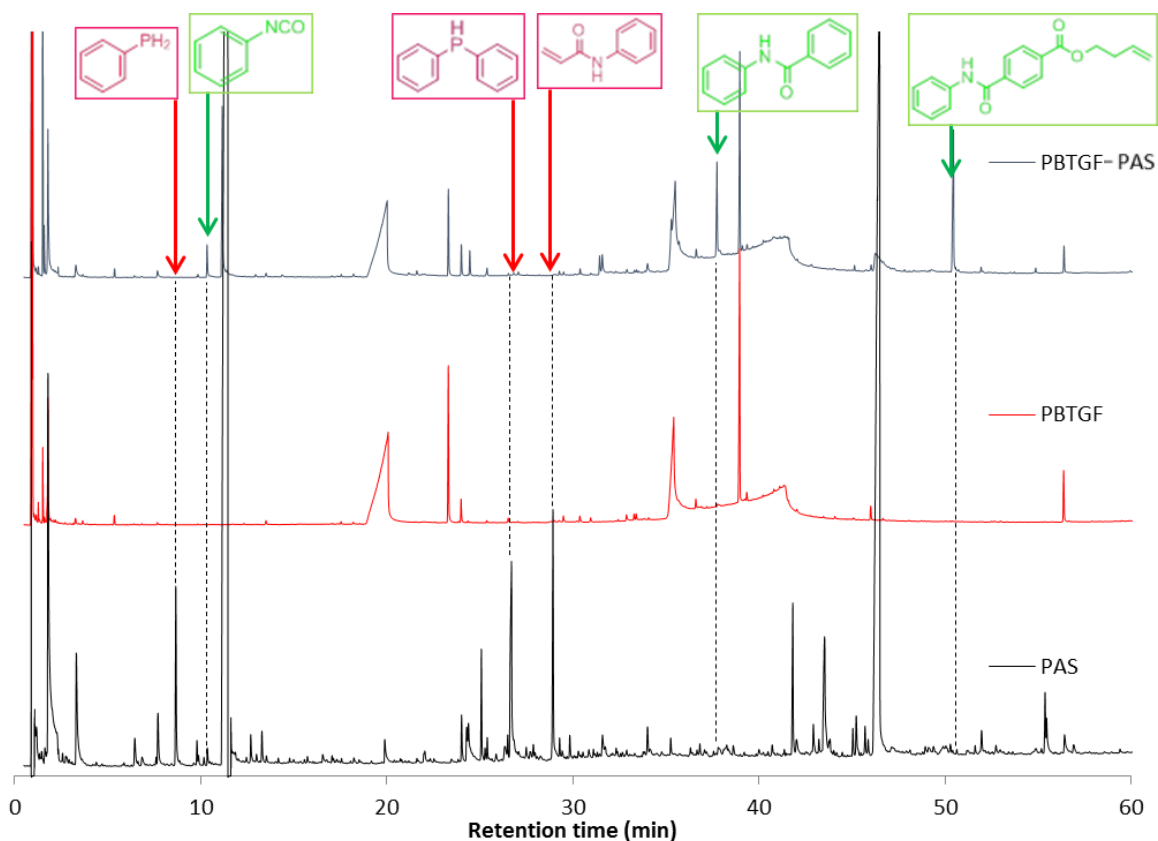
Figure 121: Overlay of py-GC/MS chromatograms of PAS, PBTGF and PBTGF 20w% PAS (flash-pyrolysis)
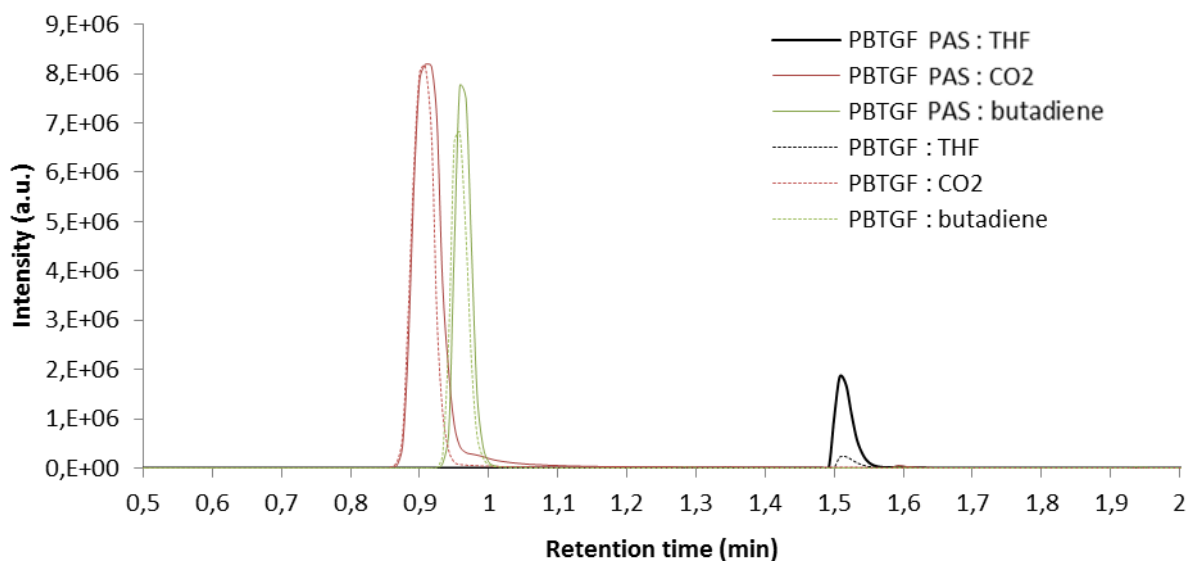
Figure 122: Chromatograms of THF, butadiene, and CO2 extracted during py-GC/MS of PBTGF and PBTGF - PAS

VI.2.2.4   Py-GC/MS : conclusion

The py-GC/MS studies, including EGA/MS, allowed determining a part of the degradation mechanism of PAS. The identification of the building blocks of the salt gives clues on the way the additive decomposes: broken bonds, recombinations. These first results were also found in the case of two other salts, which corroborates a general mechanism of decomposition of the salts. In any of the amide-phosphinate, the amide bond is the first affected. The decomposition of this bond can occur whether by scission or by intramolecular cyclization. All studied phosphinate also present the

common point of releasing phosphines, assumed to be obtained by disproportionation of the hypophosphite resulting from the breaking of the P-alkyl bond. However, in spite of a general trend in the mechanism of decomposition of the three salts, PAS presented its singularities.

The interaction between PAS and PBTGF were also studied. Upon decomposition, PAS releases aniline and phenylisocyanate, which can recombine with the various acid blocks released by the decomposition of PBT. When aniline has been released, phosphines are identified when PAS is analyzed alone, thus indicating the rupture in the alkyl phosphinate block. When PAS is combined with PBT, the phosphines are no more observed. It should be highlighted that phosphines only represent 4.6% of the corrected integrals of the products, which is a low quantity. In the formulation, two hypotheses can be drawn from these observations. On the one hand, it is possible that the quantity of phosphines is too low to be observed (20% of 4% representing about 1% of integrals). On the other hand, phosphines are very reactive species that could react with PBT fragments, forming novel species that have not been identified in the py-GC/MS spectra. Finally, the P-Ph block probably releases its phenyl group as benzene in higher temperatures.

In this first approach, a lack of information remains. Oxidoreduction reactions leading to the formation of phosphines (reduced species) would also lead to the formation of oxidized species. Moreover, many mechanisms (e.g. in Figure 113) were drawn on the basis of phosphinic acid structure. Same considerations can be given on the phosphinates. As a consequence, aluminum should remain in the condensed phase and could take part in the global mechanism of degradation of PAS.

Interestingly, in the next section, a chemical analysis of the condensed phase during the degradation of PAS and PBT-PAS will be presented. Complementary results will allow drawing a global mechanism of decomposition and action comprising gas- and condensed-phase effects.

VI.3.   ANALYSIS OF THE CONDENSED PHASE

VI.3.1   Introduction

In the previous section, the gaseous products released during degradation have been identified, in both flash and low heating ramp temperature. The potential reaction of disproportionation of phosphinic species and the cyclization of PAS to a volatile compound are key points in the mechanism of decomposition of this salt. However, some reactants and products of these reactions should belong to the condensed phase since in TGA experiment around 35 wt% residue are obtained at 800 °C for PAS.

Moreover it is suspected that in the flame-retardant mechanism, many effects occur in the condensed phase, as illustrated in the instrumented UL-94 (cooling effects, formation of a protective layer…). It is thus important to find the successive transformations to which a formulation is exposed.

The best way to identify the previously mentioned elements is the solid-state NMR analysis of the residues of thermal decomposition of PAS and PBTGF-PAS. Solid-state NMR allows finding the ^{13}C, ^{31}P and ^{27}Al structures and also drawing space correlations to confirm the presence of heteroatomic structures such as aluminum phosphinates.

In this section, the focus was made on the progressive transformation of the additive to the residue in ex-situ conditions (heat treatment was first carried out and the collected residues were then analyzed). Ex-situ conditions were chosen so as to easily identify the steps of the transformation (which may not be observed after a treatment in the conditions of a real fire scenario).

VI.3.2   1D NMR analyses

PAS and PBTGF-PAS were treated in a tubular furnace under air, at characteristic temperatures of degradation in TGA (420 and 550 °C). Residues were then collected and analyzed using ^{31}P, ^{27}Al and ^{13}C solid-state NMR. The amount of residues at 420 °C (65 wt% and 43 wt% for PAS and PBTGF-PAS respectively) and at 550 °C (41 wt% and 32 wt% for PAS and PBTGF-PAS respectively) are in accordance with the residues obtained after TGA in the same conditions.

The ^{31}P spectrum of PAS (Figure 123) after treatment at 420 °C shows two additional phosphorus structures. The band assigned to aluminum phosphinate structure (20-40 ppm) is a bit shifted due to the presence of Al^{3+} cations and is broadened after thermal treatment. An additional band comprising three peaks (0, -3, -7 ppm) is observed and attributed to aluminophosphonates [184-186]. The multiple bands observed for the supposed aluminophosphonates would be explained by the difference of chemical environment of the Al atoms involved in the aluminophosphonate structure, inducing a shift in the signal of P atoms. Another weak band at -35 ppm corresponds to PO_4 units in aluminophosphate structures. At 550 °C, only the broad PO_4 band at -35 ppm remains.

In the case of PBTGF-PAS, the ^{31}P spectrum (Figure 123) after treatment at 420 °C exhibits a broad band centered at -8 ppm, which probably corresponds to the observation carried out on PAS (aluminum phosphinates with different chemical shifts). However, it should be highlighted that the signal is not as sharp as in PAS. The potential interactions between PBT, GF and PAS could lead to a more disordered structure and so a more disordered environment of ^{31}P. The phosphinate band (20-40 ppm) is not observed, but the band at -8 ppm is broadened, which suggests presence of the bands observed in PAS at -35 ppm (aluminophosphates) and 20-40 ppm (aluminophosphonates) at

the same treatment temperature, but slightly shifted. At 550 °C, only the PO_4 structures are observed, as observed for PAS.

Figure 123: [31]**P solid state NMR (MAS, 10 kHz, 9.4T) of PAS and PBTGF-PAS before and after thermal treatments**
* denotes spinning side bands

The [27]Al spectrum for both materials heat treated in the same conditions are presented in Figure 124. The [27]Al spectrum of PAS heat treated at 420 °C shows 3 bands: 44 ppm (that can be attributed to AlO_4 units in aluminophosphonate structures), 9 ppm (a weak broad band also present in the untreated product, corresponding to octahedral aluminum atoms with phosphorus in their second coordination sphere but likely linked with Al-O-Al groups, so that the coordination sphere is incomplete **[128]**), and -16 ppm (characteristic of octahedral aluminum, AlO_6, connected by Al-O-P bonds and a complete phosphorus coordination sphere) **[129, 184-186]**. At 550 °C, the same three bands are still visible but only the band at -16 ppm is significant, other bands being very weak.

PBTGF-PAS contains glass fibers and thus an additional band is observed between 10 and 80 ppm. The spectrum corresponding to the glass fibers superimposes with the Al sites observed in PAS. This means there is no difference in term of aluminum sites when PAS is formulated in PBTGF.
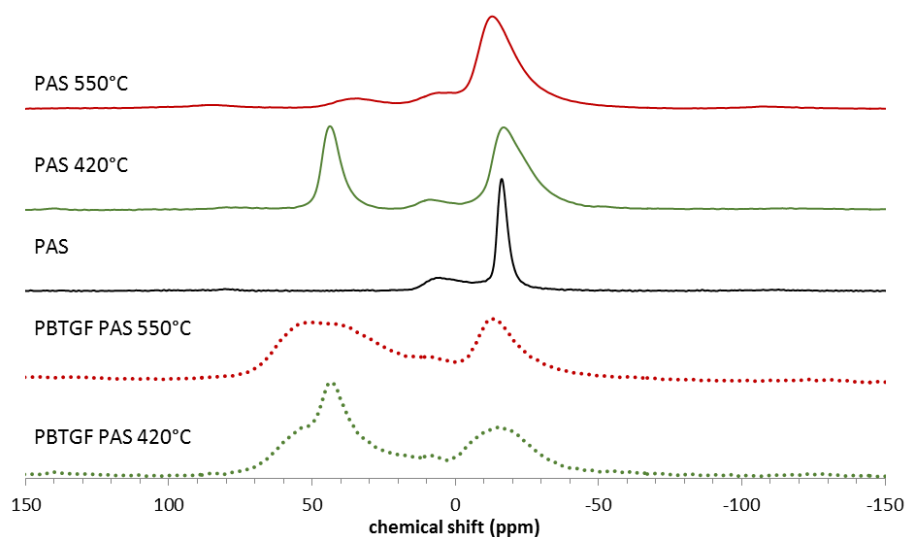
Figure 124: [27]**Al solid state NMR (MAS, 10 kHz, 9.4T) of PAS and PBTGF-PAS before and after thermal treatments**

Concerning the ^{13}C solid-state NMR (Figure 125), after treatment of PAS at 420 °C, only aromatic carbons (120-140 ppm, 4 apparent sites) can be distinguished. The aromatic site in the lower chemical shifts (115-120 ppm) attributed to the aniline ring is no more observed. In this case however, the band at 25-30 ppm corresponding to -CH_2- is overlaid with the spinning side bands and thus it is not possible to conclude about potential remaining aliphatic structures. Changing the spinning speed in the signal of PAS treated at 420 °C (Figure 126) confirms that a weak signal remains at 25-30 ppm. At 550 °C, a weak band remains in aromatic shift range, but with high noise (this spectrum was not presented). In the spectra of PBTGF-PAS, when the formulation is not thermally treated, characteristic peaks of PBTGF are observed: 30 ppm (-CH_2-), 65 ppm (O-CH_2-), 135 ppm (Ar) and 165 ppm (COO $_{ester}$). These peaks are superimposed with the peaks of PAS (already listed in the experimental section pp.49). When the formulation is treated, the peaks of PBTGF are not present anymore and the same bands as for PAS alone are observed.
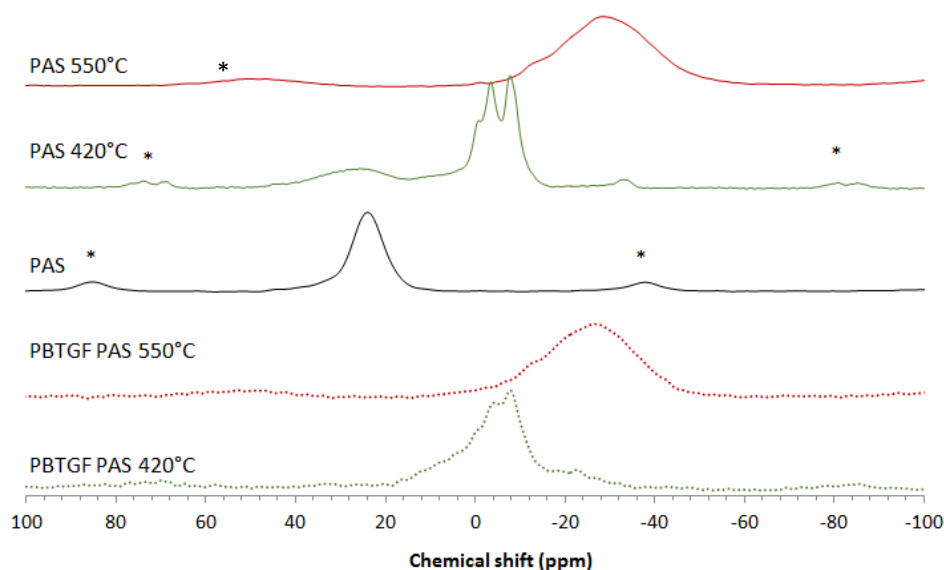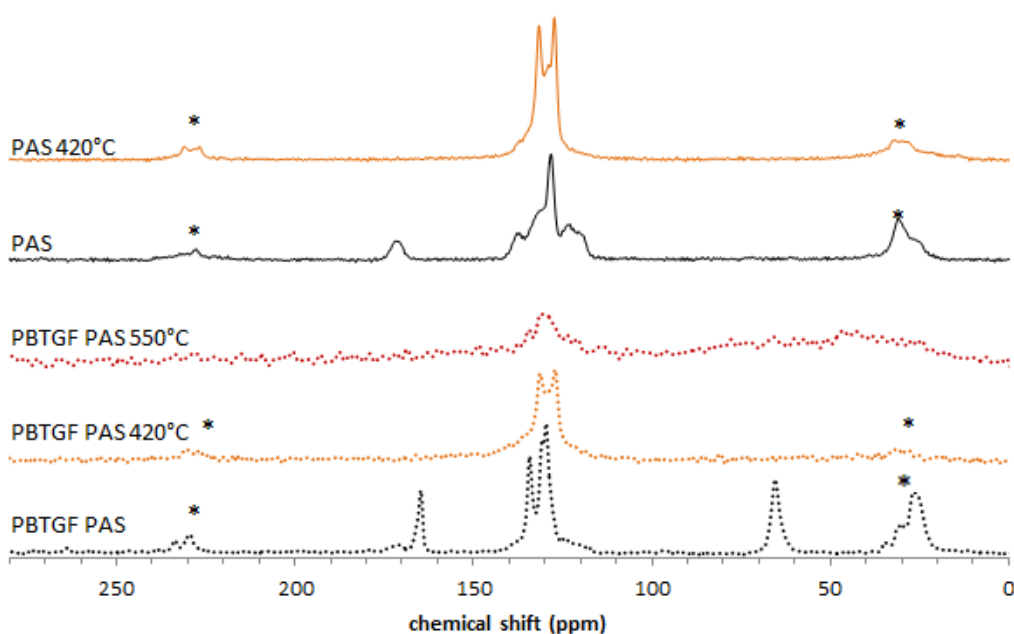

Figure 125: ^{13}C solid state NMR (MAS, 10 kHz, 9.4T) of PAS and PBTGF-PAS before and after thermal treatments
* denotes spinning side bands
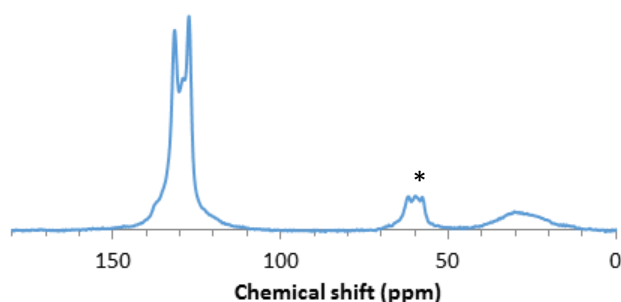
Figure 126: ^{13}C solid state NMR (MAS, 7.5 kHz, 9.4T) of PAS after treatment at 420 °C
* denotes spinning side bands

The 1D solid-state NMR analyses allow formulating many hypotheses. The ^{31}P solid-state NMR shows a progressive oxidation of the phosphinate with temperature to phosphonate and phosphate. The shift to phosphonates was also observed in the [27]Al specta (aluminophosphonates at 44 ppm). The ^{13}C analysis also allows showing that the aniline ring is no more observed in the spectrum of PAS

treated at 420 °C, whereas the P-Ph aromatic ring is still observed up to 550 °C (even if the signal exhibits low intensity). Finally, there is no visible chemical interaction between PBTGF and PAS (only a broadening of the peaks is observed). The transformation of the aluminum phosphinate to aluminophosphates is consistent with the release of phosphines observed in py-GC/MS. This phenomenon was already observed by Vannier et al. **[187]**.

VI.3.3   2D NMR analyses

In the previous section, many hypotheses were formulated on the potential heteroatomic structures formed through the transformation of PAS: aluminophosphonates or aluminophosphates with a correlation between phosphorus and different aluminum sites. So as to get more information on the spatial proximity between atoms, ^{31}P-^{27}Al Heteroatomic Multiple Quantum Correlation was carried out on thermally treated PAS. This analysis allows showing the proximity of atoms in space.

The P/Al HMQC of PAS at 420 °C (Figure 127 in 2D, Figure 128 in 3D) shows there are five correlations between phosphorus and aluminum: two intense correlations between Al at 44 ppm (P-bonded AlO_4)/-16 ppm (P-bonded AlO_6) and P at -5 ppm (aluminophosphonate), and three weak correlations (that would only be guessed due to the residual noise), between Al at 9 ppm (partially P-bonded AlO_6) and P at -5 ppm (aluminophosphonate), then between Al at -16 ppm (P-bonded AlO_6) and P at 30 ppm (phosphinate salt) and -35 ppm (aluminophosphate). The corresponding attributions are reported in Table 40.
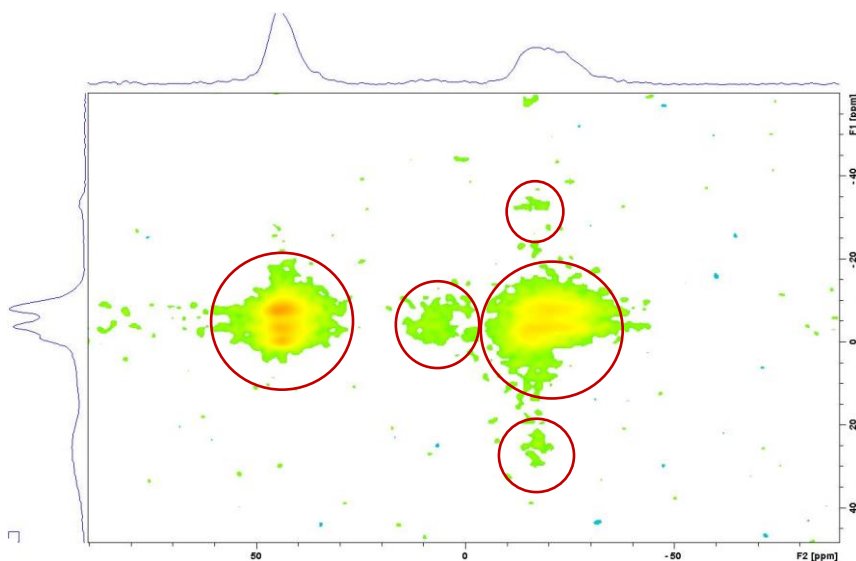
Figure 127: 2D ^{31}P-^{27}Al HMQC plot of PAS after treatment at 420 °C (2D)
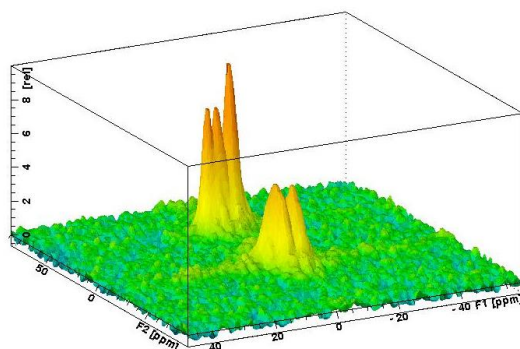
Figure 128: 3D ^{31}P-^{27}Al HMQC plot of PAS after treatment at 420 °C (3D)

Table 40: Chemical shift, attribution and correlations between Al and P in PAS treated at 420 °C
x, xx and xxx denote weak, medium, and strong correlation

Chemical shift	^{27}Al	44 ppm	9 ppm	-16 ppm
^{31}P	*Attribution*	*P-bonded AlO$_4$*	*Partially P-bonded AlO$_6$*	*P-bonded AlO$_6$*
30 ppm	*Phosphinate salt*			x
-5 ppm	*aluminophosphonate*	xxx	xx	xxx
-35 ppm	*aluminophosphate*			x

The presence of aluminophosphonates, is thus confirmed by the HMQC. This is again consistent with the hypothesis of disproportionation reaction. There exists a correlation between the phosphorus signals observed at -5 ppm and the aluminum bands attributed to Al atoms with different oxygen coordination (AlO$_4$/AlO$_6$) with phosphorus in their second coordination sphere (complete or uncomplete phosphorus coordination). The correlation of phosphorus attributed to aluminophosphonates with different aluminum sites is consistent with the shift of the phosphorus band to multiple resonances.

The P/Al HMQC of PAS at 550 °C (Figure 129 for 2D, Figure 130 for 3D) shows there is an interaction between the P band and all the aluminum bands. In this case, the residue should be constituted of definite PO$_4$ structures (-10 to − 50 ppm) intercalated in an Al network constituted of various AlO$_x$ structures (thus implying different aluminum bands due to the high structural shifts of Al in solid-state NMR, observed at 40, 10 and -15 ppm), but mainly AlO$_6$ aluminophosphates (-15 ppm) are observed.

Figure 129: 2D ^{31}P-^{27}Al HMQC plot of PAS after treatment at 550 °C (2D)

As a consequence the phosphorus band could be in fact constituted of 3 really close contributions, corresponding to the different structures and environments of the phosphorus linked to different aluminum structures, appearing as one broad band of 3 weakly shifted phosphorus, which correlate differently with Al.

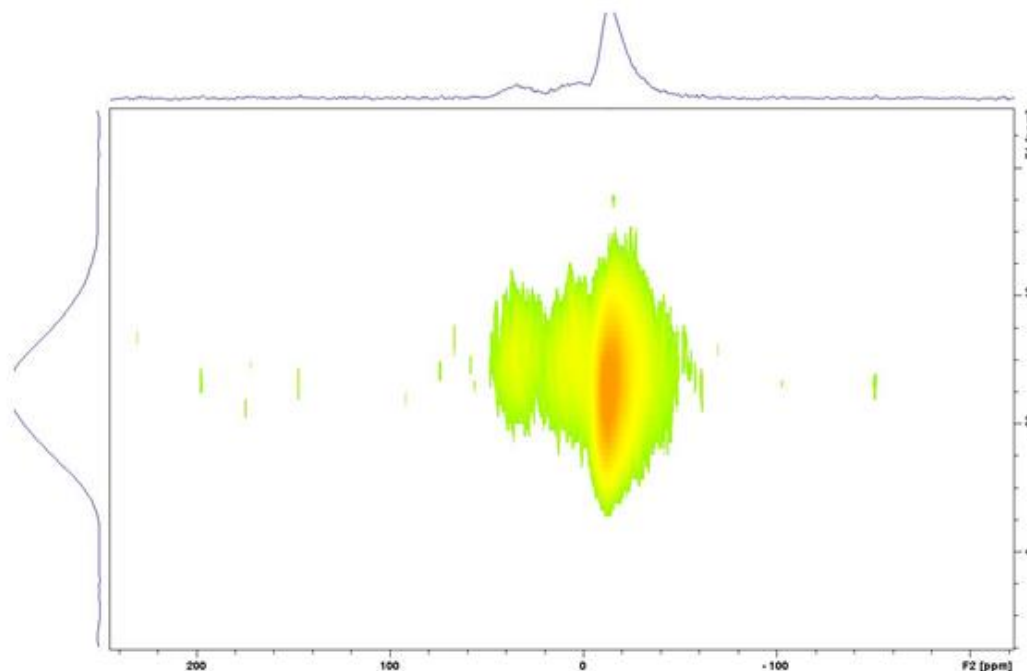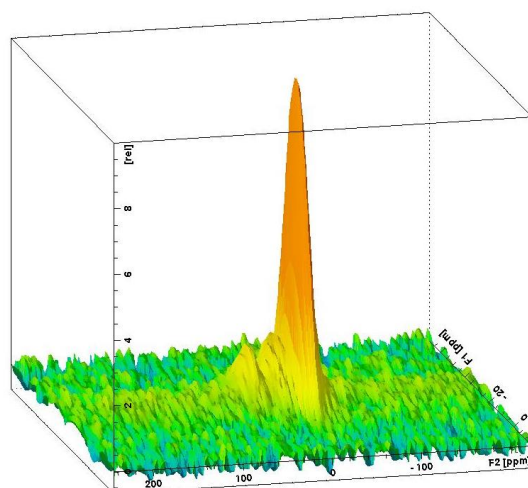**Figure 130: 3D ^{31}P-^{27}Al HMQC plot of PAS after treatment at 550 °C (3D)**

The D-HMQC analyses of the residues of PAS after thermal treatment allowed validating the hypothesis formulated in 1D solid-state NMR analyses. When it is thermally treated, PAS (aluminum phosphinate) is transformed in aluminophosphonate. The slight excess of aluminum (discussed in elemental analysis) implies the formation of Al-O-Al bonds and the observation of three different aluminum sites correlated to phosphorus: AlO$_4$ with a complete phosphorus second coordination sphere, AlO$_6$ with an incomplete phosphorus second coordination sphere (blocks linked by the Al-O-Al bonds) and AlO$_6$ with a complete phosphorus second coordination sphere. At higher temperatures, these structures are transformed in aluminophosphates, with the same three different aluminum structures correlated to the phosphorus site.

VI.3.4   Investigation of ^{13}C-^{31}P correlation: Double Cross-Polarization (DCP)

In spite of all the information gathered on the decomposition of PAS so far with solid-state NMR, no hypothesis on the attribution of the carbon bands remaining in PAS after treatment can be properly validated. Two possible cases exist in the PAS structure for aromatic carbons: the aniline ring and the phenyl ring linked to the phosphorus atom. The difference of chemical shift for the aniline ring and the P-phenyl ring would tend to indicate aniline is released after thermal treatment (as depicted in ^{13}C solid-state NMR), which is observed in the analysis of evolved gases. However, benzene is also released, which can be consistent with the rupture of the P-phenyl group. The thermal degradation of carbonaceous organic structures also generally leads to the formation of aromatic or polyaromatic structures. No conclusion can be given so far.

The HMQC techniques are powerful tools to observe the through-space correlations, in solid-state structures. However, it is not adapted to "^{13}C-^{x}Z"analyses due to the low sensitivity and abundance of ^{13}C. Another technique was needed to observe the possible spatial proximity between phosphorus and carbon in the structures obtained after thermal treatment of PAS.

A double cross-polarization (DCP) method was setup in solid-state NMR **[188]**. This technique is based on the transfer of the signal of protons to carbon (classical Cross-Polarization) and from carbon to phosphorus, or proton to phosphorus to carbon. In the resulting spectra (^{31}P or ^{13}C), a change in the cross polarization implies an increase or decrease of given bands. If a band in the ^{31}P spectrum is not correlated with a carbon, it should then disappear or at least suffer from a high decrease in intensity in the DCP spectrum.

Thermally-treated PAS was then analyzed in ^{31}P and ^{13}C DCP. Only a ^{13}C weak signal is observed in the case of the treatment at 550 °C. Thus, DCP involving shielding transfer to or from ^{13}C would not be relevant in this case. As a consequence, only the case of PAS heat treated at 420 °C was analyzed using this technique (Figure 131 and Figure 132).

In the ^{13}C DCP spectrum, the two bands observed in the CP method (25-30 ppm and 120-140 ppm) are still observed, though with a weaker intensity due to the DCP technique. This means both resonances correspond to P-bonded carbons, which would be identified as P-aliphatic (25-30 ppm) and P-aromatic (120-140 ppm). The DCP resonance of aromatic carbons is weakly shifted to 130-150 ppm. In a P-aromatic structure, the carbon atom with highest chemical shift in the aromatic band is directly bonded with phosphorus. As a consequence the shift in the aromatic band is consistent with the spatial proximity of carbons and phosphorus (higher chemical shifts closer to phosphorus are highlighted).
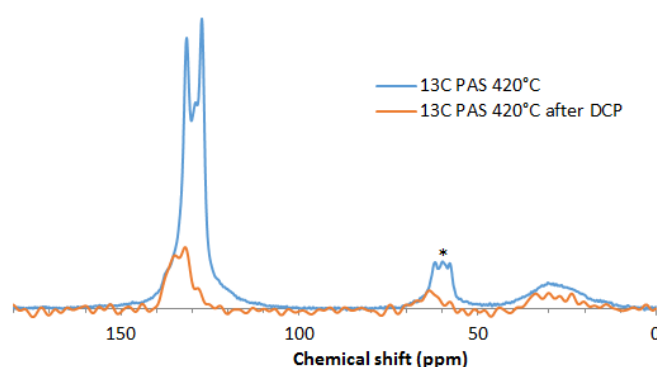
Figure 131: CP and DCP ^{13}C solid-state NMR spectra (MAS, 7.5 kHz, 9.4T) of PAS treated at 420 °C

In the case of ^{31}P, three different species were identified without DCP. The weakest band, centered at -33 ppm, is not observed anymore after DCP. This is consistent with the attribution of this band to phosphates (which do no exhibit P-C bonds) in the previous sections. However, it should be highlighted that this band was already very weak without DCP, which may explain its absence due to the signal loss through DCP.

The intensity of the band composed of three peaks at 0, -3 and -7 ppm (P_a) is sharply decreased, compared to the band centered at 30 ppm (P_b). The initial intensity ratio P_a/P_b of 9/1 decreases to 3/1. Again, this is consistent with the attribution of those bands to phosphonates and phosphinate respectively. Indeed, a phosphonate-P only exhibits one P/C spatial coordination ($P=O(OR)_2R_1$), whereas a phosphinate exhibits two ($P=O(OR)R_1R_2$).

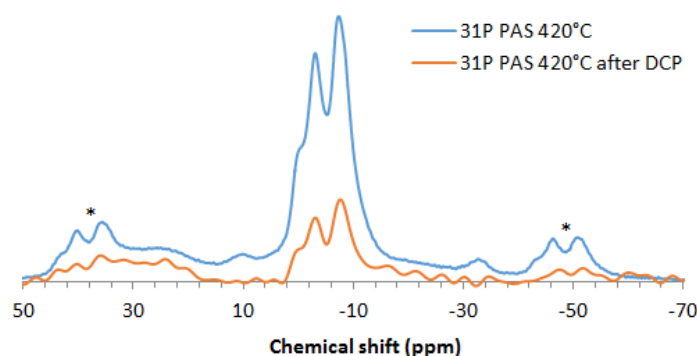**Figure 132: CP and DCP ^{31}P solid-state NMR spectra (MAS, 7.5 kHz, 9.4T) of PAS treated at 420 °C**

As a conclusion, the DCP solid-state NMR allowed demonstrating the spatial proximity between P and C, confirming the results and assumption proposed according to 1D spectra. At 420 °C, a major part of the phosphinate structure of PAS was oxidized to phosphonate, probably by rupture of the P-CH$_2$ bond. This should be consistent with the formation of the acrylanilide demonstrated in py-GC/MS, which is the lost fragment from phosphinate to phosphonate (Scheme 14). The phosphonate structure is likely to be P=O(OR)$_2$Ph in this case. Indeed, the P-Ph correlation was also illustrated, and is consistent with the release of benzene at higher temperatures. It is underlined that in his work **[188]**, Ciesielski carried out a recombination of 1D signals of the DCP to draw the 2D correlation, like a HMQC. This type of treatment was not carried out in our case.
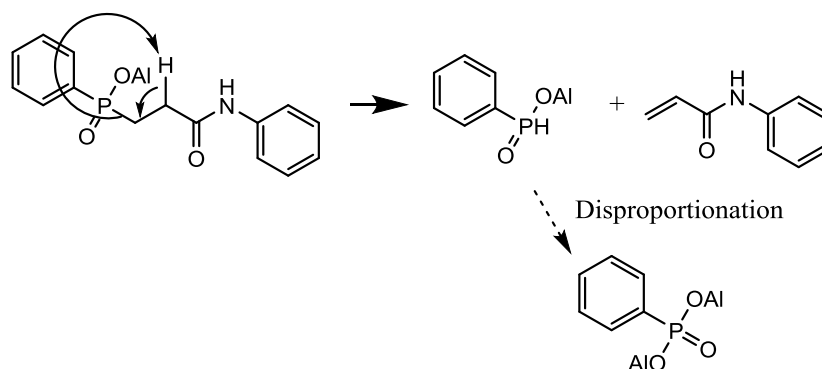
Scheme 14: Scheme of the rupture of P-alkyl bond in PAS to form a phosphonate specie

VI.3.5   *Analysis of the condensed phase: conclusion*

The analysis of the residues after thermal treatments of PAS in solid-state NMR allowed determining the reactions occurring in the condensed phase during the degradation of the phosphinate salt. It was shown that the phosphinate structure releases aniline and/or breaks at the P-alkyl bond (formation of acrylanilide, observed in the gas phase). The potentially formed hypophosphites should disproportionate and form phosphines (observed in the gas phase) and aluminophosphonates. At higher temperatures, the breaking of the P-phenyl bond (together with the release of benzene, observed in the gas phase) leads to the formation of aluminophosphates. The Al-O-P network in both steps of decomposition is intercalated with Al-O-Al bonds due to the excess of Al in the starting material.

When crossed with the data obtained through the analysis of evolved gases and TGA data, three global steps of decomposition can be drawn. It is assumed that the first step corresponds to the fragmentation of the amide fragment of the PAS molecule releasing phenylisocyanate (turning to CO$_2$ and Aniline), or directly aniline (Step 1a). This main step probably also correspond in the meantime to the cyclization mechanism highlighted in py-GC/MS. The decomposition of the rest of the molecule down to the phosphorus atom, which may be related to another mode of fragmentation of the aliphatic-amide fragments to acrylanilide (Step 1b) should also be highlighted.

The third step would correspond to the disproportionation reaction involving the release of phosphines and phosphonate from the phenylphosphonic acid.

The fourth and last step should correspond to the release of benzene from the phenylphosphonate structures, yielding aluminum phosphates in the condensed phase.

Step 1a
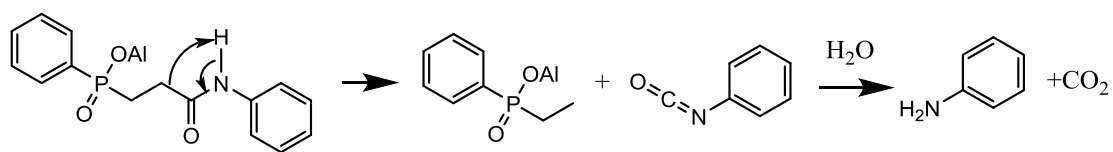
Step 1b
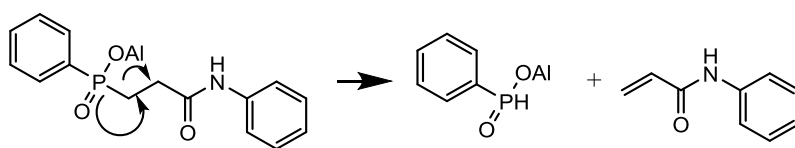
Step 2
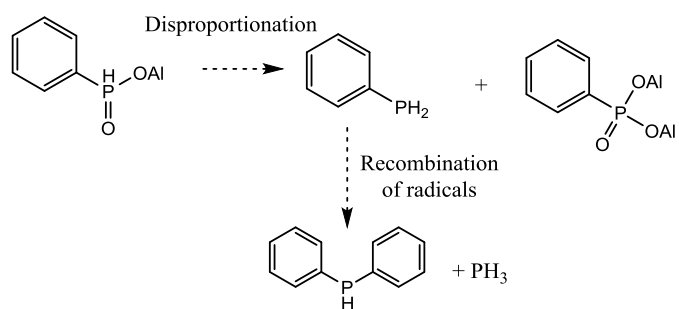
Step 3
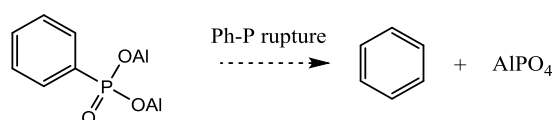
VI.4.   KINETICS

In the previous sections, the investigations of the gas- and condensed-phase led to various elements constituting the mechanism of decomposition of PAS and demonstrated that it interacts with PBTGF. To further complete the data, a kinetic modeling of the degradation of PAS was carried out.

The kinetic parameters of thermal decomposition can be calculated using methods developed by Kissinger, Ozawa, or Friedman. These classical methods are iso-convertional methods and provide only apparent results depending on the experimental conditions. In this study, the method developed by Friedman **[189]** was used. Friedman iso-convertional method is based on the intercomparison of the rates of weight loss ($d\alpha/dt$) for a given fractional weight loss (α) determined using different linear heating rates. The method is based on equation 5:

$$d\alpha/dt = A\ f(\alpha)\ exp\ (-Ea/RT)$$

Equation 5

with Ea the activation energy, $f(\alpha)$ the degradation function, R the gas constant, T the temperature and A the rate constant or pre-exponential factor. The Friedman analysis uses the resulting logarithmic differential equation:

$$ln(d\alpha/dt) =\ lnA + lnf(\alpha) - Ea/RT$$

Equation 6

Through this equation, it is possible to obtain values for Ea over a wide range of conversions.

The thermal degradation of a solid is followed by the emission of gaseous products by a heterogeneous process. It is characterized by a nucleation or diffusion (from one to three dimensions) mechanism, and thus by various decomposition model f (α). The selection of the decomposition models should be based on physical considerations (what we know about the chemistry and physics of the reaction) and on the fit quality of the simulation. For the simulation of the thermal degradation of polymers, the most used model is the n-th order function. A thermal decomposition can occur in several steps, for example with the breaking of chemical bonds, heat transfer reactions or desorption of gaseous products. Because of the complexity of the process, it is quite impossible to find an accurate equation to describe all types of thermal decomposition, especially in the case of kinetics varying during the process **[190]**.

It is recalled that logA and Ea are correlated by a compensation effect: the value of Ea determines the pre-exponential factor value and reciprocally. The Friedman analysis results (Figure 133) provided some approximate Ea values, which were used as starting values to initiate the calculations. Then, the results of the kinetic simulation allowed the determination of the best degradation models.

The model which obtains the best F-test fit quality between the computed curves and the experimental TGA curves for four heating ramps (1 °C/min, 5 °C/min, 10 °C/min and 20 °C/min) in pyrolytic conditions was four successive steps with n-th functions:

$$A \xrightarrow{\ 1\ } B \xrightarrow{\ 2\ } C \xrightarrow{\ 3\ } D \xrightarrow{\ 4\ } E$$
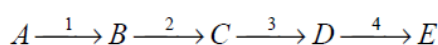
The resulting parameters for each step are reported in Table 41, and the fitted curves are reported Figure 134, correlation coefficient of 0.9997.
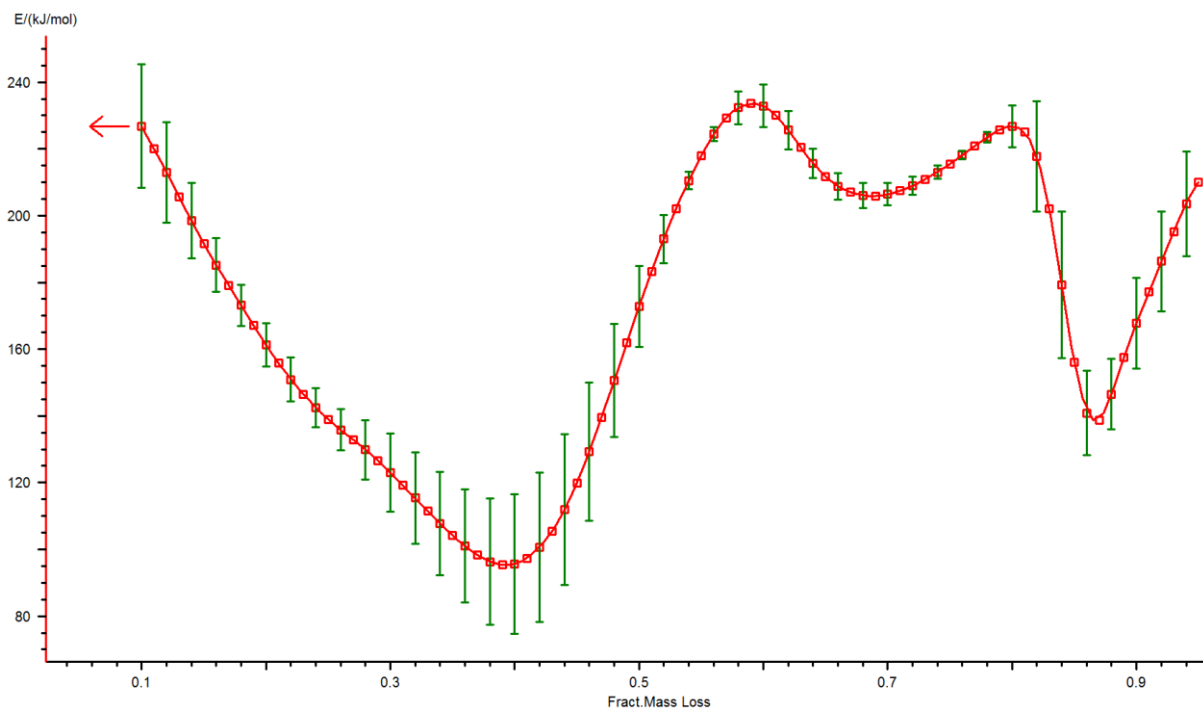
Figure 133: Friedman energy-plot of PAS in N$_2$

Table 41: Kinetic parameters of the degradation of PAS in pyrolytic conditions

Step	Log A (A: s^{-1})	Ea (kJ/mol)	n
1	15.6 ± 0.3	214 ± 4	0.73 ± 0.05
2	7.1 ± 0.3	118 ± 4	1.72 ± 0.08
3	18.6 ± 0.8	277 ± 13	1.16 ± 0.22
4	8.0 ± 1.6	175 ± 30	1.44 ± 0.17
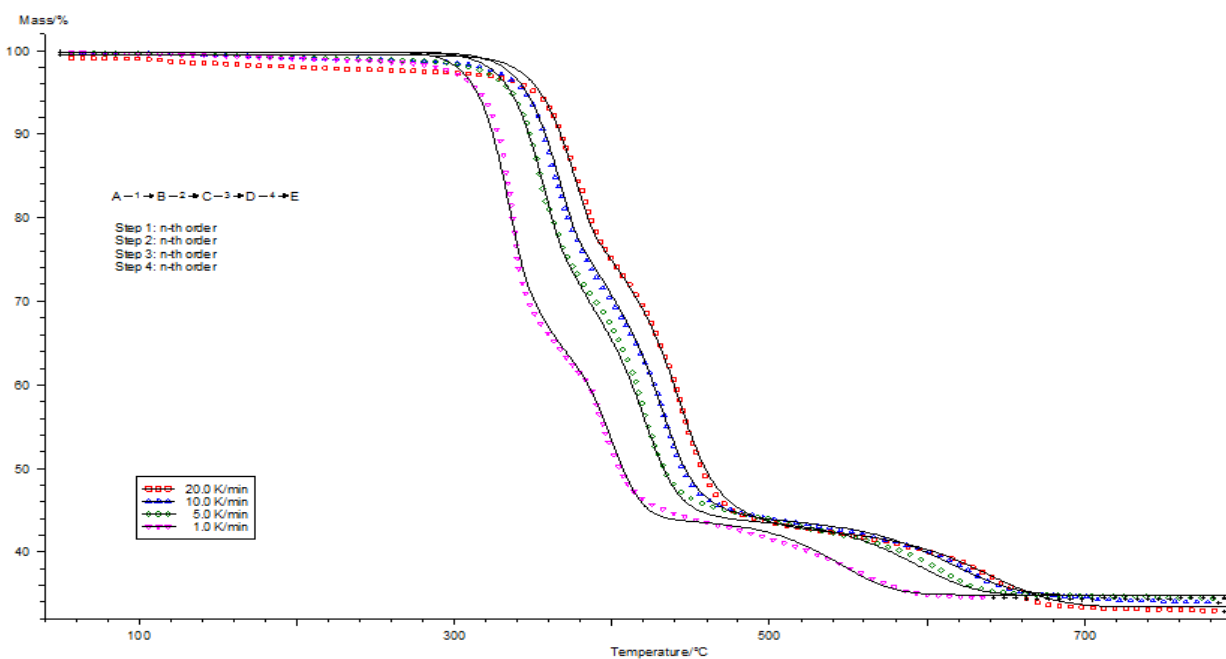
Figure 134: Simulation of the degradation of PAS in pyrolytic conditions

It should be underlined that this model does not meet the hypotheses on the different steps of the mechanisms previously presented. Only three steps were expected, but implying two potential competitive reactions in step 1. As a consequence, the following decomposition model was also tested:

$$A \xrightarrow{\quad 1 \quad} B \atop \xrightarrow{\quad 2 \quad} B \xrightarrow{\quad 3 \quad} C \xrightarrow{\quad 4 \quad} D$$
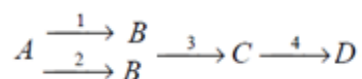
The fit was however not possible with the four heating ramps. To obtain a satisfying F-test fit quality, only the 5, 10 and 20 °C/min ramps were used for the fit. In that case, a correlation coefficient of 0.9997 is reached when the parameters reported in Table 42 are applied. The corresponding fitted curves are reported in Figure 135. The hypothesis to this fact is that the behavior of PAS is sharply different in lower heating ramps, thus making the kinetic fit more difficult.

Table 42: Kinetic parameters of the degradation of PAS considering 2 competitive reactions in step 1

Step	Log A (A: s^{-1})	Ea (kJ/mol)	n
1	15.1 ± 0.2	280 ± 3	1.70 ± 0.05
2	11.9 ± 0.3	172 ± 4	0.56 ± 0.07
3	12.3 ± 0.8	193 ± 3	1.33 ± 0.04
4	9.2 ± 1.6	195 ± 10	1.66 ± 0.08
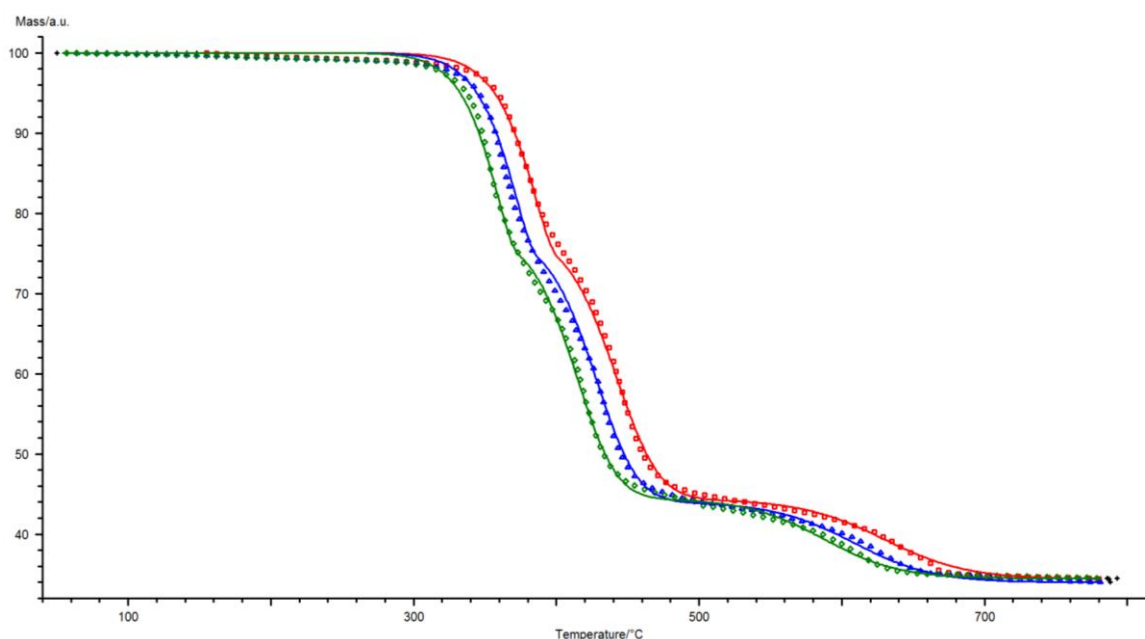
Figure 135: Simulation of the degradation of PAS considering two competitive reactions and high heating ramps

Whether the first reactions are considered successive or competitive, they exhibit really different activation energies. A sharply different energy of activation means a larger impact of the heating ramp on the corresponding step. Moreover, the difficulty to reach this model when the lower heating ramp (1 °C/min) is considered tends to indicate that the decomposition mechanism is rather different in lower heating ramps. It should be underlined that all analyses such as thermal treatments (and solid-state NMR) were carried out in standard 10 °C/min conditions. It is then possible to miss some information specific to lower heating ramps that would lead to a slightly modified mechanism of decomposition.

VI.5.   CONCLUSION

In this chapter, many analyses were carried out during the thermal decomposition of PAS and PBTGF-PAS. Gas phase and condensed phase were both analyzed to reach a global model of decomposition.

FTIR and py-GC/ or EGA/MS allowed showing the different degradation products of PAS that were released in the gas phase (acrylanilide, aniline…), and so illustrate the weakest bonds in the molecule. The former aluminum phosphinate can cyclize and leave the condensed phase as an *azaphospholidinone-oxide* (leaving aluminum moieties in the condensed phase); but in most cases, aniline is released and the amide fragment decomposes little by little. The remaining phosphinate comprising a very reactive P-H bond can disproportionate into phosphonates (remaining in the condensed phase) and phosphines (gas phase active species).

In the condensed phase, solid-state NMR on thermally treated residues allowed showing that the aluminum phenylphosphonate can keep oxidizing and turn into aluminophosphate, with various aluminum coordinations, while releasing the remaining phenyl group under the form of benzene. The release of phosphines can contribute to poison the flame, as well as the release of azaphospholidinone-oxide. The real effect of these decomposition products on the flame should be furthermore investigated **[191]**.

The endothermic decomposition of PAS occurring mostly in the early stages of the degradation could contribute to cool down the material in the fire testing conditions. Finally, the phosphorus fragments remaining in the condensed phase, probably stabilized by the presence of the phenyl group, can contribute to create an organomineral char, protecting the surface of the sample. As a consequence, a mix between gas and condensed phase activity could be proposed.

The impact of PAS can only be investigated in the formulations. TGdifference as well as gas- and condensed-phase analyses carried out on PBTGF-PAS showed that the release of aniline leads to its recombination with PBT fragments such as benzoic acid or terephthalic esters fragments. This would also be consistent with a transamidification of the PBT chains, explaining the release of THF and the predegradation of PBT observed at lower temperatures. The release of THF would have the material catch on fire more easily (illustrated by the GWIT results) but this effect would be counterbalanced by the release of the phosphorus-containing fragments, thus decreasing flammability (high LOI). On the other hand, the release of phosphine, observed in the decomposition mechanism of PAS alone, is no more observed in py-GC/MS treatments of PBTGF-PAS. This fact is unexpected and should have a negative impact on fire properties. The hypothesis of a recombination of phosphines with PBT degradation fragments has been formulated. The presence of phosphines in the decomposition of the thermally thick formulation (cone plates for example) or formulations with higher loadings of PAS should also be investigated to confirm this hypothesis or validate the second hypothesis, that is, a dilution effect of the phosphine (thus not detected).

The presence of glass fibers should have an impact on thermal conductivity (wick effect), possibly decreasing the effectiveness of the endothermic effect of PAS and could also thus contribute to the formation of a solid residue, improving the mechanical properties of the charred layer. Without glass fibers, the recombination of aniline with PBT chains would decrease melt viscosity and lead to extinguishment by dripping.
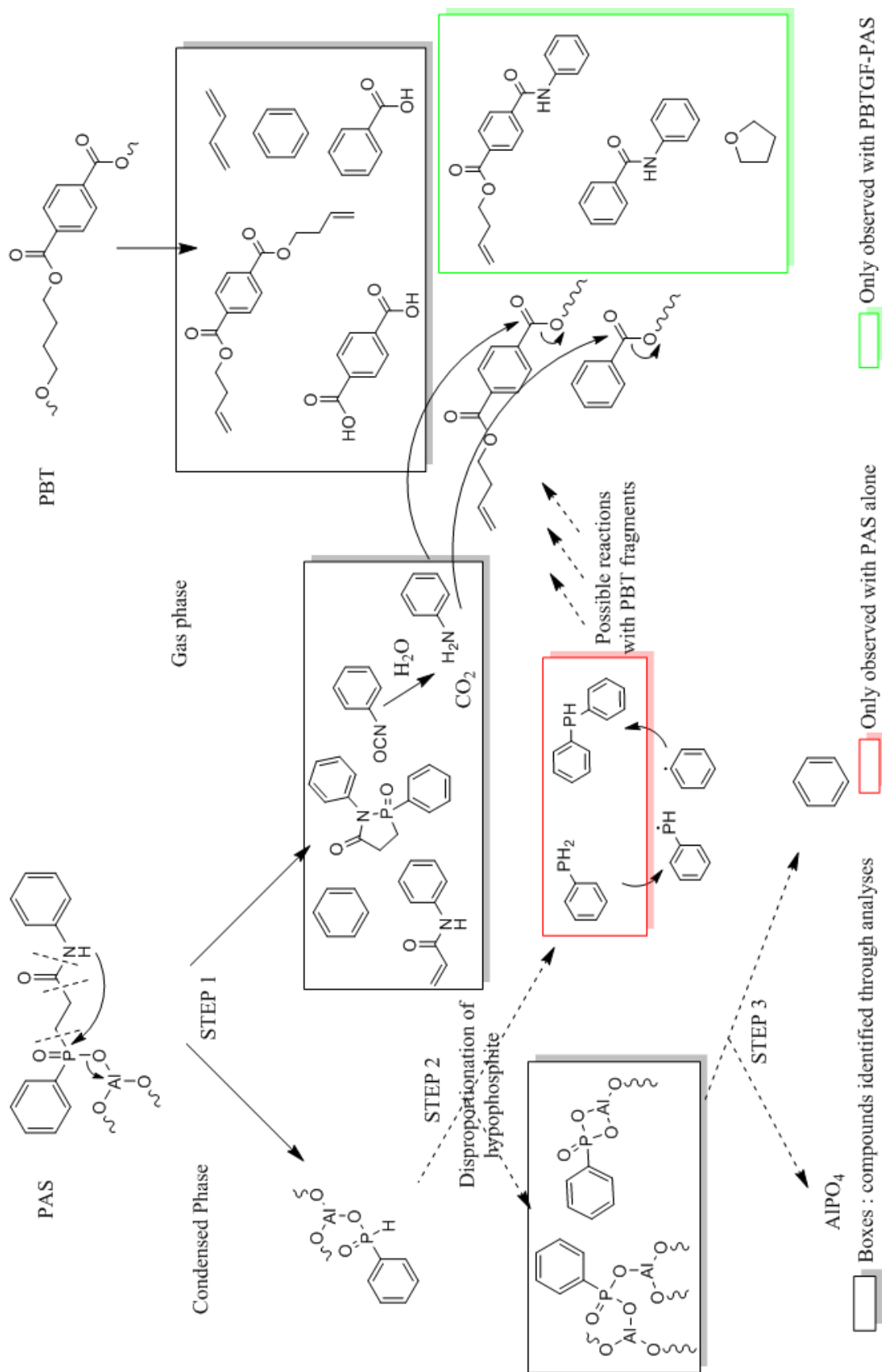
Figure 136: Global mechanism of decomposition and interactions of PBTGF-PAS

General conclusion - Outlook

This work was devoted to the development of novel phosphinate salts to flame retard glass fiber reinforced PBT and PA6, for applications in the E&E industry. These polymers are widely used in this domain to insulate electrical parts. The design of flame retardants is made on a purpose of compliance of such materials with the severe requirements to limit the flammability risks.

Based on the literature review and on the results of a previous partnership between the laboratory and BASF SE, six main starting materials were chosen to build novel flame retardants: 2-2-phenyl-1,2-oxaphospholan-5-one 2-oxide (2-POO), which is the phosphinate core common to all the products, and five amines. Aniline, benzylamine, ethylene diamine, para-phenylene diamine and piperazine were reacted with 2-POO, resulting in five phosphinic acids. These acids were converted into aluminum salts.

The first challenge consisted in yielding products that could be extruded in PBT and PA6, which process temperature is high regarding the usual stability of organic compounds. Salts with a perfect Al/P ratio were not obtained (elemental analyses, solid-state NMR), and the products were acidic, even after washing. However, their thermal stability allowed their processing in targeted matrices. Even if the degradation of the salts does not occur in the same temperature range as PBT and PA6, preliminary TGA also highlighted potential interactions between the additives and PBT as first approach.

Fire testings were then carried out to evaluate the efficiency of novel phosphinate salts as flame retardants. Promising results were achieved with the aniline-based compound, namely PAS. 20 wt% of this salt in PBTGF reached a V-1 classification in the UL-94. When 5 wt% melamine polyphosphate are used as co-additive, the highest classification, V-0, was reached. The use of PAS in PBTGF also allowed reaching the highest Glow Wire Flaming Index (GWFI, 960 °C) and a LOI of 30 vol% O_2. Unfortunately, results were not satisfying in PA6GF, and surprisingly the UL-94 ranking was higher in unreinforced PBT for PAS used without co-additive.

From the first screening of these additives, questions have been raised concerning the lack of information from the UL-94, as a same classification can correspond to different modes of action of given flame retardants or different fire behaviors. Instrumentation was thus set up on the test to collect temperature and weight loss data from the tested bars. The first setup was based on eight benchmarks, and the good agreement between observations and literature results validated the design of the instrumentation. It was then possible to compare PAS and Exolit OP1230 in this test and find an explanation on the difference of classification for PAS in PBT/PBTGF. This instrumentation approach was a first bridge to the comprehension of mechanisms involved in the effectiveness of PAS.

The understanding of these mechanisms was a crucial concern in this work. The pattern of degradation of PAS and PBTGF-PAS was built thanks to the analysis of both gas and condensed phase. TGA-FTIR and GC/MS allowed determining the different fragmentation points on the PAS molecules upon heating ramp decomposition. It was shown that PAS decomposes endothermically (thus cooling the material), releasing isocyanates and aniline, which can recombine with the PBT fragments and eventually with PBT chains, enhancing the degradation and dripping. In unreinforced material, enhanced dripping leads to high classification. This effect is prevented inGF reinforced material.

Organophosphorus compounds are also released and can contribute to poisoning the flame. The analysis of the residues in solid-state NMR showed PAS progressively turned to aluminophosphonates and aluminophosphates, with a high stability of the P-Ph bond. A model of decomposition with thermal and kinetic parameters was built, which is a simple first approach. The real decomposition pattern should be more complex.

OUTLOOK

As many fields of study were mixed in this manuscript, many perspectives emerged along the dissertation: synthesis outlook, development of the instrumentation, mechanistic studies…

The first and obvious outlook is related to the synthesis of novel phosphinates. In this manuscript, only five amine reactants were used. It could be interesting to investigate the corresponding oxygen-containing derivatives (when possible) such as phenol, benzyl alcohol, ethylene glycol…

From the first observations on the synthesized products, trends to find potential novel FR can be found. For instance, PAS does not seem as efficient in the gas phase as other phosphinates. As a consequence, other building-blocks should be considered. Triazine ring should be a good candidate (Figure 137). Other structures such as low-weight phosphinates (dimethylphosphinate) could also replace amines… The literature shows many cases of study of such compounds. It should also be possible to use the synthesized phosphinic acids to prepare oligomeric FR.
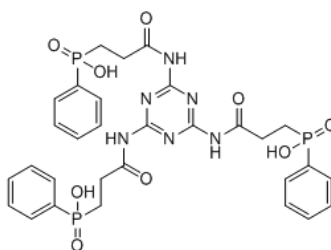
Figure 137: Triazine-based phosphinic acid derived from 2-POO

In the field of fire testing, it has been shown that instrumenting the UL-94 helped bringing much scientific information. The question raised from this instrumentation is "*Could that be possible to measure other parameters from the test?*". For instance, it is well known that the cone calorimeter presents the possibility of analyzing degradation gases during the test. Could such a measurement be carried out on the UL-94 without perturbing the flame? Could the setup of a smoke test be possible around the UL-94?

Finally, it was shown that the investigation of mechanisms is primordial in the comprehension of the flame retardancy. In this manuscript, no investigation was led on the formulations in PA6. It is not always relevant to investigate only the formulations exhibiting good results. Sometimes, the comprehension goes through finding the reasons why a formulation is not effective. More studies should be led on PA6, to help designing novel molecules that could show efficiency in polyamides. At least, it could be interesting to use the self-prepared additives in unreinforced PA6 to check if the glass fibers cause an antagonistic effect, as illustrated in the instrumented UL-94.

References

1. Plasticseurope, *Plastics - the Facts 2013 - An analysis of European plastics production, demand and waste data.* Available from : http://www.plasticseurope.org/cust/documentrequest.aspx?DocID=59108, 2013.

2. Plasticseurope, *Plastics - the Facts 2014/2015 - An analysis of European plastics production, demand and waste data.* Available from : http://www.plasticseurope.fr/Document/plastics-the-facts-20142015.aspx?Page=DOCUMENT&FolID=2, 2014.

3. Melton, G.H., Peters, E.N., and Arisman, R.K., *2 - Engineering Thermoplastics*, in *Applied Plastics Engineering Handbook*, Myer Kutz, Editor 2011, William Andrew Publishing: Oxford. p. 7-21.

4. Research and Markets, *Global Engineering Plastics Market Analysis By Product Types, Applications & Geography – Trends & Forecasts (2012 – 2017).* 2012.

5. Desbonnet, J. and Apchin, G., *Polyesters thermoplastiques PET et PBT pour injection.* Techniques de l'ingénieur, 2001.

6. *Glass-fibre reinforced PBT solves flame retardancy on French railways.* Reinforced Plastics, 2014. **58**(1): p. 7.

7. National Fire Protection Association, *Fires in the US.* Available from: http://www.nfpa.org/research/reports-and-statistics/fires-in-the-us, 2013.

8. Nelson, G. L., Morgan, A. B., and Wilkie, C. A., *Fire retardancy in 2009.* ACS symposium series, 2009. **1013**: p. 1-7.

9. *Consumer Protection Act, 1987 (a); Furniture and Furnishings Fire Safety Regulations 1988*.

10. Association Française de Normalisation (AFNOR), *NF P92-507 Sécurité contre l'incendie - Bâtiment - Matériaux d'aménagement - Classement selon leur réaction au feu.* 2004.

11. Association Française de Normalisation (AFNOR), *NF EN 13501-1 Classement au feu des produits et éléments de construction - Partie 1 : classement à partir des données d'essai de réaction au feu.* 2013.

12. National Fire Protection Association (NFPA), *NFPA 701: Standard methods of fire tests for flame-resistant textiles and films.* 2010.

13. Levchik, S.V. and Weil, E.D., *Flame retardancy of thermoplastic polyesters - a review of the recent literature.* Polymer international, 2005. **54**: p. 11-35.

14. Flame-retardants online, *Flame retardants market.* Available from: http://www.flameretardants-online.com, 2013.

15. Levchik, S. V. and Weil, E. D., *Combustion and fire retardancy of aliphatic nylons.* Polymer international, 2000. **49**(10): p. 1033-1073.

16. Duquesne, S. and Bourbigot, S., *Flame retardant nonwovens*, in *Applications of Nonwovens in Technical Textiles* 2010. p. 65-84.

17. Nass, B. and Wanzke, W., *US Patent 6207736 B1 - Non-halogenated flameproofing combination for non-halogenated polymers containing phosphinic acid salt and/or diphosphinic acid salt and nitrogen-containing phosphate* Clariant GmbH, 2001.

18. Jenewein, E., Kleiner, H.J., Wanzke, W., and Budzinsky, W., *US Patent 6365071 B1 - Mixture of diphosphinic acid an nitrogen compound* Clariant GmbH, 2002.

19. Schlosser, E., Nass, B., and Wanzke, W., *US Patent 6547992 B1 - Flame retardant combination for thermoplastic polymers*, Clariant GmbH, 2003.

20. Louisy, J., *Synthesis of novel phosphinate salts and development of formulations for the flame retardancy of glass fiber reinforced PolyButylene Terephtalate.* PhD Manuscript for BASF, 2012.

21. Heinze, H. and Wilhelm, F., *US 4680376 - Process for the continuous production of high-molecular polybutyleneterephthalate*, Davy McKee AG, 1987.

22. Heinze, H., Wilhelm, F., Mackensen, K., and Finkeldei, F., *US 4499261 - Process for the continuous production of polybutylene terephthalate of high molecular weight*, Davy McKee AG, 1985.

23. Quentin, J.P., *Polycondensation des polyesters saturés.* Techniques de l'ingénieur, 2004.

24. Fakirov, S., *Handbook of thermoplastic polyesters.* 2002. **1 & 2**.

25.   Pi Chang, E., Kirsten, R.O., and Slagowski, E.L., *The effect of additives on the crystallization of poly (butylene terephthalate).* Polymer Engineering & Science, 1978. **18**(12): p. 932-936.

26.   Cheng, Stephen Z. D., Pan, Robert, and Wunderlich, Bernhard, *Thermal analysis of poly(butylene terephthalate) for heat capacity, rigid-amorphous content, and transition behavior.* Die Makromolekulare Chemie, 1988. **189**(10): p. 2443-2458.

27.   Hobbs, S. and Pratt, C.F., *Multiple melting in poly(butylene terephthalate).* polymer, 1975. **16**: p. 462-464.

28.   Yeh, J.T. and Runt, J., *Multiple melting in annealed poly(butylene terephthalate).* Journal of Polymer Science Part B: Polymer Physics, 1989. **27**: p. 1543-1550.

29.   Kim, H.G. and Robertson, R.E., *Multiple melting endotherms in isothermally melt-crystallized poly-butylene terephthalate.* Journal of Polymer Science Part B: Polymer Physics, 1998. **36**: p. 1757-1767.

30.   Righetti, M.C. and Di Lorenzo, M.L., *Melting process of poly(butylene terephthalate) analyzed by temperature-modulated differential scanning calorimetry.* Journal of Polymer Science Part B: Polymer Physics, 2004. **42**: p. 2191-2201.

31.   Konishi, T. and Miyamoto, Y., *Crystallization of Poly(butylene terephthalate) from the Glass.* Macromolecules, 2009. **43**: p. 375-383.

32.   Tashiro, K., Y., Nakai, Kobayashi, M., and Tadokoro, H., *Solid-state transition of poly(butylene terephthalate) induced by mechanical deformation.* Macromolecules, 1980. **13**: p. 137-145.

33.   Ohtani, H., Kimura, T., and Tsuge, S., *Analysis of thermal degradation of terephthalate polyesters by high resolution pyrolysis-gas chromatography.* Analytical Sciences, 1986. **2**: p. 179-182.

34.   Sato, H., Kondo, K., Tsuge, S., and Ohtani, H., *Mechansisms of thermal degradation of a polyester flame-retarded with antimony oxide/brominated polycarbonate studied by temperature-programmed analytical pyrolysis.* Polymer Degradation and Stability, 1998. **62**: p. 41-48.

35.   Ishikawa, T., Ueno, T., Watanabe, Y., Mizuno, K., and Takeda, K., *Flame retardancy of poly(butylene terephthalate) blended with various oxides.* Journal of applied polymer science, 2008. **109**: p. 910-917.

36.   Balabanovich, A.I. and Engelmann, J., *Fire retardant and charring effect of poly(sulfonyldiphenylene phenylphosphonate) in poly(butylene terephthalate).* Polymer Degradation and Stability, 2003. **79**: p. 85-92.

37.   Braun, U. and Schartel, B., *Flame Retardancy Mechanisms of Aluminium Phosphinate in Combination with Melamine Cyanurate in Glass-Fibre-Reinforced Poly(1,4-butylene terephthalate).* Macromolecular Materials and Engineering, 2008. **293**(3): p. 206-217.

38.   Balabanovich, A.I., Balabanovich, A.M, and Engelmann, J., *Intumescence in poly(butylene terephtalate): the effect of 2-methyl-1,2-oxaphospholan-5-one 2-oxide and ammonium polyphosphate.* Polymer international, 2003. **52**: p. 1309-1314.

39.   Horrocks, A.R., *An Introduction to the Burning Behaviour of Cellulosic Fibres.* Journal of the Society of Dyers and Colourists, 1983. **99**(7-8): p. 191-197.

40.   Horrocks, A.R. and Price, D., *Fire retardant materials*, ed. Woodhead Publishing 2001.

41.   Casu, A., Camino, G., De Giorgi, M., Flath, D., Laudi, A., and Morone, V., *Effect of glass fibres and fire retardant on the combustion behaviour of composites, glass fibres–poly(butylene terephthalate).* Fire and Materials, 1998. **22**(1): p. 7-14.

42.   Hine, P. J. and Duckett, R. A., *Fiber orientation structures and mechanical properties of injection molded short glass fiber reinforced ribbed plates.* Polymer Composites, 2004. **25**(3): p. 237-254.

43.   Joshi, M., Maiti, S. N., Misra, A., and Mittal, R. K., *Influence of fiber length, fiber orientation, and interfacial adhesion on poly (butylene terephthalate)/polyethylene alloys reinforced with short glass fibers.* Polymer Composites, 1994. **15**(5): p. 349-358.

44.   Bergeret, A., Bozec, M. P., Quantin, J. C., Crespy, A., Gasca, J. P., and Arpin, M., *Study of interphase in glass fiber–reinforced poly(butylene terephthalate) composites.* Polymer Composites, 2004. **25**(1): p. 12-25.

45.   Linak, E. and Yoneyama, M., *Thermoplastic polyester engineering resins.* Chemical Economics Handbook, 2009: p. 580-1160.

46.   Palmer, R.J., *Polyamides, Plastics.* Encyclopaedia of Polymer Science and Technology, ed. John Wiley and sons2002.

47.   Odian, G., *Principles of Polymerization (4th edition)*, ed. John Wiley and sons2004.

48.   Roda, J., *Polyamides.* Handbook of Ring-Opening Polymerization, 2009: p. 165-195.

49.   Braun, E. and Levin, B.C., *Nylons: A review of the literature on products of combustion and toxicity.* Fire and Materials, 1987. **11**(2): p. 71-88.

50.   Gianchandani, J., Spruiell, J. E., and Clark, E. S., *Polymorphism and orientation development in melt spinning, drawing, and annealing of nylon-6 filaments.* Journal of applied polymer science, 1982. **27**(9): p. 3527-3551.

51.   Salem, D.R., *Structure formation in polymeric fibers*, ed. Hanser2001.

52.   Sallem-Idrissi, N., Miri, V., Elkoun, S., Krawczak, P., Lacrampe, M. F., Lefebvre, J. M., and Seguela, R., *Trichroic infrared analysis of the strain-induced structural changes in the PA6 layer of PA6/PE multilayer films under biaxial drawing.* Polymer, 2009. **50**: p. 5812-5823.

53.   Penel-Pierron, L., Depecker, C., Séguéla, R., and Lefebvre, J. M., *Structural and mechanical behavior of nylon 6 films part I. Identification and stability of the crystalline phases.* Journal of Polymer Science Part B: Polymer Physics, 2001. **39**(5): p. 484-495.

54.   Weeding, T. L., Veeman, W. S., Gaur, H. Angad, and Huysmans, W. G. B., *Structural investigation of polyamide-6 and polyamide-6 composites using carbon-13 cross polarization/magic angle spinning NMR.* Macromolecules, 1988. **21**(7): p. 2028-2032.

55.   Vasanthan, N. and Salem, D.R., *FTIR spectroscopic characterization of structural changes in polyamide-6 fibers during annealing and drawing.* Journal of Polymer Science Part B: Polymer Physics, 2001. **39**(5): p. 536-547.

56.   Devaux, E., Bourbigot, S., and El Achari, A., *Crystallization behavior of PA-6 clay nanocomposite hybrid.* Journal of applied polymer science, 2002. **86**(10): p. 2416-2423.

57.   Journal of Materials Science, Casanovas, J. and Alemán, C., *Calculated NMR chemical shifts of nylon 6: a comparison of the α and γ forms.* Journal of Materials Science, 2002. **37**(17): p. 3589-3594.

58.   Ho, J.C. and Wei, K.H., *Induced γ → α Crystal Transformation in Blends of Polyamide 6 and Liquid Crystalline Copolyester.* Macromolecules, 2000. **33**(14): p. 5181-5186.

59.   Liu, T. X., Liu, Z. H., Ma, K. X., Shen, L., Zeng, K. Y., and He, C. B., *Morphology, thermal and mechanical behavior of polyamide 6/layered-silicate nanocomposites.* Composites Science and Technology, 2003. **63**(3–4): p. 331-337.

60.   Anton, A. and Baird, B.R., *Polyamides, Fibers*, in *Encyclopedia of Polymer Science and Technology*2002, John Wiley & Sons, Inc.

61.   Levchik, S.V., Weil, E.D., and Lewin, M., *Thermal decomposition of aliphatic nylons.* Polymer international, 1999. **48**(7): p. 532-557.

62.   Davis, R.D., Gilman, J.W., and VanderHart, D.L., *Processing degradation of polyamide 6/montmorillonite clay nanocomposites and clay organic modifier.* Polymer Degradation and Stability, 2003. **79**(1): p. 111-121.

63.   Reimschuessel, H.K., Shalaby, S.W., and Pearce, E.M., *On the oxygen index of nylon 6.* Journal of Fire and Flammability, 1973. **4**: p. 299.

64.   Pearce, E.M., *Contemporary topics in polymer science*, ed. New York: Plenum Press. Vol. 5. 1984.

65.   Troitzsch, J., *Plastics Flammability Handbook*, ed. Hanser Gardener Publications2004.

66.   Laoutid, F., Bonnaud, L., Alexandre, M., Lopez-Cuesta, J. M., and Dubois, Ph, *New prospects in flame retardant polymer materials: From fundamentals to nanocomposites.* Materials Science and Engineering: R: Reports, 2009. **63**(3): p. 100-125.

67.   Price, D., Anthony, G., and Carty, P., *Fire Retardant Materials*, ed. Woodhead publishing Ltd.2001.

68.   Cusack, P. A., Heer, M. S., and Monk, A. W., *Zinc hydroxystannate as an alternative synergist to antimony trioxide in polyester resins containing halogenated flame retardants.* Polymer Degradation and Stability, 1997. **58**(1–2): p. 229-237.

69.   Kemmlein, S., Herzke, D., and Law, R.J., *Brominated flame retardants in the European chemicals policy of REACH—regulation and determination in materials.* Journal of Chromatography A, 2009. **1216**(3): p. 320-333.

70.   De Schryver, D, Landry, S.D., and Reed, J.S., *Latest developments on the flame retardancy of engineering thermoplastics–SAYTEX® HP-7010 (brominated polystyrene) in glass filled engineering thermoplastics.* Polymer Degradation and Stability, 1999. **64**(3): p. 471-477.

71.   Shaw, S., Blum, A., Weber, R., Kannan, K., Rich, D., Lucas, D., Koshland, C.P., Dobraca, D., Hanson, S., and Birnbaum, L.S., *Halogenated flame retardants: do the fire safety benefits justify the risks?* Reviews on environmental health, 2010. **25**(4): p. 261-306.

72.   Talsness, C.E., *Overview of toxicological aspects of polybrominated diphenyl ethers: A flame-retardant additive in several consumer products.* Environmental Research, 2008. **108**(2): p. 158-167.

73.   Balabanovich, A. I., *The effect of melamine on the combustion and thermal decomposition behaviour of poly(butylene terephthalate).* Polymer Degradation and Stability, 2004. **84**(3): p. 451-458.

74.   Weil, E. D. and Choudhary, V., *Flame-retarding plastics and elastomers with melamine.* Journal of Fire Sciences, 1995. **13**(2): p. 104-126.

75.   Kersies, J.Jr. and Furst, C. *Flame retardant mechanistic aspects of melamine cyanurate in polyamide 6 and 66*. 1999. Interscience Communications Ltd.

76.   Jahromi, S., Gabrielse, W., and Braam, A., *Effect of melamine polyphosphate on thermal degradation of polyamides: a combined X-ray diffraction and solid-state NMR study.* Polymer, 2002. **44**: p. 25-37.

77.   Casu, A., Camino, G., De Giorgi, M. , Flath, D. , Moronea, V. , and Zenonia, R. , *Fire-retardant mechanistic aspects of melamine cyanurate in polyamide copolymer.* Polymer Degradation and Stability, 1997. **58**(3): p. 297–302.

78.   Weil, E. D. and Levchik, S.V., *Current practice and recent commercial developments in flame retardancy of polyamides.* Journal of Fire Sciences, 2004. **22**(3): p. 251-264.

79.   Braun, U., Bahr, H., Sturm, H., and Schartel, B., *Flame retardancy mechanisms of metal phosphinates and metal phosphinates in combination with melamine cyanurate in glass-fiber reinforced poly(1,4-butylene terephthalate): the influence of metal cation.* Polymers for Advanced Technologies, 2008. **19**: p. 680-692.

80.   Mukherjee, A., *Melamine derivatives-An alternative to traditional flame retardants.* Plastics engineering, 2001. **57**(2): p. 42-43.

81.   Braun, U., Bahr, H., and Schartel, B., *Fire retardancy effect of aluminum phosphinate and melamine polyphosphate in glass fibre reinforced polyamide 6.* e-Polymers, 2010.

82.   Schlosser, E., Hoerold, S., Di Schwarz, U., and Reinemann, S., *EP2031019A2 - Flame resistant polyester compounds*, 2009, Clariant International Ltd., Switz. .

83.   Coquelle, M., Duquesne, S., Casetta, M., Sun, J., Gu, X., Zhang, S., and Bourbigot, S., *Flame Retardancy of PA6 Using a Guanidine Sulfamate/Melamine Polyphosphate Mixture.* Polymers, 2015. **7**(2): p. 316-332.

84.   Cérin, O., Development and characterization of a novel flame retardant EVM-based formulation: investigation and comprehension of the flame retardant mechanisms, PhD Thesis - Science et technologies, 2010, Université Lille 1

85.   Camino, G., Maffezzoli, A., Braglia, M., De Lazzaro, M., and Zammarano, M., *Effect of hydroxides and hydroxycarbonate structure on fire retardant effectiveness and mechanical properties in ethylene-vinyl acetate copolymer.* Polymer Degradation and Stability, 2001. **74**(3): p. 457-464.

86. Haurie, L., Fernández, A.I., Velasco, J. I., Chimenos, J. M., Lopez Cuesta, J.M., and Espiell, F., *Synthetic hydromagnesite as flame retardant. Evaluation of the flame behaviour in a polyethylene matrix.* Polymer Degradation and Stability, 2006. **91**(5): p. 989-994.

87. Hollingbery, L.A. and Hull, T.R., *The thermal decomposition of huntite and hydromagnesite—a review.* Thermochimica Acta, 2010. **509**(1): p. 1-11.

88. Miyata, S., *Composite metal hydroxide and its use*, 1995, Google Patents.

89. Shanmuganathan, K., Deodhar, S., Dembsey, N., Fan, Q., Calvert, P., Warner, S., and Patra, P.K., *Flame retardancy and char microstructure of nylon-6/layered silicate nanocomposites.* Journal of applied polymer science, 2007. **104**(3): p. 1540-1550.

90. Ballistreri, A., Montaudo, G., Puglisi, C., Scamporrino, E., and Vitalini, D., *Mechanism of smoke suppression by metal oxides in PVC.* Journal of Polymer Science: Polymer Chemistry Edition, 1981. **19**(6): p. 1397-1408.

91. Markezich, R. L. and Mundhenke, R. F., *The use of non-antimony oxide synergists with halogen flame retardants.* Annual Technical Conference - Society of Plastic Engineers, 1995. **53rd**: p. 3541-3.

92. Ballistreri, A, Montaudo, G, Puglisi, C, Scamporrino, E, Vitalini, D, and Calgari, S, *Mechanism of flame retardant action of red phosphorus in polyacrylonitrile.* Journal of Polymer Science: Polymer Chemistry Edition, 1983. **21**(3): p. 679-689.

93. Balabanovich, A. I., Levchik, G. F., Levchik, S. V., and Schnabel, W., *Fire retardance in polyamide-6. The effects of red phosphorus and radiation-induced cross-links.* Fire and Materials, 2001. **25**(5): p. 179-184.

94. Weil, E.D. and Levchik, S.V., *Flame retardants for plastics and textiles.* Hanser, 2009: p. 230-231.

95. Suzuki, M. and Saiki, N., *US 6133358 - Flame retardant resin formulation consists of a thermoplstic aromatic polyester resin, a novolak phenol resin and a coated red phosphorus powder having coating layer of a cured resin, useful for automobiles, electronics and electrical fields*, 2000.

96. Gareiss, B., Deckers, A., Klatt, M., and Weber, W., *US 6469095 B1 - Addition of the ethylene copolymers according to the invention, in particular low-molecular-weight copolymers, in combination with halogen-free flame retardants, gives a synergistic flame-retardant effect*, BASF Aktiengesellschaft, 2002.

97. Klatt, M., Gareiss, B., and Yamamoto, M., *US 6103797 - Thermoplastic molding composition comprising polyester, melamine cyanurate, phosphorus-containing flame retardant*, BASF Aktiengesellschaft, 2000.

98. Aufmuth, W., Levchik, S.V., Levchik, G.F., and Klatt, M., *Poly (butylene terephthalate) fire retarded by 1, 4-diisobutylene-2, 3, 5, 6-tetraxydroxy-1, 4-diphosphine oxide. I. Combustion and thermal decomposition.* Fire and Materials, 1999. **23**(1): p. 1-6.

99. Levchik, S.V., Bright, D.A., Alessio, G.R., and Dashevsky, S., *Synergistic action between aryl phosphates and phenolic resin in PBT.* Polymer Degradation and Stability, 2002. **77**(2): p. 267-272.

100. Chen, J., Liu, S., Jiang, Z., and Zhao, J., *Flame retardancy, smoke suppression effect and mechanism of aryl phosphates in combination with magnesium hydroxide in polyamide 6.* Journal of Wuhan University of Technology, Material Sciences, 2012. **27**: p. 916-923.

101. Artner, J., Ciesielski, M., Ahlmann, M., Walter, O., Döring, M., Perez, R.M., Altstädt, V., Sandler, J.K.W., and Schartel, B., *A novel and effective synthetic approach to 9, 10-dihydro-9-oxa-10-phosphaphenanthrene-10-oxide (DOPO) derivatives.* Phosphorus, Sulfur, and Silicon, 2007. **182**(9): p. 2131-2148.

102. Perret, B, Schartel, B, Stöß, K, Ciesielski, M, Diederichs, J, Döring, M, Krämer, J, and Altstädt, V, *Novel DOPO-based flame retardants in high-performance carbon fibre epoxy composites for aviation.* European Polymer Journal, 2011. **47**(5): p. 1081-1089.

103. Ciesielski, M, Schäfer, A, and Döring, M, *Novel efficient DOPO-based flame-retardants for PWB relevant epoxy resins with high glass transition temperatures.* Polymers for Advanced Technologies, 2008. **19**(6): p. 507-515.

104. Levchik, G. F., Grigoriev, Y.V., Balabanovich, A. I., Levchik, S.V., and Klatt, M., *Phosphorus–nitrogen containing fire retardants for poly (butylene terephthalate).* Polymer international, 2000. **49**(10): p. 1095-1100.

105. Scaffaro, R., Botta, L., La Mantia, F. P., Gleria, M., Bertani, R., Samperi, F., and Scaltro, G., *Effect of adding new phosphazene compounds to poly(butylene terephthalate)/polyamide blends. II: Effect of different polyamides on the properties of extruded samples.* Polym. Degrad. Stab., 2006. **91**: p. 2265-2274.

106. Richardson, J. and Dellar, R.J., *US 4972011 - Flame retardant polymer composition containing phosphonic acid salts*, Ciba-Ceigy corporation, 1990.

107. Kleiner, H.-J. and Budzinsky, W., *US 6270560 - Salt mixtures made from aluminum phosphinates, aluminum hydroxide &/or aluminum phosphonates &/or aluminum phosphates*, Ticona GmbH, 2001.

108. Klatt, M., Heitz, T., and Gareiss, B., *US 6306941 B1 - Flame-proof thermoplastic moulding materials*, BASF Aktiengesellschaft, 2001.

109. Yang, W., Hu, Y., Tai, Q., Lu, H., Song, L., and Yuen, R.K.K., *Fire and mechanical performance of nanoclay reinforced glass-fiber/PBT composites containing aluminum hypophosphite particles.* Composites Part A: Applied Science and Manufacturing, 2011. **42**(7): p. 794-800.

110. Kvalnes, D.E. and Brace, N.O., *US 2691566 - Organic phosphorus compounds for increasing the flame resistance of textiles*, 1954, E. I. du Pont de Nemours & Co. .

111. Racky, W., Kleiner, H.J., and Herwig, W., *DE 1972-2252258 - Fire-resistant thermoplastic polyesters*, 1974, Farbwerke Hoechst A.-G. .

112. Aoyama, T., Morikawa, M., Kato, N., Hashiba, I., Nagano, K., and Aramaki, M., *JP 51088549 - Fire resistant polyester and polyamide compositions*, 1976, Toray Industries, Inc., Japan; Nissan Chemical Industries, Ltd. .

113. Arbusow, B.A., *Michaelis-Arbusow-und perkow-reaktionen.* Pure and Applied Chemistry, 1964. **9**(2): p. 307-336.

114. Yuldashev, A., Rubtsova, I. K., and Moshkin, P. A., *Copolymerization of β,β'-dichloroethyl vinyl phosphinate with some unsaturated compounds.* Plasticheskie Massy, 1962: p. 10-11.

115. Borisov, G. and Devedzhiev, I., *Obtaining bis(p-carboxyphenoxymethyl)phosphinic acid, its esters, and polyesters.* Doklady Bolgarskoi Akademii Nauk, 1972. **25**: p. 759-62.

116. Grekov, A. P., Goncharova, L. B., Laptii, S. V., Veselov, V. Ya, Kercha, Yu Yu, and Shandruk, M. I., *Thermal degradation of phosphorus-containing polyurethanes.* Kompozitsionnye Polimernye Materialy, 1981. **9**: p. 28-32.

117. Mateva, R. and Dencheva, N., *On the behavior of organophosphorus lactam derivatives during anionic polymerization of ε-caprolactam.* Journal of Polymer Science Part A: Polymer Chemistry, 1992. **30**(7): p. 1449-1462.

118. Cho, C.-S., Chen, L.-W., Fu, S.-C., and Wu, T.-R., *Synthesis, characterization, thermal and flame retardant properties of novel aryl phosphinate diglycidyl ether cured with anhydride.* Journal of Polymer Research, 1998. **5**: p. 59-65.

119. Noetzel, S. and Herwig, W., *DE 2447727 - Flame-resistant polyamide molding materials*, 1976, Hoechst A.-G., Federal Republic of Germany.

120. Hashiba, I. and Nagano, K., *JP 52000245 - Substituted phosphinates*, 1977, Nissan Chemical Industries, Ltd., Japan .

121. Kleiner, H.J., Linke, F., and Duersch, W., *EP 1978-100073 - Carbamoyloxyalkylphosphinic acid derivatives and their use for production of flame-retardant finishes*, 1978, Hoechst A.-G., Federal Republic of Germany.

122. Nakahama, T., Mimura, K., and Aoki, K., *JP 54061124 - Fire-resisting phosphinic acid esters*, 1979, Nitto Chemical Industry Co., Ltd., Japan; Mitsubishi Rayon Co., Ltd. .

123. Kleiner, H.-J., Budzinsky, W., and Kirsch, G., *EP 699708 - Flame-retardant polyester molding compositions*, 1996, Hoechst A.-G., Germany .

124. Kleiner, H.-J., Budzinsky, W., and Kirsch, G., *EP 792912 - Fireproof polyamide molding compositions containing calcium or aluminum phosphinate salts*, 1997, Hoechst A.-G., Germany .

125. Hanabusa, K. and Matsushima, M., *WO 9856857 - Fire-resistant thermoplastic polyester compositions containing nitrogenous organic compounds and phosphinic acid salts*, 1998, Polyplastics Co., Ltd., Japan .

126. Flame-retardants online, *Phosphinates, the flame retardants for polymers in electronics (Clariant).* Available from : http://www.flameretardants-online.com/images/userdata/pdf/170_EN.pdf, 2006.

127. Braun, U., Schartel, B., Fichera, M.A., and Jäger, C., *Flame retardancy mechanisms of aluminium phosphinate in combination with melamine polyphosphate and zinc borate in glass-fiber reinforced polyamide 6.6.* Polymer Degradation and Stability, 2007. **92**: p. 1528-1545.

128. Samyn, F. and Bourbigot, S., *Thermal decomposition of flame retarded formulations PA6/aluminium phosphinate/melamine polyphosphate/organomodified clay: Interactions between the constituents?* Polymer Degradation and Stability, 2012. **97**: p. 2217-2230.

129. Duquesne, S., Fontaine, G., Cérin-Delaval, O., Gardelle, B., Tricot, G., and Bourbigot, S., *Study of the thermal degradation of an aluminium phosphinate–aluminium trihydrate combination.* Thermochimica Acta, 2013. **551**: p. 175-183.

130. Chajrullin, V.K., Sobcuk, I.I., and Pudovik, A.N., Zurnal obscej Chimii, 1967. **37**(3): p. 710-714.

131. Finke, M., Kleiner, H.J., and Lohmar, E., *US patent 4045480: Process for preparing 1,2-oxa-phospholanes*, 1977.

132. Balabanovich, A.I. and A.M., Balabanovich, *Fire retardant and charring effect of poly(sulfonyldiphenylene phenylphosphonate) in poly(butylene terephtalate)* Polymer degradation and stability, 2003. **79**: p. 85-92.

133. Noetzel, S., Herwig, W., Kern, R., and Lotz, W., *US patent 3980614: Flame retarding plastic materials*, Hoechst Aktiengesellschaft, 1976.

134. Noetzel, S., *US patent 3980615: Flame retarding plastic materials*, Hoechst Aktiengesellschaft, 1976.

135. Blöcker, E., *US patent 5281637: Flameproofed thermoplastic polyester molding material and its use*, Hoechst Aktiengesellschaft, 1994.

136. Underwriters' Laboratories, *UL 94 - Tests for flammability of plastic materials for parts in devices and appliances.* 1998.

137. Kandola, B.K., Price, D., Milnes, G.J., and Da Silva, A., *Development of a novel experimental technique for quantitative study of melt dripping of thermoplastic polymers.* Polymer Degradation and Stability, 2013. **98**: p. 52-63.

138. Acquasanta, F., Berti, C., Colonna, M., Fiorini, M., and Karanam, S., *Study of Glow Wire Ignition Temperature (GWIT) and Comparative Tracking Index (CTI) performances of engineering thermoplastics and correlation with material properties.* Polymer Degradation and Stability, 2011. **96(4)**: p. 566 - 573.

139. ISO 4589 *Determination of burning behavior by oxygen index.* 1996.

140. Lyon, R.E. and Janssens, M.L., *Polymer flammability.* U.S. Department of Transportation, Federal Aviation Administration, Final report, 2005.

141. Hugget, C., *Estimation of rate of heat release by means of oxygen consumption measurements.* Fire and Materials, 1980. **4**(2): p. 61-65.

142. Askadskii, A.A., *Chapter VII: Temperature of Onset of Intense Thermal Degradation of Polymers.* Computational Materials Science of Polymers - Cambridge International Science Publishing, 2003.

143.   Hu, B., Trébosc, J., and Amoureux, J.-P., *Comparison of several hetero-nuclear dipolar recoupling NMR methods to be used in MAS HMQC/HSQC.* Journal of Magnetic Resonance, 2008. **192**(1): p. 112-122.

144.   Brinkmann, A. and Kentgens, A.P.M., *Proton-Selective 17O-1 H Distance Measurements in Fast Magic-Angle-Spinning Solid-State NMR Spectroscopy for the Determination of Hydrogen Bond Lengths.* Journal of the American Chemical Society, 2006. **128**(46): p. 14758-14759.

145.   Parker, W.J., Jenkins, R.J., Butler, C.P., and Abbott, G.L., *Flash method of determining thermal diffusivity, heat capacity and thermal conductivity.* Journal of Applied Physics, 1961. **32**: p. 1679-1684.

146.   Bauer, H., Hoerold, S., and Krause, W., *US 2008/0188598 A1 - Salts of alkyl esters of carboxyethyl (alkyl) phosphinic acid*, Clariant GmbH, 2010.

147.   Paulik, F.E., and Weinkauff, D.J., *WO 2001070752 A1 - Process for the preparation of 2-carboxy-alkyl(aryl)phosphonic acids and anhydride(s)*, Solutia Inc., 2001.

148.   Thibaudeau, C., Stenutz, R., Hertz, B., Klepach, T., Zhao, S., Wu, Q., Carmichael, I., and Serianni, A., *Correlated CC and CO bond conformations in saccharide hydroxymethyl groups: parametrization and application of redundant 1H-1H, 13C-1H, and 13C-13C NMR J-couplings.* Journal of the American Chemical Society, 2004. **126**(48): p. 15668-15685.

149.   Ando, I., *Some aspects of the NMR chemical shift/structure correlation in the structural characterization of polymers and biopolymers.* Polym J, 2012. **44**(8): p. 734-747.

150.   Guo, X.Z. and Wang, L.S., *Solubilities of Phosphorus-Containing Compounds in Selected Solvents.* J. Chem. Eng. Data, 2010. **55**: p. 4709-4720.

151.   Lookman, R., Grobet, P;, Merckx, R., and Van Riemsdijk, W.H., *Application of 31 P and 27 Al MAS NMR for phosphate speciation studies in soil and aluminium hydroxides: promises and constraints.* Geoderma, 1997. **80**(3): p. 369-388.

152.   Jordan, P.A., Clayden, N.J., Heath, S.L., Moore, G.R., Powell, A.K., and Tapparo, A., *Defining speciation profiles of Al 3+ complexed with small organic ligands: the A1 3+-heidi system.* Coordination chemistry reviews, 1996. **149**: p. 281-309.

153.   Robinson, R. A. and Britton, H. T. S. , *The amphoteric nature of aluminum hydroxide.* Journal of the Chemical Society, 1931: p. 2817-2820.

154.   Gallo, E., Braun, U., Schartel, B., Russo, P., and Acierno, D., *Halogen-free flame retarded poly(butylene terephthalate) (PBT) using metal oxides/PBT nanocomposites in combination with aluminium phosphinate.* Polymer Degradation and Stability, 2009. **94**(8): p. 1245-1253.

155.   Dick, C., Dominguez-Rosado, E., Eling, B., Liggat, J. J., Lindsay, C. I., Martin, S. C., Mohammed, M. H., Seeley, G., and Snape, C. E., *The flammability of urethane-modified polyisocyanurates and its relationship to thermal degradation chemistry.* Polymer, 2001. **42**(3): p. 913-923.

156.   Perret, B., Pawlowski, K.H., and Schartel, B., *Fire retardancy mechanisms of arylphosphates in polycarbonate (PC) and PC/acrylonitrile-butadiene-styrene.* J. Therm. Anal. Calorim., 2009. **97**: p. 949-958.

157.   Lu, C., Liu, L., Chen, N., Wang, X., Yang, D., Huang, X.H., and Yao, D.H., *Influence of clay dispersion on flame retardancy of ABS/PA6/APP blends.* Polym. Degrad. Stab., 2015. **114**: p. 16-29.

158.   Kandola, B.K., Price, D., Milnes, J., Da Silva, A., Gao, F., and Nigmatullin, R., *Characterization of melt dripping behavior of flame retarded polypropylene nanocomposites.* ACS symposium series, 2012. **1118**: p. 311-325.

159.   Akdogan, H., Tomás, R.L., and Oliveira, J.C., *Rheological properties of rice starch at high moisture contents during twin-screw extrusion.* LWT-Food Science and Technology, 1997. **30**(5): p. 488-496.

160.   Ragaert, K., Dekeyser, A., Cardon, L., and Degrieck, J., *Quantification of thermal material degradation during the processing of biomedical thermoplastics.* Journal of applied polymer science, 2011. **120**(5): p. 2872-2880.

161.   Alexy, P., Lacík, I., Šimková, B., Bakoš, D., Prónayová, N., Liptaj, T., Hanzelová, S., and Várošová, M., *Effect of melt processing on thermo-mechanical degradation of poly(vinyl alcohol)s.* Polymer Degradation and Stability, 2004. **85**(2): p. 823-830.

162.   EC60335-1-4, *Safety of household and similar electrical appliances, 4th ed.* 2008.

163.   Schartel, B., Pawlowski, K.H., and Lyon, R.E., *Pyrolysis combustion flow calorimeter: A tool to assess flame retarded PC/ABS materials?* Thermochimica Acta, 2007. **462**(1–2): p. 1-14.

164.   Lyon, R.E., Walters, R.N., and Stoliarov, S.I., *Screening flame retardants for plastics using microscale combustion calorimetry.* Polymer Engineering & Science, 2007. **47**(10): p. 1501-1510.

165.   Sonnier, R, Ferry, L, Longuet, C, Laoutid, F, Friederich, B, Laachachi, A, and Lopez-Cuesta, J.M., *Combining cone calorimeter and PCFC to determine the mode of action of flame-retardant additives.* Polymers for Advanced Technologies, 2011. **22**(7): p. 1091-1099.

166.   Sonnier, R., Negrell-Guirao, C., Vahabi, H., Otazaghine, B., David, G., and Lopez-Cuesta, J.M., *Relationships between the molecular structure and the flammability of polymers: Study of phosphonate functions using microscale combustion calorimeter.* Polymer, 2012. **53**(6): p. 1258-1266.

167.   https://scifinder.cas.org. *Bibliometry for the keyword UL-94*. Dec. 2014.

168.   Kempel, F., Schartel, B., Marti, J.M., Butler, K.M., Rossi, R., Idelsohn, S.R., Onate, E., and Hofmann, A., *Modelling the vertical UL 94 test: competition and collaboration between melt dripping, gasification and combustion.* Fire and Materials, 2014. **2257**.

169.   Schartel, B, Pötschke, P., Knoll, U., and Abdel-Goad, M., *Fire behaviour of polyamide 6/multiwall carbon nanotube nanocomposites.* European Polymer Journal, 2005. **41**(5): p. 1061-1070.

170.   Song, Lei, Hu, Yuan, Lin, Zhihua, Xuan, Shanyong, Wang, Shaofeng, Chen, Zuyao, and Fan, Weicheng, *Preparation and properties of halogen-free flame-retarded polyamide 6/organoclay nanocomposite.* Polymer Degradation and Stability, 2004. **86**(3): p. 535-540.

171.   Levchik, S.V., Levchik, G.F., Balabanovich, A.I., Weil, E.D., and Klatt, M., *Phosphorus oxynitride: a thermally stable fire retardant additive for polyamide 6 and poly (butylene terephthalate).* Die Angewandte Makromolekulare Chemie, 1999. **264**(1): p. 48-55.

172.   Michaux, G., Fire retardancy of Polyamide 6 for electrotechnical applications, PhD Thesis - Science et technologies, 2014, Université Lille 1

173.   Morita, K., M., Hidaka, R., and Aryoshi, M., *Manufacturing method of polyamide resin compositions by extrusion*, Jpn. Kokai Tokkyo Koho, 1996.

174.   Levchik, S. V., Balabanovich, A. I., Levchik, G. F., and Costa, L., *Effect of melamine and its salts on combustion and thermal decomposition of polyamide 6.* Fire and Materials, 1997. **21**(2): p. 75-83.

175.   Liu, Y. and Wang, Q., *The investigation on the flame retardancy mechanism of nitrogen flame retardant melamine cyanurate in polyamide 6.* Journal of Polymer Research, 2009. **16**(5): p. 583-589.

176.   Dabrowski, F., Optimisation et compréhension de procédés d'ignifugation de polymères techniques PhD Thesis - Science et technologies, 2001, Université Lille 1

177.   Horacek, H., Ritzberger, K., Reichenberger, R., and Prinz, C., *DE4436281A1 - Fire-resistant, glass fiber-reinforced polyamides containing reaction products of phosphoric acid with melamine or melem as fire retardants*, 1996, Chemie Linz Deutschland Gmbh, Germany .

178.   Martens, M.M., Kasowski, R.V., Cosstick, K.B., and Penn, R.E., *Fire-resistant polyamide and polyester compositions*, 1998, E. I. Du Pont de Nemours & Co., USA . p. 10 pp., Cont.-in-part of U.S. 5,618,865.

179.   Coquelle, M., Flame retardancy of polyamide 6 fibers : the use of sulfamate salts, PhD Thesis - Science et technologies, 2014, Université Lille 1

180.   Coquelle, M., Duquesne, S., Casetta, M., Sun, J., Zhang, S., and Bourbigot, S., *Investigation of the decomposition pathway of polyamide 6/ammonium sulfamate fibers.* Polymer Degradation and Stability, 2014. **106**: p. 150-157.

181.   Schartel, B. and Braun, U., *Flame retardancy mechanisms of aluminum phosphinate in glass fiber reinforced thermoplastics.* Proc. Annu. Conf. Recent Adv. Flame Retard. Polym. Mater., 2008. **19th**: p. 36-47.

182.   Ohtani, H., Kimura, T., and Tsuge, S., *Analysis of thermal degradation of terephtalate polyesters by high-resolution pyrolysis-gaschromatography* Analytical sciences, 1986. **2**: p. 179-182.

183.   Hoffmann, T., Friedel, P., Harnisch, C., Häußler, L., and Pospiech, D., *Investigation of thermal decomposition of phosphonic acids* Journal of Analytical and Applied Pyrolysis 2012. **96**: p. 43-53.

184.   Guerrero, G., Mutin, P.H., and Vioux, A., *Organically modified aluminas by grafting and sol-gel processes involving phosphonate derivatives.* Journal of Materials Chemistry, 2001. **11**: p. 3161-3165.

185.   Chaplais, G., Le Bideau, J., Leclercq, D., Mutin, H., and Vioux, A., *Novel aluminum phenyl, benzyl, and bromobenzylphosphonates: structural characterisation and hydrazion-dehydration reactions.* Journal of Materials Chemistry, 2000. **10**: p. 1593-1601.

186.   Cabeza, A., Aranda, M.A.G., Bruque, S., Poojary, D.M., Clearfield, A., and Sanz, J., *Aluminum phenylphosphonates: a fertile family of compounds.* Inorganic Chemistry, 1998. **37**: p. 4168-4178.

187.   Vannier, A., Duquesne, S., Bourbigot, S., Alongi, J., Camino, G., and Delobel, R., *Investigation of the thermal degradation of PET, zinc phosphinate, OMPOSS and their blends— Identification of the formed species.* Thermochimica Acta, 2009. **495**(1–2): p. 155-166.

188.   Ciesielski, W., Kassassir, H., and Potrzebowski, M.J., *A practical guide for the setup of a 1H– 31P–13C double cross-polarization (DCP) experiment.* Solid State Nuclear Magnetic Resonance, 2011. **39**(3–4): p. 151-157.

189.   Friedman, H.L., *Kinetics of thermal degradation of char-forming plastics from thermogravimetry.* Journal of Polymer Science, 1964. **6**(1): p. 183-195.

190.   Zsako, J., *Kinetic analysis of thermogravimetric data.* Journal of thermal analysis, 1996. **46**(6): p. 1845-1864.

191.   Korobeinichev, O. P., Bolshova, T. A., Shvartsberg, V. M., and Chernov, A. A., *Inhibition and promotion of combustion by organophosphorus compounds added to flames of CH4 or H2 in O2 and Ar.* Combustion and Flame, 2001. **125**(1–2): p. 744-751.

Résumé

Cette étude s'intéresse aux procédés d'ignifugation de deux thermoplastiques techniques, le poly téréphtalate de butylène (PBT) et le polyamide 6 (PA6), à application dans le domaine électrique et électrotechnique. Plus précisément, l'accent est mis sur l'ajout en masse de retardateurs de flammes à base d'azote et de phosphore. L'objectif de ce projet consiste à préparer de nouveaux retardateurs de flamme par voie de synthèse organique. Dans un premier temps, cinq phosphinates d'aluminium ont été préparés par amidification de l'acide hydroxyphenylphosphoryl propanoïque et réaction avec un promoteur d'aluminium. Ces sels ont été incorporés au PBT et au PA6, seuls ou en combinaison avec des co-additifs, puis testés à l'UL-94, test témoin de la propagation verticale de la flamme, très utilisé dans l'industrie électrique et électrotechnique. Parmi les cinq sels, seul le phenylamide de l'acide hydroxyphenylphosphoryl propanoïque (PAS) s'est avéré être un retardateur de flammes efficace. D'autres tests ont été réalisés pour approfondir les résultats. Une instrumentation du test UL-94 a également été développée pour établir les bases de la compréhension du mécanisme d'action de la formulation, approfondies ensuite dans une série de microanalyses. Il a été démontré que le PAS se décompose en entraînant la scission des chaînes de PBT et le refroidissement du matériau. La libération de composés phosphorés en phase gaz, bien que moins efficace que pour d'autres composés commerciaux, suffit à donner à la formulation sa propriété d'auto-extinction.

Mots clés : Polyester, polyamide, organo-phosphoré, ignifugation, synthèse organique

Abstract

This study deals with the flame retardancy of two engineering plastics, the poly(butylene terephthalate) (PBT) and the polyamide 6 (PA6), widely used in the electrical and electronic equipment (EEE). The focus is made on the incorporation of phosphorus- and nitrogen-containing flame retardant (FR) additives. The main goal of this project was to prepare novel FR through organic synthesis. Five aluminum phosphinates were prepared by reaction of amines on hydroxyphenylphosphnyl propanoic acid and an aluminum promoter. The salts were incorporated to PBT and PA6, with or without co-additives, and the materials were tested in the UL-94, test investigating the vertical propagation of the flame and widely used in the EEE industry. Among the five salts, only the aluminum salt of phenyl amide of hydroxyphenylphosphnyl propanoic acid showed outstanding properties as FR. Other tests were carried out, among which an instrumentation of the UL-94 test, to build a way to the comprehension of mechanisms. First observations were completed by various microanalyses. It has been shown that the decomposition of PAS enhances that of PBT in parallel to its cooling. The liberation of phosphorus-containing species in the gas-phase, despite les efficient than in the case of other commercial FR, gives the formulation its auto-extinguishing character.

Keywords : Polyester, polyamide, organophosphorus, fire retardancy, organic synthesis